Fabrication and Characterization of Functionally Graded Metal and Polymer Composites by Sequential and Centrifugal Casting Techniques

Thesis submitted to

Cochin University of Science and Technology (CUSAT)

in partial fulfilment of the requirements for the Degree of

Doctor of Philosophy

in the Faculty of Technology

By

AKHIL S. KARUN

(Reg. No. 4569)

Under the Supervision of

Dr. U.T.S. Pillai & Dr. T.P.D. Rajan

Materials Science and Technology Division
CSIR-National Institute for Interdisciplinary Science and Technology (NIIST)
(Formerly, Regional Research Laboratory)
Council of Scientific & Industrial Research (CSIR), Govt. of India
Thiruvananthapuram – 695 019
INDIA

May 2017

Fabrication and Characterization of Functionally Graded Metal and Polymer Composites by Sequential and Centrifugal Casting Techniques

Ph.D. Thesis

May 2017

Author:

Akhil S. Karun
Senior Research Fellow (SRF)
Materials Science and Technology Division
CSIR - National Institute for Interdisciplinary Science and Technology (NIIST)
Thiruvananthapuram – 695 019
Email: akhilskarun@gmail.com
Tel. No.: +91-4735245587 (Residence)
Mobile No.: +91-9496325080

Thesis Supervisors:

Dr. U.T.S. Pillai
Chief Scientist
Materials Science and Technology Division
CSIR - National Institute for Interdisciplinary Science and Technology (NIIST)
Thiruvananthapuram – 695 019
Email: utspillai@gmail.com
Tel. No.: +91-4712515236 (Office)
Mobile No.: +91-9447882883

and

Dr. T.P.D. Rajan
Principal Scientist
Materials Science and Technology Division
CSIR - National Institute for Interdisciplinary Science and Technology (NIIST)
Thiruvananthapuram – 695 019
Email: tpdrajan@gmail.com
Tel. No.: +91-4712515327 (Office)
Mobile No.: +91-9447035439

Dedicated to

My well-wishers . . .

DECLARATION

I hereby declare that the thesis entitled **"Fabrication and Characterization of Functionally Graded Metal and Polymer Composites by Sequential and Centrifugal Casting Techniques"** embodies the results of bonafide research work carried out by me for the degree of Doctor of Philosophy in Faculty of Technology of the Cochin University of Science and Technology (CUSAT), Cochin, Kerala under the combined supervision of Dr. U.T.S. Pillai (Chief Scientist) and Dr. T.P.D. Rajan (Principal Scientist), Materials Science and Technology Division, CSIR-National Institute for Interdisciplinary Science and Technology (NIIST), Council of Scientific & Industrial Research (CSIR), Thiruvananthapuram, Kerala, India. I further declare that this thesis or part thereof has not previously been formed the basis for the award of any degree or diploma.

Thiruvananthapuram

02 May, 2017 **AKHIL S. KARUN**

Council of Scientific and Industrial Research
CSIR - NATIONAL INSTITUTE FOR INTERDISCIPLINARY SCIENCE AND TECHNOLOGY (CSIR-NIIST)
Industrial Estate P.O., Pappanamcode,Thiruvananthapuram, Kerala - 695 019, India

May 02, 2017

CERTIFICATE

This is to certify that the thesis entitled **"Fabrication and Characterization of Functionally Graded Metal and Polymer Composites by Sequential and Centrifugal Casting Techniques"** is a bonafide record of the research work carried out by **Mr. Akhil S. Karun**, under our supervision in partial fulfilment of the requirement for the degree of Doctor of Philosophy of Cochin University of Science and Technology (CUSAT) and further that no part of this thesis has been presented previously for the award of any other degree. All the relevant corrections, modifications and recommendations suggested by the audience and the doctoral committee members during the pre-synopsis presentation have been incorporated in the thesis.

Dr. U.T.S. Pillai
(Research Supervisor)
Chief Scientist
Materials Science and Technology Division
Email: utspillai@gmail.com
Tel. No.: 0471-2515236
Mob: +91-9447882883

Dr. T.P.D. Rajan
(Research Supervisor)
Principal Scientist
Materials Science and Technology Division
Email: tpdrajan@gmail.com
Tel. No.: 0471-2515327
Mob: +91-9447035439

Acknowledgements

I take this opportunity to express my deep sense of gratitude and sincere thanks to all who helped me to complete the thesis work successfully. My first and foremost thanks go to my research supervisors Dr. U.T.S. Pillai (Chief Scientist) and Dr.T.P.D.Rajan (Principal Scientist), Materials Science and Technology Division (MSTD) of CSIR-National Institute for Interdisciplinary Science and Technology (NIIST), Council of Scientific & Industrial Research (CSIR), Thiruvananthapuram, Kerala.

It is with great respect and profound gratefulness that I record my gratitude and deep felt devotion to Dr. B.C. Pai (Former Director, CSIR-NIIST) for his precious and valuable discussions, never failing kindness, inspiring guidance and for sharing encouraging thoughts throughout the thesis work.

I thank Dr. A. Ajayaghosh, Director and Dr. Suresh Das, Former Director of CSIR-National Institute for Interdisciplinary Science and Technology (NIIST), Thiruvananthapuram, Kerala for providing the necessary facilities for carrying out this research work.

I will forever be thankful to the network project ESC-0101 for the fellowship and Council of Scientific & Industrial Research (CSIR), Govt. of India, New Delhi for granting me the Senior Research Fellowship for the completion of this research work.

I would like to thank Dr. P. Prabhakar Rao (Head, MSTD), Dr. M.L.P. Reddy and Dr. M.T. Sebastian (Former Heads, MSTD) for their help and support during my tenure in CSIR-NIIST as Senior Project Fellow (SPF) and Senior Research Fellow (SRF).

My sincere thanks to Dr. K. Harikrishna Bhat, Dr. A. Srinivasan, Dr. M. Ravi, Mr. M.C. Shaji, Dr. U.S. Hareesh, Dr.Satyajit Shukla, Dr. S. Ananthakumar, Dr. J.D. Sudha, Dr. V.S. Prasad, Dr. A.R.R. Menon, Dr. Saju Pillai, present and retired scientists of Materials Science and Technology Division and Chemical Sciences and Technology Division, CSIR-NIIST for the help and support.

I express heartfelt thanks to my doctoral committee external expert, Prof. Dr. K.E. George, Former Professor & Head, Department of Polymer Science and Rubber Technology, Cochin University of Science and Technology (CUSAT), Kochi for his timely help extended towards me for the successful submission of the thesis.

I am deeply indebted to all my teachers especially Dr. V.R. Rajeev (Govt. Engineering College, Thrissur), Dr. K. Bindhu Kumar (College of Engineering Trivandrum), Dr. S. Narayanan (Former Principal, Sree Chitra Thirunal College of Engineering (SCTCE), Thiruvananthapuram), Mr. Sreeju U., Mr. V. Gopalakrishnan, Mrs. Vineetha A., Mr. T.S. Sigikumar, Mrs. Shimi Mohan, (Former Assistant Professors at Musaliar College of Engineering and Technology (MCET), Pathanamthitta), Prof. N. Samuel Thomas / Ennesty (Former Principal, St. Thomas College, Kozhencherry, Pathanamthitta), Mr. Suresh Babu T.G., Mr. K.S. Radhakrishnan Nair, Mr. K.K. Balakrishnan, Mr. P.K. Vijayan, Mr. Manu S. Kurup, Mrs. Prasanna Zachariah, Mrs. V. Subaida Beevi, Mrs. Rosamma Samuel and Late Mr. Thomas Samuel (Aashan - My first Teacher).

I extended my thanks to Mr. Harish Raj V., Mr. M.R. Chandran and Mrs. Soumya S. for SEM Analysis, Mr. Pruthiviraj N. for XRD Analysis, Mrs. Reshma L.R. for support during polymer based work, Dr. Abi Santhosh Aprem (Scientist, HLL), Mrs. Reshmi (HLL) for Shore D hardness testing, Ms. Anju P., Ms. Molji C. and Mrs. Bhagya Uthaman for their help, support and cooperation during the entire support for the work.

I would like to express my sincere thanks to Mr. Hari S., Mr. Graceborn L.R., Mr. Abhijith Shanker T., Mr. Akhil B. Roy and Mr. Krishnadath D., Mr. Anil Chacko, Mr. Arjun P., Mr. Manoj Balu V.B., Mr. Arun Kumar S. (M. Tech. Project Students) for their wholehearted support during the entire tenure for the successful completion of the work. Also, I avail the opportunity to express my profound thanks to Mr. M. Brahmakumar, Mr. Satheesh Kumar R., Mr. Sreelal M., Mr. Arunsankar J., Mr. Giri Sankar M., Mr. Jaganlal S.K., Mr. Sujin J.S., Mr. Anand M. and Mr. J.P. Jayaprasobh for the workshop facilities provided for fulfilling the requirements for completing the work.

I am very much indebted to the members of CSIR-NIIST family especially my friends Mrs. Praseeda S. Nair (University Assistant, University of Calicut), Mrs. Lakshmi V. (Project Scientist, Sree Chitra Tirunal Institute for Medical Sciences & Technology), Dr. Deepa J.P. (Assistant Professor, S.N. College, Punalur, Kollam), Mrs. Resmi V.G., Ms. Jerin K. Pancrecious, Ms. Ramya R., Mr. Kavin S., Mr. Rajesh Kumar R., Ms. Ulaeto, Sarah Bill (Nigeria), Dr. Williams S. Ebhota (Nigeria), Ms. Ajala, Faten (Tunisia), Mr. N. Anand, Mr. Shaiju P., Mr. E. Jayakumar (Assistant Professor, SCTCE), Late Mr. Jibin C. Jacob, Mr. Arjun B.K., Mr. Akhil M.G., Mr. Arun Kumar S., Mr. S.U. Sanjeev Kamal and the other members of Materials Science and Technology Division for their valuable support, advice and encouragement.

I genuinely express my sincere thanks to Mr. Rahul S., Mrs. Arya A. Das, and Mrs. Jeen Mariam Mathews my batch mates who have registered for Ph.D. in CUSAT.

I owe a lot to my beloved friends Deepu S., Sarath S. Nair and Anish R. (Ph.D. Scholar, IIT Madras), who encouraged and extended their helping arms towards me at every stage of my personal and academic life and longed to see this achievement come true.

Words are inadequate to express my gratitude to all my family members especially Late E.K. Neelakhandan (Kannadiachan - Grand Father), Late Kunjappi (Achacha - Grand Father), Late Podippennu (Achoyi - Grand Mother), K.K. Valliyamma (Kannadiammachi - Grand Mother), K.K. Raghunathan, Valsa C.V., P.N. Mohan, P.N. Salim, Shyla V.N., P.N. Chintha, Rachana V.P., T.V. Natarajan, Geetha C.V., Karunakaran Kadammanitta (Father), Sheeba C.V. (Mother), M.I. Gopi, Kala C.V. Thirumeni K.R., Thirumanas K.R., Sathu G. Rajan, Thampuran P.S., Devanand P.C., Sharma P.S., Rajeswary K.R., M.G.K. Vishnu, Arya G. Rajan, Midhun S. Karun (Brother), Arjun P.S. (Appu), Gopika Mangalassery, Devika P.C. (Ammalu), Nisha P., Devadathan T. (Kannan), Devanandhan T. (Nandhu), Rajeev K. Mohan, Divya M.B., Sreevidhya Ashokan and Sangeeth Mani who constantly stood as a source of happiness, encouragement, confidence and untiring support.

Akhil S. Karun

Preface

Functionally graded materials (FGMs) are comparatively new class of advanced inhomogeneous composite materials, where the material composition and/or the microstructure are locally varied to regulate the physical and mechanical properties within a component at specific locations. FGMs are in their early stages of evolution and are expected to have a strong impact on the design and development of new components and structures with better performance. The phenomena of graded structures are prevalent in nature such as bamboo, teeth, bone, wood, etc. and in some of the conventional engineering materials. The developments of FGM are still in its infancy stage and there are scopes for developing wide varieties of FGM genuine for thermal protection systems for specific engineering applications such as in aerospace, automotive industry, defence, etc. due to their high-temperature surface resistance, thermal properties, increased bonding of ceramic-matrix interface and increased fracture toughness. Most of the FGM studies are multiphase composite materials where the volume fraction of reinforcement particles or phases varies continuously from one location to the other within a component or structure leading to the formation of controlled non-uniform microstructure with continuous change in properties. Processing of FGM and their engineering components with gradient properties are very much exigent and has a lot of technological relevance. Among the various processing methods available for the production of FGM such as chemical vapour deposition, physical vapour deposition, sol-gel technique, plasma spraying, molten metal infiltration, self-propagating, centrifugal casting, diffusion bonding, laser cladding and controlled mould filling (sequential casting), etc., centrifugal casting and sequential casting are the simplest and cost effective technique for producing large-size engineering components. The added advantage of sequential casting is the non-requirement of any special casting equipment. The FGM fabrication techniques have attracted researchers and are increasingly receiving attention globally in making components for specific applications in engineering sectors. The objective of the present thesis is on the processing and characterization of functionally graded metal and polymer composites for engineering applications by sequential and centrifugal casting techniques.

Chapter 1 outlines the general background and fundamentals of the materials investigated. A critical review of functionally graded materials was carried out on up to date available literature, which was presented in Chapter 2 titled as Literature Review. Chapter 2 also contains the detailed description of the processes, applications and limitations of the materials under study. The scope and objectives of the present work were described at the end of Chapter 2. A detailed description of experimental methodology which contains the design, selection of materials, processing of the selected material systems using different techniques, characterization methods, mechanical testing and wear testing were discussed in Chapter 3 under the title Materials and Experimental Methods.

Chapter 4 deals with the study of sequential cast A390-A319 and A390-A6061 functionally graded bimetallic aluminium alloys. The effect of miscibility of the alloys at

the interface of the bimetallic aluminium alloy systems of A390-A319 and A390-A6061 are carefully evaluated using optical micrograph and scanning electron microscopy. The as-cast and heat treated studies on hardness profiles of the bimetallic systems were carried out using the T6 condition of the aluminium alloys. The modification of eutectic silicon and primary silicon at the interface was also discussed in this section. Two entirely different types of properties are attained within a single sequential cast component. The sequential cast materials provide improved tensile and compressive strength compared to parent materials exhibiting a strong interface bonding between two sequential cast alloy systems. The wear study was performed at the two different regions of the respective bimetallic systems and provides a gradient performance within the same component. The A390 alloy region shows enhanced tribological properties in both the sequential cast systems.

Chapter 5 deals with the study of the formation of centrifugally cast functionally graded in-situ primary Si reinforced Al-composite. The effect of addition of magnesium (Mg) and modifiers such as strontium (Sr) and zirconium (Zr) in hypereutectic A390 aluminium alloy and in centrifugal cast Al FGM are evaluated. The functionally graded microstructures are formed by the segregation of in-situ generated low density primary Si phases towards the inner periphery of cylinder and disc. Among the individual addition of varying content of Mg, Sr and Zr in centrifugally cast cylinders, maximum hardness in respective systems were observed in A390-1.5 wt. % Mg and A390-0.03 wt. % Sr/Zr. However, the combined addition of 1.5 wt. % Mg and 0.03 wt. % Sr in A390 hypereutectic aluminium alloy provide maximum hardness and wear resistance.

Chapter 6 includes the design and fabrication of centrifugal cast functionally graded exit vane guide using aluminium A2219 alloy reinforced with silicon carbide (SiC) of 14 μm and 23 μm average particle sizes (APS) and the evaluation of the properties. The microstructural analysis in both longitudinal and transverse direction shows graded particle distribution. The leading edges of exit vane guide provide higher hardness and wear resistance due to the increased graded particle concentration. The exit vane guide with fine SiC particles of 14 μm provides enhanced hardness and wear resistance than the base alloy and other composite system studied. Tensile strength is higher towards the interior region of the exit vane guide.

Chapter 7 deals with the study of the effect of centrifugal force in the distribution of short carbon fibers (SCFs) reinforced epoxy matrix composites by centrifugal casting technique. The distribution pattern of SCFs in the epoxy matrix from the outer region to the inner region of the polymer castings using different volume percentages (vol. %) of SCFs are evaluated. Rheological studies show that the viscosity increases as the volume percentage of SCF increases. Microstructural features of the FGMs notably exhibit a clear variation of three regions namely matrix rich region, fiber rich outer region and transition region. Hardness value is maximum for the outer periphery of epoxy polymer cast with 1 vol. % SCF reinforcement. Wear resistance is maximum in case of the specimen taken from the outer periphery of the epoxy-2 vol. % SCF. Chapter 8 presents the summary, major conclusions drawn from the present research work and future scope of the investigation.

Contents

List of Figures

List of Tables

Abbreviations

ρ_a	Density of air
ρ_l	Density of liquid (water)
W_a	Weight of the specimens in air
W_l	Weight of the specimens in liquid (water)
°C	Degree Celsius
µm	Micrometre
AC	Alternating current
Al-Si	Aluminium-silicon
AMCs	Aluminium Matrix Composites
ANSI	American National Standards Institute
APS	Average Particle Size
ASTM	American Society for Testing and Materials
BHN	Brinell Hardness Number
CCT	Centrifugal Casting Technique
CMCs	Ceramic Matrix Composites
CNC	Computer Numerical Control
CNFs	Carbon Nano Fibers
CPC	Conductive Polymer Composites
d	Diameter
DAS	Dendritic Arm Spacing
DTA	Differential Thermal Analysis
EDS	Energy Dispersive X-ray Spectroscopy
FGMMCs	Functionally Graded Metal Matrix Composites
FGMs	Functionally Graded Materials
ft	Feet
G	Gravitational Force factor
GPa	Gigapascal
HP	Horse Power
HRC	Rockwell Hardness
IIT	Impurity Induced Twinning
kg	Kilogram

kgf	Kilogram-force
kN	Kilonewton
kV	Kilovolt
m	Meter
min	Minute
ml	Millilitre
mm	Millimeter
MMCs	Metal Matrix Composites
MMLs	Mechanically Mixed Layers
MPa	Megapascal
N	Newton
OES	Optical Emission Spectrometer
OHNS	Oil Hardening Non-Shrinking
PAN	Polyacrylonitrile
PMCs	Polymer Matrix Composites
PTC	Positive Temperature Coefficient
rpm	Rotations per minute
s	Seconds
SCFs	Short Carbon Fibers
SDAS	Secondary Dentritic Arm Spacing
SEM	Scanning Electron Microscopy
SiC_p	Silicon Carbide Particles
T_f	Freezing temperature
T_m	Melting temperature
UTM	Universal Testing Machine
UTS	Ultimate Tensile Strength
vol. %	Volume percentage
XRD	X-ray Diffraction
α	Alpha
θ	Theta

CHAPTER 1

Introduction

Engineering materials are broadly classified as metals, ceramics, polymers and composites. Apart from the monolithic material properties of metals, ceramics and polymers, composite materials possess combined properties of the constituent elements contained in the particular composites. Depending on the major continuous phase in the composite materials, the composites are named as metal matrix composites (MMCs), polymer matrix composites (PMCs) and ceramic matrix composites (CMCs), if the continuous phases are metals, polymers and ceramics respectively. The properties such as high specific strength and stiffness, enhanced thermal, wear and other mechanical properties of the monolithic materials can be tailored by incorporating ceramic/particulate or fiber reinforcements. Metal matrix composites exhibit better properties than polymer matrix composites because of their capability to operate at reasonably high temperature than polymers, outstanding resistance to moisture, superior thermal and electrical conductivities, etc.

1.1 Functionally Graded Materials

Functionally graded materials (FGMs) are comparatively new class of advanced inhomogeneous composite materials, where the material composition and/or the microstructure are locally varied to regulate the physical and mechanical properties within a component at specific locations (Vieira et al., 2009; Nairobi et al., 2005 and Rajan et al., 2009). Figure 1.1 shows the schematic diagram of the functionally graded material having reinforcement rich, transition and depleted regions. FGMs are in their early stages of evolution and are expected to have a strong impact on the design and development of new components and structures with better performance. The phenomena of graded structures are prevalent in nature such as a bamboo pole, teeth, bone, wood, etc. and in some of the conventional engineering materials. The concept of making FGM was proposed in mid-1980 in Japan. The developments of FGMs are still in its infancy stage and there are scopes for developing wide varieties of FGMs genuine for thermal protection systems for

specific engineering applications such as in aerospace, automotive industry, defence, etc. due to their high-temperature surface resistance, thermal properties, increased bonding of ceramic-matrix interface and increased fracture toughness (Rajan et al., 2008). Most of the FGM studies are based on multiphase composite materials where the volume fraction of reinforcement particles or phases is being varied continuously from one location to the other within a component or structure leading to the formation of controlled non-uniform microstructure with continuous change in properties and performance. Processing of FGMs and their engineering components with gradient properties are very much exigent and has a lot of technological relevance. Out of various processing methods for the production FGMs such as chemical vapour deposition, physical vapour deposition, sol-gel technique, plasma spraying, molten metal infiltration, self-propagating, centrifugal casting, diffusion bonding laser cladding and controlled mould filling, etc. centrifugal casting is the simplest and cost-effective technique for producing large-size engineering components. Fukui of Japan first proposed FGM by centrifugal casting. The FGM fabrication techniques have attracted researchers and are increasingly receiving attention globally in making components for specific applications in the area of aerospace, defence, automotive and general engineering (Akhil et al., 2016).

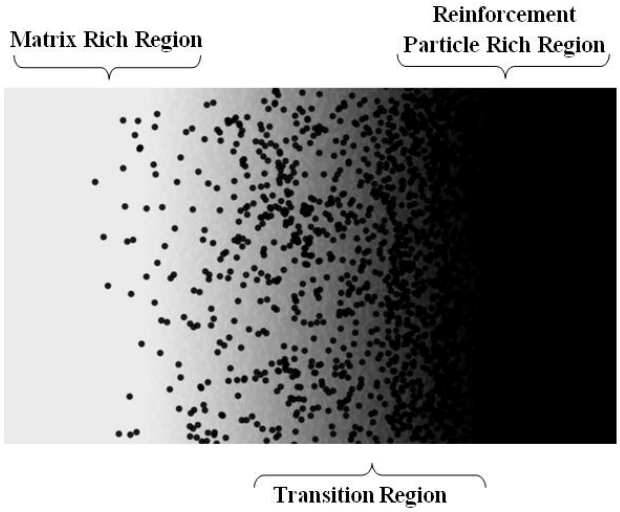

Figure 1.1 Schematic diagram of functionally graded material

1.2 Aluminium Alloys

Aluminium (Al) is the third most abundant element in the earth crust and it is the most abundant metal. It is a light weight silvery-white metal which is soft and

possesses nonmagnetic and ductile properties. The two main classifications of aluminium alloys are casting alloys and wrought alloys. The cast alloys and wrought alloys are again sub-divided into heat-treatable and non-heat-treatable alloys. More than 80 % of aluminium alloys are being used for wrought products such as rolled plates, extrusions, etc. Cast aluminium alloys have lower tensile strengths than wrought alloys and it yields cost-effective products due to the low melting point. Due to the high specific strength, corrosion resistance, high wear resistance and low thermal expansion properties of aluminium and its alloys, especially aluminium-silicon (Al-Si) alloys find various applications in automobile, aerospace, defence and other strategic sectors. Specific number series indicate the major alloying elements and certain combinations of elements in the American National Standards Institute (ANSI) numbering system [Table 1.1 and Table 1.2]. For casting alloys, the first digit of the number indicates the major alloying element of the alloy system. The second and third digits indicate the minor alloying elements of the system. The digit that follows the decimal in each alloy number indicates the product form. A zero (0) following the decimal indicates the cast product itself (die casting, for instance). A one (1) following the decimal indicates the chemistry limits for ingot used to make the XXX.0 product. For wrought alloys, the first digit indicates the principal alloying elements which have been added to the alloys and also used to describe the aluminium alloy series like 1000 series, 2000 series, etc. up to 8000 series.

Table 1.1 Different cast aluminium alloy designations

Number Series	Alloy type
1XX.X	99.0 % minimum aluminium content
2XX.X	Al + Cu
3XX.X	Al + Si & Mg or Al + Si & Cu or Al + Si & Mg & Cu
4XX.X	Al + Si
5XX.X	Al + Mg
6XX.X	Unused Series
7XX.X	Al + Zn
8XX.X	Al + Sn

Table 1.2 Different wrought aluminium alloy designations

Number Series	Alloy type
1XX	99.000 % Minimum Aluminium
2XX	Copper
3XX	Manganese
4XX	Silicon
5XX	Magnesium
6XX	Magnesium and Silicon
7XX	Zinc
8XX	Other Elements

1.3 Aluminium-Silicon Alloys

Aluminium-silicon (Al-Si) alloys are the major alloys used for the production of automobile and aerospace components mainly due to their light weight, excellent strength and workability, good corrosion resistance, high reflectivity thermal and electrical conductivity, and attractive appearance. Aluminium conducts electricity better than most of the other metals. The high thermal conductivity of aluminium is desirable due to the rapid conduction and dissipation of heat quickly and uniformly. The Al-Si alloys are age-hardenable alloys. The Al-Si alloys are of hypo-eutectic, eutectic and hyper-eutectic aluminium alloys depending upon the percentage of the silicon content in the aluminium alloys. The phase diagram [Figure 1.2] clearly shows that ~ 12.6 wt. % silicon is the eutectic composition of the aluminium alloy. If the percentage of silicon is below the eutectic point, it is called hypo-eutectic aluminium alloy and if it is above the eutectic point, then it is called hyper-eutectic aluminium alloys. The microstructure of hypo-eutectic and eutectic aluminium alloys contains α-Al dendrites that nucleate first during the solidification of the alloy followed by eutectic silicon segregated along the interdendritic region having plate-like structure. Apart from the hypo-eutectic and eutectic aluminium alloys, hyper-eutectic aluminium alloys exhibit the presence of hard cuboids of primary silicon which is less dense than the eutectic silicon. The properties of the Al-Si alloys are improved by precipitation hardening, eutectic silicon modification and grain refinement. In 1930's

by the addition of Ti in aluminium alloys (Rosenhain et al., 1930) started the concept of adding other constituent elements in the aluminium alloys for the grain refinement.

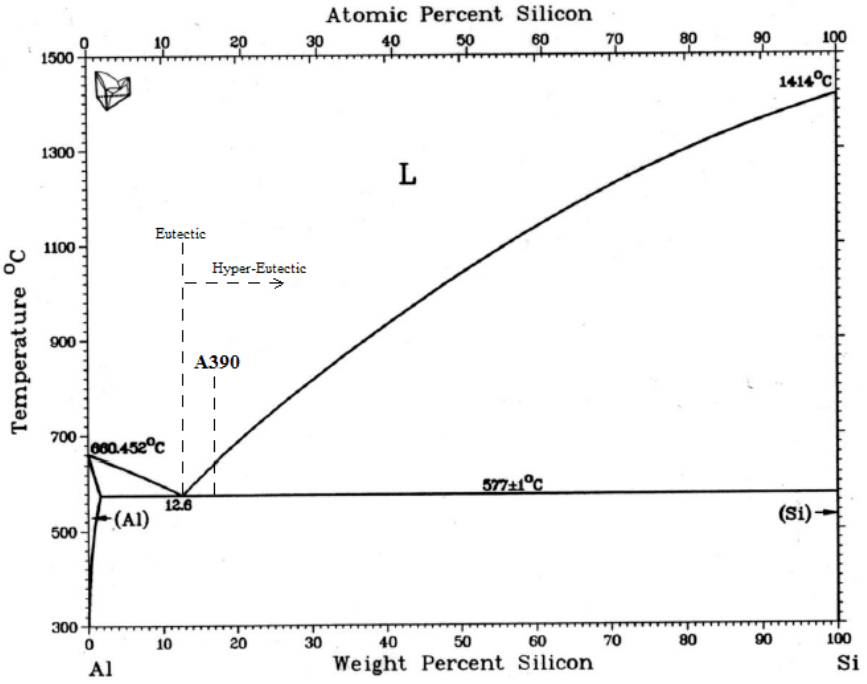

Figure 1.2 Phase diagram of Aluminium-Silicon alloy

1.4 Composites

A composite material is a material made of two or more separate phases with significantly better physical or chemical properties than one material alone which have been intimately bonded to each phase which results in a material with characteristics that different from the individual component. One constituent present in the composite is called the reinforcing phase and the one in which it is embedded, or a continuous phase is referred to as the matrix. Matrix is a light material like aluminium or magnesium or titanium which provides support to the reinforcements. Unlike from sandwiched composites, the matrix in a composite form a network path throughout the material. The reinforcements can be either continuous or discontinuous. The reinforcing phases may be in the shape of fibers, particles, or flakes. The reinforcements provide better properties like thermal conductivity, wear resistance, etc. All the composites are not human-made. There exist many natural composites such as wood, pearls, human bone, teeth, etc. The interface between the matrix and reinforcement plays a major role in determining the properties of the

composites. The bonding between the constituents at the interface is also continuous or discontinuous. The density, concentration of the element, elastic modulus, the coefficient of thermal expansion, etc. at the interface determines the quality of the composite material. Composite materials are widely used in various engineering fields such as in automobiles and space crafts, boat hulls, sporting goods, building panels, etc. Based on the matrix, composites are classified as metal matrix composites (MMCs), polymer matrix composites (PMCs), and ceramic matrix composites (CMCs).

1.5 Metal Matrix Composites

A metal matrix composite (MMC) is a composite material that contains a continuous metallic matrix phase and reinforcement that represented by volume for at least a few percentage of the total material. Metal matrix composites consist of a metallic matrix such as aluminium, magnesium, iron, cobalt, copper and a dispersed ceramic phases such as oxides, carbides or immiscible metallic phases such lead, tungsten, molybdenum, etc. Ceramic reinforcement may be of carbides of silicon (SiC) and boron, alumina, silicon nitride, boron nitride, etc. Metal matrix composites have been considered as materials of immense technological and commercial significance during the past two decades. MMC reinforced with ceramic or metallic particles are widely used in various sectors like aerospace, automobile and even in sports goods, etc. due to their high specific modulus, strength and wear resistance. Furthermore, MMC have been considered as an alternative to monolithic metallic materials or conventional alloys in many specialized applications (Gomes et al., 2000). In particular, aluminium matrix composites (AMCs) have been reported to possess higher strength and stiffness, excellent wear resistance, lower coefficient of thermal expansion and friction coefficient with increasing volume fraction of reinforcement particles when compared with the matrix alloy (Korkut et al., 2004).

1.6 Polymer Matrix Composites

Polymer matrix composites are the materials consisting of a polymer (resin) matrix combined with a fibrous/particulate reinforcing dispersed phase. Epoxy resins are extensively used in aerospace and cryogenic engineering applications. Functionally graded epoxy polymers can be exposed to tribological applications to attain better properties than the homogeneous polymers/composites. The

enhancement in the wear properties of polymers can be achieved by incorporating fibers/particles in the epoxy matrix. Thermosetting epoxy resins are normally used polymer matrix for the high temperature applications below 160 °C since it can accommodate higher temperatures than other polymers, good rheological behaviour during processing, low shrinkage, easiness in the processing, alterable structure, environmental resistance, better adhesion properties and improved mechanical properties especially for strategic sectors (Chatterley et al., 2010; Zhou et al., 2008; Green et al., 2009; Xu et al., 2008; Zhao et al., 2012 and El-Sayed et al., 1995).

1.7 Ceramic Matrix Composites

Ceramic matrix composites are a subgroup of composite materials where the matrix and the reinforcement consist of any ceramic materials. Ceramic matrix composites are materials which contain one or more distinct ceramic phases/particles that are deliberately added to the other, to attain some enhanced property that cannot be achieved through the monolithic ceramic materials. In ceramic matrix composites, ceramic matrix is reinforced either with continuous fibers or with a discontinuous type of reinforcement, such as particles, whiskers or chopped fibers. The reinforcements that are used in the ceramic matrices are carbon, oxides, non-oxides glasses and glass-ceramics. Carbon and carbon fibers are also considered as ceramic material. The most important role of reinforcement is to provide proper toughness to the brittle ceramic matrix and the main function of the matrix is to keep the reinforcing phases/particles in the pre-desired orientation in proper location that can act as a load transfer medium to protect reinforcement from the operating environment. Filler materials in matrix enhance the properties such as hardness, thermal conductivity, thermal expansion and electrical conductivity. The use of this type of reinforcements in ceramic matrix improves the properties at high temperature and also posses excellent corrosion and wear properties. The most important applications of ceramic matrix composites are in the area of production of cutting tools made up of SiC whisker reinforced aluminium oxide for the machining of hard materials. Also, ceramic matrix composites are widely used in several engineering applications such as in gas turbines components, heat shield systems, components for burners, flame holders, hot gas ducts, rocket engines, bearing

components, brake disks and brake system and components for aircraft and automobiles.

1.8 Organisation of the Thesis

The present work focuses on tailoring functionally graded structures and properties using sequential and centrifugal casting techniques in metal and polymer systems. The metallic materials used are aluminium alloys and polymer system is based on the epoxy matrix.

Chapter 1 outlines the general background and fundamentals of the materials investigated. The present research work starts with a critical review that was extensively discussed with the available works of literature, which was presented in Chapter 2 titled as Literature Review. Chapter 2 contains the detailed description of the processes, applications and limitations of the material under study. The scope and objectives of the present work were described at the end of Chapter 2. A detailed description of experimental methodology which contains the design, selection of materials, processing of the selected material systems using different techniques, characterization methods, mechanical testing and wear testing were discussed in Chapter 3 under the title Experimental Methodology.

Chapter 4 deals with the study of sequential gravity casting of A390-A319 and A390-A6061 bimetallic aluminium alloys. The effect of miscibility of the alloys at the interface of the bimetallic aluminium alloy systems of A390-A319 and A390-A6061 are carefully evaluated using optical micrograph and scanning electron microscopy. The hardness evaluation of as-cast and heat treated bimetallic systems was carried out at the T6 condition of the aluminium alloys. The modification of eutectic silicon and primary silicon at the interface was also discussed in this section. Two entirely different types of properties attained in a single material is properly described and explained. The improved tensile and compressive strength observed during the tests was explained with reasons. The wear study was performed at the two different regions of the same bimetallic systems and explained with the help of SEM.

Chapter 5 deals with the study of the formation of centrifugally cast functionally graded in-situ primary Si reinforced Al-composite. The effect of the addition of magnesium (Mg) and modifiers such as strontium (Sr) and zirconium (Zr)

in hypereutectic A390 aluminium alloy and centrifugal cast Al FGM are evaluated. Mainly this chapter focused on the modification of eutectic and primary silicon phases.

Chapter 6 includes the design of exhaust turbine exit vane guide for centrifugal casting, fabrication of vane guide using aluminium A2219 alloy reinforced with silicon carbide (SiC) of 14 and 23 μm average particle size (APS) by centrifugal casting and the evaluation of the properties. The distribution of SiC particles (SiC_p) in the aluminium A2219 alloy is carefully evaluated through optical metallography. The properties are extensively characterized using different tools reported and discussed in this chapter.

Chapter 7 deals with the study of the effect of centrifugal force in the distribution of short carbon fiber (SCF) reinforced epoxy matrix composites by centrifugal casting technique. The distribution of SCF in the epoxy matrix from the outer region to the inner region of the castings using different volume percentages (vol. %) of SCF are described and discussed in this chapter.

Chapter 8 presents the summary and major conclusions drawn from the present research work and future scope of the investigation.

CHAPTER 2

Literature Review

2.1 Introduction

Inspite of the tremendous progress that has been made in the discipline of materials science and engineering within the past three decades, there remain technological challenges including the development of more specialized and advanced materials as well as consideration of the environmental impact of material processing and production. Most materials in their natural states are deficient in many ways for engineering applications and this has not stopped the demand for specific material properties. This trend stretches on a daily basis and pushed by ever increasing the desire for hybrid materials for effective component's functional performance. The challenging requirements for the improvement of the material property and development of new components are fallout from various industries which include aerospace, automotive and general engineering industries where high quality and high-performance products are required. The required materials are expected to be stiffer, stronger, lighter, harder, higher corrosive and thermal resistance, more ductile, cheaper than existing materials. In response to material demand trend, material scientists, engineers, metallurgists and physicists, for many centuries have been conducting research to develop new materials and their production techniques (Karaköse et al., 2012). This has made material science and engineering the cornerstone of the present day technological advancement. Recently, researchers have been given attention to alloys of aluminium and other low-density materials like magnesium (Mg), titanium (Ti), etc. as engineering materials for transportation for the reduction in the fuel consumption by reducing the overall weight of the system. The important characteristics of these materials are low density and higher specific strength, which is quantified by the tensile strength to specific gravity ratio.

There is an evolution of new structural material to meet the increasing need of specific strength at the lower density as a functional requirement. This standard design requirement in fuel consumption reduction in aerospace and automotive

industries favours the application of epoxy-based composites and aluminium alloys and their composites. In this regard, monolithic aluminium alloys and their composites have yielded very exciting results and have remained the center of attraction for cheap production (Lavernia et al., 1987). In most cases, in aluminium design concepts, researchers integrate additional properties into a part and reduce the number of components for cost effectiveness.

2.2 Functionally Graded Materials

Drastic changes occurring in the machine parts within the component often resulted in sharp local transitions of stress. These intense stresses that are taking place in the material can be made gradual by reducing the stress concentrations in a homogeneous material. This can be achieved by providing the materials with a gradual transition in composition or properties. From these idea underlying the concept of the production of functionally graded materials (FGMs).

Functionally graded materials are the nonuniform advanced class of alloy or composite materials which exhibit a gradual transition in the microstructure and or in the composition with continuous changing properties in a particular direction (Mortensen and Suresh et al., 1995). FGM is a novel concept for the creation of innovative properties and/or functions that cannot be achieved by conventional homogeneous materials. FGM includes the tailoring of chemical composition and microstructure of material in an intentional manner according to the quantitative prediction of the properties to achieve the desired function is the primary essential feature. The second key feature is the availability of cheapest fabrication processes which have good reproducibility, using advanced technology for gradient properties. In simple, the FGM consists of one material on one side and a second material on the other end with a smooth/gradual intermediate composition/structural morphology vary from one material to the other at the micron level. The intermediate transition regions profiles are pre-designed and introduced artificially to achieve the desired function. Graded structures are found in ordinary engineering materials from former days (Kawasaki and Ryuzo, 1995). Regarding the properties of materials, functionally graded materials provide a reasonable compromise since the properties would not be achieved through by any other means. This is the reason that the microstructure of

the FGM is continuously changing and inhomogeneous within a part. Thus, an FGM has a broad range of applications in various fields such as in general and strategic sectors (Watanabe et al., 2009). FGM holds the key for many applications, which requiring high material performance such as in biomedical fields for dental and bone implants, nuclear areas, thermal barrier coatings, thermo electric and piezoelectric devices. Therefore, over the past two decades, FGM has received wide, increasing interest globally. Various processing techniques for producing FGM are developed to reconfigure the microstructure and composition of the material to attain the assumed graded microstructure for desired properties. Squeeze casting, sequential casting, centrifugal casting and hot pressing are some of the modified advanced casting techniques to produce FGMs and their components. Among the various advanced process to produce FGM, centrifugal casting is considered as one of the most important, cost effective and easiest casting method that is being widely studied to produce FGM. The FGM fabrication techniques have attracted researchers and are increasingly receiving attention globally in making components for specific applications in the area of aerospace, defence, automotive and general engineering (Akhil et al., 2016).

2.3 Processing Techniques of FGM

The usefulness of functionally graded materials with a graded structure was recognized 40 years before (Bever et al., 1972 and Shen et al., 1972). Due to a lack of suitable production methods for FGM at that time, the work had got an only limited impact. Systematic research on manufacturing processes for improving the production process of the functionally graded materials was carried out in the framework of a national research program in Japan. After that, a large variety of production methods has been developed on FGM and the major part of the research was dedicated to processing of these materials (Mortensen et al., 1995; Neubrand et al., 1997; Miyamato et al., 1999; Brook et al., 1996 and Kieback et al., 2003).

There are various processing techniques available for the production of graded materials. The fabrication techniques of FGMs are classified based on spatial building of graded inhomogeneous structure, i.e., gradation and transformation of this structure into a bulk material (Schatt et al., 1992). And the processing methods of

FGM are classified as constructive and transport based processes (Mortensen et al., 1995). Constitutive, homogenizing and segregating processes were classified under gradation processes. In particular, one can distinguish two principal classes of methods for the production for FGM containing a metallic phase. In the first class of constructive processes, the FGM can be constructed layer by layer through a stepwise build-up of material, in a manner that starts with an appropriate distribution of constituent elements of the FGM, often of precursor materials. Constructive processes are amenable to computer control of the gradients produced. Constructive processes which exclusively rely on natural transport phenomenon during the process to create gradients within an engineering component. In homogenizing processes, the sharp interface between the two phases/materials is converted into a gradient by material transportation technique. By the application of external forces such as electrical field, gravitational force, etc. the segregating processes in the homogeneous material can be converted into a graded material by material transport. Both homogenizing and segregating processes can produce continuous gradients in a component. But for producing all types of gradients have some limitations in homogenizing and segregating processes (Schatt et al., 1992). The transport based processes take advantage of the flow of the material in the fluid state and allow the diffusion of atomic species, or the conduction of heat to create gradients in microstructure and/or in the compositions locally such as solidification processes in case of metals or composites. The factors that responsible for macro segregation in single crystals and alloy castings during solidification are fluid flow, interfacial segregation and slow solid state diffusion. Property gradients in a component produced can still be optimized, albeit within a narrower window of possible structure if these processes are quantitatively understood and harnessed. Both heat and mass diffusion techniques have been used in steel for centuries to create functional, microstructural and/or compositional gradients (Rajan et al., 2014). Based on the state and nature of processing, Rajan et al. have classified the processing methods of FGM into three, solid state processes, liquid state processes and vapour deposition processes. The Table 2.1 shows the various techniques for fabricating the FGM (Rajan et al. 2013).

Table 2.1. Processing methods of FGM (Rajan et al. 2013)

Solid Sate Processes	Liquid State Processes	Vapour State Processes
Powder metallurgy	Infiltration	Chemical vapour deposition
Sintering	Settling	Chemical vapour infiltration
Powder stacking	Centrifugal casting	Physical vapour deposition
Powder infiltration	Directional solidification	Spray deposition
Slurry technique	Sol-Gel method	Laser deposition
Plasma activated sintering	Electro deposition	
Diffusion bonding	Electroless plating	

2.3.1 Solid state processes

Powder metallurgy

Powder Metallurgy is a highly developed method for the production of reliable ferrous and nonferrous FGM parts which is a continuously and rapidly evolving technology embracing most of the metallic and alloy materials in various shapes. Powder metallurgy is one of the simplest and easiest method for fabricating the functionally graded materials. In powder metallurgy, a preform of powder or the ceramic/reinforcement particles containing the desired gradient of metal matrix is first fabricated followed by hot pressing in closed die, hot isostatic pressing, cold pressing and pressureless sintering. Powder metallurgical processes are more malleable than casting processes and secondary processes such as forging and extrusion techniques.

In the solid state process, due to the variation in densification rate of varying volume fraction of ceramics reinforcements in a metal matrix, the densification kinetics of FGM is very complex in its nature. The matrix controls the densification rate at the low volume of the ceramics, whereas at a higher volume of reinforcements the ceramic carries the load and resists the contraction of the material. The various forms of defects observed in FGM are distortion or crack in the sintered bodies; warpage due to the differences in the thermal, mechanical and shrinkage properties (Zhang et al., 2002).

Sintering

Sintering is a method of manufacturing products from powder reinforcements, by sintering (heating) the material in a sintering furnace particularly below its melting point (solid state sintering) until the particles get adhered to each other. There are many types of sintering techniques that have been used for the fabrication of graded composites and ceramics such as pressureless sintering and hot isostatic pressing (with pressure). Traditionally, sintering is used for the manufacturing of ceramic products and has also found some uses in such fields of powder metallurgy. With a nano-particle sintering aid and bulk molding technology, pressureless sintering is possible with graded metal-ceramic composites.

Depending on material properties like green density, particle size, compositional gradients and geometry, the sintering of graded compacts shows various behaviours (ranging from elastic to viscous and then come back to elastic) at different stages of sintering (Rajan et al., 2014). Zhang et al. used graded sintering under ultra-high pressure (GSUHP) to develop W/Cu FGM containing 1 % La_2O_3 and 1 % TiC. W/Cu FGM shows excellent thermal-shock resistance, good shear strength between layers and also low porosity (11.57 % and 11.35 %, respectively). The specimens with 1 % La_2O_3 have not damaged anywhere in the component, whereas crack initiated in 1 % TiC containing specimen when the power density of the laser is 200 MWm^{-2} (Zhang et al., 2007).

Powder stacking

Powder stacking technique is a solid state process for the fabrication of graded composites. The complex interdependence of many processing variables makes the production of graded composites challenging. Particle size distribution, additives, compaction pressure, and consolidation method are some of the tools available to make adjustments that can be made fabrication of functionally graded materials. The powder stacking approach is based on the concepts from fundamental sintering behaviour (Kieback et al., 2003).

2.3.2 Liquid state processes

Infiltration

The process of infiltrating liquid metal into porous ceramic performs with or without the application of pressure or vacuum. The process of infiltration involves not only the infiltration of liquid metal into the porous perform, but also the preparation of graded ceramic perform containing graded porosity. The light weight cermets having durability, elasticity, improved porosity, toughness strength, etc. are fabricated from pre-sintered ceramic powder infiltrated with a molten material. The different cermets are useful for the manufacture of surgical instruments, engine parts, cutting tools, etc. Aluminium functionally graded composites produced for automobile applications using infiltration displays a graded a graded transition from the aluminium phase to the ceramic reinforced aluminium phase on the surfaces. The process of making preform with the required percentages of the reinforcements being one of the critical steps involved. Conventional binder and slurry methods are used to make preform with uniform porosity. For the penetration of the liquid metal into the cavity, the porous structure must be sufficiently large enough for the penetration and proper solidification.

Now a day, many researchers are concentrating on this area in particular for the application of automotive engine components like a piston. The crown portion of the pistons is locally varied with various percentages 21, 25, 40 and 41 vol. % of aluminium titanate particles and alumina short fibers (hybrid reinforcements) organized by common slurry and binder methods shows superior thermal crack-resisting performance compared with the conventional pistons and metal matrix composites (Henning et al., 1992).

Settling

In the method of settling, the metal matrix composites are developed by the liquid metal stir casting process and the reinforcements and the graded ceramic reinforced metals are allowed to separate by holding the full slurry under gravity. A uniform volume fraction of particle reinforcements can be achieved by using the various range of particle sizes to create gradation in the components. Aluminium-SiC functionally graded metal matrix composites are fabricated in different experimental

components by using this method (Zhao et al., 2014). Also, sequential pouring of slurries containing reinforcements will result in the graded structure and varying volume fractions (Lajoye et al., 1998). The tendency to produce separate zones of relatively constant fraction in functionally graded materials is one of the significant limitations of this process. This can be overcome by using the particle size of wide ranges. Moreover, because of the terminal velocity, the larger size particles present in the melt slurry settle faster than the smaller size particles.

Centrifugal casting

Centrifugal casting is a process for the production of functionally graded materials that delivers castings of very high material soundness. The applications of the components produced by centrifugal castings are in petrochemical furnace tubes, cases of jet engine compressors, defence sectors, and other high-reliability applications. Centrifugal casting is one of the promising methods for the production of FGM. The graded structure in the components by centrifugal castings is achieved through the centrifugal pressure involved. The components produced by centrifugal castings have good micro structural properties and less porosity compared with conventional casting techniques and provides excellent mechanical properties. The details of the centrifugal castings are explained and reported in section 2.6.

2.4 Bimetallic Systems

Bimetals are materials that composed of two separate metals or metals of the same kind with their alloys joined to achieve certain specific properties at different regions like co-efficient of thermal expansion, corrosion, wear properties, etc. For example the blades of band saws, power saws are made of bimetals and nowadays, bimetallic bearings are also available in the market. Bimetallic design and fabrication comes into play and may be an ideal solution when a single type of material does not satisfy the functional requirements of a high performance and efficiency at low cost and are widely used in various industries due to their superior physical, chemical and mechanical properties (Kim et al., 1947; Zhang et al., 2014; Lee et al., 2013; Li et al., 2009 and Strzelecka et al., 2015). The outstanding combined properties from the bonding of the bimetal components of Al/Al, Mg/Al and Mg/Mg attracted the researchers more, and more attention had given in the last few years (Volder, 1993;

Papis et al., 2008; Papis et al., 2009; Papis et al., 2010; Hajjari et al., 2011; Hajjari et al., 2012 and Song et al., 2012). Roll bonding, explosive welding, diffusion bonding, extrusion cladding, and spray deposition technique are some of the conventional methods of fabrication of bimetals (Eizadjou et al., 2008; Akbari-Mousavi et al., 2008; Wang et al., 2007; Lee et al., 2007 and Ning et al., 2002). The limitations of these processes are high cost, low efficiency and low bonding strength. Sequential casting and continuous casting are two simple techniques for producing bimetal slabs which can overcome the low bonding strength at the interfaces. Excellent metallurgical bonding can be obtained by these two methods that involve the direct contact of two liquid metals during the process (Benedyk et al., 2006; Marukovich et al., 1998; Marukovich et al., 1999 and Marukovich et al., 2006). Sound metallic bonding between metals can be achieved by these methods and the characteristics of the interfaces have a lot of research interest. A good interface can be accomplished by the direct contact of two liquid metals or one liquid–one solid metal (Marukovich et al., 2006).

The aluminium alloy bimetal slab consisting of Al–10 % Si alloy and Al–1 % Mn alloy was fabricated by continuous casting and can combine their superior advantages of high corrosion resistance and low strength of Al-1 % Mn and poor corrosion resistance and high strength of Al-10 % Si alloy bimetal. The silicon content gradually decreases at the interface in the diffusion layer. The Al-1 % Mn alloy in the bimetal acts as a heterogeneous nucleation center for the Al-Si alloy region at the interface. The Al-1 % Mn/Al-10 % Si bimetal have got good tensile properties at the interface at the different region of the bimetal castings (Sun et al., 2012). Aluminium–aluminium bimetal were fabricated with the application of pressure during solidification using liquid A356 aluminium alloy onto 6101 aluminium extrusion bars. With controlling the temperature, a small layer of zinc was coated over the aluminium 6101 alloy. Moreover, this method seems to be an effective approach to produce Al/Al bimetal for advanced structural and functional application by using aluminium inserts and aluminium liquid melts that provides better tensile strength than produced by conventional casting methods (Liu et al., 2015). The combination of aluminium and copper to produce bimetals will give light weight, low density, the corrosion resistance of aluminium and amazing high electrical and thermal

conductivity of copper has drawn the great attention of researchers due to these unique properties. Aluminium–copper bimetal was prepared and solidified with the aid of squeeze pressure by compound casting technique using liquid aluminium on to copper bars. The bimetal was extensively characterized and studied the effect of pouring temperature and applied pressure on microstructure, mechanical and electrical properties. By applying thermal spray zinc coating onto copper inserts and by controlling the squeeze pressure, sound metallurgical bonding between the copper substrate and liquid aluminium was achieved. The bimetal of Al-Cu shows best electrical and mechanical properties of the metal poured at 700 °C. Al_4Cu_9, Al-Cu eutectic and Cu-rich Al solid solution layers are the four possible layers that formed due to the interfacial reactions of aluminium and copper (Liu et al., 2016). Al/Cu bimetals are produced by diffusion bonding provided by coating a layer of nickel-based material on the pure Al substrate at a temperature range of 450-550 °C. The Ni layer over the Al substrate eliminates the formation of aluminium-copper intermetallic compounds and improves the tensile shear strength (Zhao et al., 2014). The integral properties of Al and Ti made the combination of the Al and Ti bimetal attracted for various engineering applications, such as low weight, better strength, etc. However, the combining of the Al and Ti is not that easy as in the other cases due to the metallurgical incompatibility. Diffusion bonding process was used to process the Al/Ti bimetal and studied the microstructural characteristics at the interface (Enjoy et al., 1977 and Jiangwei et al., 2002). Interface evolution and shear strength of Al/Ti bi-metals processed by a spark plasma sintering (SPS) was investigated under various conditions and the mechanism of interfacial layer growth was discussed with the help of various characterisation techniques and observed that the formed $TiAl_3$ layer diffusion layer along the interface grew mainly into the Ti region and a very few towards the Al region (Miriyev et al., 2016). Compound casting is also used to produce bimetallic composites of Ti/Al and Mg/Al. The process is widely accepted due to its superior properties at the interface in terms of good metallurgical bonding, protection provided to the surfaces from oxides, and advantages such as simple production procedure, low energy consumption during the process and low production cost. Ti/Al bimetal composites had obtained shear strength at the interface which is much greater than that of the aluminium matrix (Dezellus et al., 2008; Nie et al., 2014; Nie et al., 2015 and Liu et al., 2015).

Like aluminium (Al), magnesium (Mg) is also a widely used material in various engineering sectors such as in automobile industry, defence, etc. due to its light weight, high specific strength and specific stiffness and good casting and machining properties (Polmear et al., 1994; Mordike et al., 2001 and Shen et al., 2015). Mg/Al bimetal composites are fabricated by insert moulding and good mechanical behaviour at the interface was achieved (Liu et al., 2015). Fabrication of Mg/Mg bimetallic composite by using insert moulding technique treated as a new insight in the area of bimetallic composites. Studies on Mg/Mg bimetal are very limited. Laminated Mg bimetal composites of AZ31/AZ31 was fabricated through warm roll bonding and found that it could achieve better tensile properties than a single AZ31 material. The only limitation of this warm roll bonding is that the oxides on the surfaces of the metals would influence the interface of the laminated sheets and thereby the bonding strength (Liu et al., 2012). In laboratory scale, Mg/Mg bimetal composites are produced by dropping magnesium melt (pure Mg or AJ62) onto a solid magnesium alloy substrate (AZ31) in an argon atmosphere to obtain good interfaces without any interfacial defects. For avoiding the interfacial defects that may come into action due to the presence of oxides on the surfaces of Mg alloys, the solid substrates are subjected to zinc pre-treatment process (Papis et al., 2010). By varying various parameters such as volume ratio and temperature, Mg/Mg bimetal composites were also prepared by insert moulding method to achieve good metallurgical bonding between the AZ31 insert and AZ91 matrix. At an insert temperature of 675 °C and a volume ratio of 2:1 (VAZ91:VAZ31), the bimetal was equipped with sound metallurgical interface bonding. Moreover, the material got 100 MPa average tensile strength at the interface which is close to the tensile value of the AZ91 alloy (Zhao et al., 2016).

2.5 Sequential Casting

Sequential casting technique involved the pouring of two different alloys/composite melts having similar co-efficient of contraction and having similar freezing ranges into a mould sequentially to produce a continuous FGM (Kieback et al., 2003; Wagstaff et al., 2011 and Liu et al., 2015). It is a facile and fairly new technique for the production of functionally graded materials (FGM) and components with controlled mould filling process by the sequential pouring of two different alloys

or composite melts. Sequential casting is a potential and effective approach for developing good interface bonding between two different aluminium alloys to develop advanced functional and structural materials for various engineering applications. As already described in the FGM section, functionally graded materials can have either a continuous or stepwise graded microstructure. The sequential casting technique finds an imminent place due to its ease of the fabrication of the process that can produce FGMs having distant or stepwise graded microstructure by simple gravity casting method without any special equipment setup with controlling the mould filling parameters (The Aluminium Automotive Manual, 2011 and Ragab et al., 2013). Sound interface bonding between the metals can be achieved by sequential casting technique which is one among the best methods for the production of bimetals. The interesting feature in the fabrication of functionally graded Al bimetal by sequential casting technique is the properties of the interface of the two Al alloys formed due to the direct contact of liquid metals during the process of solidification. Bimetals of aluminium alloys with two different alloys of aluminium can combine their properties to form an FGM and can be used for a variety of applications such as in corrosive environments and in heat exchangers.

So far there are no papers published or reported related to the sequential casting of metals that involved the joining of two dissimilar metals during solidification from the liquid state. However, two patents were reported in 1985 and 2011 from United States (US). In the continuous sequential casting of the metals and there alloys with molten metal poured from the rotating furnace about an axis. A series of moulds are continuously conveyed to the furnace and the moulds are sequentially filled with the desired dissimilar metals. The motions of the mould are controlled in a synchronous manner so that the filling of the metals takes place synchronously. During the continuous sequential casting, the metal is filled into the corresponding moulds from below the slag level to avoid the entry of slag into the moulds (Navarre et al., 1985). An ingot or a component having two layers fabricated by sequential solidification of metals also reported in US Patent No. US 7,882,887 B2. It is reported that the apparatus must contain one cooled divider wall at the entry end portion of the mould to carve the portion into two feed chambers. The metals can be fed through this portion to form the inner and outer layer/layers. The surface of

the divider wall was kept sloping away from the metal for the last layer in a downward direction providing atleast one metal contacting surface on the dividing wall to ensure the proper metal contact in the outer layer (Wagstaff et al., 2011).

2.6 Centrifugal Casting

Centrifugal casting technique (CCT) is one of the most sought processes for the fabrication of functionally graded components. Centrifugal casting or roto casting is a pressure casting technique which is used to produce functionally graded metal matrix composites with the help of centrifugal force that applied to the pool of molten metal for the high quality of the results attainable, particularly for precise control of their metallurgy and crystal structure at specific locations of the cast component by rotating the casting mould and the cast is allowed to solidify before rotation stops (Sufei et al., 2008; Vieira et al., 2009 and Akhil et al., 2016). The idea of employing centrifugal force was introduced by A.G. Eckhardt's in original patent of 1809 which revealed the basic principles and understanding involved in the centrifugal casting to make castings. Both horizontal and vertical centrifugal casting methods are used for making FGMs. The main parts of a centrifugal cast machine are shown in Figure 2.1. Due to the possibility of gradient control using process parameters, centrifugal casting has been described as a striking method for the manufacturing of FGM. In vertical centrifugal casting method, a centrifugal force applied to a homogeneous semi-liquid composite, (containing ceramics or intermetallic compound particles) drives the formation of the desired gradient, resulting composition gradient is produced by the difference in density between the molten metal and the particles under the same centrifugal force in a vertical axis. This process ensures the production of FGMs in the desired shape, microstructural and compositional gradient within a component. The method can be used for almost all materials that can be melted and poured as the liquid into the mould. The method is used in the casting of metal such as aluminium alloys, magnesium alloys, steels alloy, copper alloys, etc.; non-metals such as ceramics, glasses, and plastics; FGM such as aluminium alloy-ceramic composite (SiC, B_4C, etc.), copper alloy-ceramic composites, etc. Several functionally attractive metal-ceramic based FGM have been developed through this centrifugal casting technique for a wide range of engineering applications such as automobile, aircraft and aerospace, general engineering industries, etc. and in the

defence sector for FGM armours (Williams et al., 2016). Mechanical properties of FGM fabricated by this method have been evaluated using relatively large samples (Watanabe et al., 2000; Rodríguez-Castro et al., 2002a; Rodríguez-Castro et al., 2002b and Velhinho et al., 2003). For both vertical and horizontal centrifugal casting processes, the effects of processing condition on the structure, morphology and properties of the functionally graded composites have been well studied (Chirita et al., 2009). Typically, in centrifugal casting, the following structure or zones may occur, chill zone – this layer is of fine equiaxed structure which forms almost instantaneously at the mould wall, columnar zone – this is next to chill zone. It consists of directionally oriented crystals approximately perpendicular to the mould surface, equiaxed zone – this region may occur next to columnar zone characterized by a large number of uniformly grown crystals. Due to the differences in the solidification rates, a gradient in the microstructure and the hardness of the centrifugally cast Al alloy is also observed in FGM. A smoother gradient in the distribution of the reinforcing particles is obtained in the lower centrifugal speeds and sharper in the higher speeds (Vieira et al., 2009).

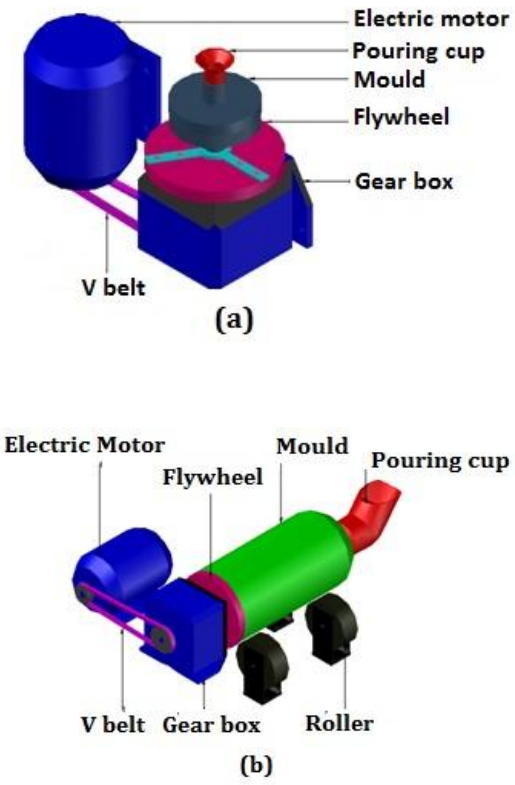

Figure 2.1 Schematic diagrams of (a) vertical centrifugal casting machine and (b) horizontal centrifugal casting machine (Williams et al., 2016)

A dense structure is observed in the centrifugally cast spun pipes near the outer periphery, and also columnar grains are radially aligned giving superior strength, fracture toughness and improved corrosion resistance properties. Segregation of the alloying elements in the matrix due to the centrifugal action was also found to be responsible for the changes in the morphology and structure of the grains and thereby the properties of the component. The centrifugally cast steel-backed babbit materials for bearing applications have also shown better bonding with superior functional properties. Compared to gravity castings, centrifugal casting gives much superior property depending on the alloy system and solidification conditions in single phase alloy systems (Diouf et al., 2010). In two or multi-phase alloys and composites systems during the centrifugal casting, depending on the density differences of the phases or reinforcement particles participating in the casting processes, either a continuous or distinct graded separations will take place upon solidification during the processes. For metal matrix composites products, centrifugal casting involves the preparation of MMC by stir casting method followed by centrifugal casting to form gradients in microstructural morphology. Generally, the centrifugal casting is only suitable for the production of axially symmetric components which gives gradient structure in the radial direction either at the outer or the inner periphery depending upon the constituent elements present in the molten pool of metal.

When particles containing liquid/slurry is subjected to centrifugal casting with the aid of centrifugal force, two distinct zones are normally attained at the two ends of the component - particle enriched region and depleted region. The extent of particle segregation and relative locations of enriched and depleted particles zones within the casting are mainly depends on the processing parameters such as the metal viscosity, melt temperature, solidification direction, cooling rate, the densities of the reinforcement particles and the constituent elements present in the matrix liquid, particle size and the rotational speed of the mould during the casting process. During centrifugal casting for the manufacturing of FGM, depending on the relative density of particles/phases present in the liquid melt, the denser particles propagates towards the outer periphery of the casting and the less dense particles segregate towards the innermost region near the axis of rotation. In the case of aluminium

matrix composites, the particle enriched zone of the heavier particles such as B_4C, SiC, alumina and zirconium silicate (zircon) are segregated at the outer periphery and the lighter phases such as primary silicon in hyper-eutectic silicon alloy and the particles such as graphite, mica and the microbalance of carbon residuals are usually observed at the inner periphery of vertical and horizontal cylindrical centrifugal castings. The thickness of particle-enriched zone can be increased with the decreasing pouring temperature and speed of rotation and decrease in thickness of the graded portion can be produced by doing it vice versa. Figure 2.2 shows the segregation of zircon (denser particle) and graphite particles (less dense) towards the outer and inner periphery of the vertical centrifugal castings, respectively (Krishnan et al., 1984 and Baneerji et al., 1985).

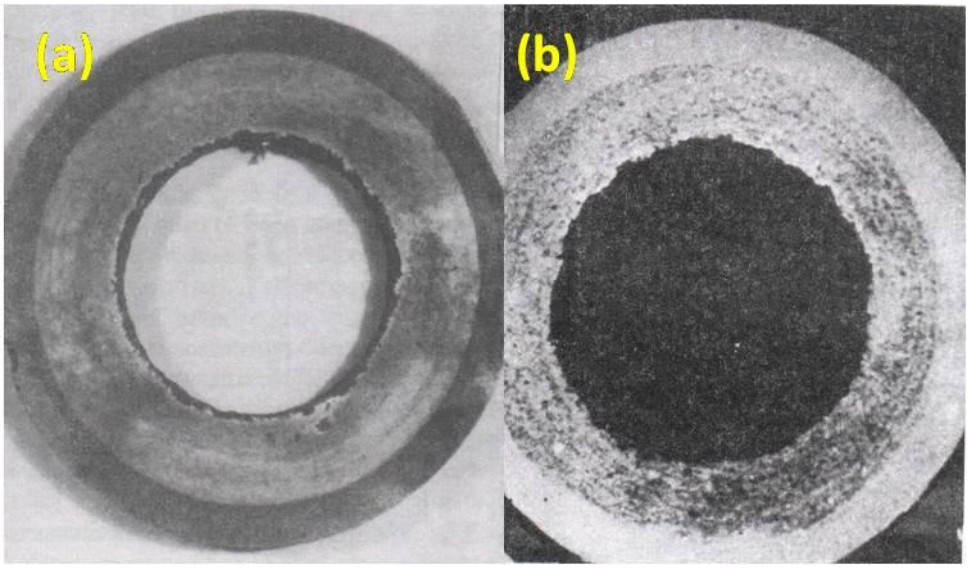

Figure 2.2 Centrifugal casting of (a) Al-Zircon and (b) Al- Graphite composites (Krishnan et al., 1984 and Baneerji et al., 1985)

Silicon carbide particles (SiC_p) are partially clustered with some pores due to imperfect wetting of ceramic particles by the molten aluminium alloy have observed during the production of functionally graded SiC_p reinforced aluminium-matrix composites by centrifugal casting. Hence, for reducing particle clustering, proper wetting between the particles and the matrix is very necessary. As a result of decreasing melt temperatures during solidification/cooling and the crowding of particles occurring in progressively narrow zones, the segregation of particles due to particle movement is slowed down (Velhinho et al., 2003). The segregation of particles occurs not only because of the solidification but also the entrapment of

gases in the molten composite melts that have a tendency to get attached with some un-wetted or partially wetted reinforcements and thus the virtual density of the agglomerate un-wetted particles being much lower than the actual density of the reinforcements in the composite slurry, resulting in higher concentration of the gas porosities with higher concentrations of clusters of reinforcements in the inner periphery of the cast components. Hence, proper wetting of particles with the matrix is necessary to reduce the agglomeration of the particles and gas porosities inside.

The methods available for the bulk and mass production of FGMs of large parts are not yet reliable and are very expensive. Amongst the fabrication techniques available, centrifugal casting technique is easiest, attractive and economical method for the production of functionally graded materials (Gao et al., 2001; Babu et al., 2004; Wang et al., 2011 and Akhil et al., 2016). Several experimental and numerical studies on FGMs of pure metal, pure metal-ceramics, metal alloy-ceramics and metal-intermetallic compounds have been developed by centrifugal casting were carried out.

2.6.1 Principle of centrifugal casting

The principle behind centrifugal casting technique is the usefulness of forces generated from centripetal acceleration obtained during the rotation of the centrifugal mould to distribute the constituent elements present in the liquid metal. Centrifugal force shapes and feeds the molten metal into the designed and provided crevices in the mould. During the initial stage of this casting process, almost all moulds were cylindrical and mainly fabricated from steel and graphite. Foundry sand or refractory lining materials were used to make cores in the mould were complexity involved. However, objects with the cross section like square and other shapes can also be produced by centrifugal casting technique, but the only limitation is that the inner surface will always maintain a curved surface due to the centrifugal force. The centrifugal casting was mainly used for the manufacturing of tubes and pipes such as gas pipes, water supply lines, sewage pipes, bearings, rings, engine cylinders liners, piston, brake drums, street lamp posts, etc. The centrifugal force is tangential to the circular path of rotation and it is a function of radius and density. The centrifugal forces play significant role during the pouring and solidification which results in

higher density elements at the outer periphery of the cast component and the non-metallic slag inclusions in the liquid melt and the gas bubbles which are less dense comparatively forced to the inner surface as depicts by Figure 2.3 (Willaims et al. 2016).

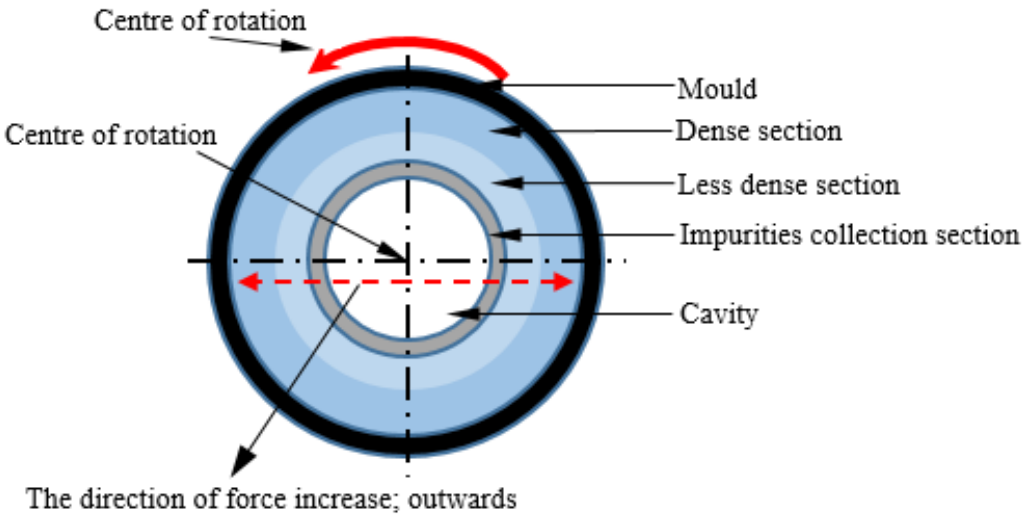

Figure 2.3 A schematic of a centrifugal casting system (Willaims et al. 2016)

The centrifugal force improves homogeneity, finishing and accuracy of the final cast product. The centrifugal force exerts acceleration:

$$F_c = mr\omega^2$$

$$= mv^2$$

Where, F_c = centrifugal force (N), m = mass (kg), r = radius (m), ω = angular velocity (rad/s) and v = peripheral speed (m/s)

This acceleration given above can be 100 or more times the acceleration due to gravity (g), thus the contact of the molten metal with the wall of the rotating mould is better than the conventional type of castings. The gravitational force on the mass is given by:

$$F_g = mg$$

Where g = acceleration due to gravity (m/s^2)

Hence the 'G' factor is given by,

$$G = \frac{F_c}{F_g} = \frac{r\omega^2}{g}$$

$$= \frac{r}{g(\frac{\pi}{30})^2 N^2}$$

$$\mathrm{G} = \frac{0.01rN^2}{G}, \text{Where N} = \text{revolutions per minute (rpm)}$$

On the other hand,

$$N = \sqrt{\left(\frac{Gg}{0.01r}\right)} = 29.9\sqrt{\left(\frac{G}{r}\right)}$$

$$\mathrm{N} = 42.3\sqrt{\left(\frac{\mathrm{G}}{\mathrm{D}}\right)}, \text{where D} = \text{rotational diameter (m)}$$

2.6.2 Classification of centrifugal casting

The following Figure 2.4 shows the classifications of centrifugal casting.

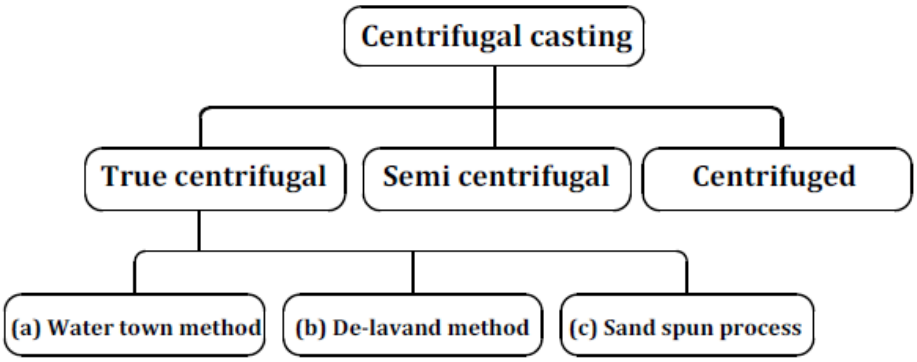

Figure 2.4 Classification of centrifugal casting

Centrifugal casting is mainly classified as true centrifugal casting, semi-centrifugal casting and centrifuged casting. Figure 2.5 shows the different centrifugal casting methods.

True centrifugal casting

In true centrifugal casting, the molten melt for the cast part is poured to the mould rotates on its axis, which may be horizontal, vertical or inclined at any suitable angle between 0 ° to 90 ° from an external source usually using a spout. While rotating, the centripetal forces from the spinning mould carried the molten metal to the walls of the cavity by centrifugal force. The rotation continues till the metal

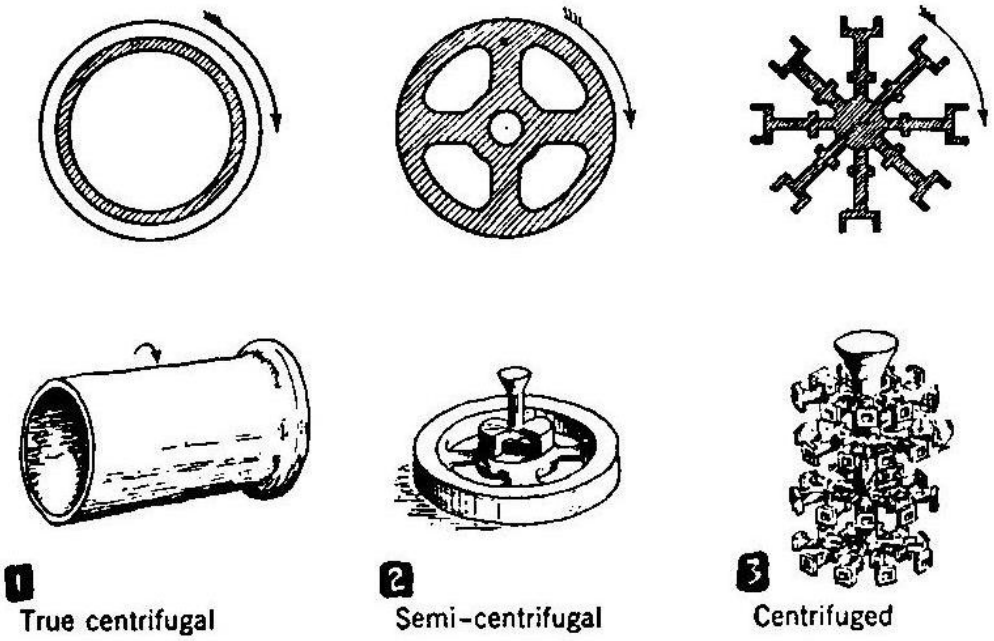

Figure 2.5 Different centrifugal casting methods (1) true centrifugal casting, (2) semi-centrifugal casting and (3) centrifuged casting

solidifies forming a hollow casting without the use of the central ore. By varying the flow rates, the quantity of the metal poured and movement of the pouring orifice the wall thickness of the final product can be changed. The outer contour of the casting can be varied according to the design of the mould, while the inside remains cylindrical for every casting. True centrifugal casting has three methods - water town method, De-lavand method and sand spun process.

(a) Water town method

Water town method is a method of which, a heavy cast-iron rotor is used as a chill mould for the manufacturing of larger gun tubes. The mould is coated with refractory wash and normally rotates at 1300 rpm. A weighed amount of liquid metal is poured into a pouring basin provided with a short spout in the mould where the diameter of the spout can be varied and rate of entry of melt can be adjusted so that the melt can evenly distribute into the mould cavity without cracking the solidification. The rate of flow should be accurately maintained otherwise, if the rate of entry of the molten metal is too slow, surface laps result from premature freezing occurs and if it is too fast, the cracking will takes place in the casting because of the centrifugal force of molten metal on the solidified thin skin will be too higher.

(b) De-lavand method

In De-lavand method, a thin walled metal mould is provided with a water jacket for cooling, is used for making of soil pipes and similar tubular like objects. The rotating machine and the mould are mounted on a plane inclined at a slight angle to the horizontal. A pouring trough for the liquid material to flow is extended into the rotating mould. By this method pipes as large as 13 inch (330 mm/0.3 m) in diameter and 20 ft (6096 mm/6.096 m) long can be manufactured.

(c) Sand spun process

In the process of sand spun, the chilling rate of the metal is lower than other methods because of the sand lining rammed inside the steel mould. The thermal protection barrier provided by the sand layer provided inside the mould as lining reduces heat shock lessens checking of the mould surface and prevents surface laps on castings caused by premature freezing of the metal. After the mould is partially filled with liquid melt, then the effect of thermal barrier disappears quickly.

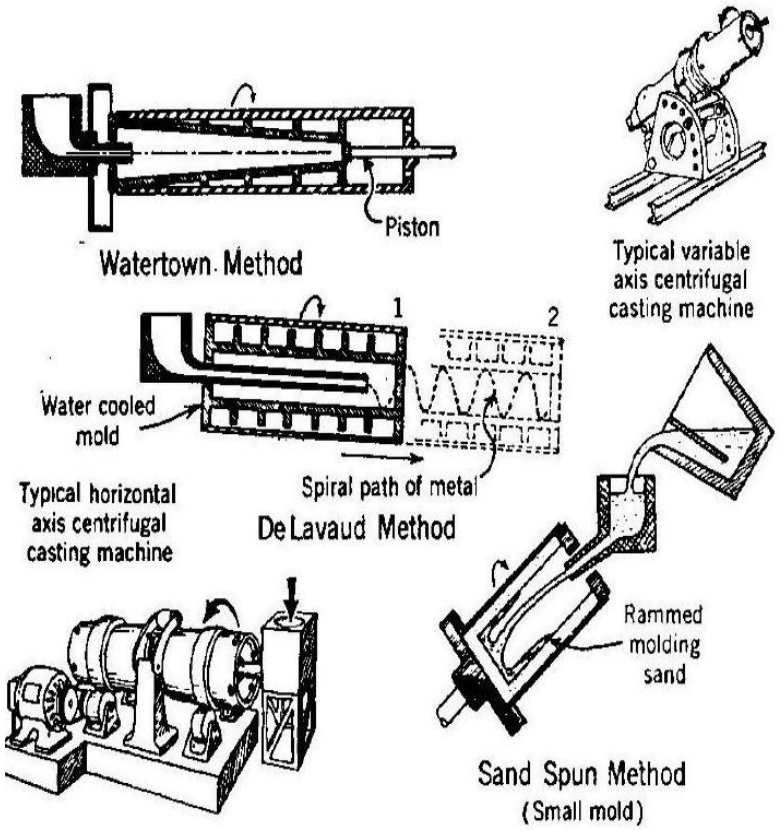

Figure 2.6 Methods of true centrifugal casting

Semi-centrifugal casting

Semi centrifugal casting method is especially used for the manufacturing of symmetrical shapes about the axis of rotation, mostly vertical. This process is almost similar to true centrifugal casting. The main difference of the semi centrifugal casting is that the mould is completely filled with molten metal that was introduced through a gate and flows outward to the rim by centrifugal force. Permanent or expendable type of moulds can be used. Compared with other processes the rotational speeds are much lower in semi centrifugal castings. Due to the lower speeds, the impurities are not segregated towards the inner periphery even high pouring temperatures are involved. Gears, pulleys, nozzles, wheels for tracked vehicles and propellers can be manufactured by using this technique.

Centrifuged casting

Centrifuge casting is the third main classification of centrifugal casting. This process is mainly used for the manufacture of industrial cast parts. Centrifuging is used for forcing metal from the spruce at the central axis into individual complex mould cavities that are provided at the circumference. The centrifuge method is always used investment casting of metals. Using this technique, several identical moulds can be placed radially about a vertically arranged central riser that feeds the metal into the cavities through a number of radially arranged gates. The mould is rotated with the central spruce along with the similar cavities arranged radially. This method of production is suitable for small, precise and complex parts where feeding problems of metals are encountered.

2.6.3 Advantages of centrifugal casting

- Centrifugal casting does not need a gating system for elements to direct the flow of metals, so it is a time saving process.
- Good quality castings can be produced in terms of surface finish, accuracy in the tolerances, dimensions, and reduced porosity such as gas porosities.
- A faster solidification can be achieved with a high quality of metallurgical properties due to the centrifugal force.
- The centrifugal force generated is about 150 times as compared with to gravitational force.

- A Simple and cost effective method for the production of functionally graded materials.

2.7 Aluminium Alloys and Structural Modifications

Modification is defined as the change that intentionally introduced to the base material to any characteristic features or phases of a product without losing its essence (Wasilewski et al., 1993). Structural modifications of aluminium and its alloys by grain refinement of primary phases and other phase modifications such as eutectic silicon modification are found to be one of the effective methods for improving the properties. Especially aluminium silicon (Al-Si) alloys are being widely used in various engineering applications including automobile, aeronautical and defence sectors due to its light weight/low density, high strength, wear resistance, etc. Grain refiners and modifiers are added in the form of master alloys to the liquid metal before pouring. Combined addition of grain refiner and modifier results in the drastic reduction in the size of grains and eutectic silicon leading to enhancement of mechanical and wear properties (Tavitas-Medrano et al., 2008).

Various investigations have been carried out by researchers on the role of Si and its percentage in relation with mechanical and wear properties. The volume of eutectic silicon phases formed during the solidification depends on the silicon content of the alloy. The percentage of eutectic silicon phases significantly influences the properties of the Al-Si alloy (Caceres et al., 2003 and García-García et al. 2007). The properties of hypo eutectic alloys can be enhanced by grain refinement (titanium and boron) and modification of eutectic silicon using sodium (Na), strontium (Sr) and zirconium (Zr) that helps to change the morphology of silicon from an acicular to the fibrous form along with the reduction in the grain size (Samuel et al., 1998 and Zhang et al., 2014). However, in hyper eutectic alloys the properties are determined to a large extent by the morphology, size and distribution of primary as well as eutectic silicon in the microstructure (Abramov et al., 1997 and Choi et al., 2012). The star-shaped coarse, hard primary silicon particles always show deteriorating mechanical properties. The addition of phosphorous in hyper eutectic Al-Si alloys results in the change of size and morphology of the primary silicon (Kyffin et al., 2001; Hogg et al., 2005 and Cui et al., 2009). The mechanical properties of the alloys mainly depend

upon the size, shape and distribution of Si particles in the matrix. Moreover, silicon forms intermetallics with the combination of magnesium (Sigworth et al., 1989). Even though the modification and properties of hyper eutectic alloys are studied using various modifiers or grain refiners, but its effect on centrifugal casting are not reported in the literature anywhere.

2.7.1 Grain refinement of Al and Al-Si alloys

Grain refinement normally occurs by increasing the nucleation sites during solidification. The nucleation in alloys during solidification is defined as the formation of the tiny crystals from the molten metal which is capable of gaining the size by developing the nucleus. The magnitude of the difference between the equilibrium melting temperature T_m and the solidification temperature (freezing temperature T_f), i.e., under cooling of the alloys are responsible for the rate of nucleation. An enhanced nucleation rate is achieved by a higher under cooling. The addition of inoculants helps aluminium and its alloys for the grain refinement phenomenon. The two main theories on nucleation are homogeneous and heterogeneous nucleation.

Homogeneous nucleation is defined as the formation of critically sized solid crystals from the liquid melt by clustering of a large number of atoms at a high undercooling. In homogeneous nucleation when a second phase particle forms a surface is also created. So a large driving force is required to overcome the energy of the created new surface during homogeneous nucleation. Likewise, the formation of the critically sized solid substances from the melt on an impurity surface is said to be heterogeneous nucleation. The substrate in the form of added inoculants or the impurities diminishes the thermodynamic barrier that required for the nucleation. Heterogeneous nucleation process occurs in the majority of the casting processes since it is not possible to eliminate the impurities completely. The kinetics of nucleation during heterogeneous nucleation is guided by the equilibrium of the interfacial energies (Murty et al., 2002). Wetting between the heterogeneous nuclei and the melt affects the nucleation efficiency. The interaction between solid heterogeneous nuclei surface and the melt is characterized by the wetting angle theta (θ) as shown in Figure 2.7.

Grain refinement has a significant role in improving the mechanical properties of the cast component mainly because of the change in the distribution of the secondary phases in the material. Figure 2.8 depicts the typical grain structure in aluminium 3004 alloy casting. It is clear that in the non-refined casting a small area near the chill zone provides equiaxed grains but, the other areas are enriched with feathery grains. The porosities formed in the material and the brittle intermetallic phases are always located between the larger grains. However, at the bottom figure, the grains are refined and fine structured which will provide isotropic mechanical properties throughout the material. The grain refinement will reduce the volume and amount of porosity; hence it will enhance the mechanical properties, especially the fatigue strength. Titanium (Ti) additions will improve the structure of the matrix material. Titanium refines the grains by raising the melting point of the aluminium alloy matrix. The melting point of aluminium is at 660.3 °C; when Ti is added into the aluminium, the melting point will raise to 665 °C. This effect of an increase in melting point has rampifications for the nucleation and growth of the aluminium phases or grains. Usually, titanium additions are accomplished with the help of aluminium master alloys with a maximum of 5-10 % of titanium. The master alloys contain a numerous number of crystals of titanium aluminide compound, $TiAl_3$ (Guzowski et al., 1987). After the addition of master alloy, typically few minutes before the casting, the microscopic titanium aluminide particles are released into the liquid melt. When the Al_3Ni particles come in contact with the molten aluminium, the particles starts to dissolve in the matrix and the molten melt at the surface of the particle becomes enriched in titanium. The titanium rich molten melt with the aluminide begin to solidify at a temperature above the melting point of the base alloy.

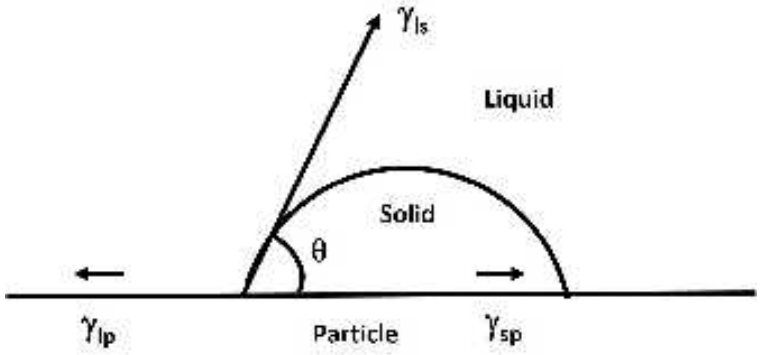

Figure 2.7 Schematic showing the equilibrium of interfacial energies during heterogeneous nucleation (Murty et al., 2002)

Figure 2.8 Grain structure in Al 3004 alloy (top: without grain refinement and bottom: with grain refiner 5Ti-1B alloy) (Geoffrey et al., 2007)

2.7.2 Modification of silicon in Al-Si alloys

Eutectic silicon modification

Eutectic silicon modification in aluminium-silicon alloys was initiated in early 19th century. The modifications are carried out through rapid cooling of the poured melt that prevents the further growth of the eutectic silicon. The rapid cooling process of casting is called chill casting. Due to the modification of the eutectic silicon by chill casting, the mechanical properties are found to be deteriorating. To avoid the deteriorating properties due to the chill casting usually, modification of eutectic silicon is achieved through the addition of chemical modifiers. In the chemical modification of Al-Si alloys, the addition of certain constituent elements such as sodium (Na), strontium (Sr), zirconium (Zr) and antimony (Sb) in hypoeutectic aluminium alloys results in the formation of fibrous eutectic silicon or in a finer laminar structure during solidification (Sigworth et al., 1983, 1989). With the addition of Na, the chemical modification of the Al-Si alloys was first reported in 1921 (Pacz, 1921). The fibrous silicon phases are heavily twinned in chemically modified alloys. The atoms of the modifiers are absorbed into the growth steps of the solid-liquid interface of the silicon in impurity induced twinning creating a twin plane re-entrant edge (TPRE) (Wagner et al., 1960).

The influence of strontium modification using varying strontium content from 0.0004 % to 0.03 % in the Al-Si-Cu alloys produced by the expandable casting process

on microstructure, porosity and tensile properties are studied and found that the optimum concentrations of strontium are between 0.01 % and 0.015 % and produces fibrous silicon structure. Moreover, the increase in the strontium content results in the higher porosity level and size of the porosity in the casting (Wang et al., 1995). The modification by strontium improved the ductility, impact, fatigue and fracture properties. Also, the further addition of strontium effectively leads to the reduction of the T6 solution treatment time (Apelian et al., 1989). The effects of additions of barium, calcium, yttrium and ytterbium on porosity formation in an aluminium A356 alloy was examined and reported that all the additions increased the porosity level with increased addition level compared with the unmodified alloy (Knuutinen et al., 2001). Apart from the common modifiers, the addition of alkali, alkaline earth and rare earth metals are also used for the modifications of the base alloys (Chiu et al., 1966; Lu et al., 1987; Chang et al., 2001 and Nogita et al., 2003). With the addition of Na and Sr the impurity induced twinning (IIT) mechanism for eutectic silicon modification was proposed for the first time (Lu et al., 1987). Complete modification of the eutectic in Al-7Si alloy is attained by two minutes of melt holding time after the addition of 0.02 wt. % Sr at a temperature of 720 °C (Kori et al., 2000b).

Primary silicon modification

Excellent properties such as good castability, low thermal expansion and high wear resistance of eutectic and hypereutectic Al-Si alloys made them be used widely in the field of automobile and general engineering industry (Hernandez et al., 2006; Xiangfa et al., 2004 and Asensio-Lozano et al., 2006). The superior mechanical properties of hypereutectic Al-Si alloys depend on the size and shape of the primary silicon (Yu et al., 2007). The refinement of primary silicon in the eutectic and hypereutectic silicon can be achieved through many methods such as mechanical or electromagnetic stirring process (Hernandez et al., 2006 and Lu et al., 2007), rapid cooling (Ge at al., 2004), rheocasting, thixocasting (Fuxiao et al., 2001 and Chen et al., 2005), rare earth elements (Xiangfa et al., 2004; Yilmaz et al., 1992 and Jinlong et al., 2005) and melt inoculation by the addition of phosphorous. In hypereutectic alloys the hard cuboids of primary silicon particles are modified using phosphorous addition, due to the AIP particles formed in the liquid melt on which the effective nucleation of the primary silicon taking place, but it will not modify the eutectic

silicon (Crosley et al., 1966; Adachi, 1984; Jorstad, 1971; Telang, 1963 and Jorstad et al., 2004). In a study, ZL109 alloy (contains 12Si) have shown the primary silicon precipitating in a size of about 15 μm by fast modification in response to the addition of 0.5 % Al-15Si-3.5P master alloy at a temperature of 720 °C. The coarse primary silicon in Al-30Si was refined from 150 μm to 37 μm due to the addition of 2 % Al-15Si-3.5P master alloy at a temperature of 850 °C (Zuo et al., 2009). The hypereutectic aluminium silicon alloys with more than 0.3 wt. % Mg forms Mg_2Si in the α-Al matrix. The morphology of the Mg_2Si decreases the mechanical properties compared to the base alloy. A combination of strontium and misch metal was usually used to change the morphology of the Mg_2Si to spherical that is obtained after the T6 heat treatment condition. Recently, the addition of Mg in hypereutectic Al-Si-Mg reported that when the Mg exceeds a certain percentage, the Si particles intrinsically refined and distributed uniformly in the matrix alloy (Mandal et al., 2007). The formation of Mg_2Si is desirable in the aluminium alloys due to its high melting point (1085 °C), low coefficient of thermal expansion (7.5×10^{-6} K^{-1}), low density (1.99 g/cm^3), high hardness (4.5 GPa) and reasonably high elastic modulus (Chang et al., 1998). The primary silicon was refined by the addition of 20 % FSM master alloy with a melt holding of 15 minutes after the addition results to a smaller size and the eutectic silicon is also modified to fibrous structure (Zhang et al., 2015).

2.8 Functionally Graded Aluminium Alloys and Composites by Centrifugal Casting Technique

As mentioned in the previous sections, centrifugal casting is one of the simplest methods for the production of functionally graded materials. The centrifugal casting of specific aluminium alloys such as hypoeutectic, eutectic and hypereutectic alloys can be used to obtain graded properties by varying the main elemental compositions (aluminium and silicon). The mechanical properties like hardness, tensile properties and fracture behaviour of the cast A356 and A357 aluminium alloys are influenced by the secondary dentritic arm spacing (SDAS), magnesium content in the alloys, the iron intermetallics in the component microstructure and the size and shape of the eutectic silicon present in the alloys (Wang, 2003). The properties of Al-Si alloys not only depends upon the chemical composition of the alloy but also the morphologies of the elements in the microstructure such as the

dendritic arm spacing of α-aluminium, eutectic silicon, intermetallics, etc. The varying grain size, shape, dendritic arm spacing of α-aluminium, eutectic silicon and intermetallic structure can be easily achieved by centrifugal casting technique through the centrifugal force and difference in the solidification rate at different locations. Centrifugal cast A356 ring exhibits a finer size primary aluminium and eutectic silicon phase towards the outer periphery of the casting than the inner periphery (Akhil et al., 2016). Figure 2.9 shows the optical microstructures of centrifugal cast A356 ring from outer to the inner periphery of the casting. The structural morphology of A356 centrifugal as cast ring reveals that the size of the eutectic and primary aluminium phase increased from outer to inner periphery and also an average DAS (Dendritic Arm Spacing) of 29, 31, 38 and 41 μm (Figure 2.9a-d) are observed from outer to inner periphery. The outer periphery showed higher hardness than the subsequent inner regions due to the difference in the grain size and shape of primary aluminium phase and eutectic silicon. Moreover, this variation of hardness also reflects in the wear rates as that showed better wear resistance at the outer regions than the inner. The variation in the properties is due to the variation in the composition and segregation of phases of different densities in the cast component from outer to inner periphery. The centrifugal casting of AS12UN aluminium alloy (Fe-0.75 %, Si-(11.50–13.00) %, Zn-0.20 %, Mg-(0.75–1.30) %, Ni-(0.80–1.30) %, Pb-0.10 %, Sn-0.05 %, Ti-0.20 %) increases rupture strength and strain up to about 35 % and 160 % respectively over the conventional gravity casting technique. The properties of the castings depend on the relative positions of the specimens taken from the castings. The greater the distance of the specimens from the axis of the rotation in centrifugal castings, higher the properties due to the higher G value due to the centrifugal force (Chirita et al., 2008).

Nowadays, different aluminium alloys with varying percentages of silicon and other constituent elements are extensively using for the manufacturing of functionally graded materials of desired properties. Moreover, the structure and properties of the alloys not only depends on the chemical composition but also due to many factors act during the time of solidification. The primary silicon particles formed in Al-20 vol. % silicon fabricated by vertical centrifugal casting shown in Figure 2.10 are segregated in the inner region of the cast cylinder due to the less

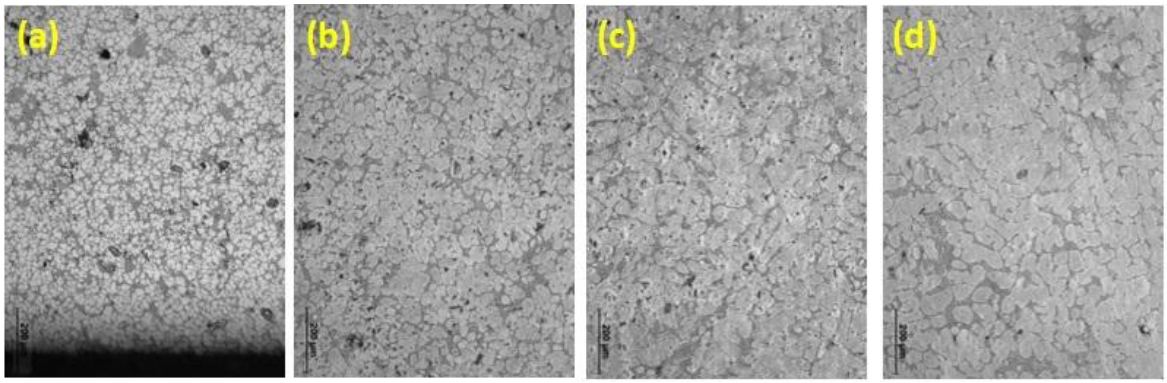

Figure 2.9 Optical microstructures of functionally graded material formed from A356 base alloy [(a) at 0.5 mm, (b) at 21 mm, (c) at 35 mm and (d) at 49 mm from outer periphery of the centrifugal castings] (Akhil et al., 2016)

density leading to higher hardness and superior wear resistance properties. The sizes and volume fraction of primary silicon decrease from inner to outer periphery up to 25 % of the total length of the inner region.

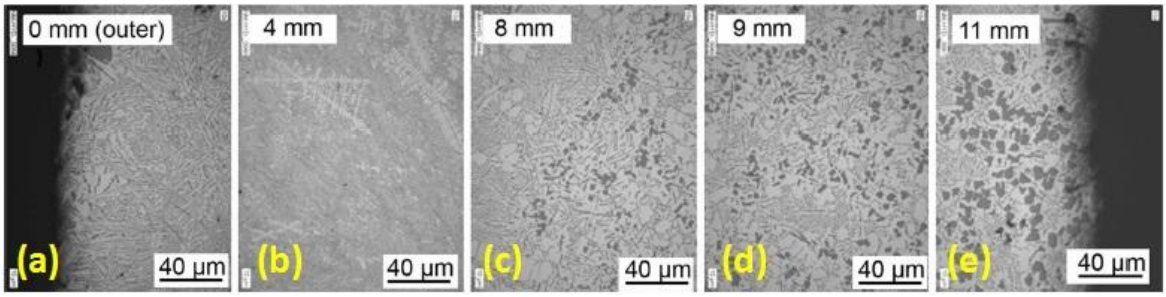

Figure 2.10 Optical microstructures of Al-20 % Si FGM fabricated by vertical centrifugal casting

Centrifugal casting is widely used for the production of functionally graded composite materials mainly reinforced with SiC, B_4C, other aluminium based FGM's and metallic materials with large differences in the densities. Cylindrical and non-cylindrical components can be produced by centrifugal casting. Through centrifugal casting, superior metallurgical cleanliness and soundness of casting can be easily achieved by centrifugal pressure caused by segregation of oxides and gas porosities towards the inner surface which can be machined off for final application of the component (Halvaee et al., 2001 and Gao et al., 2000). Optical microstructures of A6061-SiC FGM at different locations are depicted in Figure 2.11.

Table 2.2 Observations made on centrifugal casting of different aluminium matrix composites (Rajan et al., 2014)

Composite system	Observations
Al-SiC (Rajan et al., 2004; Babu et al., 2005 and Srinivasan et al., 2006)	Graded distribution of SiC particles near the outer periphery of the casting. Higher strength and modulus near outer periphery. A smooth and gradual distribution of particles is observed when mixture of particle sizes is used.
Al-graphite (Krishnan et al., 1984)	Higher volume fraction of graphite particles observed near the inner periphery of the casting.
Al-Si	Primary Si particles are observed near the inner periphery of the hollow casting.
Al–Al_3Ni (Rajan et al., 2008 and Fukui et al., 1994)	Primary Al_3Ni phases near the inner periphery of the casting. Al–20 % Ni forms the best graded distribution compared to Al–10/30/40 % Ni. Young's modulus vary from 81 to 100 GPa across the 6 mm tube wall thickness from the inner to outer surface, reflecting 15.2 and 43.2 vol. % Al_3Ni second phase.
Al-Al_2Cu (Watanabe et al., 2005)	Graded structure of Al_2Cu is observed in Al–33 mass % Cu eutectic system.
Al-Al_3Ti (Watanabe et al., 1999 and 2001)	Al_3Ti platelets are distributed gradually near the outer periphery of cylindrical casting.
Al–AlB_2(Melgarejo et al., 2006)	AlB_2 particles with higher bulk density than liquid aluminium segregate towards the outer surface regions leading to higher wear resistance.
Al–SiC–graphite	Graded distribution of SiC and graphite particles near the inner periphery of the casting. Few percentage of SiC is also observed near outer periphery.

Al–(Al_3Ti+Al_3Ni) (Watanabe et al., 2001)	Hybrid Al–(Al_3Ti+Al_3Ni) show superior wear resistance than pure Al. The wear resistance at outer region of ring is higher compare to inner region.
A356-(5, 10 & 15 wt. %) SiC (Akhil et al., 2016)	The sizes of the primary aluminium and eutectic silicon phases are finer towards the outer periphery due to the higher solidification rate achieved through centrifugal casting. Functionally graded Al–SiC_p composite rings show higher concentration of SiC_p towards outer periphery, a gradient transition region in between and the inner particle depleted zone.

The SiC particles are segregated towards the outer most region and gradually reduces the volume percentage towards the inner region. The measured volume fractions at different locations of A6061-SiC functionally graded metal matrix composites are indicated in the Figure 2.12. The volume percentages dropped from 41 vol. % at the outermost region to 15 vol. % at 5 mm from the outer region shows a gradual gradation of SiC particles with respect to the distance. Moreover, after 5 mm from the outer region, there are no particles observed other than the pure aluminium A6061 alloy structures (Babu et al., 2005). When a mixture of different SiC particle sizes are used for the manufacturing of FGM with an average particle size (APS) of 14, 23 and 42 μm in equal proportions in A356 aluminium matrix, a smooth gradation and a gradual distribution of SiC particles are observed. However, for the A356 matrix reinforced with SiC particles of 23 μm APS alone showed a sharp transition from the outer to the inner periphery (Srinivasan et al., 2006).

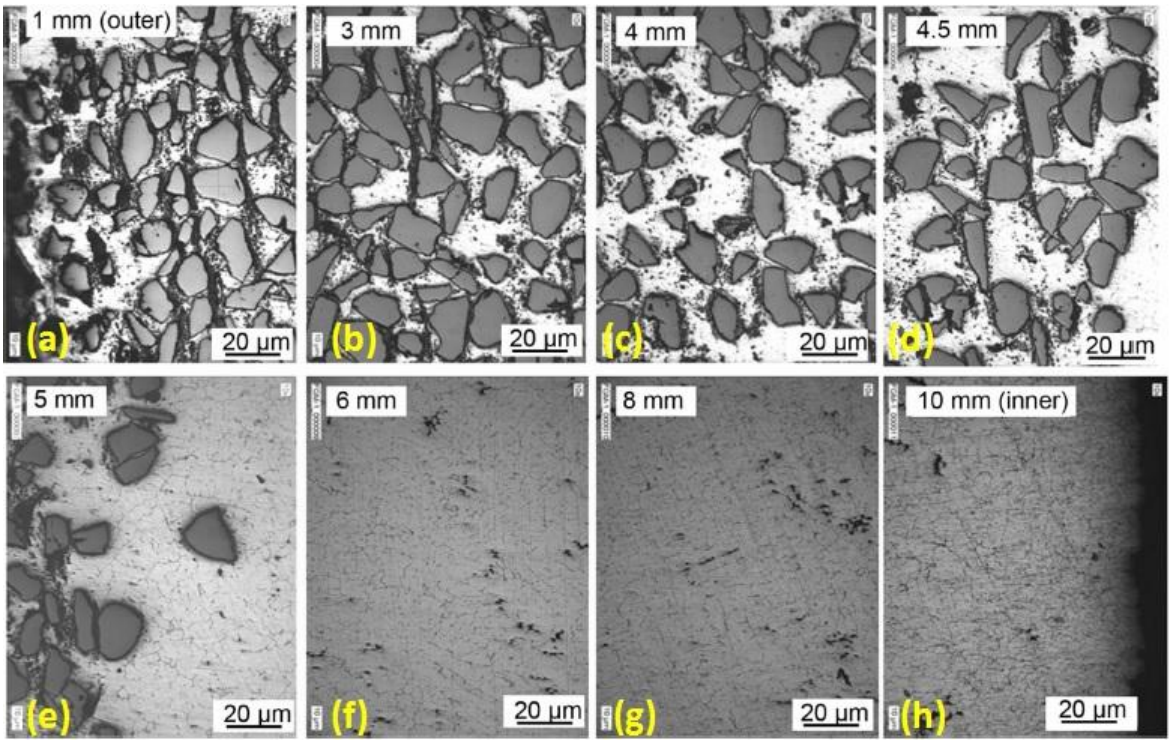

Figure 2.11 Optical microstructures of Al 6061-SiC FGM from outer to inner periphery (Babu, 2005)

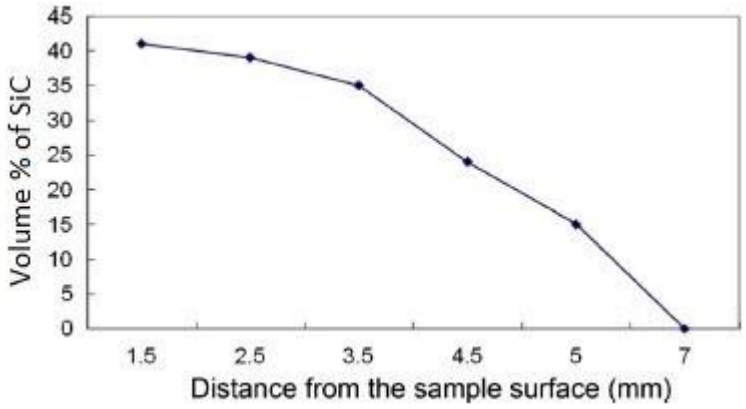

Figure 2.12 Distribution of silicon carbide particles in Al 6061-SiC FGM (Babu, 2005)

Microstructures of centrifugally cast hollow cylinder of Al-20 wt. % Ni from outer to the inner periphery are shown in Figure 2.13. The Al-Al_3Ni FGM shows a gradual gradation from outer to inner periphery. The outer region is enriched with Al_3Ni primary crystals can be clearly seen in Figure 2.13a and b, but the inner region of the cast component is full of the matrix. The primary Al_3Ni phases show both acicular and equiaxed structures, whereas the inner region shows very fine eutectic phases. The microstructure reveals the transition from hypereutectic to near eutectic

or hypoeutectic composition in the component 10 mm from the outer periphery (Fukui et al., 1994 and Rajan et al., 2008).

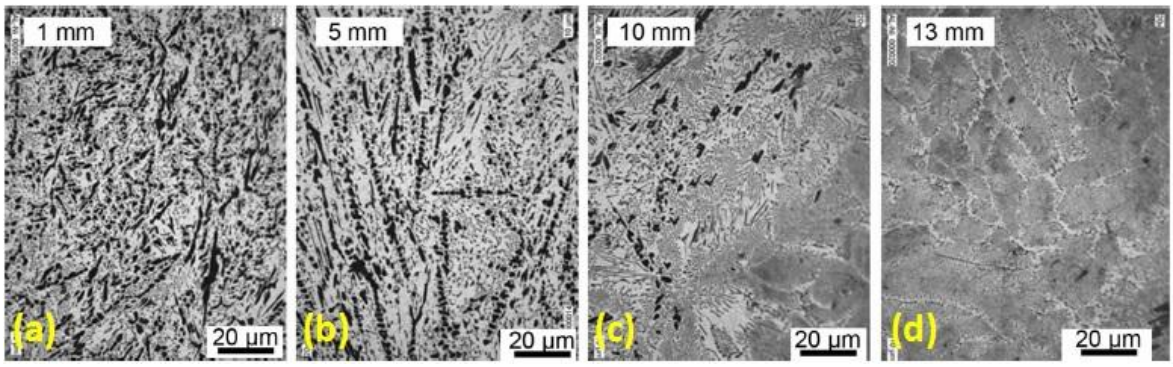

Figure 2.13 Optical microstructures of Al-Al_3Ni insitu functionally graded composite from outer periphery to inner periphery of Al-20 % Ni (Rajan et al., 2008)

The microstructural features of hybrid functionally graded hollow cylinder of LM 25-10 % SiC-5 % graphite produced by vertical centrifugal castings are presented in Figure 2.14. The microstructural observation shows that the distribution of a part of SiC in the outer periphery of the casting and the other part in the inner periphery along with the graphite particles leading to a hybrid functionally graded composite. The hindered settling phenomenon is responsible for the segregation of hybrid particles to the inner periphery of the castings (Rajan et al., 2014).

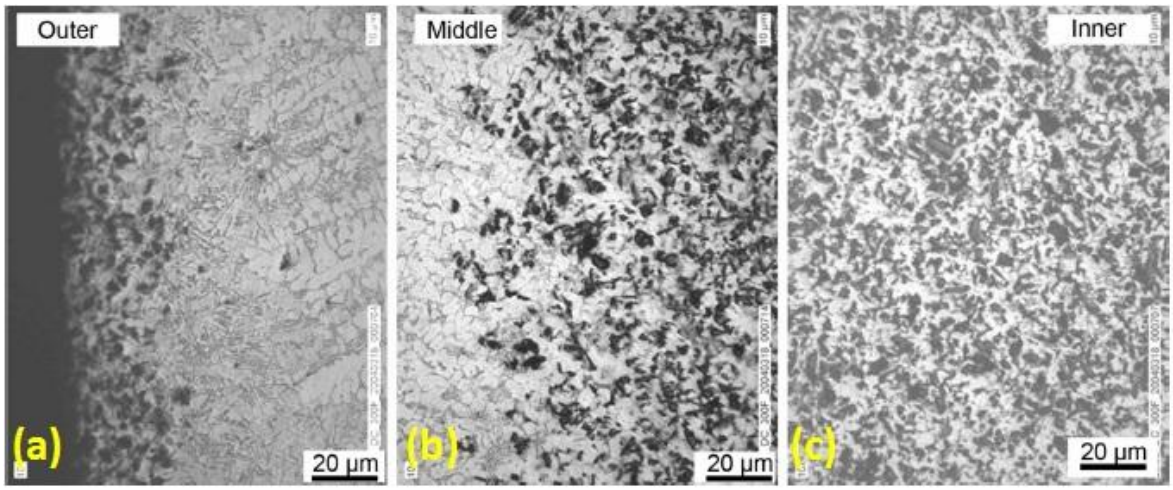

Figure 2.14 Optical microstructures of Al-10SiC-5 graphite functionally graded metal matrix composites by centrifugal casting from outer to inner periphery (Rajan et al., 2012)

Functionally graded MMC rings of 5, 10 and 15 wt. % SiC_p reinforced A356 aluminium matrix was fabricated by centrifugal casting and the microstructural observation have shown a higher concentration of SiC particles are segregated towards the outer periphery of the rings immediately after the chilled zone. (Akhil et al., 2016). The FGM reinforced with 15 wt. % SiC shows a higher percentage of gradation towards the outer periphery (at 35 mm) than the subsequent inner regions compared with the centrifugally cast A356 alloy and other FGM composites (Figure 2.15). The centrifugal cast FGMMCs show higher hardness and wear resistance (both rotating and reciprocating wear) towards the outer periphery of the castings due to the presence of higher percentage of SiC particles near the outer periphery.

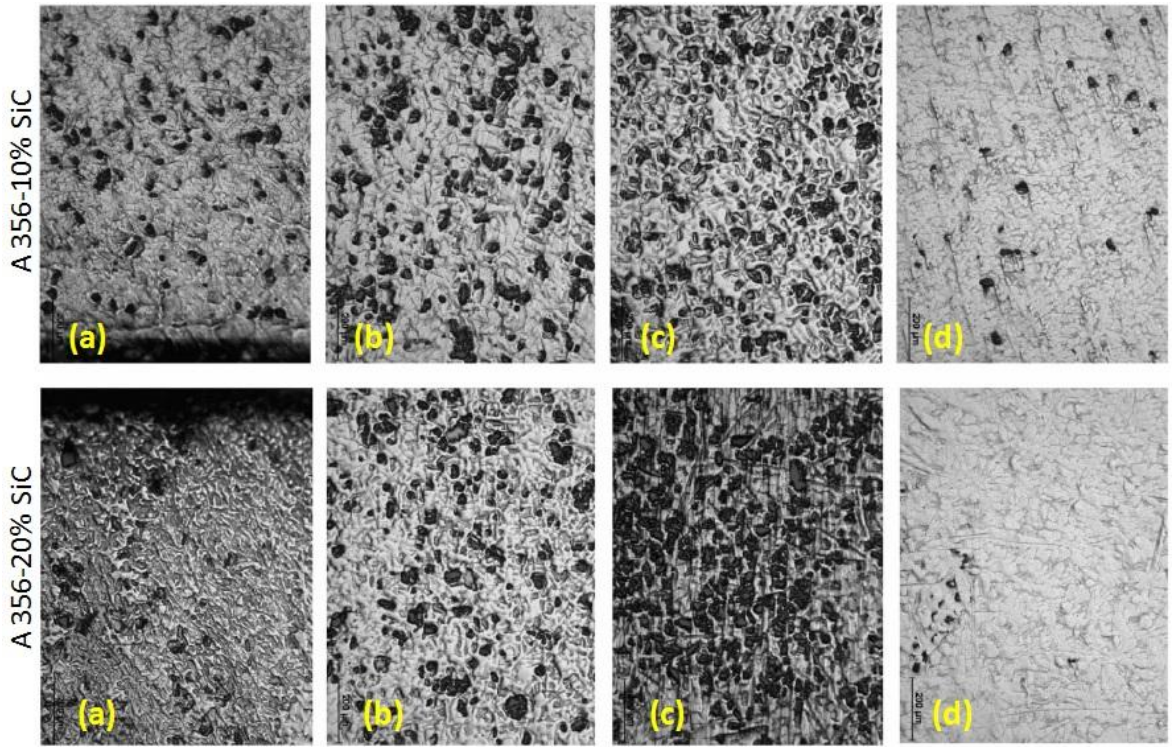

Figure 2.15 Optical microstructures of functionally graded materials formed from A356–10 and 20 wt. % SiC [(a) at 0.5 mm, (b) at 21 mm, (c) at 35 mm and (d) at 49 mm from outer periphery of the centrifugal castings] (Akhil et al., 2016)

The graded distribution of primary silicon and Mg_2Si particles developed by the in-situ process of hypereutectic Al-Mg_2Si alloy tubes fabricated by centrifugal casting was reported (Zhang et al., 2000). The microstructure in correlation with the distribution of particles in the casting with the influence of rotational speed of the centrifugal mould and the cooling rate of the castings (solidification rate) were investigated. Higher volume fractions of castings defects are associated with lower

rotation speed, but better gradient distribution of primary Mg_2Si particles are observed in the investigation. An increase in rotation speed resulted in an apparent change in the particle distribution profile in the outer region. The rotational speed has only a less influence on the particle distribution at the inner periphery. An extremely high solidification rate (cooling rate) was obtained by using a copper mould rather than graphite mould. The usage of the copper mould with water cooling leads to the formation of very fine microstructure in the outer region that when compared with the same region in the other tubes produced using graphite mould. Hence, it is evident that the macro and microstructures in the centrifugal cast tubes are tailorable.

An FGM development process called selectively reinforced casting (SRC), was developed by Pacific Northwest National Laboratory by centrifugal casting process to develop FGM components with inhomogeneously reinforced particles from stir-cast particulate metal matrix composites (Herling et al., 2004). The SRC process uses the radial component of forces that generated from centrifugal force to segregate a second discrete phase from the matrix of MMCs. This process can produce components with a high density of particles at the desired reinforced region. The density of the reinforcement is in the order of more than 50 vol. % with starting feedstock levels of 10 vol. %. This process can reduce the overall material cost of a component; by reducing the quantity of the costly reinforcements with selective reinforcements at the specific locations.

The centrifugal casting process for making FGM was modelled (Lajoye et al., 1988) by considering the movement of solid reinforcement particle in the liquid melt from the moment the solid particles experience the segregative force up to the moment it is trapped in place by the moving solidification front. The calculation was made for the time dependent particle distribution by integration of the trajectories of the solid particles participated in the casting process.

2.9 Functionally Graded Polymer Matrix Composites

Studies on functionally graded carbon fiber reinforced polymer composites are limited and hence the detailed discussion of literature related to homogenous short carbon fiber reinforced composites is carried out. Due to the difficulty in the

proper dispersion and proper wetting of the reinforcements with the polymer matrix, FGM fabrication process and controlling the polymerization process in the making of polymer matrix FGM composites, only a few works have been reported in this area by centrifugal casting. Thermosetting epoxy resins are the common polymer matrix used for the fabrication of polymer matrix composites. The epoxy resins can only be used at a temperature below 160 °C. The epoxy polymers are extensively used for various engineering applications due to low cost, low shrinkage, easiness in the processing, good rheological behavior during the fabrication, superior adhesion, improved mechanical properties and recyclability (El-Sayed et al., 1995; Zhou et al., 2008; Xu et al., 2008; Green et al., 2009; Chatterjee et al., 2010 and Zhao et al., 2012;). A few fillers like glass and carbon fibers are incorporated into the polymer matrix to obtain enhanced tribological properties. In epoxy matrix composites carbon fibers are widely used as the reinforcements due to their high specific strength and modulus (Smith et al., 1987; Donnet et al., 1990 and Tiwari et al., 2014).

The short carbon fibers (SCF) are added to the conductive polymer composites (CPC) with polyester and epoxy and its effect was studied and found that the electrical properties showed a small amplitude positive temperature coefficient (PTC) effect between 90 and 160 °C. For both the CPC, it was found that the electrical property decreases between the fibres in spite of the potential contact. Figure 2.16 shows the SEM images of unsaturated polyester reinforced with short carbon fiber (SCF) CPC. From the figure, it is seen that the aggregation process promotes the formation of sheaves and thereby deteriorating the electrical conduction. Good electrical and mechanical properties are obtained over 3 % v/v SCF, but for good thermal properties, the polymer composites with 2.5 % v/v found better (Feller et al., 2002).

Pitch-based short carbon fibers are used to improve the mechanical properties of polymer matrix composites. The compatibility of the adhesion between the epoxy and the SCF mainly depends on the surface roughness of the fibers. Higher the surface roughness leads to better bonding strength by the mechanical interlocking mechanism. Various oxidative and cryogenic treatments are provided to improve the surface roughness of the SCF. The SEM images provided in the Figure 2.17 ensure the

Figure 2.16 SEM micrographs of unsaturated polyester-SCF CPC (Feller et al., 2002)

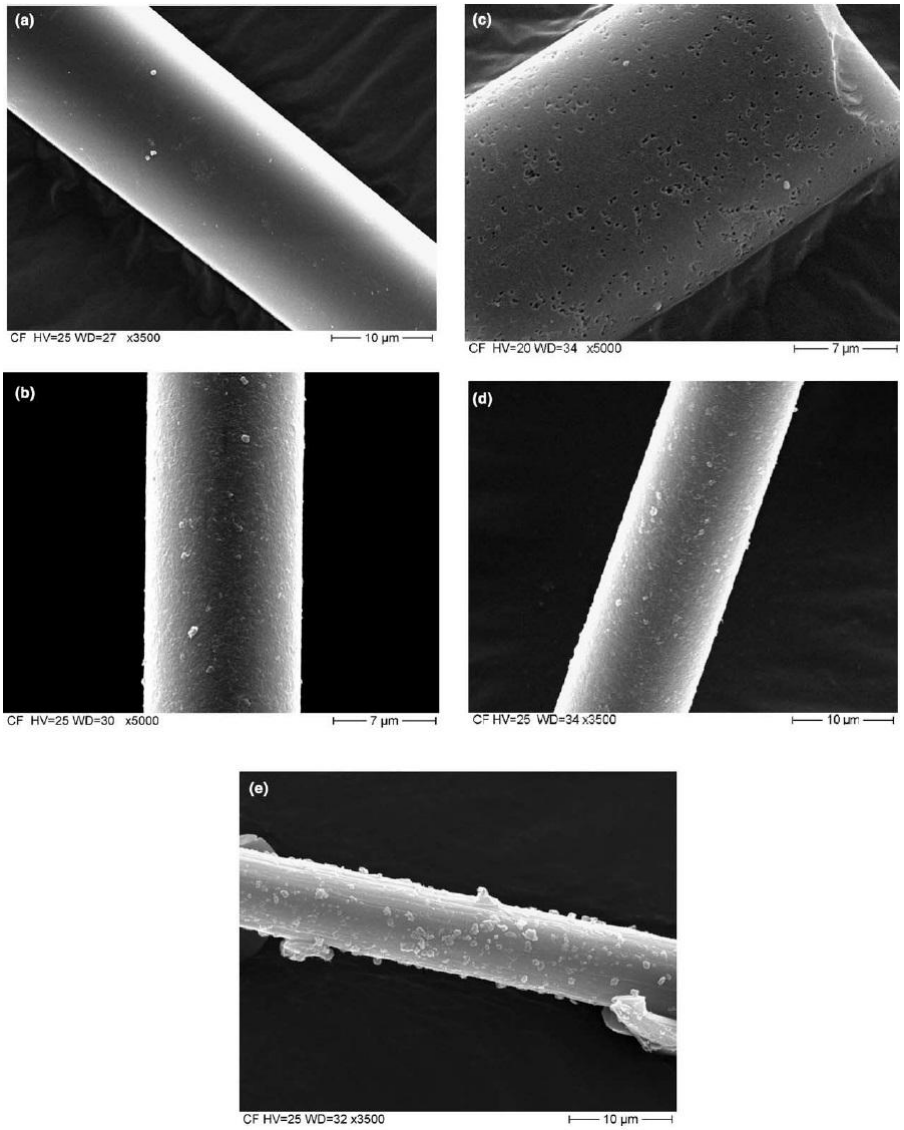

Figure 2.17 SEM images of carbon fibers treated under different conditions (a) as received; air oxidised at (b) 500 °C/1 h and (c) 600 °C/1 h; cryogenic treated in liquid nitrogen for (d) 1 min and (e) 10 min (Hui et al., 2004)

surface roughness of the treated short carbon fibers compared with the untreated fibers. Out of the treatment methods cryogenic treatments found to be good enough for short span of treatment time and eco-friendly media to improve both modulus and strength (Hui et al., 2004).

Epoxy composites reinforced with different percentages of SCF were developed and investigated the wear properties (Nay et al., 2014). The wear studies showed that the wear rate reduces significantly with increase in the SCF content. This trend was due to the solid lubricating effect that produced by the reinforced carbon fibers while rubbing during the wear test. Figure 2.18 and 2.19 shows the morphology of worn epoxy and epoxy-SCF composite that slid against a chromium steel pin inclined at 45 ° to the vertical. The SEM structures also reveal that the epoxy composites are less sensitive to surface fatigue caused by repeated sliding than the unreinforced epoxy.

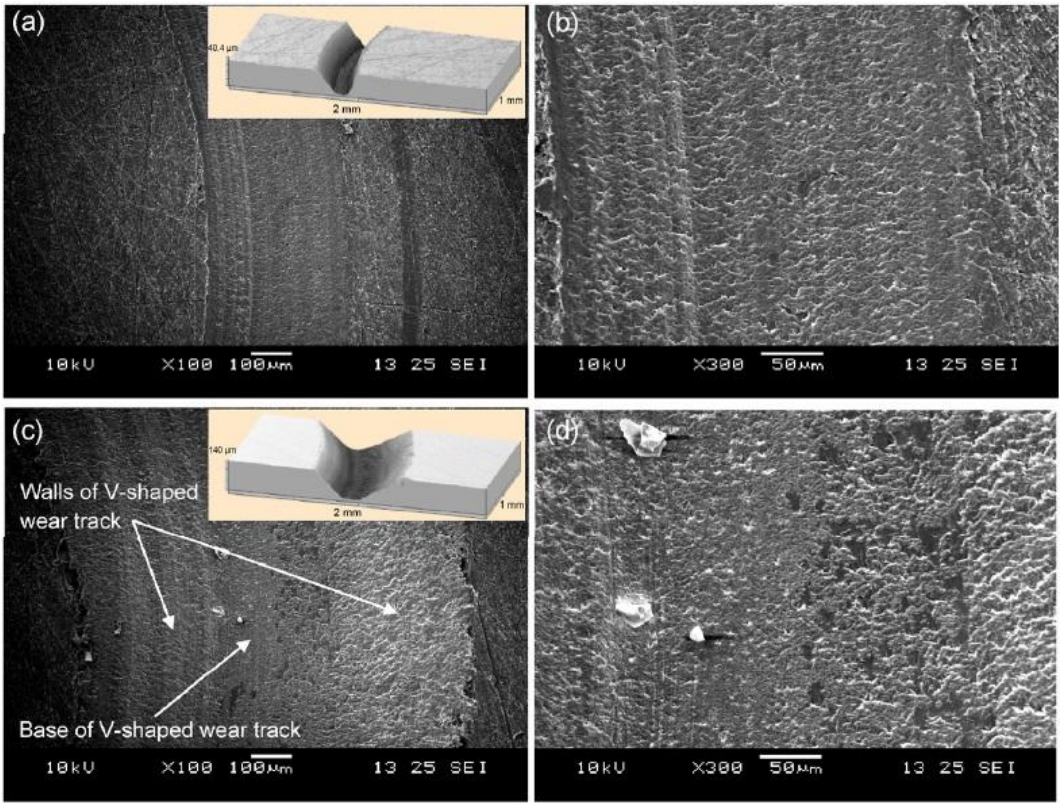

Figure 2.18 SEM images showing surface morphologies of worn epoxy, (a) and (b) 2 N and (c) and (d) 6 N, observed at different magnifications. Insets (a) and (c) show surface topographies of the same samples measured using surface profilometry (Nay et al., 2014)

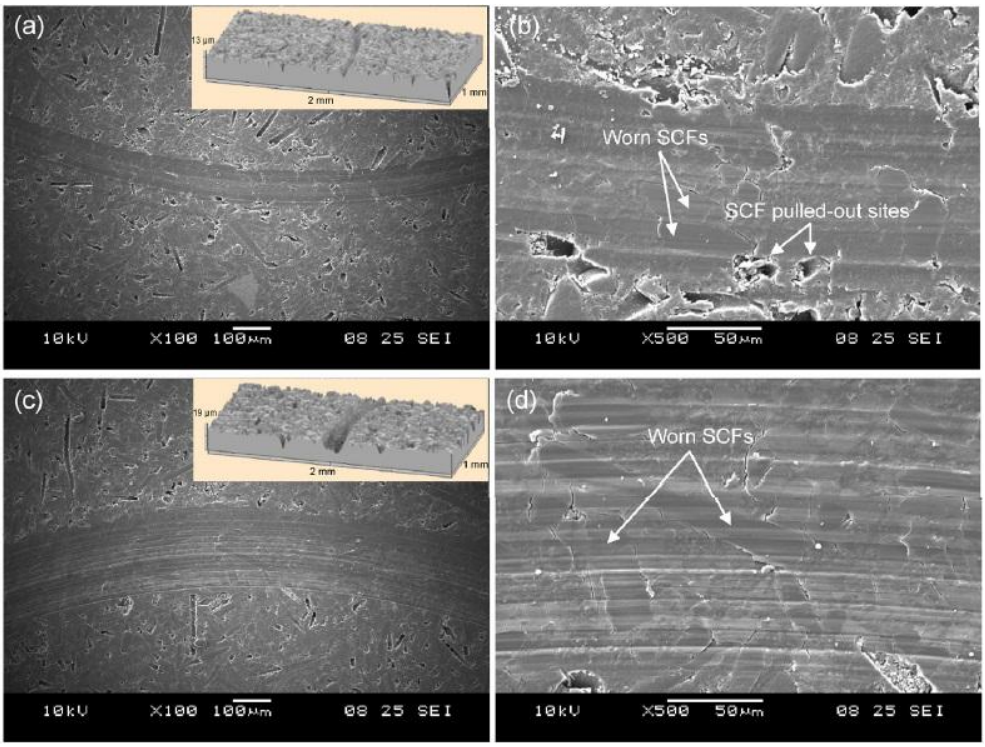

Figure 2.19 SEM images showing surface morphologies of worn epoxy composite with 20 wt. % SCFs (a) and (b) 2 N and (c) and (d) 6 N, observed at different magnifications. Insets (a) and (c) show surface topographies of the same samples measured using surface profilometry (Nay et al., 2014)

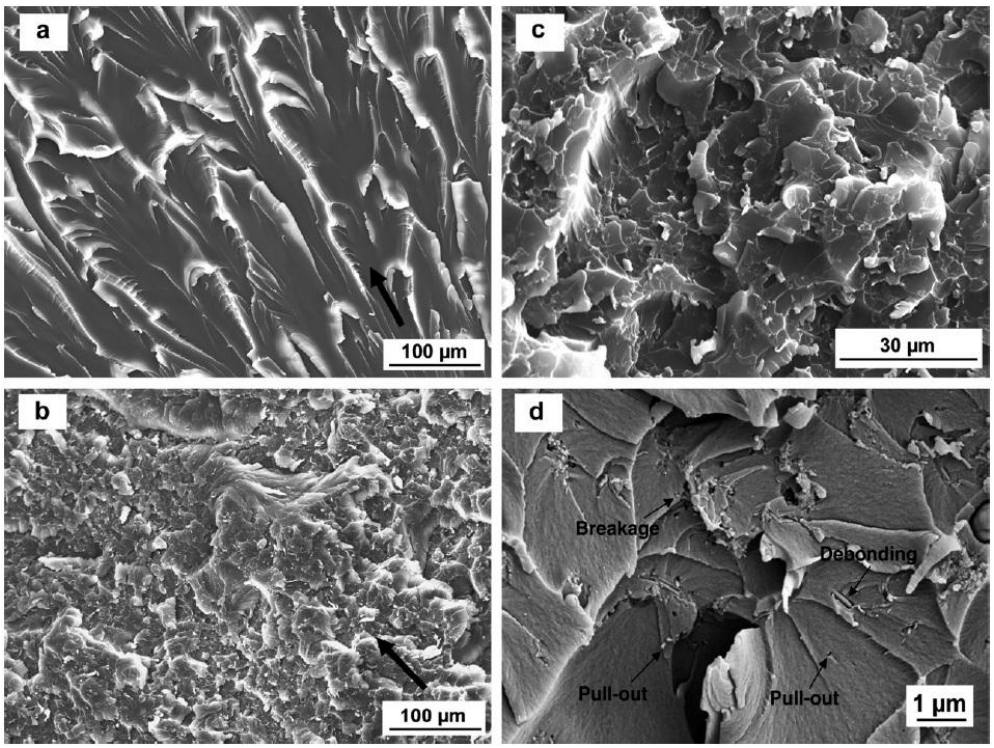

Figure 2.20 SEM micrograph of tensile fracture surfaces of (a) epoxy and (b-d) epoxy filled with 0.75 % CNFs (Zhang et al., 2010)

The combined effect of carbon nano fibers (CNFs) and short carbon fibers on the mechanical and fracture properties of epoxy resin were investigated (Zhang et al., 2010). The combined effect showed much higher tensile strength, modulus and fracture properties than the composites reinforced with single fillers. Figure 2.20 shows the SEM images of the fracture surface of 0.75 NF. In all the composite systems pull-out, breakage and debonding of CNFs were noticed over the fracture surface in SEM analysis.

2.10 Scope of the Investigation

The product developments based on functionally graded materials are still in the infancy stage. Hence there is a large scope for research and development of metal and polymer based FGMs and their engineering components.

- Most of the research work on bimetallic systems was studied as one metal in solid and the other in the liquid state or both in solid states. There are no additional process facility requirements for the production of bimetals if both the metals are made in the liquid state. However, the additional advantage is the better interfacial bonding between the metals/alloys.
- The addition of inoculants or modifiers in high silicon aluminium alloys for automotive applications are widely studied and reported but, the effect of the modifiers and minor alloying additions in the aluminium alloy when it is subjected to centrifugal casting are rare.
- The literature on centrifugal casting is mainly used for the production of components that has axial symmetry. For making non-axial symmetric components which involve complicated profiles, the design of mould and dies are challenging and critical.
- Studies on short carbon fiber (SCF) reinforced polymer composites by dispersing the SCFs for making a component is not reported.

2.11 Objectives of the Present Work

The objectives of the present work are:

1. Fabrication and characterization of functionally graded cast bimetallic A390-A319 and A390-A6061 aluminium alloys by sequential gravity casting technique with enhanced interfacial bonding and properties.
2. To study the effect of magnesium (Mg), modifiers such as strontium (Sr) and zirconium (Zr) on morphology and distribution of eutectic/primary silicon in A390 hyper-eutectic aluminium alloy during centrifugal casting.
3. Design, fabrication and characterization of functionally graded aluminium A2219-SiC metal matrix composites for turbine exit vane guide application for aero-engines by centrifugal casting technique.
4. To study the effect and distribution of short carbon fiber (SCF) reinforced epoxy matrix composites processed by centrifugal casting.

CHAPTER 3

Materials and Experimental Methods

3.1 Materials

3.1.1 Matrix

The materials used for the present investigation were aluminium A390, A319, A6061, A2219 alloys for aluminium matrix related FGM studies and epoxy matrix for polymer matrix based FGM studies. A390 is a hypereutectic cast alloy, A319 is a hypoeutectic cast alloy and A6061 as well as A2219 are wrought aluminium alloys. The detailed elemental compositions, properties of the aluminium alloys and standard properties of epoxy matrix are furnished in Table 3.1, 3.2 and 3.3 respectively.

3.1.2 Reinforcements

The different types of discontinuous reinforcements used for the present investigation were silicon carbide particles (SiC_p) of 14 and 23 μm in aluminium matrix and polyacrylonitrile (PAN) based short carbon fiber (SCF) of 3 mm length and 7 μm diameters for the manufacturing of the epoxy-SCF composite. The properties of SiC and SCF are given in Table 3.4.

Table 3.1 Elemental composition of alloys used for the present investigation (wt. %)

Alloy	Al	Si	Cu	Mg	Fe	Mn	Zn	Ti	Ni	Cr	V
A319	85.8-91.5	5.5-6.5	3.0-4.0	0.10	1.0	0.50	3.0	0.25	0.35	-	-
A390	75.3-79.5	16-18	4.0-5.0	0.50-0.65	0.40	0.10	0.10	0.20	-	-	-
A6061	95.8-98.6	0.4-0.8	0.15-0.4	0.8-1.2	Max 0.7	Max 0.15	Max 0.25	Max 0.15	-	0.04-0.35	-
A2291	91.5-93.8	Max 0.2	5.8-6.8	Max 0.02	Max 0.3	0.2-0.4	Max 0.1	0.02-0.1	-	-	0.05-0.15

Table 3.2 Properties of A319, A390, A6061 and A2219 aluminium alloys

Properties	A319	A390	A6061	A2219
Density	2.79 g/cm^3	2.72 g/cm^3	2.7 g/cm^3	2.84 g/cm^3
Liquidus Temperature	604 ^{o}C	649 ^{o}C	652 ^{o}C	643 ^{o}C
Solidus Temperature	516 ^{o}C	507 ^{o}C	582 ^{o}C	543 ^{o}C
Co-efficient of Thermal Expansion	22.9 µm/m-^{o}C at 20-300 ^{o}C	22.5 µm/m-^{o}C at 20-300 ^{o}C	25.2 µm/m-^{o}C at 20-300 ^{o}C	24.1 µm/m-^{o}C at 20-300 ^{o}C
Thermal Conductivity	109 W/m-K at 25 ^{o}C	134 W/m-K at 25 ^{o}C	167 W/m-K at 25 ^{o}C	121 µm/m-^{o}C at 20-300 ^{o}C
Solutionizing Temperature	502-507 ^{o}C	496 ^{o}C	528 ^{o}C	535 ^{o}C
Aging Temperature	163-191 °C for 8 hr	177 °C for 8 hr	160 $^\circ$C	163-191 °C for 18 to 36 hr
Yield Strength	214 MPa	310 MPa	276 MPa	393 MPa
Hardness	70-100 BHN	145 BHN	95 BHN	130 BHN
UTS	>=193 MPa	310 MPa	310 MPa	476 MPa
% Elongation	>=1.5	<=1.0	12%	10%
Modulus of Elasticity	74 GPa	81.2 GPa	68.9 GPa	73.1 GPa
Poisson's Ratio	0.33	0.33	0.33	0.33
Fatigue Strength	115 MPa	115 MPa	96.5 MPa	103 MPa
Shear Modulus	28.0 GPa	27 GPa	26 GPa	27 GPa
Shear Strength	165 MPa	187 MPa	207 MPa	280 MPa

Table 3.3 Standard properties of epoxy matrix

Properties	Values
Density	1.22 g/cm^3
Tensile strength	68 MPa
Young's modulus	4.5 GPa
Thermal stability	Low
Machinability	Medium
Hardness	Low
Moisture absorption (24 hours , 23 $^\circ$C)	Low

Table 3.4 Properties of reinforcements

Property	SiC Particle	Short Carbon Fiber (SCF)
Density	3.2 g/cm^3	1.8 g/cm^3
Average particle / Fiber size	14 and 23 µm	7 µm diameter and 3mm length
Thermal conductivity	20 (polycrystal) Wm^{-1}K^{-1}	355 Wm^{-1}K^{-1}
Specific heat capacity	1300 JKg^{-1}K^{-1}	-

Silicon carbide (SiC)

Silicon Carbide (SiC) is also known as carborundum. Silicon carbide particulates (SiC_p) have been widely used as reinforcements in aluminium matrix from 20th century onwards, among the various dispersoids available for the processing of metal matrix composites. The SiC have got wide exposure due to its enhancement of strength, modulus, thermal stability and higher wear resistance. The SiC is mainly used with aluminium alloys due to its good wetting property with aluminium alloys and also due to their closeness in the density values (2.8 for Al and 3.2 g/cm^3 for SiC_p). The SiC_p chosen for the present investigation is green in colour with 14 and 23 μm average particle size (APS) (procured from Carborundum Universal Limited) and it is easily available, cost effective and importantly it imparts significant improvement in composite properties. The photograph of commercially available green SiC is shown in Figure 3.1.

Figure 3.1 Photograph of commercially available green SiC_p

Short carbon fiber (SCF)

Polyacrylonitrile (PAN) based short carbon fibers of density 1.74 g/cm^3 with 3 mm length and 7 μm diameters supplied by Courtaulds Company were used as the reinforcements for the manufacturing of the epoxy-SCF reinforced composite. Photograph of SCF used for the fabrication of epoxy-SCF composites are depicted in Figure 3.2.

Figure 3.2 Photograph of short carbon fibers used for fabricating polymer FGM composites

3.2 Sequential Casting Process

Sequential casting technique is a simplest and cost effective method of casting, where two different alloys/composite melts having similar freezing ranges are poured into a mould sequentially without turbulence to produce functionally graded materials and components by controlled mould filling process. The process involves the pouring of two molten metals, one followed by the other providing an optimized gap between the pouring of the two melts for obtaining a proper bonding between the metals. Sequential casting is a liquid state processing technique since the process involves the pouring of liquid metals.

3.3 Composite Processing

3.3.1 Aluminium based MMC's

The composites were mainly processed in a clay graphite crucible using a resistance-heated pit furnace by liquid metal stir casting technique. The composite syntheses were carried out using 12 kg aluminium alloys melted in pit furnace. SiC particles of 23 μm average particle size and a density of 3.2 g/cm^3 were used to process the MMC's/FGM's by adding 15 weight percentages (15 wt. %) into the alloy matrix. The schematic diagram of composite processing setup is given in Figure 3.3 (a) and the photograph of pit furnace is shown in Figure 3.3 (b). Magnesium was added to compensate its loss in the alloy melt due to oxidation and to improve the wettability of the matrix with the reinforcement. Preheated SiC_p at 600 °C was introduced into the molten melt at 740 °C with a controlled feed rate. Meanwhile, the alloy melt was mechanically stirred using a specially designed impeller driven by an eddy current electric motor of 2 HP capacity with a dynamometer to control the

stirring speed. Degassing process was done by passing N_2 gas to the slurry of metal through sulphuric acid to avoid hydrogen entrapment. The melt was then superheated above the liquidus temperature and poured at 760 °C into the permanent mould to obtain the homogeneous distribution (metal matrix composite) of SiC_p and into the centrifugal mould (ring/disc mould - 240 mm diameter and 30 mm height) rotated at 1300 rpm to obtain the functionally graded materials. The detailed processing parameters used for various experiments are provided in the respective chapters. The processed alloy/composite melt is then shaped by gravity and centrifugal casting techniques. The moulds used in the present investigation for the gravity and centrifugal castings are presented in Figure 3.4.

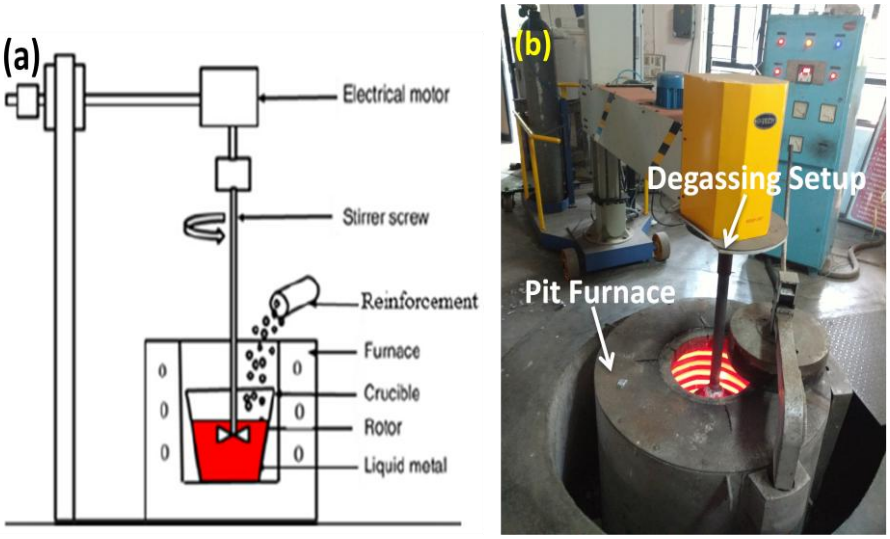

Figure 3.3 (a) Schematic diagram of composite processing setup for liquid metal stir casting (Jebeen et al., 2016 and Ebhota et al., 2016) and (b) photograph of pit furnace

Figure 3.4 Permanent moulds used in the fabrication of aluminium alloys and composites in both gravity and centrifugal casting (a) pencil mould (b) slab mould (c) cylindrical mould for cylinder application (d) cylindrical mould for the fabrication of polymer FGM (e) ring/disc mould (f) turbine fan blade for centrifugal casting

3.3.2 Epoxy based composites

The epoxy polymer composites were processed in a 600 ml capacity plastic beaker. A quantity of 340 ml epoxy resin was used for each experiment. The short carbon fibers were added to the epoxy matrix as small bunches of fibers. The epoxy resin was continuously stirred with a mechanical impeller. The curing agent was added in correct proportion to the composite liquid after the addition of carbon

fibers. Then, the epoxy composite liquid was poured into a cylindrical mould that rotated at 1300 rpm.

3.4 Physical Properties

3.4.1 Density measurement

The densities of the samples are measured using a density meter that works on Archimedes principle and calculated using the expression given below:

$$\rho = \frac{(W_a \rho_l - W_l \rho_a)}{(W_a - W_l)}$$

Where, W_a is the weight of the specimens in air, W_l is the weight of the specimens in liquid (water) and ρ_l and ρ_a are the densities of liquid and air. Using the density values, the % porosity can be calculated using the expression below:

$$\% \text{ Porosity} = \frac{(\text{Theoritical density} - \text{Measured density})}{\text{Theoritical density}} \text{ x } 100$$

Where, theoretical density is the density of the individual elements in the component. Figure 3.5 shows the photograph of density meter.

Figure 3.5 Photograph of density meter

3.5 Structural Evaluation

3.5.1 Optical microscopy

The specimens for the structural evaluation were taken and cut in a particular dimension that suite to the machine from the castings using hack-saw and band saw. The cut samples were then undergone turning operation in lathe to ensure the parallelism of the specimens at the both ends and then properly filed the edges and corners of the specimens for the smoothening of sharp edges formed during the machining operation. The sectioned surfaces so obtained were polished progressively with silicon carbide embedded emery paper of grit sizes varying from 80 to 1000 (ie., 80, 100, 220, 400, 600 and 1000 grit sizes). The samples were rotated by 90 ° between the papers and washed thoroughly with liquid soap and water. During the polishing using paper water can be used as cleaning agent, if necessary. After the completion of the polishing using emery paper, the specimens were undergone cloth polishing using different grades of diamond paste i.e., 6, 3 and 0.25 μm, over a rotating disc at a controlled rpm. The cloths used were fine sylvet clothes for cloth polishing using diamond paste. The polishing cloths were changed between the usages of the different grades of the diamond paste. Filtered kerosene was used as the lubricant during the cloth polishing. The specimens should hold and pressed against the rotating disc at a moderate pressure to avoid scratches and excessive surface contamination. The specimens were then subjected thorough wash with liquid soap and distilled water. The specimens have been viewed and analysed under polished and etched condition. The etchant used was Keller's reagent. Keller's reagent is a mixture of nitric acid, hydrochloric acid, and hydrofluoric acid. The optimum etching time was found to be 10-15 seconds. The etching time may vary from samples to samples.

Microstructural evaluations of as-cast samples of alloys and composite specimens were carried out using a Leica DMRX optical microscope. The photograph of the Leica optical microscope is depicted in Figure 3.6. The microstructures were taken from different locations and at different magnifications from the polished specimens.

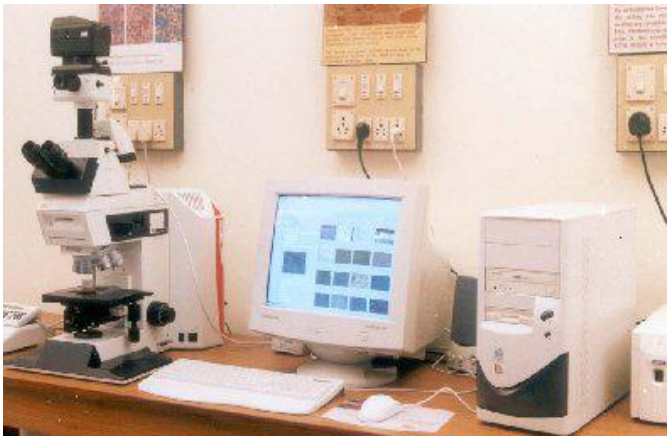

Figure 3.6 Photograph of Leica optical microscope

3.5.2 Scanning electron microscopy (SEM)

Scanning electron microscopy was used to identify the constituent part responsible for the failure of the materials and to study the micro mechanisms behind fracture. The as-received, treated reinforcements, alloy as well as composite specimens, the fractured surfaces of tensile and compression samples and worn surfaces of wear specimens were examined using the SEM. Some samples have been coated with gold to make the surface conductive to reveal good SEM images. The SEM was operating under an accelerating voltage ranging from 10 to 20 kV. The samples used for optical microstructure can also be used for the SEM observations. The JEOL JSM-5600LV and Carl Zeiss EVO-18 scanning electron microscopes were used for the SEM analysis during the present work. The photograph of SEM is shown in Figure 3.7.

Figure 3.7 Photograph of JEOL JSM-5600LV scanning electron microscope

3.6 Energy Dispersive X-ray Spectroscopy (EDS)

The composition at various locations, phases, precipitates, interfaces, intermetallics and surfaces of the reinforcements were analysed using energy dispersive X-ray spectroscopy (EDS) that attached to SEM equipment. Most of the SEM images are taken using secondary electrons (SE) although some images have been acquired using back scattered electrons (BSE). Only selected samples were subjected to EDXS analysis. The EDAX and OXFORD EDS attached to SEM were used for the present studies.

3.7 Optical Emission Spectroscopy (OES)

An optical emission spectrometer (OES) was used to analyse the chemical composition of the cast aluminium alloys and composites. OES is using arc and spark excitation (Arc Spark OES) method to determine the chemical compositions of metallic samples at different locations, to carry out the metal analysis. In the present investigation, the chemical compositions of the alloys, composites and functionally graded material systems were carried out by using SPECTROMAXx-AMETEK optical emission spectrometer. The photograph of optical emission spectrometer is shown in Figure 3.8.

Figure 3.8 Photograph of optical emission spectrometer

3.8 Differential Thermal Analysis (DTA)

The differential thermal analytical technique was used to study the thermal characteristics of as-cast alloys, composites and FGM samples with a standard HITACHI STA 7300 at different regions of the cast component. The photograph of

HITACHI STA 7300 equipment is as shown in Figure 3.9. The studies were normally performed at a standard heating rate of 10 °C/min up to a temperature of 800 °C beyond the melting point and alloy, composite or FGM processing temperature under normal air atmosphere. The metals were then cooled to the ambient temperature to examine the phase transformation temperatures that might be occurred while heating and cooling, from the large exothermic and endothermic peaks, obtained from the differential thermal analysis (DTA).

Figure 3.9 Photograph of HITACHI STA 7300 DTA equipment

3.9 X-ray Diffraction (XRD)

X-ray diffraction analysis at different locations of the cast specimens was carried out with the help of XRD-PAN analytical machine. Figure 3.10 shows the photograph of XRD-PAN analytical machine.

Figure 3.10 Photograph of XRD-PAN analytical machine

3.10 Mechanical Properties

3.10.1 Hardness

Hardness may be defined as a material's resistance to permanent indentation. Physically speaking, hardness is the resistance offered by the crystal for the movement of dislocations and practically it is the resistance offered by the crystal for localized plastic deformation.

Hardness measurement in Brinell Hardness Number (BHN)

An Indentec Brinell hardness tester and TINUS OLSEN were used to measure the Brinell hardness number (BHN) of the as-cast and heat-treated alloy and composite samples for studying the effect of the heat-treated condition over the as casts using a 2.5 mm diamond/steel ball indenter with an applied load of 62.5 kg for a dwell time of 20 seconds. Photographs of Indentec Brinell hardness tester and TINUS OLSEN hardness tester are shown in Figure 3.11. Five readings are taken from each sample to get representative data. The surface of the specimens on which the indentation is made has been turned and polished up to 400 grit size emery paper since hardness is dependent on surface roughness. The parallelisms of the samples are taken care to ensure accurate measurements. Always, maintained a distance of two times diameter ($2d$) of the indentation with the consecutive indentations to avoid the work hardening effect of the previous indentation that may affect the readings of hardness. Also, by knowing the indentation diameter, the hardness values can be obtained from a standard table for a particular applied load and indenter ball diameter. The hardness values in BHN can be manually calculated by using the formula,

$$\mathrm{BHN} = \frac{2\mathrm{P}}{\left[\pi D\left(D - \sqrt{(D^2 - d^2)}\right)\right]}$$

Where, P is the applied load in *kgf,* D is the diameter of the ball indenter in *mm* and d is the diameter of the indentation in *mm.*

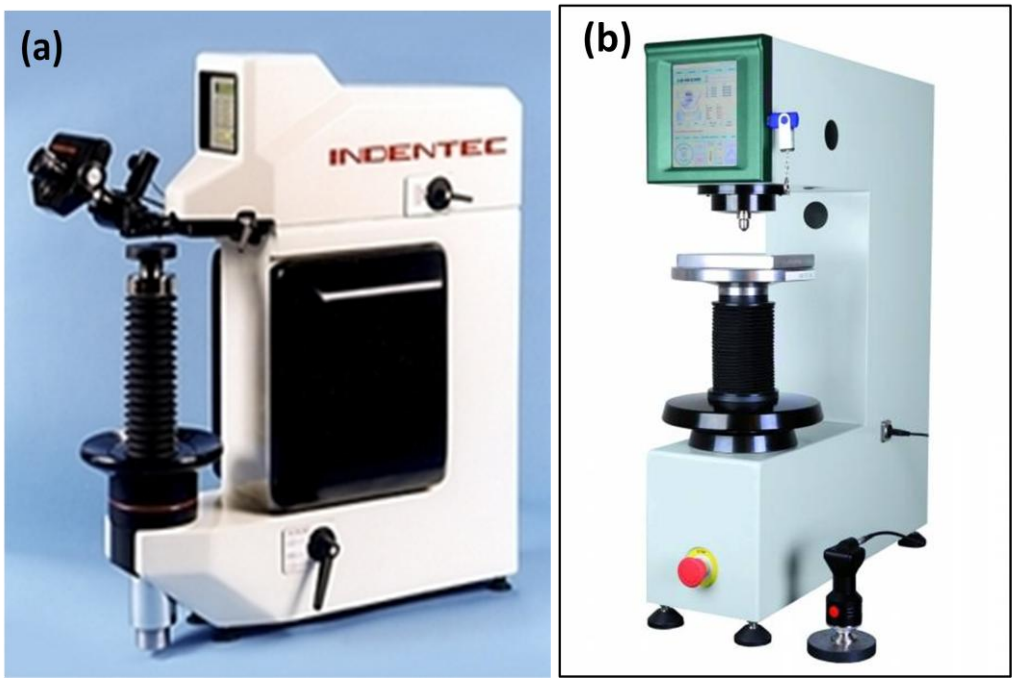

Figure 3.11 Photograph of (a) Indentec Brinell hardness tester and (b) TINUS OLSEN hardness tester

Hardness measurement in Shore D

The hardness of the polymer and composite systems are measured using a Shore D hardness durometer STD-D confirming ASTM D 2240 standard. The durometer scale was defined by Albert Ferdinand Shore, who developed a measurement device to measure Shore hardness in the 1920s. The term durometer is often used to refer to the measurement as well as the instrument itself. Durometer is typically used as a measure of hardness in polymers, elastomers, and rubbers. There are several scales of durometer, used for materials with different properties. The two most common scales, using slightly different measurement systems, are the ASTM D2240 type A and type D scales. The scale A is for softer plastics, while the scale D is for harder ones. The shore hardness scale is represented in Figure 3.12 (a) and the photograph of shore hardness durometer is shown in Figure 3.12 (b). The cut samples from the cured polymer systems perpendicular to the direction of the centrifugal force are polished using fine emery papers to ensure the parallelism of the surfaces. The durometer is held vertical with the point of the needle indenter at least 12 mm away from the smooth surface of the sample. The pressure foot is applied to the specimen without shock, keeping the foot parallel to the surface of the specimen.

Figure 3.12 (a) Shore hardness scale and (b) photograph of shore hardness durometer

3.10.2 Mechanical testing

Tensile and compression testing of alloys and composites are carried out using a fully computer-controlled Instron universal testing machine (UTM) No.1195-5500R. The photograph of the universal testing machine Instron is shown in Figure 3.13. The ultimate tensile strength (UTS), yield strength and percentage elongation were obtained directly from the computer. The tensile specimens are fabricated confirming to ASTM B557M Standard and have been tested according to ASTM E-8 standard. From each set of alloy or composite systems, five tests are carried out and an average value is reported in this work. The dimensions of the tensile and compression samples are provided in the Figure 3.14.

Figure 3.13 Photograph of Instron 1195-5500R universal testing machine

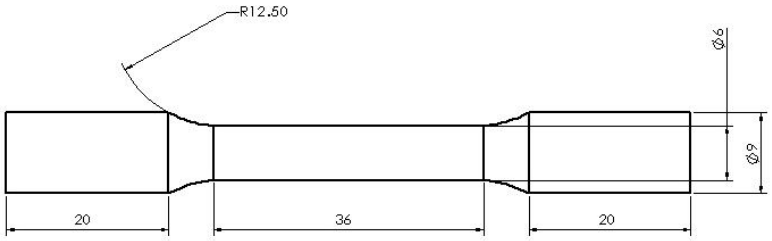

(a)

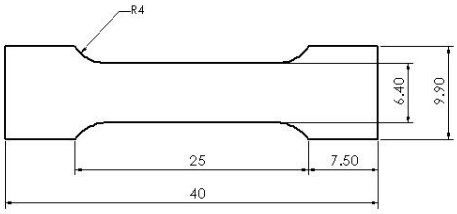

(b)

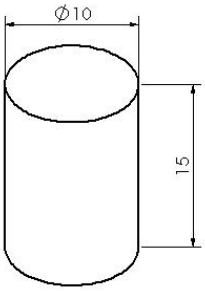

(c)

Figure 3.14 Schematic of (a) round tensile, (b) flat tensile and (c) compression sample

3.11 Wear Testing

The wear test was carried out using standard pin-on-disc wear testing machine (wear and friction monitor – 20LE) that measures tribological properties such as the frictional force, coefficient of friction and wear volume between two surfaces in contact. The photograph of pin-on-disc wear test rig is shown in Figure 3.15. Pin-on-disc tribometer consists of a stationary pin holder of 6 mm diameter, where the normal load was applied to the pin specimen by using dead weights with the help of string and special pulley arrangement, which can bear a maximum load capacity of 15 kg (147.15 N). The cylindrical pin specimens having a dimension of 6 mm diameter and 30 mm length was used as the wear specimen. Wear specimens of 6 mm circular cross section were in full contact with the counter body in the entire test duration. The counter surface disc used was En 31, high-carbon alloy steel of 165 mm diameter and 10 mm thickness which possesses a high degree of hardness (63 HRC) with compressive strength and abrasion resistance and material composition of Cu 1.00 %, Mg 0.50 %, Cr 1.40 % and Si 0.20 %. A constant sliding distance of 1800 m and a velocity of 1 m/s were maintained throughout the tests, and accordingly the track was adjusted to obtaining the specific needs. The tests were continued with the same composition of the materials with different loads of 1 kg (9.81 N), 2 kg (19.63 N), 3 kg (29.43 N), 4 kg (39.24 N), 5 kg (49.05 N), 6 kg (58.86 N), 7 kg (68.67 N), and 8 kg (78.48 N).

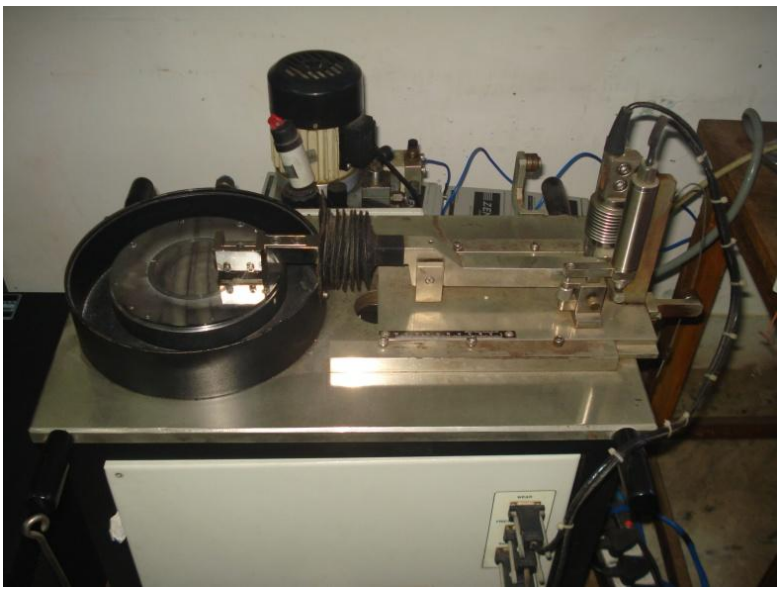

Figure 3.15 Photograph of pin-on-disc wear testing machine

3.12 Rheology

A rheometer is a device used to measure the way in which a material responds to applied force. There are three types of rheometer classified according to the sensor used to study the properties. They are:

- Rotational cylinder type
- Cone and plate type
- Plate and plate type

In rotational cylinder type rheometer, one cylinder is rotated in the annulus of the other, and is mainly used to measure the shear rate inside the cylinder. Parallel plate rheometers are widely used to measure the visco-elastic properties. Oscillatory shear experiments are widely used to characterize visco-elastic materials, while rotational mode experiments are used to measure the viscosity of material. The visco-elastic behaviour of the polymer and polymer based composite system was studied using parallel plate rheometer. Anton Par Physical Modulated Compact Rheometer 150 with disposable parallel stainless steel plates of 50 mm diameter are used for the purpose. Figure 3.16 shows the photograph and schematic illustration of rheometer. A typical parallel plate rheometer consists of:

- Two stainless plates placed parallel to each other
- A spindle to provide the shear to the sample
- Pressure transducer to measure the property variation in the sample
- Temperature sensor to set the temperature
- Computer to monitor the process

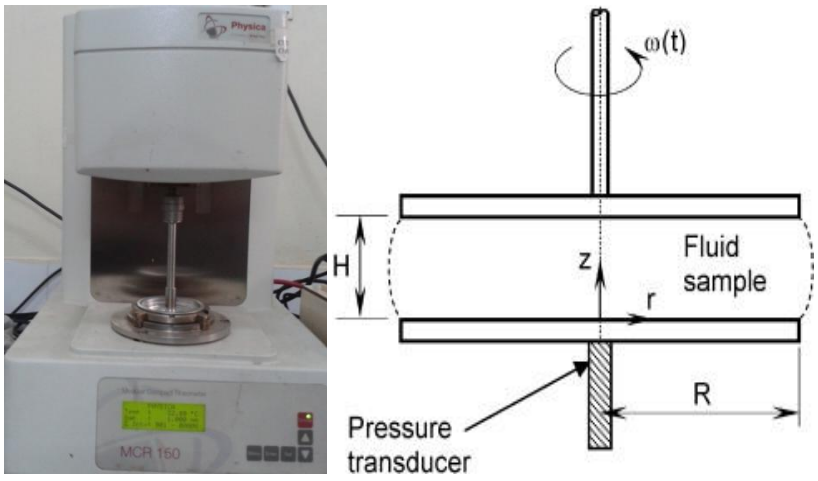

Figure 3.16 Photograph and schematic illustration of parallel plate rheometer

CHAPTER 4

Sequential Cast Functionally Graded Bimetallic Al Alloys

4.1 Abstract

Sequential casting is a facile and fairly new technique to produce functionally graded materials (FGMs) and components by controlled mould filling process. In the present investigation, functionally graded bimetallic aluminium alloys are produced by sequential gravity casting using A390–A319 and A390–A6061 alloy combinations. The control in pouring time between two melts has shown a significant effect on the quality and nature of interface bonding. The microstructure reveals good interface miscibility achieved through diffusion bonding between the alloys. A higher hardness of 160 BHN in the A390 region is obtained in both sequential cast systems, and a minimum value of 105 and 91 BHN is observed in the A319 and A6061 regions, respectively. The tensile and compression strength for A390–A319 are 337 and 490 MPa, whereas for A390–A6061, they are 364 and 401 MPa, respectively, which are significantly higher compared with the standard values of the base alloys, which confirms strong interface bonding. The A390 region shows higher wear resistance compared with other regions of the sequential cast system. The process described in this study is a potential and efficient approach to create good bonding between two different aluminium alloys to develop advanced functional and structural materials.

4.2 Introduction

Functionally graded materials (FGMs) are the nonuniform advanced class of alloy or composite materials that exhibit a gradual transition in the microstructure or in the composition with continuous changing properties in a particular direction (Mortensen et al., 1995). Various processing techniques are developed to reconfigure the microstructure of material to attain the assumed graded microstructure for desired properties. Some advanced casting techniques such as squeeze casting, sequential casting, centrifugal casting, and hot pressing are modified to produce functionally graded materials and their components. Centrifugal casting is considered to be one of the most important casting processing techniques that is being widely

studied to produce FGM. Functionally graded materials can have either a continuous or a stepwise graded microstructure. The sequential casting technique finds an inevitable place due to the simplicity of the process, which can produce FGMs having a stepwise graded microstructure by simple gravity casting method while controlling the mould filling parameters without any special equipment setup (The Aluminium Automotive Manual, 2011 and Ragab et al., 2013). The FGM fabrication techniques have attracted researchers and are increasingly receiving attention globally in making components for specific applications in the area of aerospace, defense, automotive, and general engineering (Akhil et al., 2016). Sequential casting is one of the best methods for the production of bimetals with sound interface bonding between the metals. The interesting feature in the fabrication of functionally graded Al bimetal by sequential casting technique is the properties of the interface of the two Al alloys formed due to the direct contact of liquid metals during the process of solidification. Bimetals of aluminium alloys can combine their properties and can be used for various applications such as in heat exchangers and corrosive environments.

The standard design requirement for fuel consumption reduction in the aerospace and automotive industries favors the application of aluminium alloys and their composites. In this regard, aluminium alloys and their composites have yielded very exciting results and have remained the centre of attraction for cheap production (Lavernia et al., 1987). Due to the reasonable magnitude of hardness, high thermal conductivity, excellent castability and good weldability, good ductility, excellent resistance to corrosive environments, and pressure tightness of aluminium alloys, potential applications are found in diverse fields of engineering. In most cases, in aluminium design concepts, researchers integrate additional properties into a part and reduce the number of components for cost effectiveness. In a study by Ika Aachen on ‘‘Stiffness and Crash Relevance of Car Body Components,’’ it was observed that a weight reduction possibility in the use of high-strength steel in a car is about 11 %, but 40 % reduction is possible when steel is substituted with optimized aluminium materials. This has led to the continued increase in the necessity for improved Al-Si cast alloy components with consistent mechanical attributes for applications in strategic sectors. Aluminium casting alloys like the 319 series (Al-Si-Cu) have been

found useful due to reflective mechanical, casting, and heat treating properties possessed by the alloys. Several Al-Si based alloys, the 319 alloys, are increasingly being used in various engineering industries (Miller et al., 2000; Boileau et al., 2003 and Wang et al., 2004).

Bimetallic design and fabrication comes into play and is an ideal solution when a single type of material does not satisfy the functional requirements of high performance and efficiency at low cost. In this process, a continuous metallic transition occurrence is made by bringing two metals of different states (one solid and the other liquid) together to form contact with each other (Papis et al., 2008 and Perez-Bustamante et al., 2012). The process has attracted a lot of attention in the fabrication of aluminium/aluminium alloys, aluminium alloy/copper, aluminium alloy/cast iron, magnesium alloy/magnesium alloy, gray iron/copper, etc (Liu et al., 2015; Divandari et al., 2009; Lee et al., 2013; Viala et al., 2002 and Yang et al., 2003). Hajjari et al. have reported the dissimilar joining of Al/Mg light metals by compound casting process (Hajjari et al., 2011). Al/ Mg couples, aluminium and magnesium solid cylindrical inserts, were used for the compound casting. Aluminium molten metal was cast around the magnesium insert, while the magnesium insert was cast around by aluminium molten metal. During this process, a diffusion reaction takes place between two materials with one being solid and the other being in the liquid state, and thus, a continuous metallic transition occurs from one material to the other. But in casting aluminium melt around a magnesium insert, a gap was formed at the interface due to the formation of oxide layers around the aluminium melt and magnesium insert and because of the higher coefficient of thermal expansion of magnesium insert than aluminium. The sequential casting method involved the pouring of two different alloys/composite melts having similar freezing ranges into a mould sequentially to produce a continuous FGM (Wagstaff et al., 2011 and Kieback et al., 2003). Nevertheless, the application of this technique is still limited in aluminium alloys due to the formation of a thin layer of aluminium oxide. This layer makes aluminium alloy thermodynamically stable and has poor wettability by metallic melts. Also this oxide layers restricts the formation of metallic bonds between the metals with one part being solid and the other being liquid. This can only be rectified by permanent activation of the metal surfaces by reactive coatings like

zinc (Papis et al., 2008 and Rubner et al., 2011) or by pouring both metals in liquid condition. Recently, A356/A6101 aluminium bimetallic alloy was fabricated by squeeze-compound casting; A356 aluminium alloy molten metal was poured onto a 6101 aluminium solid bar and pressed together. The impact on the mechanical attributes and microstructure of the bimetal by pouring temperature, surface treatment, and pressure applied was studied. A sound metallic bonding was obtained between the two alloys of A356 and A6101, thereby good hardness and tensile strength were also yielded because of the squeeze pressure involved in the compound casting process (Liu et al., 2015). Bimetallic foils of 0.1 mm thick A1050/A6061 aluminium alloy were produced by accumulative roll bonding and asymmetric rolling using foils in a solid state condition. For roll speed ratios of 1 or 1.4, residual voids were observed and good interface bonding was obtained at a speed ratio of 1.2 between the bimetallic foils (Yu et al., 2014). Most studies on formation of bimetallic or two alloys in a single component are carried out by solid-state diffusion bonding process or by keeping one alloy as a solid or insert and casting the other liquid metal over it. Nevertheless, studies on formation of bimetallic FGM using two different alloys in molten state are limited and hence there is a large scope for investigation in this area.

In this study, a fairly new casting technique called ‘‘sequential casting’’ is used to produce functionally graded aluminium alloys by controlled mould filling of A390 aluminium alloy with A319 and A6061 aluminium alloys to form two different combinations of graded microstructures and the properties are evaluated at the alloy regions and at the interface. The versatility of this process lies in the achievement of enhanced properties at the interface with a good interfacial bonding between the two alloys by a simple sequential gravity casting method.

4.3 Experimental Methods

The alloys used for the formation of bimetallic functionally graded materials were A390, A319, and A6061 aluminium alloys, and their standard elemental compositions are depicted in Table 4.1.

Table 4.1. Standard elemental compositions of A390, A319 and A6061 alloys (wt. %)

Alloy	Al	Si	Cu	Mg	Fe	Mn	Zn	Ti	Ni	Cr
A319	85.8-91.5	5.5-6.5	3.0-4.0	0.10	1.0	0.50	3.0	0.25	0.35	-
A390	75.3-79.5	16-18	4.0-5.0	0.50-0.65	0.40	0.10	0.10	0.20	-	-
A6061	95.8-98.6	0.4-0.8	0.15-0.4	0.8-1.2	Max 0.7	Max 0.15	Max 0.25	Max 0.15	-	0.04-0.35

Two sets of FGM were fabricated by sequential casting viz. (1) A390–A319 alloy based FGM and (b) A390–A6061 FGM. The cleaned alloys were melted in two different clay graphite crucibles and degassed using hexachloroethane at 720 °C of melt temperature to remove the entrapped hydrogen from the melt and oxides formed. The oxide layers formed are removed from the top of the melt by skimming before pouring into the mould to ensure the melt quality. The melts were then superheated to a higher temperature of 760 °C. First, an A319 hypoeutectic cast alloy was poured into a permanent rectangular slab mould (165 mm x 90 mm x 45 mm) to fill half of the mould at 760 °C, and then the A390 hypereutectic cast alloy was poured over the first melt without any time delay to get the medium- and high-silicon combination of bimetallic FGM. In the second set, the A6061 alloy was used instead of A319 alloy to get the low- and high-silicon alloy combination leading to sequential cast bimetallic FGM. The second melt of A390 aluminium alloy was poured along the mould wall to avoid the creation of turbulence in the already poured first aluminium alloy. Since two different alloys were used in a single component, the effects of heat treatment conditions (T6) of both alloys were investigated. The typical heat treatment procedure applied to the discussed sequential cast systems were the T6 condition. The prescribed heat treatment conditions for A390 is a solution treatment at 495 °C for 8 hours and hot water quenched and age hardening at 175 °C for 8 hours; for A319, the solution treatment is 505 °C for 8 hours and age hardening at 155 °C for 5 hours; and for A6061 alloys, the solution treatment is 535 °C for 4 hours and age hardening at 175 °C for 8 hours. The heat treatment procedure of different alloy systems had been used and evaluated for its effect on hardness behaviour. The best conditions were chosen and used for other characterizations.

A Leica-DMRX optical microscope was used for the microstructural characteristics of as-cast samples of A390–A319 and A390–A6061 alloy systems by using standard metallographic procedures. The detailed surface analysis of the sequential cast specimens was carried out by using JEOL JSM-5600LV and Carl Zeiss EVO-18 scanning electron microscope (SEM). An Indentec Brinell hardness tester was used to measure the Brinell hardness number (BHN) of the as-cast and heat-treated sequential gravity cast samples for studying the effect of the heat-treated condition over the as-casts using a 2.5 mm diamond ball indenter with an applied load of 62.5 kg for 20 seconds. The chemical compositions of the functionally graded sequential cast alloy systems were carried out by using an optical emission spectrometer (SPECTROMAXx-AMETEK). The differential thermal analytical technique was used to study the thermal characteristics of the sequential gravity cast FGM samples with a standard HITACHI STA 7300 at different regions (A390, A319, and the interface of both alloy regions in the A390–A319 alloy system and A390, A6061, and the interface region of the A390–A6061 alloy system). The studies were performed at a standard heating rate of 10 °C/min up to a temperature of 800 °C beyond the melting point and alloy processing temperature. Later the alloys were cooled to the room temperature to examine the phase transformation that occurred while heating and cooling, from the large exothermic and endothermic peaks, obtained from the differential thermal analysis (DTA). X-ray diffraction analysis of the sequential cast specimens was done with the XRD-PAN analytical machine. The tensile and compression tests were carried out at a strain rate of 1 mm/min with a universal testing machine KIC-2-1000-C (capacity 100 kN). The tensile samples were prepared according to the ASTM standards B557M and were tested confirming the E-8 standard. The tensile and the compression samples were prepared such that the interface of both sequential alloy systems came at the centre or within the gauge length of the samples. The dry sliding wear tests were performed on a standard pin-on-disc wear testing machine (Ducom wear and friction monitor—20LE) that can measure tribological properties of the specimens from different portions of the cast slabs such as the frictional force, coefficient of friction, and wear volume between the surfaces in contact during the tests. A stationary pin holder of 6 mm diameter was accommodated in the pin-on-disc machine where the normal load was applied by using dead weights with the aid of string and special pulley arrangement, which can

bear a maximum load of 15 kg (147.15 N) directly onto the pin specimen of 6 mm diameter and 30 mm length. A high-carbon hardened En31 alloy steel of 165 mm diameter having a hardness of 63 HRC with a high degree of abrasion resistance, compressive strength, and material composition of Cu 1.00 %, Mg 0.50 %, Cr 1.40 %, and Si 0.20 % was used as the counter body. The tests were performed with eight different loads 1 kg (9.81 N), 2 kg (19.63 N), 3 kg (29.43 N), 4 kg (39.24 N), 5 kg (49.05 N), 6 kg (58.86 N), 7 kg (68.67 N), and 8 kg (78.48 N). All tests were continued with a constant sliding distance of 1800 m, and a velocity of 1 m/second was maintained throughout the test. The surface morphologies of worn-out pin surfaces were evaluated with the SEM to study the types of wear mechanisms during dry sliding. The sequential cast wear samples were heat treated to the T6 condition of A390 hypereutectic aluminium alloy since the region of aluminium 390 alloys was supposed to be exposed for the applications during the actual time of operation.

4.4 Results and Discussion

4.4.1 Microstructural observations

Figure 4.1 shows the optical images of a sequential gravity cast slab taken from the A390 region to the A319 region. After the pouring of 319 aluminium alloy at 760 °C into the mould, the melt started solidifying. During the solidification process, when the temperature reaches below 660 °C, the Al present in the 319 alloy starts solidifying as α-Al in the form of dendrites by rejecting the silicon into the liquid melt from the solidification front. The silicon has much less solid solubility in aluminium (<0.02 %) at this temperature. Thus, the liquid melt becomes enriched with silicon. When the temperature of the melt reaches down to the eutectic temperature, then the rich silicon containing Al alloy liquid transform into eutectic structure giving a lamellar structure of silicon and aluminium. The eutectic silicon is precipitated inside the interdendritic spacing of α-Al. The entire melt of 319 aluminium alloy will solidify within 10 seconds after the pouring. The 390 aluminium alloy is poured over 319 alloy at 780 °C within 5 seconds after the pouring of 319 aluminium alloy. If the pouring of the second melt is delayed by more than 5 to 7 seconds, the first melt poured starts solidifying and the chances of diffusion of the two melts to obtain good interface bonding is much less. This was observed during the process parameter

optimization. As soon as the 390 liquid melt comes in contact over the semisolid 319 alloy, it remelts the latter, which is already in the process of solidification and intermingling of the elements takes place because of the higher superheat involved in the 390 aluminium alloy. The remelting and intermingling of the elements are not only a result of the higher superheat of the melt but also depends on the difference in the liquidus temperatures of the 319 (604°C) and 390 (649°C) alloys. During the process of remelting and intermingling of two alloys, both the liquid and solid states co-exist. The 390 alloy also starts solidifying from the solidification front by precipitating out the α-Al by rejecting the silicon into the liquid. As the silicon is moving toward the liquid, the liquid melt becomes richer in silicon and it approaches the eutectic composition. So the intermingled region will get more time for the solidification and it solidifies only when the temperature drops to eutectic temperature. As the percentage of silicon in the liquid melt exceeds the eutectic point, silicon precipitates out in the form of cuboids. Figure 4.1(a) shows the A390 alloy region of the sequential gravity cast slab (A390–A319) that contains both eutectic and cuboids of primary silicon. The primary silicon phases can easily be identified as the large gray color cuboidal structure that can be found in the microstructures. Figure 4.1(b) is showing the interface region of the two metals (A390 and A319) that is intermingled between the two melts of aluminium 390 and 319 alloys during the time of solidification. The interface in Figure 4.1(b) contains cuboids of primary silicon and eutectic silicon because at this region the solidification of the first poured 319 already gets solidified. The silicon is not completely developed to the cuboidal structure because the solidification takes place rapidly and the intermingling of the elements has not occurred properly at this mould wall side. The interface at Figure 4.1(c) indicates a diffused interface containing more of the eutectic silicon because this region is the last solidified region among the interface and proper intermingling and redistribution of silicon happens. Also, the solidification takes places in the direction of heat transfer. Some alpha aluminium dendrites grow in the direction of heat flow toward the mould side, which interlocks the melts at the interface. The interface region is the combination of the two melts that are well bonded to each other during the solidification. The elements, mainly silicon in the A390, diffuse into the A319 alloy reconfiguring the composition and maintaining the equilibrium at the interface. Figure 4.1(c) also contains intermediate regions of A390

and A319 alloy depicting the natural infiltration of the 390 aluminium melt into the shrinkage portions of the 319 aluminium metal that occurred during the process of solidification. The region of A319 alloy indicated in Figure 4.1(d) contains some clusters of eutectic silicon diffused from the high-silicon A390 alloy as a result of the natural infiltration and redistribution of silicon from the 390 melt into the 319 metal through alpha aluminium. The diffusion type of the bonding pattern is mainly observed throughout the interface of the bimetal alloy.

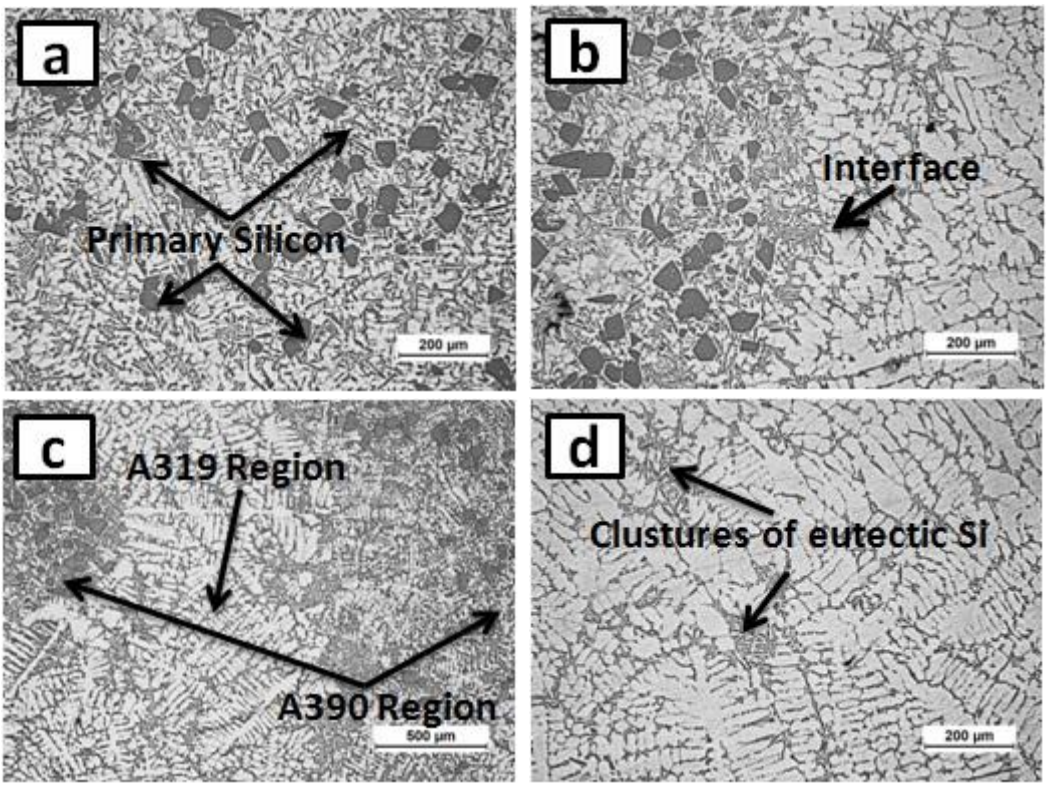

Figure 4.1 Optical micrographs of sequential gravity cast A390-A319 bimetallic aluminium alloy, taken from A390 portion to A319 portion at different locations (a) A390 region at 10x (b) Interface near mould side at 10x (c) Interface at the centre at 5x and (d) A319 region at 10x

Figure 4.2 shows the optical micrographs of A390–A6061 sequential gravity cast slab aluminium alloys. The optical micrographs are taken from the A390 region to the A6061 region. The pouring of 6061 aluminium alloy at 780 °C to the half of the slab mould results in the solidification of 6061 within 5 to 8 seconds by precipitating pure aluminium nearer to the mould side. The liquid melt becomes richer with silicon composition during the solidification of the aluminium as α-Al and rejection of silicon from the solidification front. During this process, the 390 alloy is poured into the

balance half of the mould within 5 seconds after the first pouring. The primary silicon, eutectic silicon, and alpha aluminium are observed in Figure 4.2(a), which is present in the hypereutectic A390 aluminium alloy at the top of the cast slab. A sharp interface between A390 and A6061 is obtained in the A390–A6061 sequential cast system, which is clearly evidenced from Figure 4.2(b). The liquidus temperature of 6061 aluminium alloy is 652 °C and that of 390 is 649 °C. The sharp interface is formed as a result of the immediate solidification of the low-silicon A6061 alloy. The sharp interface at Figure 4.2(b) is enriched with eutectic silicon and small-sized cuboids of silicon. This is caused by the intermingling of silicon, which has not properly happened because of the rapid solidification at the mould side; nevertheless, a minor scale interfacial diffusion has occurred. The solidification of the 6061 alloy is faster than when compared with 390 aluminium alloy because the superheat involved in the 390 alloy is not sufficient enough to remelt the solidified layers of 6061 aluminium alloy and the difference in the liquidus temperature is only 3 °C. The 390 liquid melt diffuses into the 6061 melt at the centre portion, and it remelts some layers of already solidified 6061 metal and bonding takes place. Apart from the aluminium 390–319 sequential cast combination, the 390–6061 aluminium alloy bimetal has a sharp interface, which is mainly a result of the minor difference in their liquidus temperatures. As described in the previous section, this combination of sequential cast system also shows a shrinkage portion in the first metal, which was naturally infiltrated by the 390 melt into the 6061 aluminium alloy, and the infiltrated portions [Figures 4.2(c) and (d)] are also enriched with smaller sized cuboids and eutectic silicon. Figure 4.2(d) represents the region that belongs to A6061, which contains alpha aluminium and a minuscule amount of eutectic silicon. Here, in the case of a 6061–390 sequential cast slab combination, diffusion type bonding is observed throughout the interface.

4.4.2 Scanning electron microscopy (SEM) and EDS analysis

Figure 4.3 shows the SEM micrographs at the interface of sequential cast A390–A319 and A390–A6061 aluminium alloys. Figure 4.3(a) corresponds to the interface of the A390–A319 aluminium alloy, which indicates the presence of primary silicon in the 390 aluminium region and the alpha aluminium-rich area in the A319

aluminium alloy with a small amount of eutectic silicon. Nevertheless, the interface region of these two alloys is considered a distinct interface; it is perfectly bonded as it

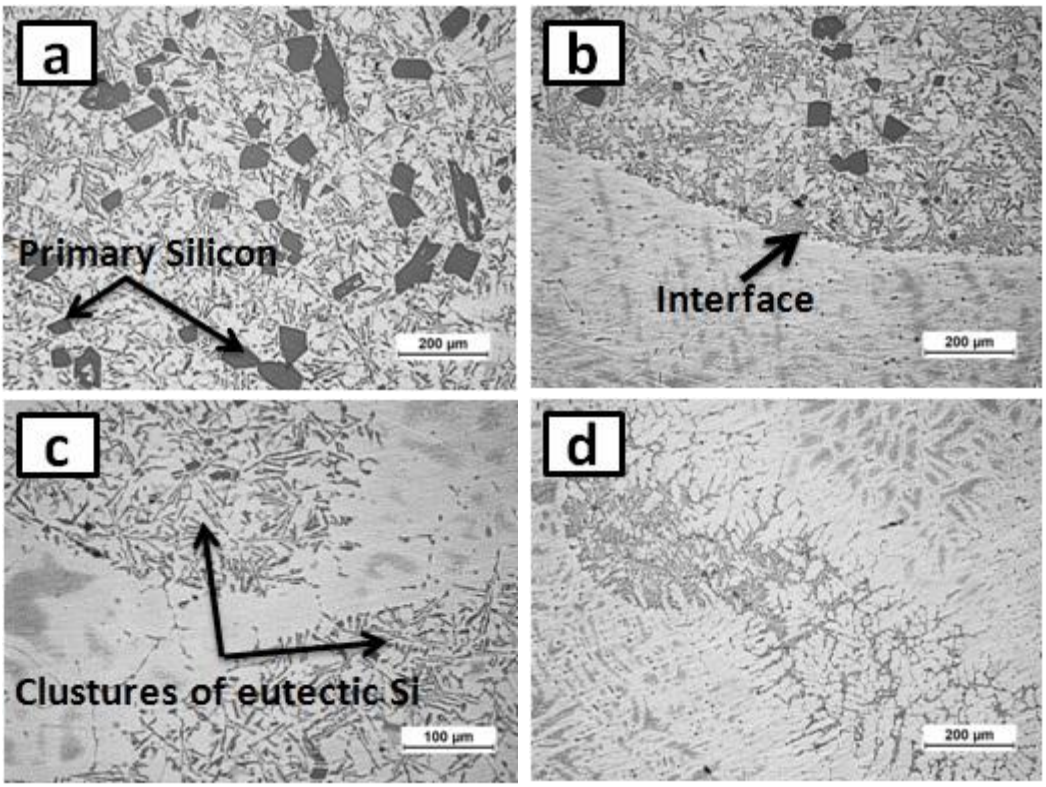

Figure 4.2 Optical micrographs of sequential gravity cast A390-A6061 bimetallic aluminium alloy, taken from A390 portion to A6061 portion at different locations (a) A390 region at 10x (b) Interface near mould side at 10x (c) Interface at the centre at 5x and (d) A6061 region at 10x

is clearly observed in the SEM image. The interface of the A390–A6061 sequential cast alloys shows [Figure 4.3(b)] both characteristics of the parent metal. From the interface of both alloy systems, i.e., the high–medium silicon alloy system and high–low silicon alloy systems, show perfect bonding of the metals. A few porosities are observed in the high–low silicon alloy system. The SEM analysis at the interface further confirms the proper bonding between the metals in both sequential cast systems.

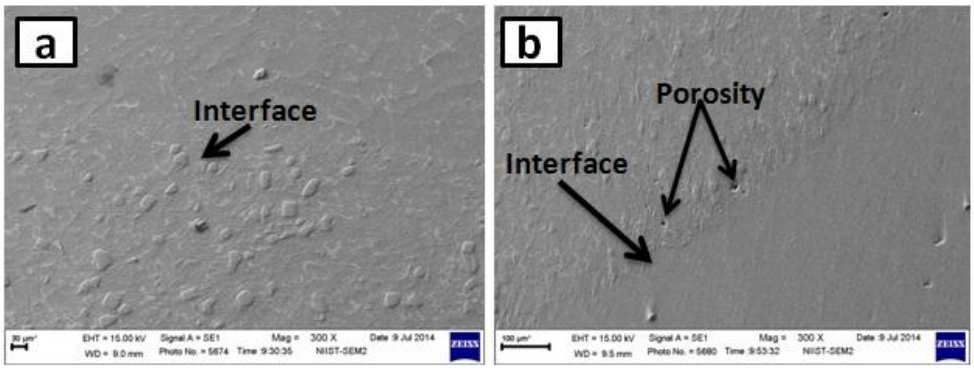

Figure 4.3 SEM images of sequential gravity cast (a) A390-A319 and (b) A390-A6061 bimetallic aluminium alloy at interface

EDS analyses of sequential cast A390–A319 and A390–A6061 aluminium alloy systems are shown in Figures 4.4 and 4.5. The EDS analyses at the interface of the both systems also confirm the diffusion of the two metals at the interface. The silicon percentages at the interface show an intermediate percentage of two alloys in both types of sequential alloy systems.

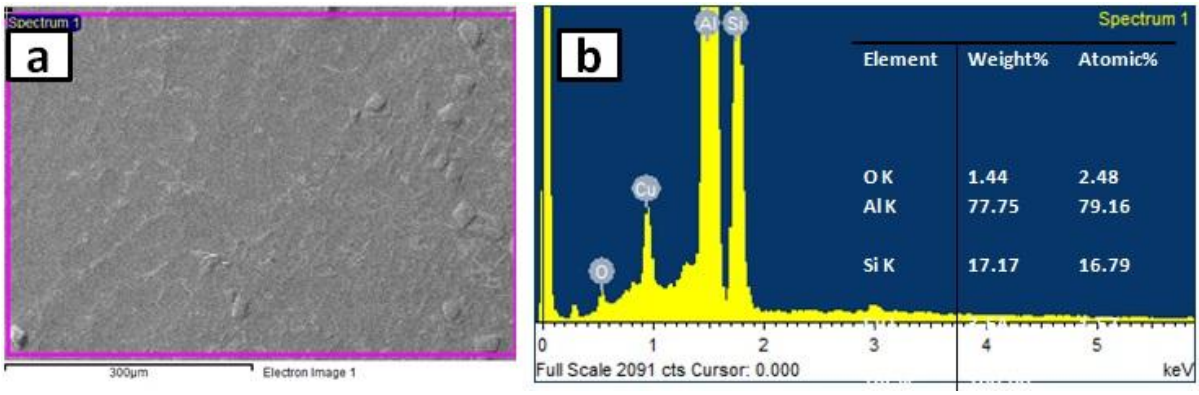

Figure 4.4 EDAX analysis at interface of sequential gravity cast A390-A319 bimetallic aluminium alloy (a) SEM and (b) EDAX analysis

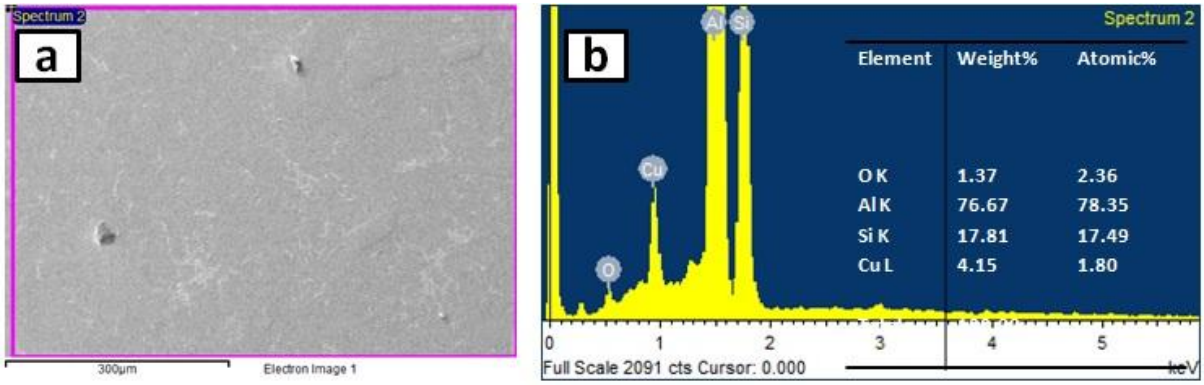

Figure 4.5 EDAX Analysis at interface of sequential gravity cast A390-A6061 bimetallic aluminium alloy (a) SEM and (b) EDAX analysis

4.4.3 Optical emission spectroscopy (OES)

Tables 4.2 and 4.3 show the optical emission spectroscopy results of as-cast and heat-treated condition of A390–A319 sequential gravity slab cast.

Table 4.2. Optical emission spectroscopy results of as-cast samples of sequential cast A390-A319 aluminium alloys at regular intervals of 10 mm on either side of the interface (wt. %)

Condition	Location	Si	Cu	Mg	Fe
As-Cast	A 390 Portion	18.943	4.082	0.335	0.404
	Conical Interface	14.204	3.668	0.332	0.37
	Straight Interface	16.814	4.113	0.331	0.4
	A 319 Portion	5.91	3.744	0.038	0.209

Table 4.3. Optical emission spectroscopy results of heat treated samples of sequential cast A390-A319 aluminium alloys at regular intervals of 10mm on either side of the interface (a) heat treatment of A390 and (b) heat treatment of A319 (wt. %)

Condition	Location	Si	Cu	Mg	Fe
Heat Treatment of A 390 (T6)	A 390 Portion	18.83	2.824	0.192	0.357
	Conical Interface	21.072	1.800	0.679	0.236
	Straight Interface	14.880	1.800	0.934	0.264
	A 319 Portion	6.256	2.639	0.016	0.183

(a)

Condition	Location	Si	Cu	Mg	Fe
Heat Treatment of A 319 (T6)	A 390 Portion	20.276	2.489	0.432	0.525
	Conical Interface	16.744	2.599	0.185	0.324
	Straight Interface	18.980	2.872	0.338	0.712
	A 319 Portion	5.960	2.480	0.019	0.174

(b)

The tests are conducted in three regions; A390 region, interface, and A319 region. Two types of interfaces, namely, conical interface at the centre of casting and straight interface near the mould wall surface, are observed. The conical interface is formed in the centre of the bimetallic casting as a result of the diffusion of liquid

metal into the shrinkage portion of the first poured metal and the better miscibility of two different alloys provided good bonding in this region. The straight interface is observed near the mould wall at the outer surface because of faster cooling rate experienced by the alloy near the mould wall.

It is observed that the A390 region shows 18.94 % of Si, which is the permissible limit of the A390 alloy system, whereas the A319 region shows a silicon percentage of 5.91 that is also within the limit for A319 aluminium alloy. Meanwhile, the interface of the two metals shows a value of 16.81 % Si as a result of the diffusion of the second melt into the first melt during its solidification process. Thus, the interface acts as a combination of the two metals. As the newly fabricated sequential cast product contains two types of aluminium alloys, specific heat treatment must be provided to the product according to the particular application.

Table 4.3 gives the optical emission spectroscopy results of samples of A390–A319 sequential slab cast with heat treatment of A390 and A319 aluminium alloys, respectively. Table 4.3(a) shows the elemental analysis of a heat-treated A390–A319 sequential slab cast with T6 condition of A390 alloy. The regions belonging to A390 and A319 alloy show the permissible limits of the silicon percentage, whereas the interface shows a slight higher percentage of silicon than the standard composition. This is a result of the diffusion of primary silicon present in the hypereutectic A390 aluminium alloy and of the eutectic silicon present in the hypoeutectic A319 aluminium alloy.

Optical emission spectroscopy results of A390–A6061 sequential gravity slab cast are depicted in Tables 4.4 and 4.5. The OES examination is carried out (Table 4.4) at three regions, in A390, A6061, and the interface region of both metals, and it is found that the regions other than the interface region show the percentage of the silicon within its standard composition limit. The interface gives an intermediate composition of both alloys analogous to the A390–A319 system. Table 4.5(a) and (b) shows the OES results of heat-treated (T6 condition for A390 and A6061) samples of the A390–A6061 system. In this case of heat-treated samples, there is not much diffusion of primary and eutectic silicon of the A390 and A6061 aluminium alloys because the solidification in A6061 is faster than when compared with the

hypereutectic A390 alloy. Also, the parent alloy region showed the percentage of the elements within the limits only under both heat-treated conditions.

Table 4.4. Optical emission spectroscopy results of as-cast samples of sequential cast A390-A6061 aluminium alloys at regular intervals of 10mm on either side of the interface (wt. %)

Condition	Location	Si	Cu	Mg	Fe
As-Cast	A390 Portion	19.635	2.397	0.476	0.557
	Conical Interface	10.58	1.342	0.535	0.26
	Straight Interface	9.302	1.80	0.506	0.233
	A 6061 Portion	0.945	0.301	0.696	0.122

Table 4.5. Optical emission spectroscopy results of heat treated samples of sequential cast A390-A6061 aluminium alloys at regular intervals of 10mm on either side of the interface (a) heat treatment of A390 and (b) heat treatment of A6061 (wt. %)

Condition	Location	Si	Cu	Mg	Fe
Heat Treatment of A 390 (T6)	A 390 Portion	20.954	2.668	0.365	0.355
	Conical Interface	16.709	2.69	0.419	0.348
	Straight Interface	10.306	1.916	0.425	0.271
	A 6061 Portion	2.034	0.479	0.559	0.11

(a)

Condition	Location	Si	Cu	Mg	Fe
Heat Treatment of A 6061 (T6)	A 390 Portion	21.409	3.084	0.452	0.537
	Conical Interface	16.893	2.585	0.405	0.355
	Straight Interface	11.485	2.878	0.577	0.392
	A 6061 Portion	1.065	0.574	0.586	0.137

(b)

4.4.4 Differential thermal analysis (DTA)

Figure 4.6 shows the DTA of different regions of sequential cast A390–A319 and A390–A6061 aluminium alloys, respectively. In all three regions, i.e., A390, A319, and the interface of both, almost the aluminium and eutectic silicon melts at the temperature of 560 °C indicated by the endothermic peak [Figure 4.6(a)]. At a temperature of 512 °C, the $CuAl_2$ phase starts melting. In the case of A319 alloy, the primary Al melting is observed at 605 °C. From Figure 4.6(b), it is clearly evident that

the solidification range of the A390 and A6061 is not close and the solidification is very fast in the case of A6061 as already discussed in the microstructural evaluation. The major component aluminium in A390 melts at same 560 °C in this instance also, but in A6061, it is nearly 645 °C. Since low-silicon alloys are enriched with alpha aluminium, no other main phase transformation is observed in the DT Analysis. From the Figures 4.6(a) and (b), it is observed that the interface is having an intermediate curve among the curves obtained from the differential thermal analysis.

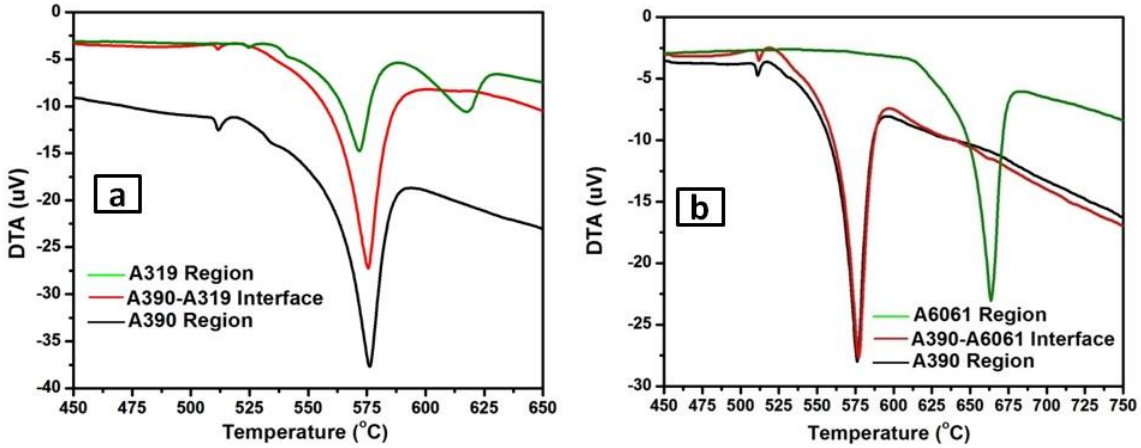

Figure 4.6 DTA of sequential gravity cast (a) A390-A319 and (b) A390-A6061 bimetallic aluminium alloy

4.4.5 XRD analysis

Figure 4.7 presents the X-ray diffraction analyses carried out at the pure alloy regions and interfaces of sequential gravity cast systems. The diffraction analyses show the intensity peaks of major composition aluminium at different diffracted angles of 2θ at 38.47 ° and the succeeding peaks at 44.74 °, 65.13 °, 78.23 °, and 82.43 °, as per the JCPDS database, which is also similar to the peaks identified by Bustamante et al. (Perez-Bustamante et al., 2012). The peaks of silicon are also present in the analysis at a 2θ angle of 28.44 °, 47.29 °, 56.11 °, 69.13 °, 76.37 °, and 88.02 ° (Perez-Bustamante et al., 2012).

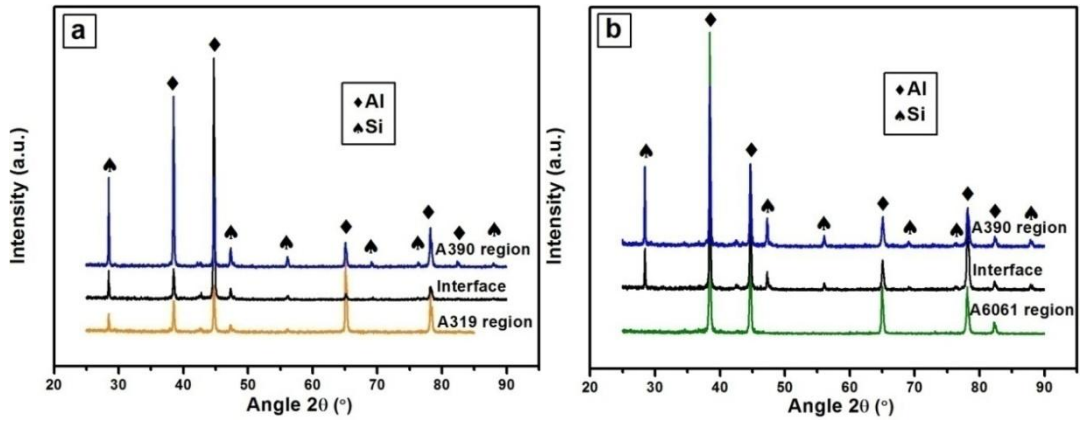

Figure 4.7 XRD analysis of sequential gravity cast bimetallic aluminium alloys (a) A390-A319 and (b) A390-A6061

4.4.6 Hardness

As-cast and heat-treated hardness values of sequential gravity cast FGM samples of A390–A319 and A390–A6061 under different heat treatment conditions are shown in Figure 4.8. An average of five hardness values were taken and plotted in each condition. Figure 4.8(a) shows the as-cast and heat-treated (T6 condition for A390 and A319) hardness of A390–A319 combination of sequential gravity slab. The hardness results in BHN yields a maximum hardness of 160 in the heat-treated sample at the A390 region and a minimum hardness of 105 BHN at the A319 region of the A390–A319 alloy system. The specimen heat treated using the standard A390 T6 heat treatment condition shows higher hardness values compared with the A319 alloy heat treatment parameters. Hence, for further studies on the A390–A319 sequential cast alloy system, the standard A390 T6 heat treatment procedure is followed.

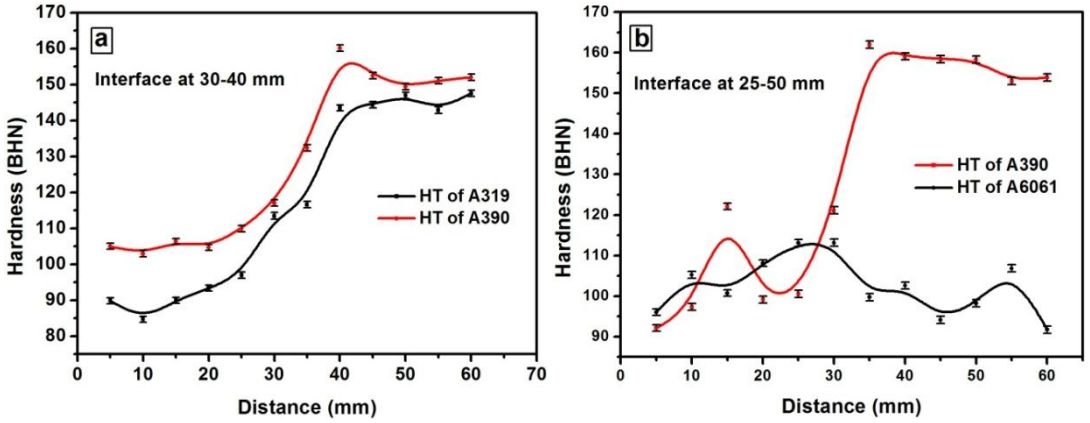

Figure 4.8 Hardness profile of sequential gravity cast bimetallic aluminium alloys (a) A390-A319 and (b) A390-A6061

As-cast and heat-treated hardness of A390–A6061 combinations are shown in Figure 4.8(b). The hardness profile of A6061 region (0-25 mm) shows lower hardness values than A390 region from one end of the sample to the other, when the heat treatment procedure for A390 alloy is followed (red line curve). A maximum hardness of 160 BHN and a minimum of 91 BHN is obtained at the A390 region and the A6061 region, respectively, for the heat-treated sample (T6 condition of A390) of the A390–A6061 alloy system. Using the standard T6 heat treatment procedure of A6061 to the A390–A6061 sequential gravity cast slab, a maximum of 113 BHN at the A390 region, and a minimum of 91 BHN is obtained at the A6061 region. The hardness of the A390 alloy is reduced from 160 BHN to 113 BHN since the region of A390 underwent the heat treatment of A6061. An intermediate hardness of 132 BHN and 116 BHN is observed at the interface of the A390–A319 aluminium alloy system; and 121 BHN and 113 BHN for the A390–A6061 system. The hardness value at 15 mm of A390–A6061 alloy system heat treated using 390 procedure shows a higher hardness of 122 BHN due to the diffusion of higher silicon 390 alloy into the low silicon 6061 region (Figure 4.2d). The variation in hardness behaviour is having good correlation with the observed results of the optical microstructures, SEM, EDS, OES and XRD of the respective regions. Since the standard T6 heat treatment procedure of 390 alloy have provided better hardness values that the 6061, for all the remaining studies, the A390 heat treatment conditions are used in both sequential cast FGM systems.

4.4.7 Tensile and compression properties

A390–A319 sequential cast heat-treated samples show a tensile strength of 337 MPa and a compressive strength of 490 MPa. The sequential cast aluminium A390–A6061 alloy shows a tensile strength of 364 MPa and a compressive strength of 401 MPa, and the values obtained are within the ranges of the strengths of the parent alloys. It was noticed that the interfaces of the bimetallic systems are robust enough to withstand the loads because the fracture has not occurred at the interface rather than at the base alloy region of A319 and A6061 during the tensile and compression tests.

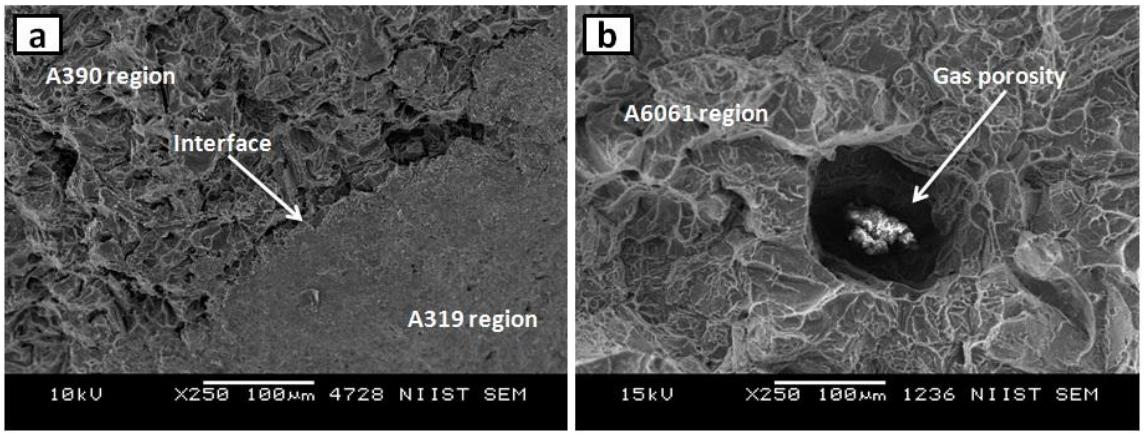

Figure 4.9 SEM analysis of fracture surface of tensile specimens (a) A390-A319 and (b) A390-A6061

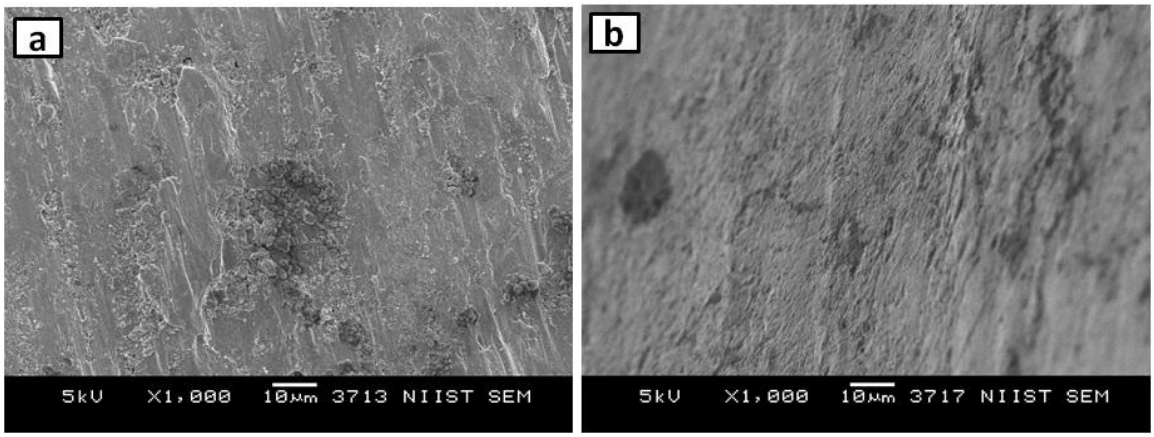

Figure 4.10 SEM analysis of fracture surface of compression specimens (a) A390-A319 and (b) A390-A6061

Figure 4.9 shows the SEM analyses of the fractured tensile surface of sequential cast bimetallic aluminium alloy systems. Figure 4.9(a) reveals the interface region of the A390–A319 system; it is clear that the crack occurs at the interface region and proceeds through the weakest 319 alloy region. Nevertheless, the tested tensile specimen does not reveal the occurrence of fracture at the interface. Even though the fracture analyses show the interface of both alloys, it has a tensile strength of 337 MPa that is sufficient for standard engineering applications. Fractured SEM analyses of the A390–A6061 system presented in Figure 4.9(b) reveals that the region of A6061 is highly ductile and the presence of porosity observed on the surface leads to the fracture of the tensile specimen. The presence of gas porosity is also found in the interfacial region in A390–A6061 sequential cast FGM as observed in Figure 4.3. The standard tensile properties of the base alloys of A390, A319, and A6061 are 310, 234, and 310 MPa, respectively, under respective

T6 conditions. From the present study, the tensile and compressive strength properties of the sequential cast systems are higher than the standard tensile values of A390, A319, and A6061 base alloys as a result of better bonding formed by diffusion of alloy melts at the interface of the bimetallic alloy systems. The compression fracture takes place normally at a 45° angle to the loading axis for brittle materials. The typical compressive fracture of A390–A319 and A390–A6061 sequential cast aluminium alloys are shown in Figure 4.10. Unlike a tensile fracture, the compressive fracture takes place by sliding of fracture parts one over the other. The fractured compressive structures are partially brittle in nature showing surface irregularities. The crack propagation in compressive test samples have occurred near the interface in the A319 and A6061 area of A390–A319 and A390–A6061 sequential cast aluminium alloys specimens, respectively. The sliding of the specimen initiates at the high stress concentration area or in the defective area. The hardness studies have shown higher hardness in the 390 region compared with the 319 and 6061 regions. In relation to hardness values, the tensile and compressive fracture also occurs near the interface and proceeds toward the 319 and 6061 alloy regions in the respective sequential cast systems.

4.4.8 Wear studies

The wear rate of the sequential gravity cast A390–A319 and A390–A6061 systems are shown in Figure 4.11. The wear rate is computed in mm^3/Nm by taking the difference in the initial and final weights of the respective pin specimens before and after the test. Figure 4.11(a) illustrates the wear rate of the A390 region of the sequential gravity cast A390–A319 alloy. The wear of A319 region shows a decrease in the wear rate upto 39.24 N, then increase upto 58.86 N and almost closest value of 58.86 N upto 78.48 N. But in A390 region, the wear rate values decreases upto 29.43 N, then increases upto 49.05 N, then decreases to 58.86 N and maintains almost close values afterwards. This increase and decrease in the values of wear rates at different loads are due to the formation of protective layers of MML and its breaking due to high pressure of further loading. The A390 region shows less wear rate compared with the wear rate of the A319 region. An oxidative and delamination wear mechanisms are the dominant wear mechanisms found at lower and higher loads, respectively (Gui et al., 2001). The primary silicon present in the hypereutectic

aluminium 390 alloy gives a higher hardness. Thus, a high wear resistance is obtained in the 390 region of the specimen. A low wear rate of 3.60887 x 10^{-12} mm^3/Nm is attained at a normal load of 58.86 N at the A390 region as compared with other higher loads. Since A319 is a hypoeutectic Al-Si alloy, the specimens from the 319 aluminium alloy region always show a higher wear rate in almost all loads because it contains only eutectic silicon, which is less hard than the primary silicon present in the A390 aluminium alloy. Figure 4.11(b) shows the wear rate graph of sequential gravity cast A390–A6061 aluminium alloy. From the graph, it is clear that the A390 region specimens show greater resistance to wear as a result of the presence of primary silicon as discussed in the previous section. Samples of the A6061 region suffer a high magnitude of wear even at the lowest load of 29.43 N. At this load, the specimens of the A6061 region undergo severe wear as the material undergoes severe plastic deformation because the material contains mainly aluminium phases with less silicon. It is further noticed that mild-to-severe wear transition takes place in the 6061 alloy region at lower loads of 29.43 to 49.05 N.

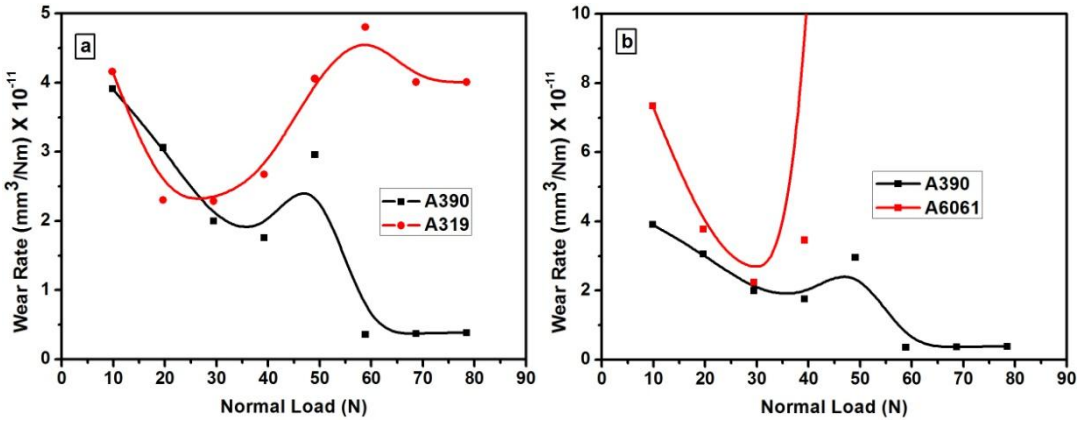

Figure 4.11 Wear rate values of sequential gravity cast bimetallic aluminium alloys (a) A390-A319 and (b) A390-A6061

4.4.9 Worn surface analysis

Figure 4.12 shows the SEM micrographs of the worn surface of sequential gravity cast A390-A319 alloy specimens tested on different loads. The hypereutectic aluminium alloys are extensively used in the automobile industry, especially for cylinder liner applications. The wear resistance is provided by the fine and even distribution of homogeneous primary silicon particles present in A390 alloy (Gautam et al., 2015). Figure 4.12(a) through (d) comprises the SEM micrographs showing

worn surfaces of the A390 region and Figure 4.12(e) through (h) shows the micrographs of 319 region at various loads of 19.62 N, 39.24 N, 58.86 N, and 78.48 N respectively in A390–A319 sequential gravity cast samples. At a lower load of 19.62 N, the worn surface shows very fine wear scars in Figure 4.12(a) compared to Figure 4.12(e) which is due to comparatively lower wear rate in 390 alloys. Figure 4.12(b) shows the wear debris detached from the surface of the specimen during the wear test. The hard debris particles or phases separated from the surface of the specimen lead to two-body or three-body abrasive wear further. A large number of grooves and dimples are present in the worn-out surfaces. Formation of the dimples took place at lower loads, and the dimples became larger when the applied normal load was increased (Gui et al., 2001). Figures 4.12(c) and (d) show the plastic deformation happened to the surface of the specimen (A390 region) under the action of higher loads. The debris detached from the parent material during wear removed from the surface as a result of the plastic deformation at higher loads. The width of the wear scar is wider at a maximum load of 78.48 N compared with the width of scars at the 58.86 N load. The plastic deformation leads to excessive wear of the specimen. The hard primary silicon cuboids have an abrasive action on the En 31 counter surface steel. During the process of sliding, the iron is detached from the counter surface as a result of the micro cutting of the steel disc by the hard primary silicon particles and gets part into the wear debris (Gui et al., 2001; Alshmri et al., 2014 and Show et al., 2014).

From Figures 4.12(e) it is clear that at a lower load of 19.62 N wearing of surface forms oxide layers. These oxide layers protect the specimen surface leading to severe wear. Since the region of experiment belongs to hypoeutectic composition, the ductile nature of the materials helps the material to suppress the formation of wear debris and thereby reduces the chances of three-body abrasions. At higher loads, the plastic deformation occurs, which is evident from Figures 4.12(g) and (h). Figure 4.12(h) shows a tear in the surface of the material that is a result of the detachment of a hard phase and rubbing between two surfaces (specimen and the counter surface). Earlier studies reported that a small amount of Fe_2O_3 and Al_2O_3 was found on the worn surface analysis (Gui et al., 2001 and Kumar et al., 2013). Iron oxides have only a low coefficient of friction and provide a lubrication effect during

rubbing that helps in reducing the rate of wear. This ensures the surface had undergone an oxidative type of wear. The formation of oxide layers protects the specimen surface from direct metal-to-metal contact (Kumar et al., 2013). Also, mechanically mixed layers (MMLs) play a vital role in the reduction and increase of wear rate in some cases. Iron, oxides of iron and aluminium, and intermetallic compounds of aluminium-iron formed during the rotational sliding in the pin-on-disc wear test helps in the development of the MML that is getting sandwiched between the rubbing surfaces of the specimen and the counter surface. The wearing and tearing of the MML formed on the rubbing surface of the specimen leads to an increase or decrease in the wear rate depending on the certain conditions such as the pressure at higher loads and sliding velocity. All the time, MML cannot protect the surface from severe wear conditions because that depends on the service conditions like lower sliding speeds at higher loads and higher sliding speeds at lower loads. The steady and low wear rates at the lower loads are a result of the less effective contact area between the two surfaces in sliding (Show et al., 2014). At higher loads, delamination wear takes place because of the subsurface cark formation and penetration into the pin material causing higher wear rate (Gui et al., 2001). Delamination always happens as a result of the local adhesion of surfaces in contact and its consequent breakdown followed by the work-hardening effect of the subsurface. This causes the initiation and propagation of the cracks which will ultimately result in layer by layer delamination of metals in the form of thin sheared sheets (Show et al., 2014). Hard cuboids of primary silicon help prevent the hypereutectic aluminium alloy from severe wear rate.

Figures 4.13(a) through (h) shows the SEM images of worn surface analysis of A390-A6061 at 19.62 N, 39.24 N, 58.86 N, and 78.48 N loads, respectively, as in the A390–A319 alloy system. In the case of hypoeutectic and eutectic aluminium alloys, the size and shape of the eutectic silicon decides the rate of wear and the resistance (Chandrashekharaiah et al., 2009; Vencl et al., 2010 and Cruz et al., 2010). A similar phenomenon is observed in this case also as in the case of the A390 region in the A390–A319 system because both alloys are the same. The worn surface analysis of the A6061 region in the A390–A6061 system is depicted in Figure 4.13(e) through(h). Here the loads used in the wear tests are 19.62 N, 29.43 N, 39.24 N, and

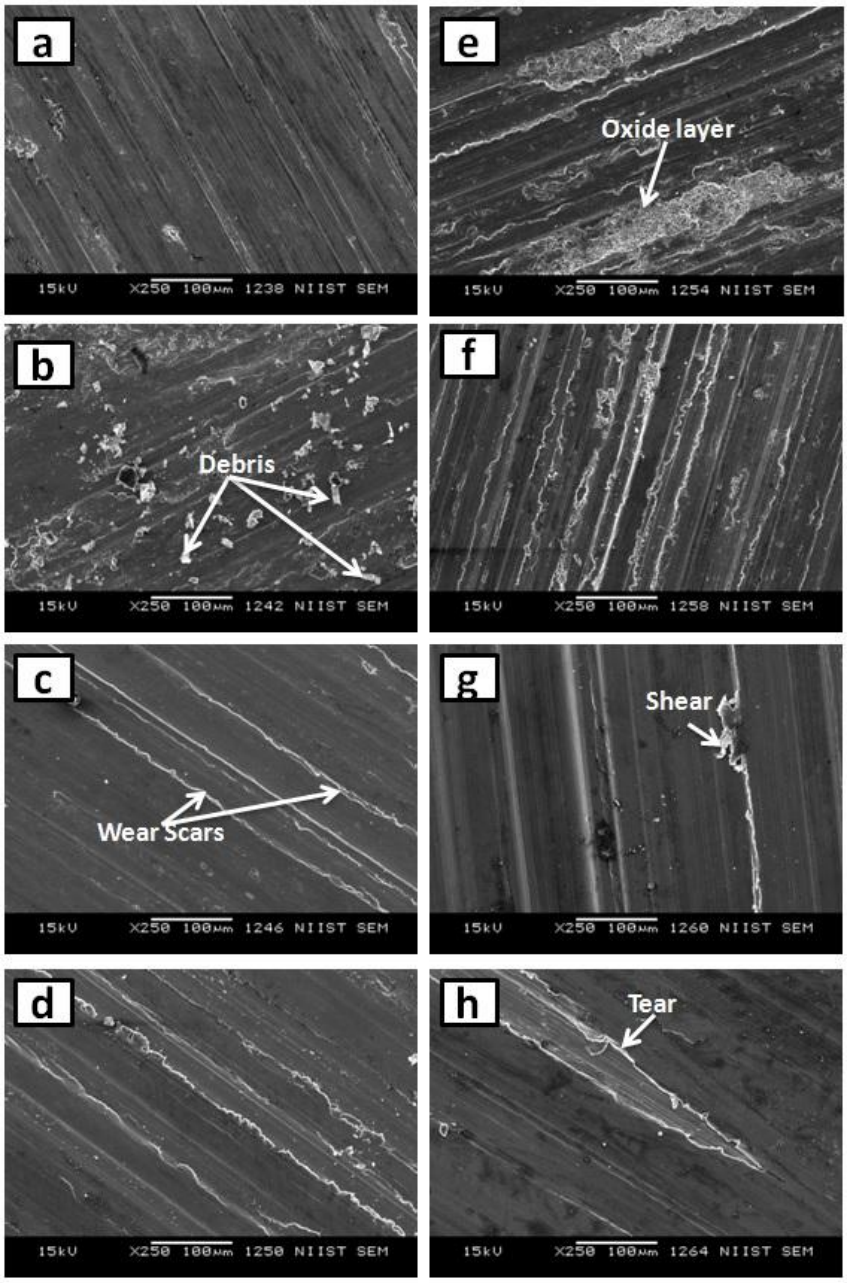

Figure 4.12 SEM micrographs of the worn surface of sequential gravity cast A390-A319 bimetallic aluminium alloy (a-d) A390 region and (e-h) A319 region at loads of 19.62 N, 39.24 N, 58.86 N and 78.48 N respectively

49.05 N, respectively. The 6061 aluminium alloy has a composition of almost pure aluminium, and the specimens possess lower hardness and cannot withstand higher loads. At the lower load itself, the material started to deform plastically during the test, which is visible from the micrographs. Formation of laminar planes is also visible in the micrographs of the specimen of the A6061 region as a result of severe plastic deformation. In both sequential cast systems, the A390 region had undergone only less wear than the other region. The presence of primary silicon in A390 blocks

the starting of delamination wear of the material. Because of the higher frictional heating at higher loads, the ploughing marks become deeper and generated oxide is more. The wear is proportional to the load and the running distance. A lower load with longer running distance and higher load with shorter running distance also leads to excessive wear of the material.

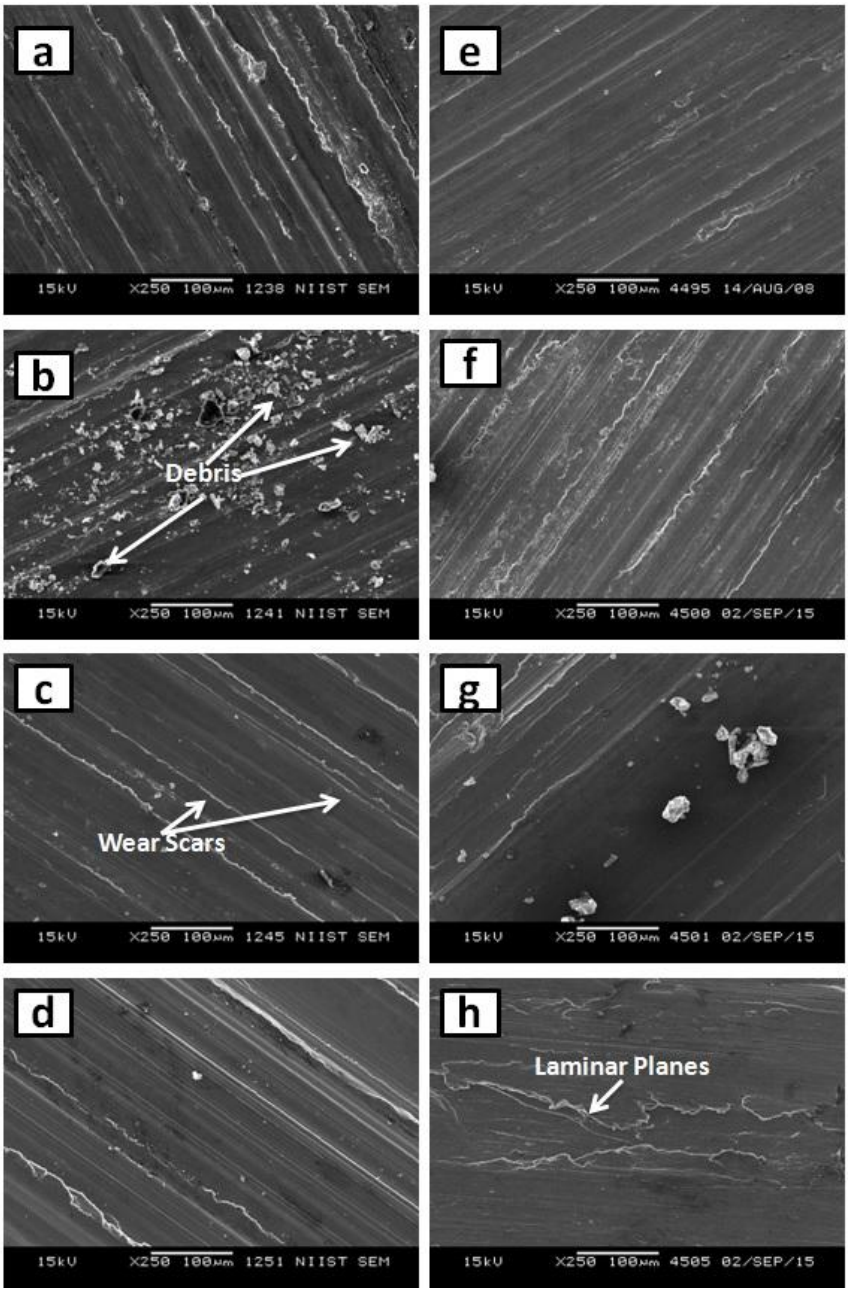

Figure 4.13 SEM micrographs of the worn surface of sequential gravity cast A390-A6061 bimetallic aluminium alloy (a-d) A390 region at loads of 19.62 N, 39.24 N, 58.86 N and 78.48 N and (e-h) A6061 region at loads of 19.62 N, 29.43 N, 39.24 N and 49.05 N respectively

4.4.10 Conclusions

A sequential gravity casting technique is used successfully to fabricate functionally graded cast A390–A319 and A390–A6061 aluminium alloys. During the process of casting, the temperature of the second pouring metal remelts the first poured metal that is already in the process of solidification. The heat treatment is based on the region that is useful for the engineering applications during the actual time of operation. A maximum hardness of 160 BHN is obtained in both sequential gravity cast alloys at the A390 region, and a minimum hardness of 105 BHN and 91 BHN are obtained in A390–A319 and A390–A6061 systems, respectively, at the heat-treated samples. The microstructure and OES results are in excellent agreement with the magnitude of hardness. The A390–A319 system has a tensile strength of 337 MPa and a compressive strength of 490 MPa, whereas A390–A6061 shows 364 and 401 MPa, respectively. The tensile and compression tests proved that the interface has excellent bonding between the metals. The region of A390 aluminium in A390–A319 and A390–A6061 sequential gravity cast system shows better wear resistance properties than do the A319 and A6061 regions. Both abrasive and adhesive types of wear mechanisms were observed in the sequential cast systems.

CHAPTER 5

Functionally Graded in-situ Al A390 with Mg, Sr and Zr Additions

5.1 Abstract

Functionally graded materials (FGMs) with locally varied specific properties at selected locations are extensively used for automobile applications such as engine cylinder. The present investigation focuses on the fabrication, optimization and characterization of Mg, Sr, Zr and combined addition of Mg-Sr and Mg-Zr in A390 aluminium alloy for cylinder liner applications by centrifugal casting technique. The microstructural observation reveals that the phases are homogeneously distributed in the gravity cast components. In the centrifugal cast samples, the α-aluminium phases seem to be finer towards the outer periphery and the less density particles such as primary silicon phases are segregated towards the inner periphery of the centrifugal cast cylinders. A maximum hardness of 158 BHN is achieved at the inner periphery of the combined addition of 1.5 wt. % Mg and 0.03 wt. % Sr in A390 alloy, whereas the minimum hardness of 111 BHN is obtained at the inner region in the combined addition of 1.5 wt. % Mg and 0.03 wt. % Zr in A390 alloy, which are the highest and lowest hardness values compared with the other centrifugal cast alloy systems. A higher tensile strength of 295 MPa and 264 MPa are obtained at the outer and inner region of the A390-0.03 wt. % Sr alloy system, respectively. The middle transition region of A390-1.5 wt. % Mg and outer specimens of A390-0.03 wt. % Sr showed an enhanced wear resistance than the other aluminium FGM systems under investigation. The SEM and EDAX wear analysis shows an abrasive, adhesive and oxidative type of wear mechanisms.

5.2 Introduction

Functionally graded materials (FGMs) are one of the potential and emerging classes of advanced non-uniform alloy or composite materials which exhibit a progressive transition in the composition and or in the microstructure at the macroscopic or continuum scale which intentionally varied with continuous changing properties leading in a particular direction depending upon the process of fabrication

(Mortensen et al., 1995; Akhil et al., 2016; Hirai et al., 1996 and Watanabe et al., 2006). FGM's are best alternatives for the applications where the conventional homogeneous monolithic materials cannot serve in the severe service conditions (Kawasaki et al., 1997). The gradual change in the properties helps the FGM to prevent the material from the mismatch in the thermal expansion. The centrifugal casting method is the easiest and economical method to produce FGM with varying properties at different locations, among the other synthesising techniques such as the sol-gel technique (Miao et al., 2002), the vapour-liquid-solid method (Wu et al., 2000), electro deposition (Martín-González et al., 2002 and Ji et al., 2002), chemical and physical vapour deposition (Cheng et al., 2000; Liu et al., 2000; Heremans et al., 2000 and Moroz et al., 1999), rapid solidification (Li et al., 1993), thermal evaporation (Lao et al., 2002 and Banerjee et al., 2003), plasma spraying, spray forming, etc. All the techniques other than the centrifugal casting technique have certain limitations such as delamination of the FGM surface coatings due to the imbalanced thermal stresses, wear and tear, evaporation, oxidation, crystallization, and melting hence the life of the coatings were reduced, the nano-level thickness of the coatings and also due to the difficulties in the production continuous layer of coatings at limited thickness (Kumar et al., 2010). FGM's have a wide range of applications in aerospace, defence, structural and automotive components such as in brake discs, cylinder liners, piston, bearings, pulleys, rail wheels and other general engineering applications. The processing of the FGM with gradient properties and their application in engineering fields has a lot of technological importance as they are very much exigent (Akhil et al., 2016). The centrifugal casting process is used to produce aluminium based FGM's.

Centrifugal casting is a pressure casting process that is widely used to produce aluminium based FGM with the help of the centrifugal force applied to the liquid metal by rotating the mould (Akhil et al., 2016). Recently, most of the researchers are drawn attention to centrifugal casting methods for the production of FGM components due to its uniqueness and merits. For the fabrication of FGM components, both vertical and horizontal centrifugal casting methods can be used depending upon the diameter and length of the component to be fabricated. Horizontal methods are used to make cylindrical or tubular castings such as large

spun pipes at low speeds, automotive and compressive cylinder liners, etc. When compared to horizontal centrifugal casting, vertical centrifugal casting has a wider range of applications like impeller wheels, pulleys, electric motor rotors, gear blanks, valve bodies, etc. Even non-symmetrical castings are made by vertical centrifugal castings. Also the centrifugal cast components have a very high degree of metallurgical quality and cleanliness due to the propagation and settlement of low density impurity and gas bubbles towards the interior portion of the castings that can be further machined as a final operation (Chirita et al., 2008; Liu et al., 2005 and Halvaee et al., 2001). There are various advantages for centrifugal casting process over other processes such as the component can maintain a particular composition and property at specific location throughout the cast component from equal distance from the centre of the cast component, the parameters for the castings can be easy to maintain such as speed of rotation of the mould, preheating temperature of the mould, melt temperature, etc, the centrifugal casting process is a most effective and efficient process to produce FGM components and by applying a force only to create a graded structure rather than using chemicals or electrolyte (Kuo et al., 2007). The gradation in centrifugal casting is mainly achieved through the density difference in the constituent elements in the alloy system or due to the difference between the densities of the matrix and the reinforcement particles present in the alloy with the help of centrifugal force. The reinforcement phases can be placed either at the inner periphery or the outer periphery of the castings depending upon the density of the reinforcement particles. The FGM's can be prepared by ex-situ or by in-situ composite preparation methods. The ex-situ FGM preparation method is also known as centrifugal solid particle method. For making the ex-situ FGM's, the reinforcement ceramic particles should be added externally to the matrix and for the in-situ, the reinforcing phases should be generated inside the matrix itself with the addition of other reactive elements. For the ex-situ method, the processing temperature of the FGM is lower than the melting temperature of the reinforcement particle. The type of gradation such as smooth, sharp and the thickness of the gradation can be varied with the help of the size, shape, type of reinforcements and the processing temperature of the material. The limitation of the centrifugal casting is that it cannot produce complex structures other than axisymmetric components (Kumar et al., 2010).

In aggressive environments functionally graded metal matrix composites have great interest since it shows excellent mechanical properties among the functionally graded materials (Clyne et al., 2001). The increase in the volume fraction of the reinforcement phases in the matrix alloy drastically increases the performance of the composites as a whole. The aluminium metal matrix composites (MMCs) reinforced with particles gives superior metallurgical properties such as specific strength, improved strength, thermal stability, compressive properties, toughness and high resistance to wear. A large number of research works has been reported with different aluminium alloys and different particulate reinforcements by centrifugal casting such as A356 with varying percentage additions of SiC particles (Akhil et al., 2016), Al-TiC (Nai et al., 2004), Al-SiC (Fukui et al., 1996), Al-SiC-Graphite (Rajan et al., 2008), Al-Al_2O_3 (Kang et al., 2008), etc. Watanabe and Fuki reported the dispersion of ceramic reinforcement particles in a ductile aluminium matrix. In this method, the researchers have mainly achieved the gradient structure and composition due to the density difference between the molten matrix and the dispersed ceramic or intermetallic compounds (Watanabe et al., 2000; Watanabe et al., 2000; Watanabe et al., 2001; Sequeira et al., 2005; Sequeira et al., 2005 and El-Hadad et al., 2010). A very large amount of research works have been reported and published based on aluminium based FGM reinforced with carbides of silicon, titanium and boron and also titanium diboride (Akhil et al., 2016; Kennedy et al., 2001 and Kennedy et al., 2002). Functionally graded A356 aluminium alloy reinforced with 10 and 20 wt. % SiC particles produced by ex-situ centrifugal casting was reported (Akhil et al., 2016). The SiC particles are segregated at the outer periphery of the ring castings due to the higher density of the SiC particles compared to that of aluminium 356 alloys. Higher hardness and wear resistance are achieved at the SiC particle rich outer region than the inner surface. Velhinho et al. also reported the processing of SiC reinforced functionally graded composites with aluminium matrix by centrifugal casting technique. He reported that due to the imperfect wetting of the SiC particles, some pores are formed due to the partially clustered SiC particles (Velhinho et al., 2003). So it is necessary to obtain properly wetted particles to achieve quality castings. The studies of aluminium reinforced with B_4C by centrifugal castings are also reported. The B_4C possesses superior metallurgical properties like high value of hardness close to that of the diamond and remarkable

thermal stability (Rao et al., 2010). The formation of Al_3BC and AlB_2 was restricted since the reaction time is less. The Al-B_4C FGM composite also shows a higher hardness values towards the outer region due to the higher volume fraction of B_4C particles towards this region with an increase of centrifugal force from 110 G to 220 G. The main disadvantage of the MMC's is the high cost that involved in the synthesis methods. This can be diminished by the replacement of the bulk FGM's by FGM coatings or cladding which can serve the similar function that of the bulk systems (Kevorkijan et al., 2003). The aluminium alloys itself strengthened by the intermetallic dispersoids that leads to the enhancement of the mechanical, corrosion and wear properties of aluminium alloy components (Das, 2000). Apart from the particulate functionally graded composite materials, the aluminium alloys alone can produce functionally graded materials with the aid of difference in the densities and properties of the phases present in the aluminium alloys. Due to the physical properties of the aluminium-silicon alloys influenced by their chemical composition and the improved mechanical properties that influenced by the microstructure and the composition of the alloy, the aluminium-silicon alloys are used as structural materials for various engineering applications. The strength of the aluminium alloys mainly depends on the presence of the secondary phases present between the primary aluminium phases. The well established commercial aluminium alloys A356 have good tensile and fracture properties. These properties are mainly achieved through the magnesium (Mg) content in the alloy, the secondary arm spacing (SDAS), the intermetallics of iron and its primary based on the structure, size and shape of the eutectic and primary silicon phases in the alloy system (Wang , 2003). There are many works reported based in the centrifugal casting in-situ method, Al-AlB_2, Al-Mg_2Si, Al-$NiAl_3$, Al-$TiAl_3$, and Al-$NiAl_3$-$TiAl_3$ (Watanabe et al., 2001; Duque et al., 2005; Melgarejo et al., 2006; Melgarejo et al., 2008; Zhou et al., 1998; Fukui et al., 1994; Matsuda et al., 2001; Watanabe et al., 1999 and Watanabe et al., 2001). Watanabe reported the processing of the Al-Al_3Ti FGM by the solid-particle centrifugal casting method where the processing temperature of the dispersed solid phase Al_3Ti particles and the master alloy was lower than the liquidus temperature. The dispersed Al_3Ti particles find a place which is normal to the direction of the centrifugal force (Clyne, 2001; Watanabe et al., 1999; Watanabe et al., 1997 and Watanabe et al., 2001). The control of elemental composition in the alloy,

microstructural variations and thereby improving the mechanical properties is possible by introducing special elements in the form of pure elements or master alloys at very low percentages into the base alloy for the grain refinement of the elements in the alloy system. Nevertheless, the easiest and the general procedure is the casting technology of aluminium-silicon alloys (Liao et al., 2002; Stefanescu et al., 1988 and Shabestari et al., 2004). The studies with combined addition of grain refiners and the modifiers showed superior mechanical and wear properties in the alloys due to the reduced structure of silicon phases, shape and grain size (Tavitas-Medrano et al., 2008). The addition of strontium (Sr) as a modifier to the aluminium alloys changes the morphology of eutectic silicon to the fibrous from the acicular nature (Samuel et al., 1998). Wang et. al., reported that the varying percentage of 0.0004 wt. % to 0.03 wt. % in the Al-Si-Cu alloys, the tensile properties are found to be increased at an optimum concentrations of strontium between 0.01 % and 0.015 %. The increase in the concentration of strontium in the alloys results in increase in the porosity level and the size of the porosity in the component. The addition of strontium in the alloys also improves the ductility, fatigue, fracture and impact properties (Wang et al., 1995 and Apelian et al., 1989). In hyper eutectic alloys the properties like hardness, wear and toughness are mainly depend on the size, morphology and the distribution of the star-shaped hard cuboids of primary silicon on the micrograph (Abramov et al., 1997). Also the silicon forms Mg_2Si intermetallics in combination with Mg in aluminium alloys, which is the precipitation hardening and in-situ reinforcing phase in many of the aluminium based alloys (Sigworth et al., 1989). The Mg_2Si phase has very high hardness, melting point, good thermo-electric property and elasticity modulus. Centrifugal casting of Al-Si-Mg alloys by in-situ method was reported and found the enriched Mg_2Si in the surface of the component (Zhang et al., 1998). The primary silicon phases are formed towards the inner layers of the cylindrical parts produced through the centrifugal casting due to the low density of the particles (Wang et al., 1997). So these materials are highly advisable for the automotive and defence applications since it serves the functions at the extreme conditions.

In this study, centrifugal casting is used for the fabrication of functionally graded aluminium alloy by separate (Mg, Sr and Zr) and combined addition of Mg-Sr

and Mg-Zr into A390 aluminium alloy and the properties are evaluated from the outer to the inner periphery of the castings, particularly the effect of Mg, Sr and Zr addition in the centrifugal cast components.

5.3 Experimental Methods

The composition and properties of A390 matrix alloy is depicted in Tables 5.1a and 1b respectively. The alloy was processed in a clay graphite crucible melted with the help of a resistance heated furnace. The degassing process was done by using hexachloroethane at 720 °C of the melt. Mg was added into the A390 alloy of varying percentages, 0.5 wt. %, 1 wt. %, 1.5 wt. % and 2 wt. % at 740 °C. Sr and Zr was added into the A390 alloy at 0.01 wt. %, 0.02 wt. %, 0.03 wt. % and 0.04 wt. %. The melt was then superheated above the liquidus temperature at 760 °C and poured into the permanent slab mould for gravity casting and cylindrical mould of diameter and height 90 mm for the centrifugal casting rotated at 1300 rpm to obtain the functionally graded cylinder. The as-cast samples of A390, Mg, Sr and Zr added aluminium A390 were heat treated as per T6 condition at 495 °C for 8 hours; quenched in hot water and then aging at 175 °C for 8 hours.

Microstructural evaluations were carried out using a Leica-DMRX optical microscope used to study the microstructural characteristics of as-cast samples of A390, Mg, Sr and Zr added A390 alloy systems by using standard metallographic procedures. A TINUS OLSEN hardness tester was used to measure the Brinell hardness number (BHN) of the as-cast and heat-treated alloy samples for studying the effect of the heat-treated condition over the as-casts using a 2.5 mm steel ball indenter with an applied load of 62.5 kg for a dwell time of 20 seconds. A standard HITACHI STA 7300 instrument was used for the differential thermal analysis to study the thermal characteristics of the different FGM samples at different locations. The thermal studies were carried out at a heating rate of 10 °C/min up to a temperature of 800 °C beyond the melting point of the alloy and the processing temperature and the alloys were allowed to cool to the room temperature to examine the phase transformation from the large exothermic and endothermic peaks that obtained from the differential thermal analysis (DTA) while heating and cooling. XRD-PAN analytical machine was used to study the X-ray diffraction analysis of the FGM specimens.

Table 5.1a Standard elemental composition of A390 aluminium alloy (wt. %)

Alloy	Al	Si	Cu	Mg	Fe	Mn	Zn	Ti
A390	75.3-79.5	16-18	4.0-5.0	0.50-0.65	0.40	0.10	0.10	0.20

Table 5.1b Standard properties of A390 aluminium alloy

Properties	A390
Density	2.72 g/cm^3
Liquidus Temperature	649 ^{o}C
Solidus Temperature	507 ^{o}C
Co-efficient of thermal Expansion	22.5 µm/m- ^{o}C at 20-300 ^{o}C
Thermal Conductivity	134 W/m-K at 25 ^{o}C
Solutionizing Temperature	495 ^{o}C
Aging Temperature	177 ^{o}C for 8 hr
Hardness	145 BHN
UTS	310 MPa
% Elongation	<=1.0
Modulus of Elasticity	81.2 GPa
Fatigue Strength	115 MPa
Shear Strength	187 MPa

The tensile and compression tests were carried out in a universal testing machine KIC-2-1000-C (capacity 100 kN) at a standard strain rate of 1 mm/min. The tensile samples were machined according to the ASTM standards B557M and the samples were tested confirming the E-8 standard. The sliding wear tests were performed for the FGM samples at different locations on a standard Ducom wear and friction monitor—20LE pin-on-disc wear testing machine without lubrication, that can measure wear volume between the surfaces in contact during the tests. The pin-on-disc consist of a 6 mm diameter stationary pin holder, where the load was normally

applied to the pin specimen of 6 mm diameter and 30 mm height by using dead weights with the support of string and special pulley arrangement that can carry a maximum load of 15 kg directly. An En 31 high-carbon hardened alloy steel of 165 mm diameter and a hardness of 63 HRC were used as the counter surface with a high degree of abrasion resistance and compressive strength. The wear tests were executed with four different loads 2 kg (19.63 N), 4 kg (39.24 N), 6 kg (58.86 N), and 8 kg (78.48 N). All the tests were conducted at a constant velocity of 1 m/second and sliding distance of 1800 m was critically maintained throughout the tests. The surfaces of the worn out pin surfaces was then further studied using JEOL JSM-5600LV and Carl Zeiss EVO-18 scanning electron microscope (SEM) and EDAX to study the types of surface morphologies, the wear mechanisms and the oxide layer formation on the specimen surface during dry sliding wear test.

5.4 Results and Discussion

5.4.1 Characteristics of gravity cast materials

5.4.1.1 Microstructural observations

Figure 5.1 shows the optical microstructure of gravity cast A390 aluminium alloy. The figure represents the presence of silvery whitish coloured α-aluminum, needle shaped eutectic silicon and the polygonal shaped cuboids of primary silicon. The dark cuboidal structured primary silicon gives the hardness to the alloy.

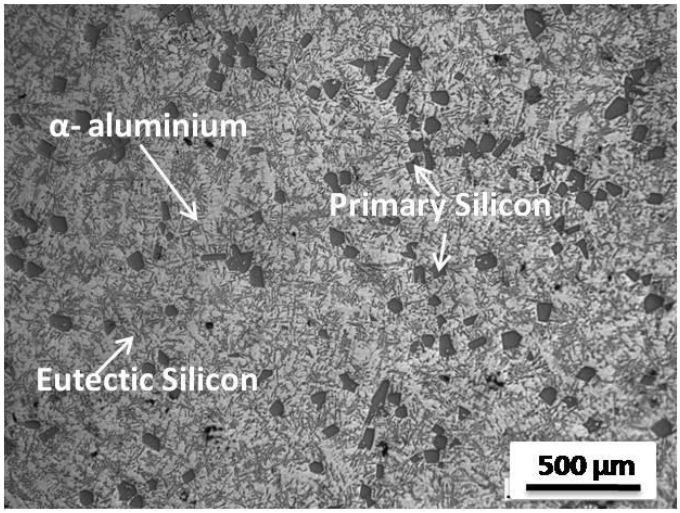

Figure 5.1 Optical microstructure of gravity cast A390 aluminium alloy

Figure 5.2a-d shows the optical microstructures of gravity cast A390-0.5 wt. % Mg, A390-1 wt. % Mg, A390-1.5 wt. % Mg and A390-2 wt. % Mg respectively. In Figure 5.2a α-aluminium, eutectic silicon and primary silicon phases are observed. The eutectic silicon in A390-0.5 wt. % Mg is seen as small-small clusters which tend to the formation of the primary silicon in the next level. Also very few primary silicon can be seen in this region. The Figure 5.2b corresponds to the microstructure of A390-1 wt. % Mg, it shows the presence of α-aluminium, eutectic and primary silicon. The microstructure of A390-1.5 wt. % Mg in Figure 5.2c shows the presence of α-aluminium and eutectic silicon in clusters. This cluster of eutectic silicon improves the hardness and mechanical properties of the cast component. The formation of primary silicon restricted by the addition of the 1.5 wt. % Mg and the presence of Mg in hypereutectic aluminium alloy A390 always form Mg_2Si. This Mg_2Si phase acts as a hard phase and gives strength and hardness to the alloy. Figure 5.2d shows the microstructure of A390-2 wt. % Mg that reveals the presence of α-aluminium, eutectic silicon and Mg_2Si. The black spots in the microstructure represent the Mg_2Si phase. In this case, also the presence of a higher percentage of Mg (2 wt. %) restricts the formation of primary silicon.

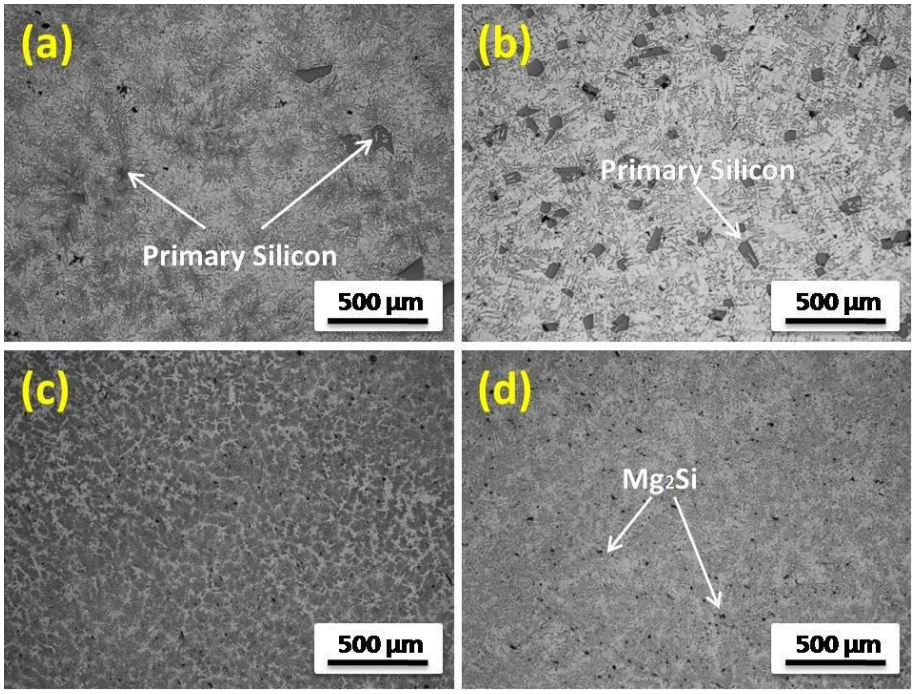

Figure 5.2 Optical microstructures of gravity cast (a) A390-0.5 wt. % Mg (b) A390-1 wt. % Mg (c) A390-1.5 wt. % Mg and (d) A390-2 wt. % Mg

Figure 5.3 shows the optical microstructures of Sr added A390 aluminium alloy gravity casting. The Sr is added at 0.01 wt. %, 0.02 wt. %, 0.03 wt. % and 0.04 wt. % to the A390 aluminium alloy. Figure 5.3a-d shows the microstructure of A390-0.01 wt. % Sr, A390-0.02 wt. % Sr, A390-0.03 wt. % Sr and A390-0.04 wt. % Sr. In A390-0.01 wt. % Sr, the

presence of aluminium phase, eutectic phase and the primary silicon phases are visible in Figure 5.3a. However, for A390-0.02 wt. % Sr in Figure 5.3b there is no trace of primary silicon due to the more number of nucleation sites acted due to the addition of 0.02 wt. % of Sr. Also the clusters of eutectic silicon phases are more in this system. However, the further addition of Sr at 0.03 and 0.04 wt. % shows increase in the size of primary silicon in both the cases and reduction in number of primary silicon which is due to larger heterogeneous nuclei sites. Microstructures also clearly reveal the presence of aluminium and eutectic silicon clusters.

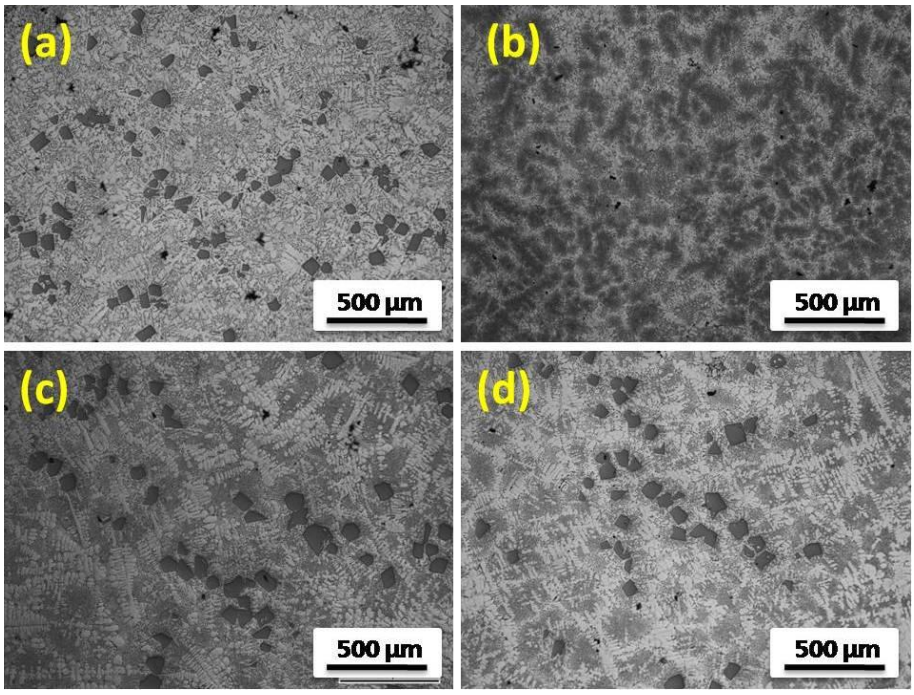

Figure 5.3 Optical microstructures of gravity cast (a) A390-0.01 wt. % Sr (b) A390-0.02 wt. % Sr (c) A390-0.03 wt. % Sr and (d) A390-0.04 wt. % Sr

Figure 5.4a-d represents the optical microstructures of gravity cast Zr added at 0.01 wt. %, 0.02 wt. %, 0.03 wt. % and 0.04 wt. % to the A390 aluminium alloy. The presence of primary silicon is seen from 0.01 wt. % addition upto 0.03 wt. % addition, but the size is finer than that of the size of the pure A390. At 0.04 wt. % addition of Zr the number of eutectic silicon phases increases and the primary silicon phases started disappearing and the eutectic phases are more fibrous than from the other percentage additions of Zr. This is clearly evident from the Figure 5.4d.

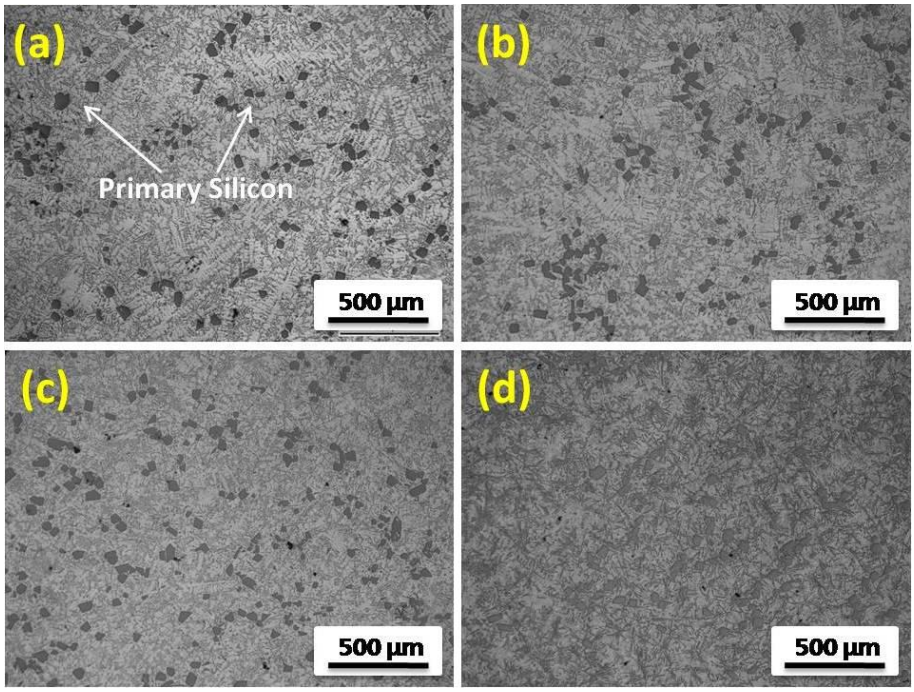

Figure 5.4 Optical microstructures of gravity cast (a) A390-0.01 wt. % Zr (b) A390-0.02 wt. % Zr (c) A390-0.03 wt. % Zr and (d) A390-0.04 wt. % Zr

5.4.1.2 Hardness

Table 5.2 depicts the hardness values of gravity cast pure A390 alloy, Mg added at 0.5, 1, 1.5 and 2 wt. % and Sr and Zr added at 0.01, 0.02, 0.03 and 0.04 wt. % in A390 aluminium alloy. The heat treated condition of the alloy systems shows higher hardness values than the as-cast condition. The base A390 aluminium alloy shows a hardness value of 134 BHN in the heat treated condition while the Mg added A390 alloy systems shows 147.5, 140.5, 137.5 and 144.5 BHN for the A390-0.5 wt. % Mg, A390-1 wt. % Mg, A390-1.5 wt. % Mg and A390-2 wt. % Mg respectively. Addition of Mg tends to increase the formation of Mg_2Si phases in aluminium alloy and also refines the eutectic phases in the system, hence the Mg added alloy provides higher hardness. Among the Mg added systems, the A390-1.5 wt. % Mg shows the lower hardness (137.5 BHN) due to disappearance of primary silicon phases as observed in Figure 5.2(c). Again the A390-2 wt. % Mg shows higher hardness (144.5 BHN) due to the formation of primary Mg_2Si phases.

The Sr added A390 alloy with 0.01, 0.02, 0.03 and 0.04 wt. % showed higher hardness values of 152.5, 147, 150 and 140.5 BHN respectively compared to base A390 alloy. Among the various Sr added systems, 0.04 wt. % Sr added system shows lower hardness, which may be due to over modification and grain coarsening in the alloy. The addition of Zr in A390 shows 145, 149, 145.5 and 146.5 BHN for 0.01 wt. % to 0.04 wt. % respectively. The Zr added systems show hardness values in the closer range (145-149 BHN). A maximum

hardness of 152.5 BHN is achieved in A390-0.01 wt. % Sr in the heat treated condition due to the refined structure of aluminium and eutectic phases.

Table 5.2 Hardness of A390 alloy systems (BHN)

Alloy System	As-cast	Heat treated
A390 base alloy	103	134
A390-0.5 wt. % Mg	113.5	147.5
A390-1.0 wt. % Mg	111.5	140.5
A390-1.5 wt.% Mg	110.5	137.5
A390-2.0 wt. % Mg	109	144.5
A390-0.01 wt. % Sr	102	152.5
A390-0.02 wt. % Sr	108	147
A390-0.03 wt. % Sr	112	150
A390-0.04 wt. % Sr	111	140.5
A390-0.01 wt. % Zr	96	145
A390-0.02 wt. % Zr	112	149
A390-0.03 wt. % Zr	107	145.5
A390-0.04 wt. % Zr	110	146.5

5.4.2 Characteristics of FGM cylinder

5.4.2.1 Microstructural observations

Figure 5.5 shows the optical microstructure of A390 aluminium alloy produced by centrifugal casting in cylinder mould taken from the outer to the inner periphery of the casting at 0.5 mm, 6 mm, 12 mm and 15 mm. Figure 5.5a is the microstructure at 0.5 mm from the outer diameter of the casting that shows the presence of very fine α-aluminum, eutectic silicon and small amount of primary silicon. The refined structure of the α-aluminum at this region is because of the forced solidification of the A390 melt during the process of the casting and is also due to the formation of the chilled zone at the outer most region due to the higher preheat temperature of the mould. The microstructures of the subsequent areas from the outer regions show coarser sized α-aluminum phase and longer needle shaped eutectic silicon because of the lesser cooling rate of the melt at the subsequent regions than the outer region. The Figure 5.5b represents the optical microstructure at 6 mm from the outer surface of the casting; this region is the transition region from primary silicon particle depleted outer to particle rich inner region. Apart from the presence of coarse α-aluminum and eutectic silicon at 6 mm, also seen the presence of hard cuboids of the primary silicon which is less denser than the α-aluminium. The primary silicon moved towards the inner region of the casting due to the low density of the primary silicon compared to α-aluminium and eutectic silicon and also due to the centrifugal force. The transition region separates the α-aluminum rich region and primary silicon rich region. The Figure 5.5c and d shows the microstructures of the inner regions of the castings at 12 mm and 15 mm respectively that shows the presence of a higher percentage of primary silicon at these regions that will give higher hardness and toughness in this region which is a desirable property for cylinder liner application.

Figure 5.6-5.9 shows the microstructures of magnesium added (at 0.5 wt% Mg, 1 wt. % Mg, 1.5 wt. % Mg and 2 wt. % Mg) A390 cylinder by centrifugal casting. The microstructures are taken from outer to the inner periphery of the castings at 0.5 mm, 9 mm, 18 mm, and 21mm from the outer periphery of the cylindrical casting. The microstructures of Mg added alloy systems at 0.5 mm from the outer surface of

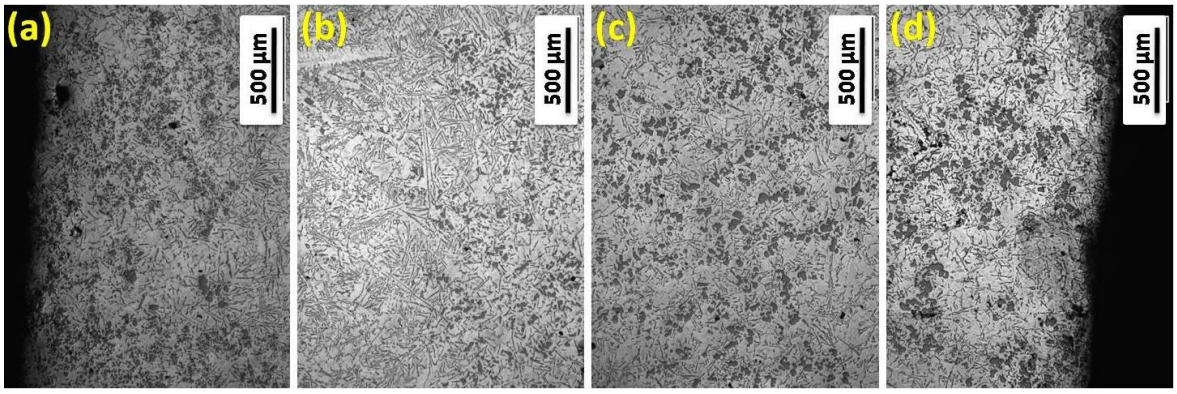

Figure 5.5 Optical microstructures of functionally graded A390 base alloy cylinder at (a) 0.5 mm (b) 6 mm (c) 12 mm and (d) 15 mm from the outer periphery of the centrifugal casting

the cylindrical castings shows almost similar structures of fine grains of α-aluminium and short sized eutectic silicon because of the preheat temperature of the mould when the liquid melt touches the mould during the casting process. As the distance increases from the outer periphery of the cylinder to the inner periphery, the structure of the α-aluminium become coarser and coarser and the quantity of the silicon phases increases. The increase in the percentage of the silicon towards the inner periphery is due to the relative density of the phases during the processing of the component. Microstructures of A390-0.5 wt. % Mg added centrifugal cast cylinder is depicted in Figure 5.6c and at 18 mm it shows the presence of primary silicon. The primary silicon is accumulated in the inner periphery of the cylindrical casting due to the low density of the primary silicon compared to that of aluminium. When the liquid metal falls into the rotating mould, the melt propagates towards the outer diameter of the mould and the melt moves to the top of the cylinder along the inside wall of the cylindrical mould due to the centrifugal force. The outermost layer of the melt that in contact with the cylindrical mould gets immediately solidified and that is why the microstructures show the presence of small amount of the small sized primary silicon at the region near the outer periphery. The primary silicon present at this region did not get enough time to travel towards the inner periphery even the density is lower than that of the aluminium due to the sudden solidification of the melt at this region. However, the inner most region in the Figure 5.6d shows the presence of primary silicon due to the propagation of low density primary silicon towards the inner most regions of the cylinder due to the rotation of the mould during the process of casting.

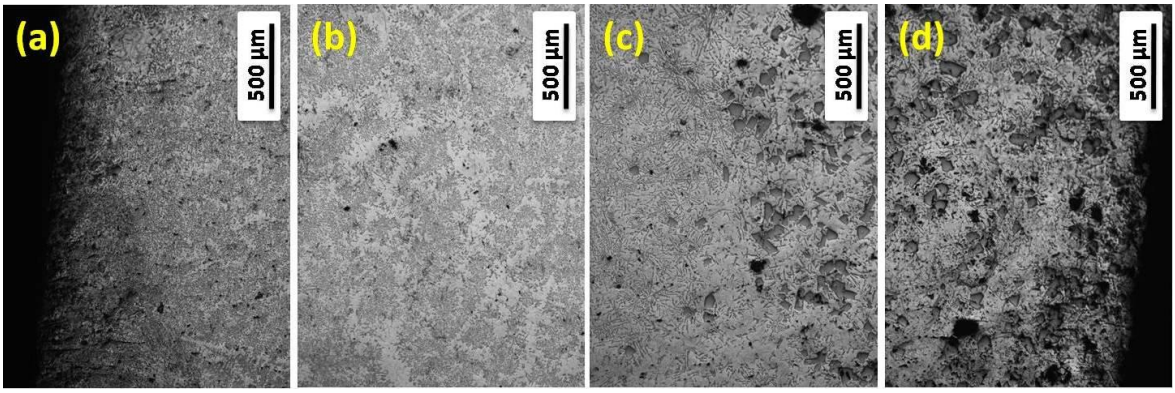

Figure 5.6 Optical microstructures of functionally graded A390-0.5 wt. % Mg cylinder at (a) 0.5 mm (b) 9 mm (c) 18 mm and (d) 21 mm from the outer periphery of the centrifugal casting

The Figure 5.7c is also showing the transition region between the aluminium rich region at the outer periphery and the primary silicon region between the inner peripheries of A390-1 wt. % Mg. At the transition region, the presence of primary silicon as well as clusters of eutectic silicon is clearly visible. The primary silicon is formed as a result of the accumulation of silicon beyond the eutectic point. The accumulation of eutectic silicon to form primary silicon is clearly evident from the transition region. However, due to the addition of the higher percentage of Mg in the case of A390-1.5 wt. % Mg and A390-2 wt. % Mg [Figure 5.8 and 5.9] restricts the formation of primary silicon, also almost all the silicon phases appear as eutectic silicon and some part appear as Mg_2Si. The outer periphery of the casting is enriched with fine grains of aluminium phase and inner periphery is enriched with silicon phases, especially primary silicon in the regions near the inner surface. In pure A390 cylindrical casting the primary silicon appears at 9 mm from the outer periphery of the transition region but in the other alloy systems it appears near the inner periphery at 18 mm, this is because of the increase in the nucleation sites and the dilution effect of Mg in A390 alloy.

Figure 5.10-5.13 shows the optical microstructures of Sr added at 0.01, 0.02, 0.03 and 0.04 wt. % to the A390 hypereutectic aluminium alloy. The addition of Sr in aluminium alloys changes the morphology of the silicon phases, i.e., eutectic as well as the primary silicon phase to some extent. The morphology changes from the coarse plate-like structure to the fine fibrous structures. Figure 5.10a-d represents the optical microstructures of centrifugally cast A390-0.01 wt. % Sr. from outer to the

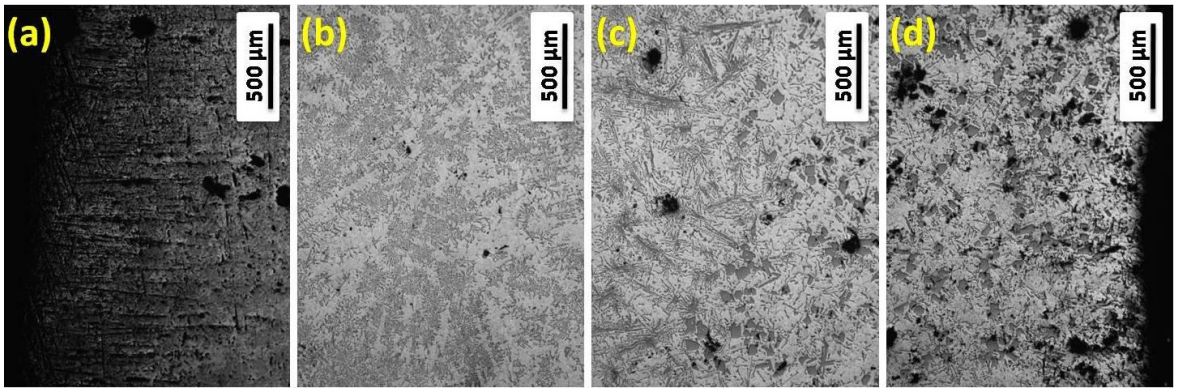

Figure 5.7 Optical microstructures of functionally graded A390-1 wt. % Mg cylinder at (a) 0.5 mm (b) 9 mm (c) 18 mm and (d) 21 mm from the outer periphery of the centrifugal casting

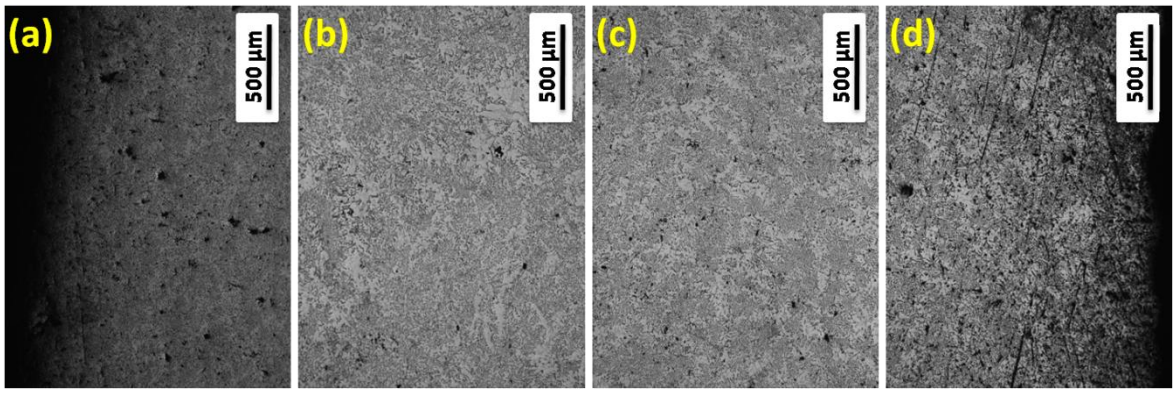

Figure 5.8 Optical microstructures of functionally graded A390-1.5 wt. % Mg cylinder at (a) 0.5 mm (b) 9 mm (c) 18 mm and (d) 21 mm from the outer periphery of the centrifugal casting

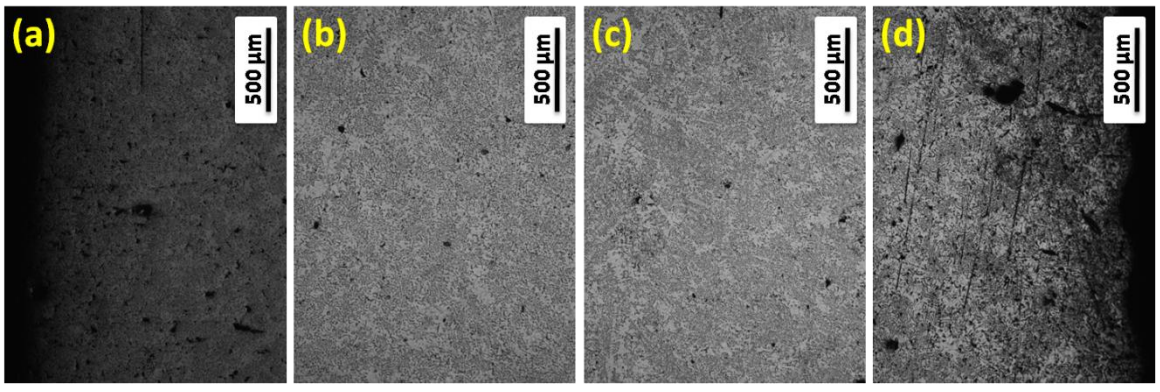

Figure 5.9 Optical microstructures of functionally graded A390-2 wt. % Mg cylinder at (a) 0.5 mm (b) 9 mm (c) 18 mm and (d) 21 mm from the outer periphery of the centrifugal casting

inner periphery. In Figure 5.10a it is clear that the presence of primary silicon is not seen anywhere because of the numerous number of nucleation sites acts in the alloy due to the addition of Sr. At 0.5 mm, instead of primary silicon at the outer diameters, clusters of primary silicon can be seen in the microstructures. At 12 mm the transition region is also visible which ensures the clear sign of propagation of low density primary silicon towards the inner most regions of the silicon. The primary silicon phases change from large block to small block in the regions beyond 12 mm from the outer periphery towards the inner periphery. Also, the eutectic silicon phases are seen as fibrous structures rather than the needle shaped structures in the base alloy. The Figure 5.11 corresponds to the optical microstructures of centrifugal cast A390-0.02 wt. % Sr. In this, at 3 mm from the outer most surface the transition region is seen as the clusters of eutectic silicon which will form as primary silicon in the next process parameters. The microstructure at 12 mm shows the transition of eutectic silicon to the primary silicon. The centre portion of the cluster of eutectic silicon converted to primary silicon. The primary silicon formation starts from the centre of the eutectic silicon cluster and develops in the outward direction. The size and the shape of the primary silicon depend on the size of the clusters of eutectic silicon and the way it develops according to the processing parameters. However, the inner most regions are enriched with fully developed primary silicon which will provide good hardness properties at this region. Figure 5.12 is the optical microstructures of A390-0.03 wt. % Sr by centrifugal casting. The outer regions of the cast component show fine structured aluminium phases and small clusters of eutectic silicon. As the distance proceeds from the outer to the inner periphery, the size of the eutectic silicon clusters become larger and then the clusters transformed to primary silicon (at 15 mm from the outer periphery in Figure 5.12c). In Figure 5.13c for A390-0.04 wt. % Sr the transition region is clearly seen between eutectic silicon phase and the primary silicon phase which will provide better toughness at the inner most regions. The inner regions of A390-0.03 wt. % Sr and A390-0.04 wt. % Sr in Figures 5.12d and 13d shows the presence of fine primary silicon phases as compared with base alloy microstructures.

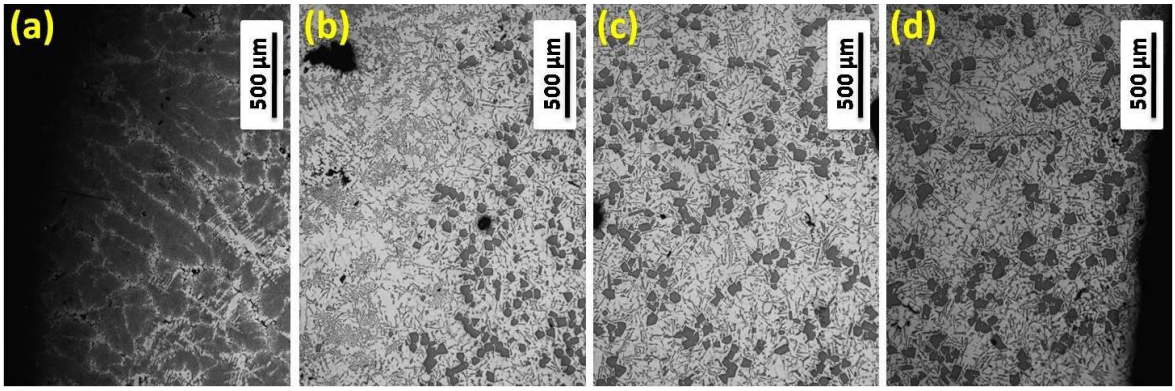

Figure 5.10 Optical microstructures of functionally graded A390-0.01 wt. % Sr cylinder at (a) 0.5 mm (b) 12 mm (c) 15 mm and (d) 21 mm from the outer periphery of the centrifugal casting

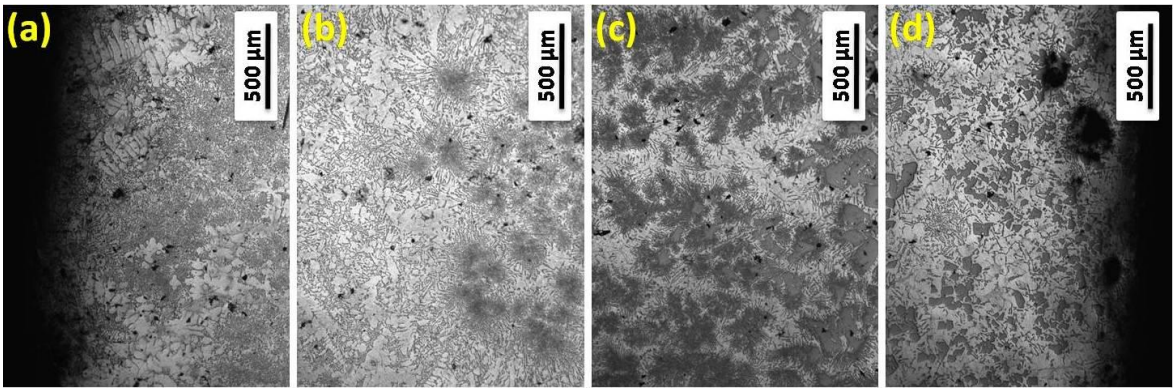

Figure 5.11 Optical microstructures of functionally graded A390-0.02 wt. % Sr cylinder at (a) 0.5 mm (b) 3 mm (c) 12 mm and (d) 18 mm from the outer periphery of the centrifugal casting

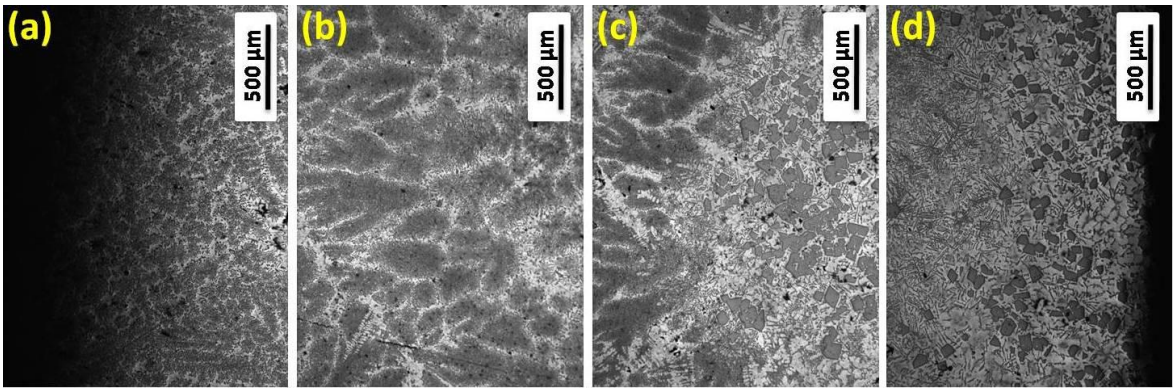

Figure 5.12 Optical microstructures of functionally graded A390-0.03 wt. % Sr cylinder at (a) 0.5 mm (b) 9 mm (c) 15 mm and (d) 18 mm from the outer periphery of the centrifugal casting

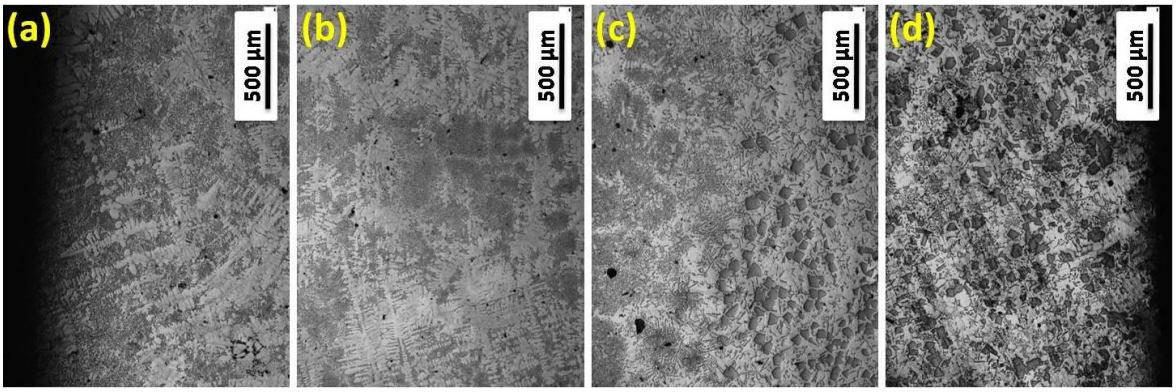

Figure 5.13 Optical microstructures of functionally graded A390-0.04 wt. % Sr cylinder at (a) 0.5 mm (b) 6 mm (c) 12 mm and (d) 18 mm from the outer periphery of the centrifugal casting

Figure 5.14-5.17 shows the optical microstructures of centrifugal cast A390 with 0.01 wt. %, 0.02 wt. %, 0.03 wt. % and 0.04 wt. % Zr. The addition of Zr in A390 changes the morphology of eutectic as well as the primary silicon phases. As in the previous cases, the low density primary silicon phases are travelled and segregated to the inner periphery of the castings at 0.01 wt. % Zr addition in Figure 5.14a. At 0.02 wt. % addition of Zr in A390 shows that the primary silicon is completely absent in the microstructures from outer to the inner periphery [Figure 5.15a-d]. The Figure 5.16 and 5.17 represents the microstructures of 0.03 wt. % Zr and 0.04 wt. % Zr in A390 alloy. At this percentage, the microstructures exhibit only very few traces of primary silicon phases towards the inner periphery of the cast cylinder. Also, it is carefully noted that the primary silicon appears in the Zr added A390 towards the outer periphery of the castings are very finer as compared with the Mg and Sr added cylindrical systems.

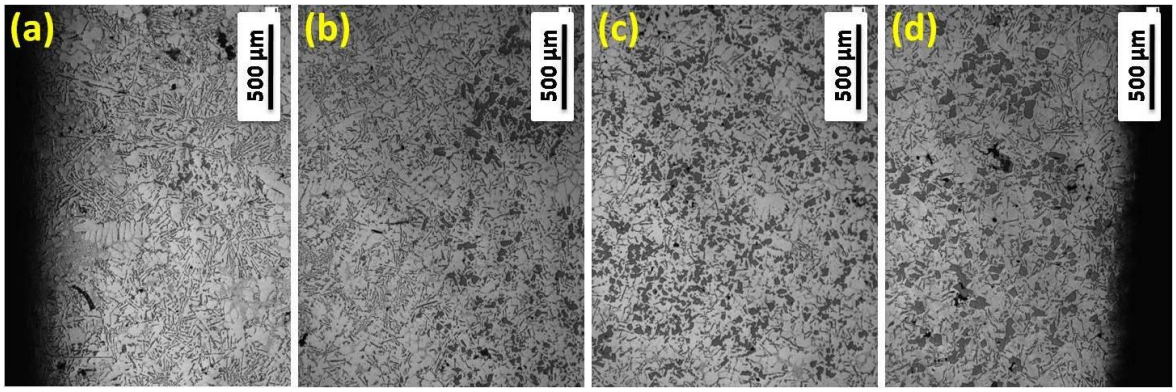

Figure 5.14 Optical microstructures of functionally graded A390-0.01 wt. % Zr cylinder at (a) 0.5 mm (b) 6 mm (c) 9 mm and (d) 15 mm from the outer periphery of the centrifugal casting

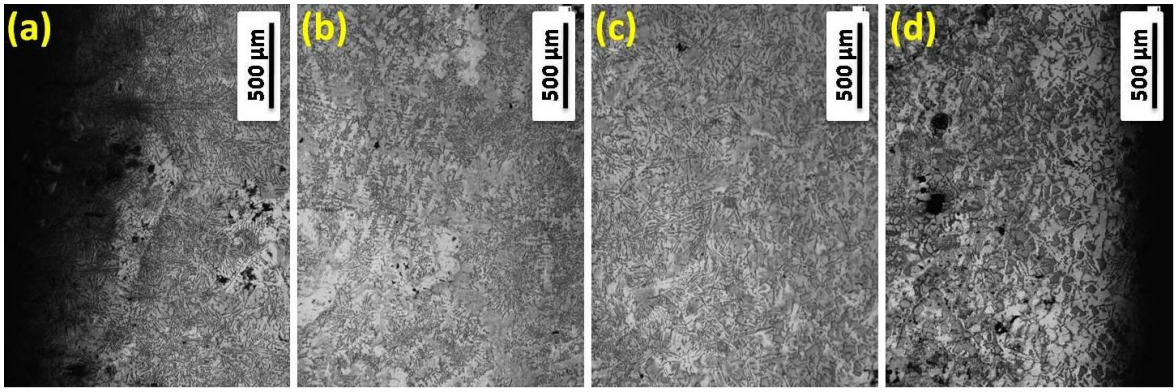

Figure 5.15 Optical microstructures of functionally graded A390-0.02 wt. % Zr cylinder at (a) 0.5 mm (b) 6 mm (c) 12 mm and (d) 15 mm from the outer periphery of the centrifugal casting

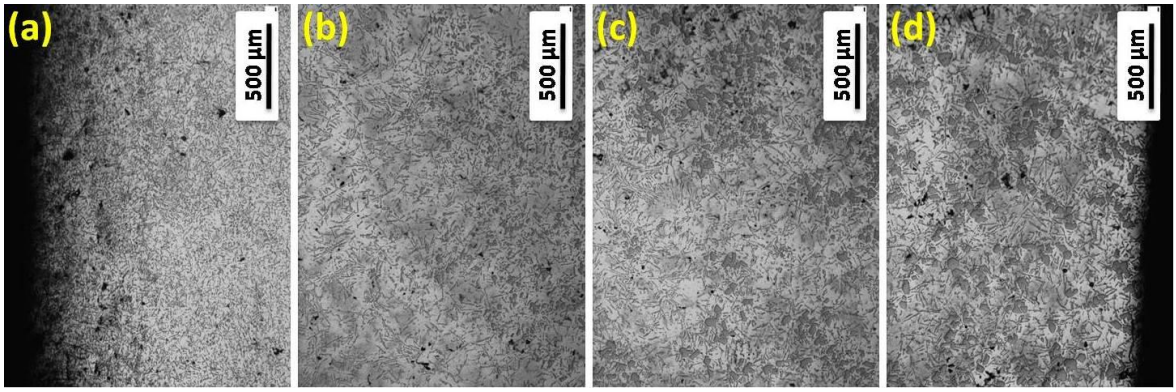

Figure 5.16 Optical microstructures of functionally graded A390-0.03 wt. % Zr cylinder at (a) 0.5 mm (b) 6 mm (c) 12 mm and (d) 15 mm from the outer periphery of the centrifugal casting

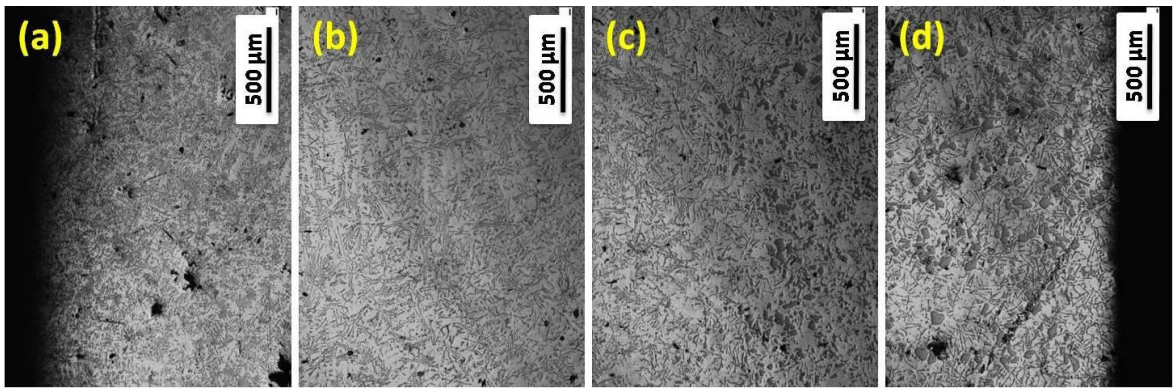

Figure 5.17 Optical microstructures of functionally graded A390-0.04 wt. % Zr cylinder at (a) 0.5 mm (b) 6 mm (c) 12 mm and (d) 15 mm from the outer periphery of the centrifugal casting

5.4.2.2 Hardness

Figure 5.18 shows the hardness profile of A390 base alloy from outer to the inner periphery of the centrifugally cast cylinder. The values of hardness are taken at 1 mm interval from 2 mm from the outer periphery of the cylinder towards the inner periphery. The hardness values in heat treated condition always show higher values over as-cast condition. During heat treatment precipitation hardening takes place leading to enhancement in hardness. The hardness profiles show an increase in the hardness values from the outer to inner periphery of the cast cylinder. The increase in the hardness values are due to the presence of low density in-situ primary silicon particles segregated towards the inner periphery of the casting by centrifugal force. In the as-cast condition, it shows a minimum hardness value of 108 BHN at 2 mm from the outer periphery and a maximum hardness of 114 BHN at the inner most region (i.e., 13 mm from the outer periphery). The lower hardness near outer periphery from 2-6 mm is because of the coarse grains of the α-aluminium phase and the lack of primary silicon phases at this region. The outer surface is harder than the region before 6 mm from the outer, even in the absence of silicon phases due to the fine grain sizes achieved due to the forced solidification attained during the centrifugal action. The heat treated samples show a minimum of 124 BHN at 2 mm from the outer most region and it shows a higher hardness of 148 BHN at the inner most region due to the presence of low density hard primary silicon particles. The higher concentration of primary silicon phases accumulated towards the inner periphery of the centrifugally cast cylinder is clearly shown in the Figure 5.5b-d which provides the hardness to the inside of the cast cylinder. As the concentration of the primary silicon phases increases from the transition region to the inner portion of the cylinder, the hardness also increases.

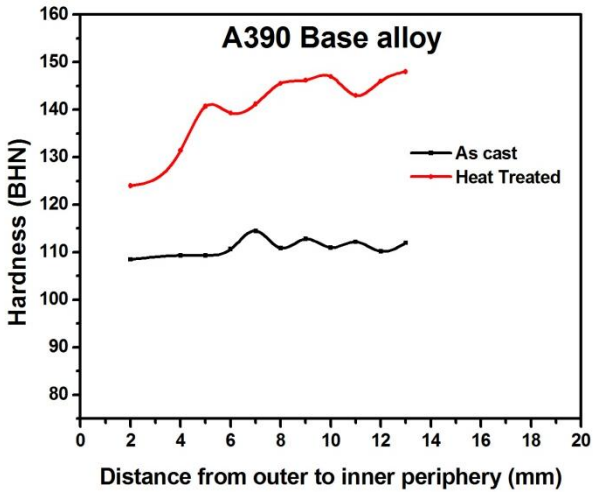

Figure 5.18 Hardness profile of A390 base alloy centrifugal cast cylinder for the as-cast and precipitated treated samples

A390-2 wt. % Mg) as clearly visible in the microstructures in Figures 5.6-5.9. The as-cast hardness towards inner region of A390-2 wt. % Mg shows a decrease in the hardness due to the dilution effect and the absence of primary silicon particles from the other systems (Figure 5.9d). of A390The hardness vales in centrifugal cast cylinder always show higher hardness towards the inner periphery of the casting due to the presence of primary silicon phases in case of A390-0.5 wt. % Mg and A390-1 wt. % Mg alloy systems.

Figure 5.20a-d shows the hardness values of centrifugally cast Sr added A390 aluminium alloy cylinder from outer to inner periphery. As in the previous cases, the heat treated samples shows an improved hardness over as-cast hardness. The steep/ considerable increase in hardness values after 12 mm is due to the accumulation of primary silicon particles towards the inner periphery of the castings. The increase in the hardness at this region depends on the volume of primary silicon particles and size of primary silicon particles segregated due to the centrifugal gravitational force. As mentioned in the literature survey, studies have been reported that the strontium added systems exhibits micro-porosities. These micro-porosities will locally increase and decrease the hardness at particular positions. For 0.01 wt. % Sr added A390 a minimum hardness of 93 BHN and a maximum hardness of 109 BHN obtained for as-cast condition at 2 mm and 18 mm respectively. The heat treated condition shows 108 BHN at 2 mm and 145 BHN at 18 mm respectively as the minimum and maximum values of hardness. Figure 5.20b shows the hardness curves of A390-0.02 wt. % Sr. The hardness values shows 117 BHN at the outer surface and 144 BHN at the inner surface for the heat treated samples. As the size of the primary silicon reduces towards the inner periphery of the castings, the hardness seems to be increasing. For A390-0.03 wt. % Sr alloy system a maximum hardness of 144 BHN is achieved at 18 mm from the outer surface (i.e., inner most region) and a minimum

Figure 5.19 a-d shows the hardness profiles of centrifugal cast A390-0.5 wt. % Mg, A390-1 wt. % Mg, A390-1.5 wt. % Mg and A390-2 wt. % Mg. The general trend of the hardness profile of the A390-Mg as-cast systems show a decrease in the hardness values from the outer periphery of the cast cylinder upto 14-16 mm towards inner region and then after 16mm, shows an increase in the hardness values to the inner most region of the cast cylinder. But in heat treated samples it shows always an increase in the hardness from the outer to the inner periphery of the castings. The decrease and increase trend of the hardness values in the as cast condition from the outer to the inner region is because of the difference in the solidification rate of the alloy experienced due to the centrifugal casting process. The hardness at the outer region is due to the smaller grain size of the alpha aluminium phase attained during the forced solidification. The subsequent regions have grain size larger than the outer most regions and these region will show only lesser hardness compared to the outer regions. As the distance from the outer region increase the grain size also increases. This increase in the grain size towards the inner regions leads to lesser values of hardness than in the preceding regions. The value of hardness increases from certain position in the casting towards the inner regions due to the segregation of the low density harder primary silicon particles due to the centrifugal force. But the precipitation hardening during heat treatment aids to an increase in the hardness values from the outer to the inner regions of the casting. In A390-0.5 wt. % Mg a minimum hardness of 121 BHN at 5 mm from the outer periphery and a maximum hardness of 141 BHN obtained at the inner most region in the heat treated condition [Figure 5.19a]. For 1 wt. % of Mg added A390 alloy in Figure 5.19b, it gives 120 BHN and 144 BHN hardness as minimum and maximum hardness values at heat treated condition. The minimum hardness of 120 BHN is due to the coarse grains of the aluminium phase and maximum hardness is due to the presence of primary silicon at that region. The Figure 5.19c shows a minimum of 127 BHN at 9 mm and a maximum of 142 BHN at 18 mm from the outer periphery of the casting for A390-1.5 wt. % Mg and A390-2 wt. % Mg the minimum and maximum values are 119 at 2 mm and 140 at 15 mm, respectively. In the case of A390-1.5 wt. % Mg and A390-2 wt. % Mg the maximum hardness values are lesser than the values that compared with the values of the inner most region. This is because the primary silicon particles are completely disappeared due to dilution effect in these two systems (A390-1.5 wt. % Mg and

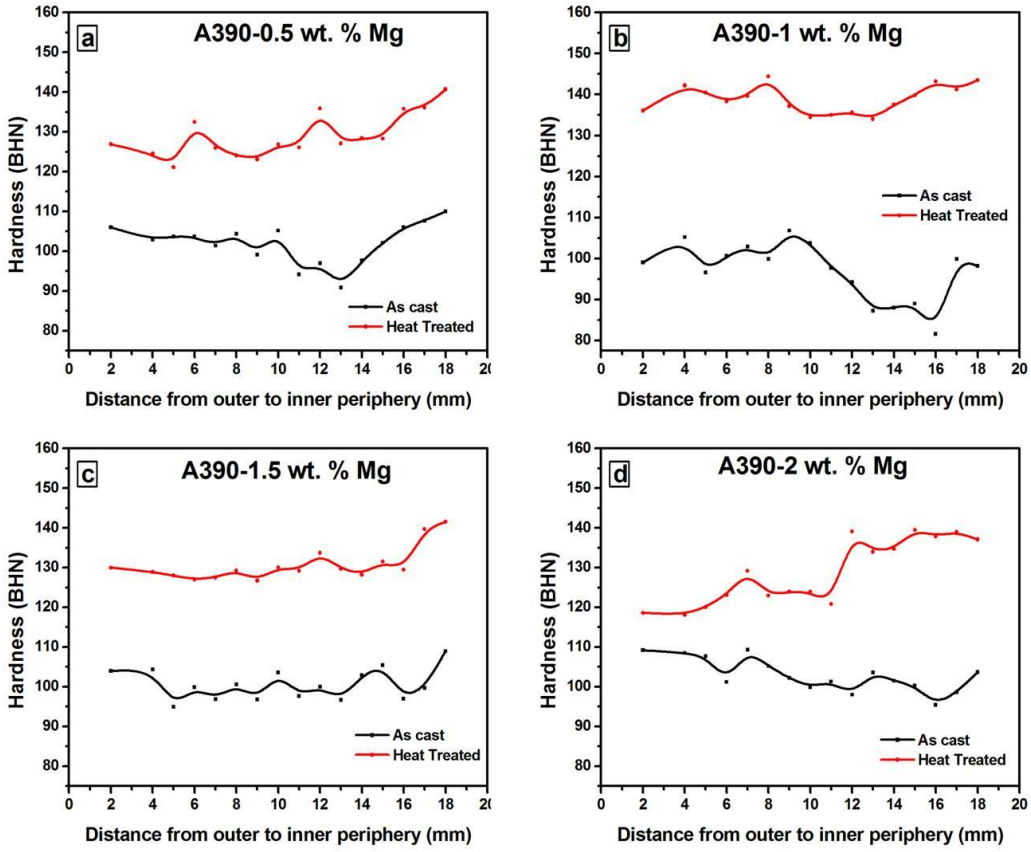

Figure 5.19 Hardness profile of Mg added A390 centrifugal cast cylinder for the as-cast and precipitated treated samples (a) A390-0.5 wt. % Mg (b) A390-1 wt. % Mg (c) A390-1.5 wt. % Mg and (d) A390-2 wt. % Mg

value of 125 BHN is obtained at the outer diameter of the component. At the outer most region of A390-0.04 wt. % Sr indicates 121.5 BHN and 139.5 BHN at the inner region of the cylindrical casting. Among the Sr added A390 alloy system by centrifugal casting, A390-0.03 wt. % shows better hardness than the other alloy systems.

Figure 5.21a-d indicates the hardness values of centrifugal cast Zr added A390 aluminum alloy at 0.01 wt. % to 0.04 wt. %. Here also the heat treated samples show the best hardness than the as-cast samples. The hardness profiles of A390-Zr modified cast cylindrical systems generally shows almost steady increase in the hardness values upto a certain region (10 – 12 mm) and then increases the values to a maximum towards the inner most regions. In all the Zr modified A390 systems, there is a point between 10 mm and 14 mm that shows an increase in the hardness values that the other regions upto 10 mm. This region is called transition region. Primary silicon phases are accumulated from the transition region to the innermost region where, the volume of primary silicon phases gradually increases from the transition region to the inner most regions

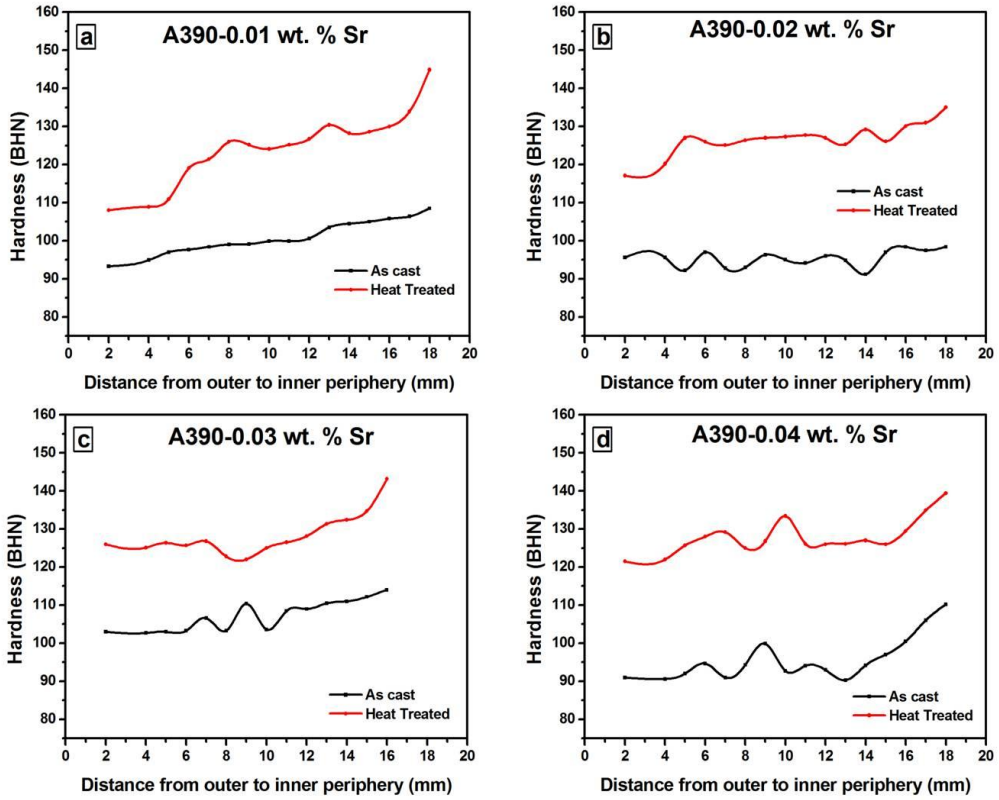

Figure 5.20 Hardness profile of Sr added A390 centrifugal cast cylinder for the as-cast and precipitated treated samples (a) A390-0.01 wt. % Sr (b) A390-0.02 wt. % Sr (c) A390-0.03 wt. % Sr and (d) A390-0.04 wt. % Sr

depending upon the size and relative density of the phases present at that region. A minimum hardness of 123 BHN at 9 mm and a maximum of 146 BHN at 18 mm are obtained in the heat treated condition for 0.01 wt. % addition of Zr in A390 alloy. As the percentage addition of the Zr is increased from 0.01 to 0.02 wt., the minimum value falls to 119 BHN at 2 mm and the maximum value raised to a value of 158 BHN at 18 mm. Further the formation of Al_3Zr phases enhances the hardness of the Zr added alloys. At 0.03 wt. % addition of Zr in A390 exhibits a minimum hardness value of 125.5 BHN at 8 mm and a maximum hardness of 149 BHN was obtained at 18 mm in the heat treated condition. The maximum value at 0.04 wt. % addition of Zr in A390 falls to 139 BHN at 18 mm. The Zr added at 0.03 wt. % proves the best hardness among the other Zr added alloy systems. The best conditions that obtained from the microstructural and hardness characterizations of the Mg, Sr and Zr added A390 cylindrical component are again fabricated in disc mould of diameter 240 mm and 30 mm height for further characterizations such as tensile, compression and wear tests since the FGM cylinder produced are not sufficiently larger enough to prepare samples out of it. The best conditions for hardness are obtained for A390-1.5 wt. % Mg, A390-0.03 wt. % Sr and A390-0.03 wt. % Zr. The effect of combined addition of 1.5 wt. % Mg-0.03 wt. % Sr and 1.5 wt. % Mg-0.03 wt. % Zr in A390 aluminium alloy are also studied.

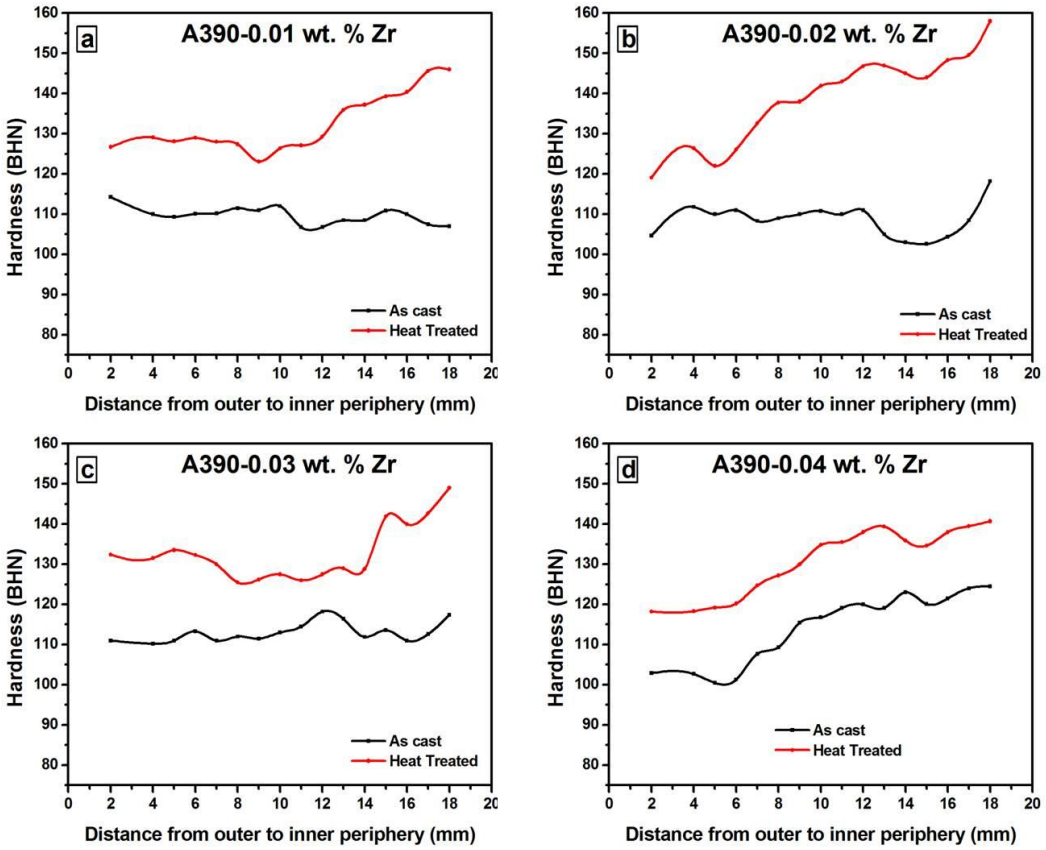

Figure 5.21 Hardness profile of Zr added A390 centrifugal cast cylinder for the as-cast and precipitated treated samples (a) A390-0.01 wt. % Zr (b) A390-0.02 wt. % Zr (c) A390-0.03 wt. % Zr and (d) A390-0.04 wt. % Zr

5.5.3 Characteristics of FGM discs

5.5.3.1 Microstructural observations

Figure 5.22 shows the microstructures of A390-1.5 wt. % Mg centrifugal cast disc. The microstructures are taken from outer periphery of the casting to the inner periphery. The microstructures shown are at 0.5 mm, 20 mm, 60 mm and 90 mm from the outer periphery of the cast disc. The outer most regions at 0.5 mm in Figure 5.22a shows fine grains of aluminium phase and eutectic silicon phases. The fine grains of aluminium phases are due to the forced solidification of the liquid melt and due to the preheat temperature of the mould. The Mg added into the A390 aluminium alloy combine with Si present in the alloy system forms the Mg_2Si phases. In Figure 5.22c, the transition region shows the presence of α-aluminium, eutectic silicon, clusters of eutectic silicon, primary silicon and also the transformation of eutectic silicon clusters to primary silicon. Moreover, the innermost region of the centrifugal

cast disc at 90 mm in Figure 5.22d shows a higher concentration of primary silicon. Figure 5.23 shows the optical microstructures of 0.03 wt. % Sr in A390 aluminium alloy. The eutectic silicon changes the morphology from needle shaped structure to the fibrous network structure. From outer to inner periphery the microstructures reveals the affinity of eutectic silicon sustain as clusters. Even though the strontium added A390 shows better hardness properties than the base alloy system, some porosity is visible in the microstructures. Figure 5.24 represents the optical microstructures of 0.03 wt. % Zr added in A390 aluminium alloy FGM disc from outer to the inner periphery of the casting. The aluminium phases are finer towards the outer region and coarser towards the inner region whereas the eutectic silicon changes the morphology as short and broken needle shaped structures. Also, the primary silicon segregated towards the inner region due to the low density during the centrifugal action is seen as finer at the transition region and coarser towards the inner region [Figure 5.24c and d] as compared with the other FGM alloy systems. Figure 5.25 represents the microstructures of combined addition of 1.5 wt. % Mg and 0.03 wt. % Sr in A390 aluminium alloy centrifugal disc. As in the previous alloy systems, the microstructures exhibit a fine α-aluminium phase towards the outer periphery and coarser towards the inner periphery. Also, the eutectic silicon appears as clusters at 65 mm and primary silicon particles are finer towards the inner periphery. The porosities at the inner most regions are generally because of the accumulation of low density gas bubbles at this region due to the centrifugal casting effect. Figure 5.26 displays the optical microstructures of combined addition of 1.5 wt. % Mg and 0.03 wt. % Zr in A390 aluminium alloy. The outer region of the disc shows fine and short eutectic phases. The inner region of the centrifugal FGM disc showed equally sized and shaped primary silicon from the transition to the inner region. Moreover, at the inner region the number of eutectic silicon phases are very less as compared with the A390-1.5 wt. % Mg-0.03 wt. % Sr. Also the innermost region exhibits some porosities due to the segregation of low density materials and gas bubbles since the gravitational G factor is less towards the axis of the rotation during centrifugal casting.

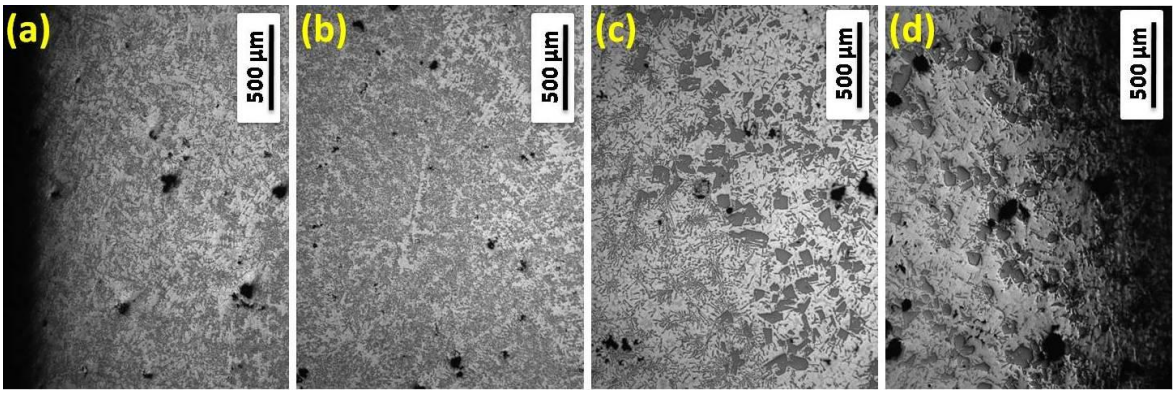

Figure 5.22 Optical microstructures of A390-1.5 wt. % Mg functionally graded disc at (a) 0.5 mm (b) 20 mm (c) 60 mm and (d) 90 mm from the outer periphery of the centrifugal casting

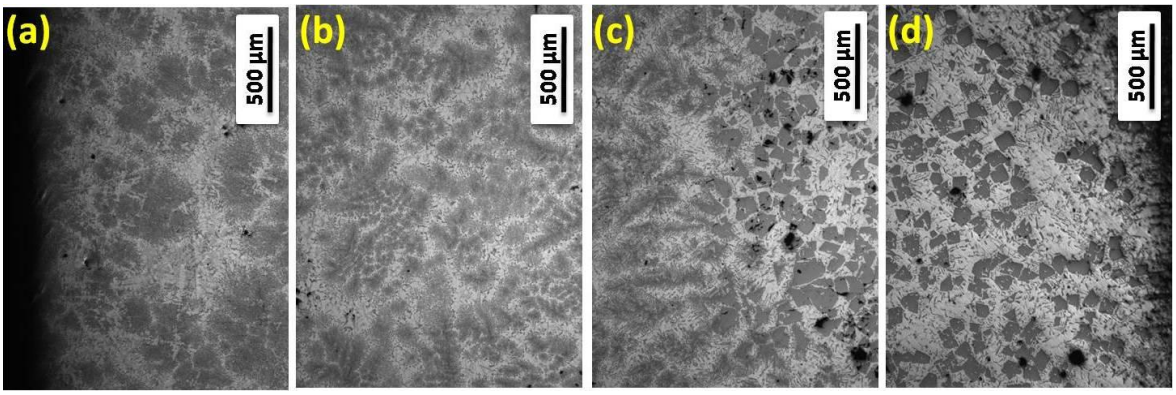

Figure 5.23 Optical microstructures of A390-0.03 wt. % Sr functionally graded disc at (a) 0.5 mm (b) 20 mm (c) 60 mm and (d) 70 mm from the outer periphery of the centrifugal casting

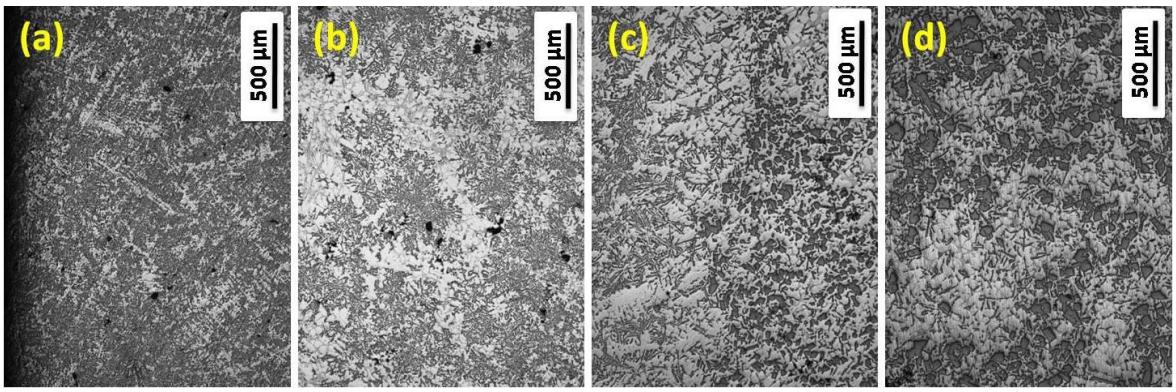

Figure 5.24 Optical microstructures of A390-0.03 wt. % Zr functionally graded disc at (a) 0.5 mm (b) 20 mm (c) 65 mm and (d) 90 mm from the outer periphery of the centrifugal casting

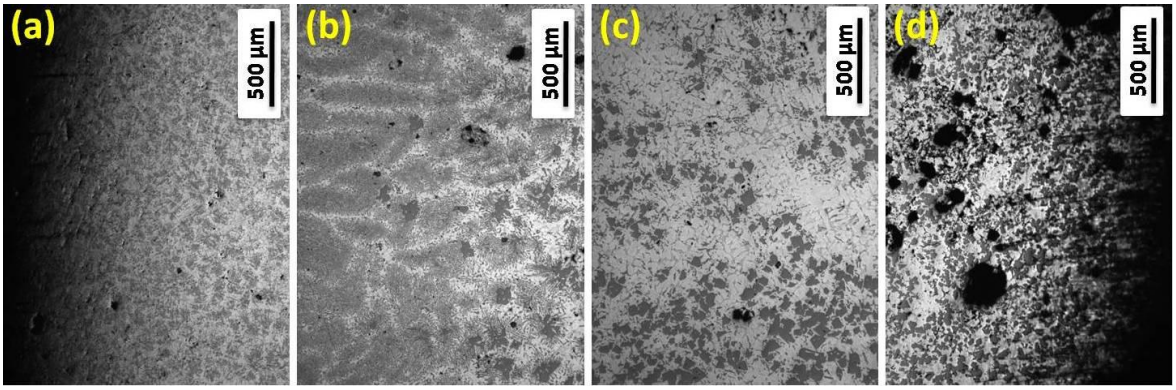

Figure 5.25 Optical microstructures of combined addition of 1.5 wt. % Mg and 0.03 wt. % Sr in A390 (A390-1.5 wt. % Mg-0.03 wt. % Sr) functionally graded disc at (a) 0.5 mm (b) 20 mm (c) 60 mm and (d) 90 mm from the outer periphery of the centrifugal casting

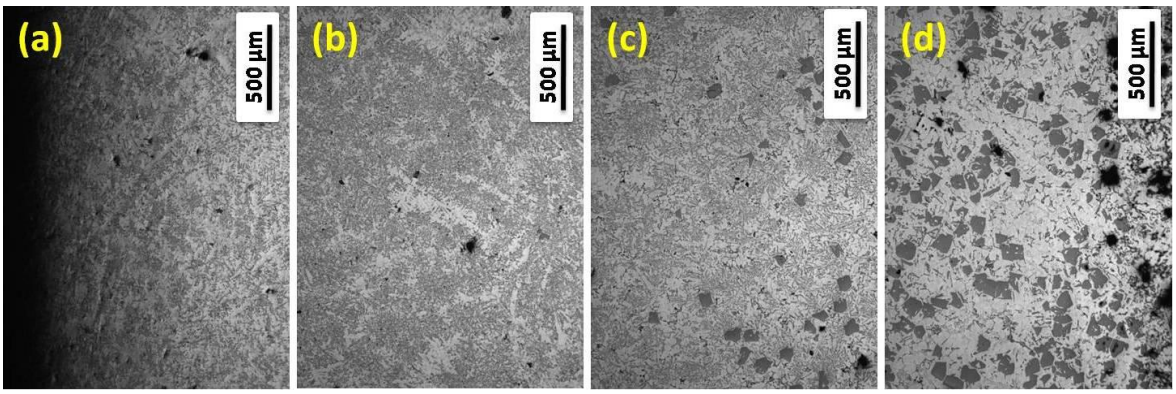

Figure 5.26 Optical microstructures of combined addition of 1.5 wt. % Mg and 0.03 wt. % Zr in A390 (A390-1.5 wt. % Mg-0.03 wt. % Zr) functionally graded disc at (a) 0.5 mm (b) 20 mm (c) 60 mm and (d) 90 mm from the outer periphery of the centrifugal casting

5.5.3.2 Hardness

Figure 5.27 shows the as-cast and heat treated hardness profiles of centrifugally cast A390-1.5 wt. % Mg disc. The hardness in BHN is measured from the outer to the inner periphery of the cast disc at 5 mm interval. In the as-cast condition the hardness maintains almost a steady value (100 ± 5 BHN) up to 55 mm and then decreases, which may due to the coarse microstructures and microporosities at the inner region of the cast disc. But in the heat treated condition it is observed that after 55 mm the hardness towards the inner region increases due to the formation of more precipitation hardening phases and the presence of primary silicon particles segregated at this region during centrifugal casting. The outer most periphery of the disc indicates a hardness of 100 BHN and slightly less towards the next regions. The higher hardness value at the outer region is because of the fine grain size of α-aluminium and eutectic silicon. Moreover, the hardness values at 10 mm and 15 mm show less hardness as compared with the outer due to the coarse grains of the aluminium phase. Then the hardness drops to certain values and maintains almost the range of hardness due to

the similarity in the sizes of the α-aluminium and eutectic silicon phases. The harness increases to 138 BHN at 60 mm and reaches a maximum value of 158 BHN at 75 mm. The increase in the hardness from 60 mm onwards is due to the presence of primary silicon and Mg_2Si appears in the microstructures in Figure 5.22c and d. Even the inner periphery of the as-cast component shows a lower hardness than the previous regions, but after the heat treatment, the inner periphery shows an improved hardness than the as-cast condition due to the dilution effect of the Mg addition. The Figure 5.28 shows the hardness graphs for the centrifugal cast disc of A390-0.03 wt. % Sr. The region close to outer periphery shows slightly higher hardness due to the chill zone formation and finer grain size. Then the hardness values decreases from the outer region of the casting to a distance of 30 mm and increases to 50 mm and then decreased and increased. The intermediate increase in the hardness values is due to the presence of primary silicon particles precipitated at those regions due to the solidification front from the top and bottom of the disc mould during centrifugal casting. In this, a minimum value of 127.5 BHN is achieved at 55 mm and a maximum value of 151 BHN is achieved at 75 mm from the outer periphery which is less than that compared with the Mg added centrifugal cast alloy system. It is because the hardening phase of Mg_2Si is absent in the case of Sr added system and also due to the higher porosity level observed in the Sr added system. Figure 5.29 indicates the hardness profile of A390-0.03 wt. % Zr centrifugal cast FGM disc from outer to the inner periphery at 5 mm apart. The Zr modified system shows a general trend of decreasing hardness towards the inner region of the cast disc even in the presence of primary silicon particles. The FGM disc shows an enhanced hardness in the heat treated condition which gives a minimum value of hardness of 101 BHN at the inner region and a maximum hardness value of 143 BHN at 40 mm. Apart from the other centrifugal cast FGM discs with the individual addition of Mg and Sr in A390 the Zr added alloy system shows a reduced hardness towards the inner region of the casting even in the presence of hard primary silicon particles. The combined addition of Mg and Sr in A390-1.5 wt. % Mg-0.03 wt. % Sr alloy system in Figure 5.30 shows 124.5 BHN at 30 mm and 143.5 BHN in the inner most region at 65 mm from the outer diameter of the disc. Figure 5.31 shows the hardness graph of A390-1.5 wt. % Mg-0.03 wt. % Zr alloy from outer to the inner region of the cast disc. However, apart from the combined addition of Mg and Sr in A390, the Mg and Zr added A390 alloy system revels that the hardness values from the outer to the inner periphery decreases even in the presence of primary silicon particles. This decrease in the hardness values towards the inner region of the cast disc is due to the segregation of high density (4.1 g/cm^3) Al_3Zr phases towards the outer region of the casting. However, the combined addition shows only lesser hardness than the Mg added at 1.5 wt. % in A390 aluminium alloy.

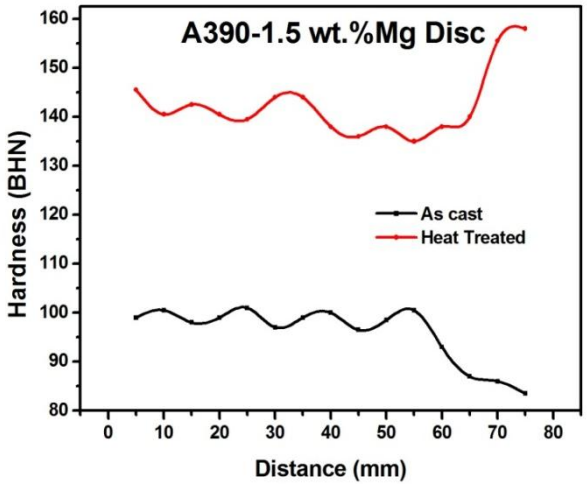

Figure 5.27 Hardness profile of A390-1.5 wt. % Mg centrifugal cast disc from outer to inner periphery of the castings at 5 mm interval

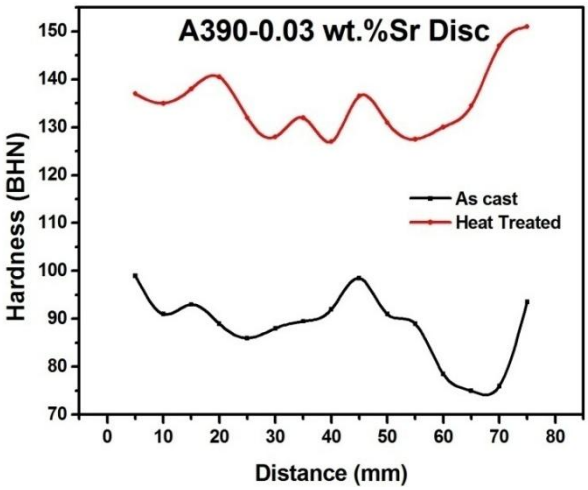

Figure 5.28 Hardness profile of A390-0.03 wt. % Sr centrifugal cast disc from outer to inner periphery of the castings at 5 mm interval

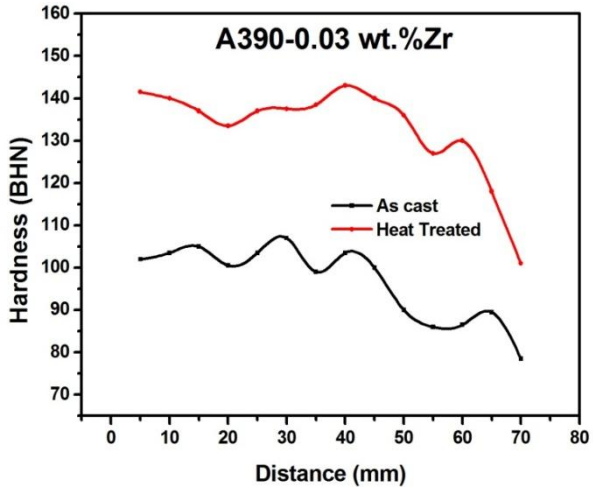

Figure 5.29 Hardness profile of A390-0.03 wt. % Zr centrifugal cast disc from outer to inner periphery of the castings at 5 mm interval

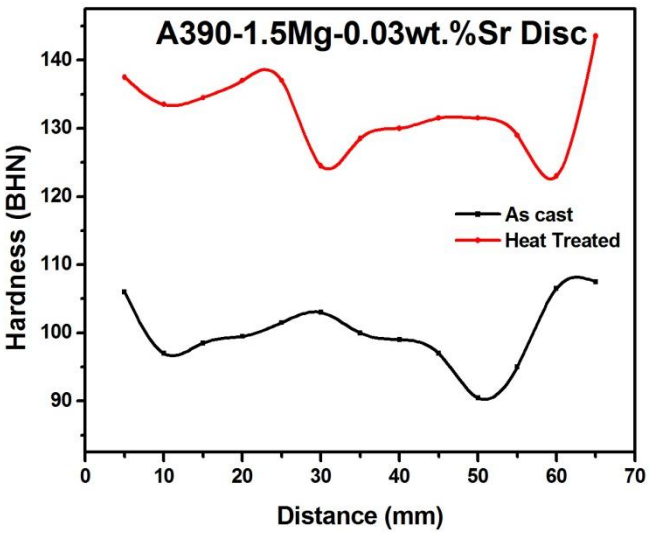

Figure 5.30 Hardness profile of A390-1.5 wt. % Mg-0.03 wt. % Sr centrifugal cast disc from outer to inner periphery of the castings at 5 mm interval

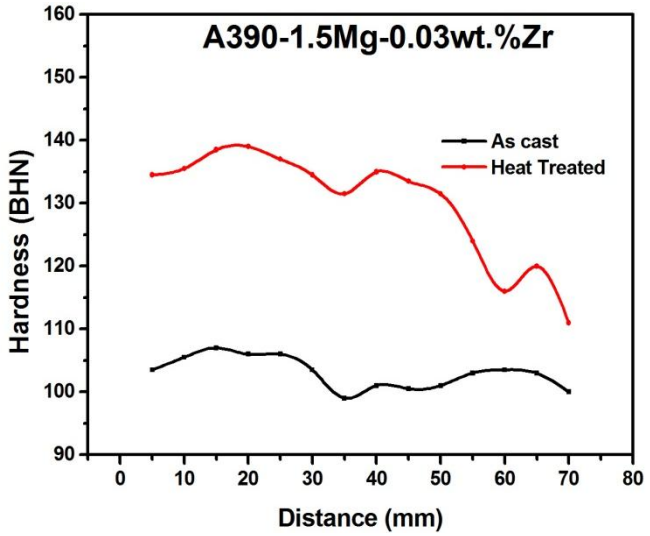

Figure 5.31 Hardness profile of A390-1.5 wt. % Mg-0.03 wt. % Zr centrifugal cast disc from outer to inner periphery of the castings at 5 mm interval

5.5.4 Differential thermal analysis (DTA)

Figure 5.32a-e represents the DTA analyses of A390-1.5 wt. % Mg, A390-0.03 wt. % Sr, A390-0.03 wt. % Zr, A390-1.5 wt. % Mg-0.03 wt. % Sr and A390-1.5 wt. % Mg-0.03 wt. % Zr of centrifugal cast disc at outer, middle, transition and inner region from 300 to 650 °C. The $CuAl_2$ phase starts melting nearly at a temperature of 515 °C for the sample from the outer surface in the five alloy systems. But for the samples from the middle, transition and the inner regions exhibits a shift in the melting of $CuAl_2$ phase below 515 °C from outer to the inner specimens due to the variation in the elemental composition of the elements from the outer to the inner periphery achieved

through the centrifugal casting process. Also the major elements aluminium and silicon melts at a temperature of 560 °C which is represented by the endothermic peaks in the DT analysis. The differential thermal analysis curves of all the samples of all the alloy systems shows a shift in the curves depending upon the position of the samples (i.e., outer to inner periphery) due to the addition of Mg, Sr, Zr and the combined addition of the both Mg, Sr and Zr.

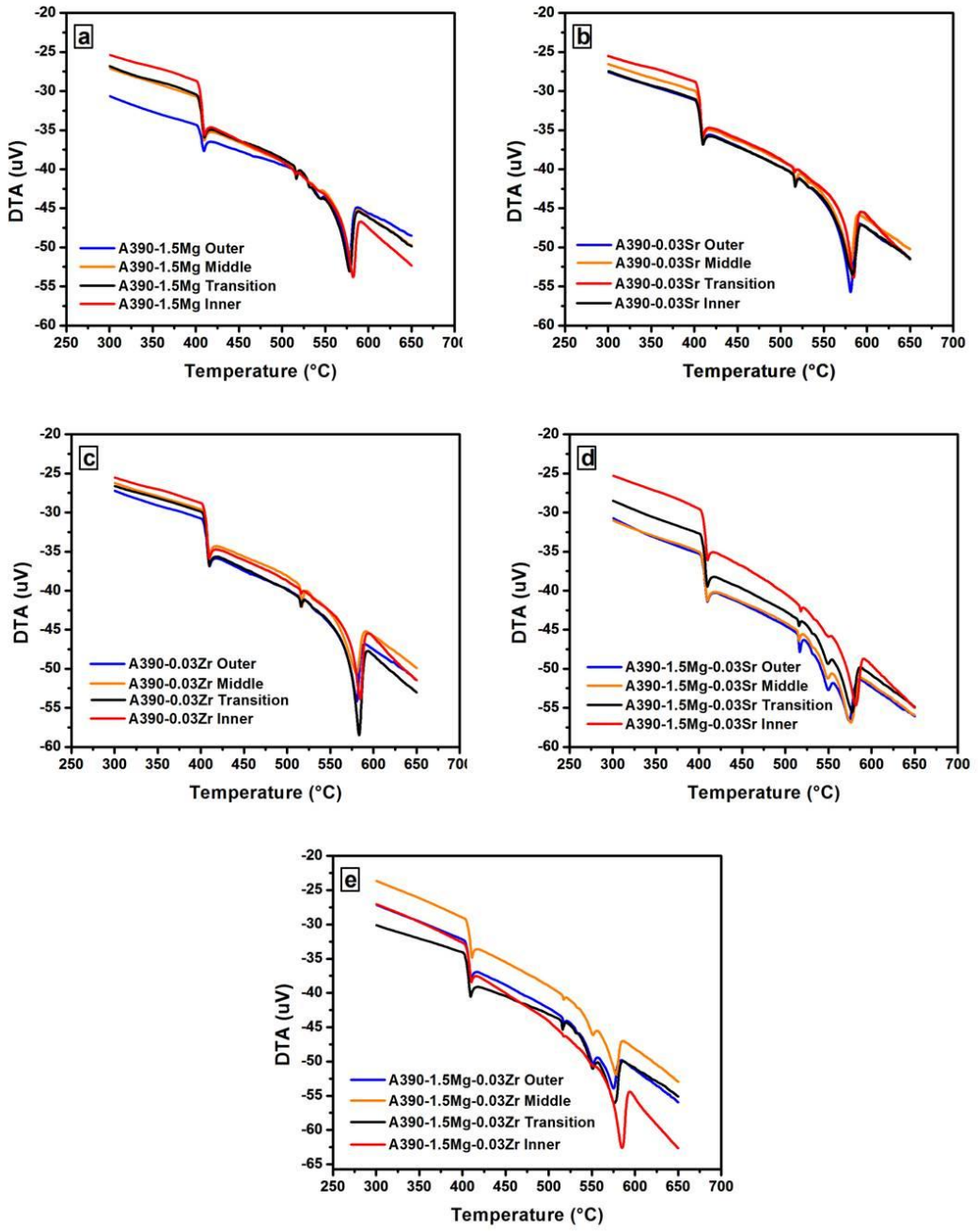

Figure 5.32 DTA of centrifugal cast A390 aluminium alloy disc (a) A390-1.5 wt. % Mg, (b) A390-0.03 wt. % Sr, (c) A390-0.03 wt. %Zr, (d) A390-1.5 wt. % Mg-0.03 wt. % Sr and (e) A390-1.5 wt. % Mg-0.03 wt. % Zr

5.5.5 Tensile and compression properties

Figure 5.33 and 5.39 shows the tensile and compression strengths of outer, middle and inner specimens of A390-1.5 wt. % Mg, A390-0.03 wt. % Sr, A390-0.03 wt. % Zr, A390-1.5 wt. % Mg-0.03wt. % Sr and A390-1.5 wt. % Mg-0.03 wt. % Zr aluminium alloy systems. The centrifugal cast disc A390-1.5 wt. % Mg aluminium alloys at outer, middle and inner regions gives an ultimate tensile strength values of 271, 274 and 214 MPa, respectively while that of A390-0.03 wt. % Sr and A390-0.03 wt. % Zr gives 280, 250 and 246 MPa for Sr added system and 271, 276 and 260 MPa for Zr added system at outer, middle and inner regions, respectively. The combined addition of 1.5 Mg and 0.03 Sr in A390 aluminium alloy shows a tensile strength of 295, 266 and 264 MPa at outer, middle and inner regions and the combined addition of 1.5 Mg and 0.03 Zr indicates a tensile strength of 292, 249 and 253 MPa respectively at the three regions of the centrifugal cast disc. The variation in the tensile strengths can be clearly distinguishable from the bar graph provided in Figure 5.33. From the tensile values of Mg, Sr, Zr and combined addition of Mg-Sr and Mg-Zr in A390 aluminium alloy systems, the values at middle region shows higher values than the outer and inner regions of the Mg added alloy systems. This variation in the tensile values at the outer and middle regions is due to the grain size of aluminum phases in these regions due to the addition of Mg at 1.5 wt. % in A390-1.5 wt. % Mg and A390-1.5 wt. % Mg-0.03 wt. % Sr alloy systems. The outer region of the cast component shows very fine α-aluminium phases and short eutectic silicon phases but, the middle region is enriched with coarser phases of aluminium as compared with the outer region and this gives more ductility than the outer region. This is the reason that the middle regions of A390-1.5 wt. % Mg and A390-1.5 wt. % Mg-0.03 wt. % Sr gives higher ultimate tensile strength than the outer regions. In the A390-0.03 wt. % Sr system, the strength of the middle region is comparatively lesser than the outer region when compared with the other alloy systems, due to the microporosities found in the microstructure in Figure 5.23 b and c because of the addition of Sr in the alloy. The addition of Sr always exhibits the presence of micro-porosities throughout the castings. The inner regions of Zr added A390 centrifugal cast alloy disc shows lesser values as compared with the other regions. The inner regions are enriched with the silicon and primary silicon particles accumulated due

to the low density of primary silicon particles during the rotation of the centrifugal mould during the casting process. The presence of silicon and primary silicon gives brittle nature at the regions they are present. The inner region of the cast component in Figure 5.22-5.25 shows a higher percentage of silicon and primary silicon. The newly developed alloy systems achieved closer tensile strengths in comparison with the standard tensile strength of A390 aluminium alloy. Figure 5.34-5.37 shows the SEM analysis of fracture surface of tensile specimens at the outer, middle and inner regions. The SEM analysis of the fractured surface of A390-1.5 wt. % Mg tensile specimen at Figure 5.34a-c shows a combination of ductile and brittle nature of fractures at outer, middle and inner regions, respectively where, the ductile nature is due to the α-aluminium and the brittle nature is because of the eutectic silicon and primary silicon phases. The inner region had undergone the brittle type of fracture due to the presence of primary silicon at this region. The fractograph of A390-0.03 wt. % Sr at outer, middle and inner regions is depicted in Figure 5.35a-c. From the fractograph, it is revealed that the failure of the tensile specimens occurred at the outer and middle regions are due to the presence of micro-porosities that is evident from the optical microstructures [Figure 5.23] and the surface analysis of tensile specimens in Figure 5.35. The inner region in Figure 5.35c shows cracks in the surface morphology due to the presence of primary silicon and brittleness provided by the primary silicon to these specimens at this region. The surface morphology of 0.03 wt. % Zr added A390 alloy reveals from the Figure 5.36 that the failure at the outer region is due to the presence of gas porosities and the inner region is due to the presence of both shrinkage and gas porosities and brittleness achieved through the segregation of primary silicon. The combined addition of the 1.5 wt. % Mg-0.03 wt. % Sr and 1.5 wt. % Mg-0.03 wt. % Zr [Figure 5.37 and 5.38] in A390 alloy tensile specimens also shows some porosities in the microstructures at outer, middle and inner regions in Figure 5.25 and 5.26 . Also, the SEM analysis shows ductile nature throughout the tensile experiments which are evident from the fractograph.

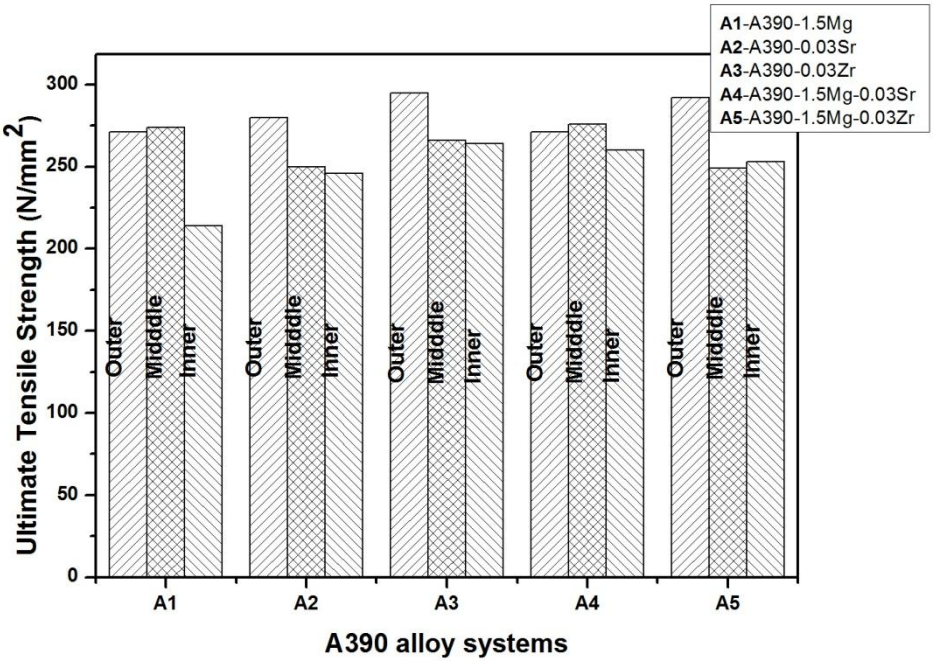

Figure 5.33 Tensile strengths of Mg, Sr, Zr, combined addition of Mg-Sr and Mg-Zr in A390 aluminium alloy

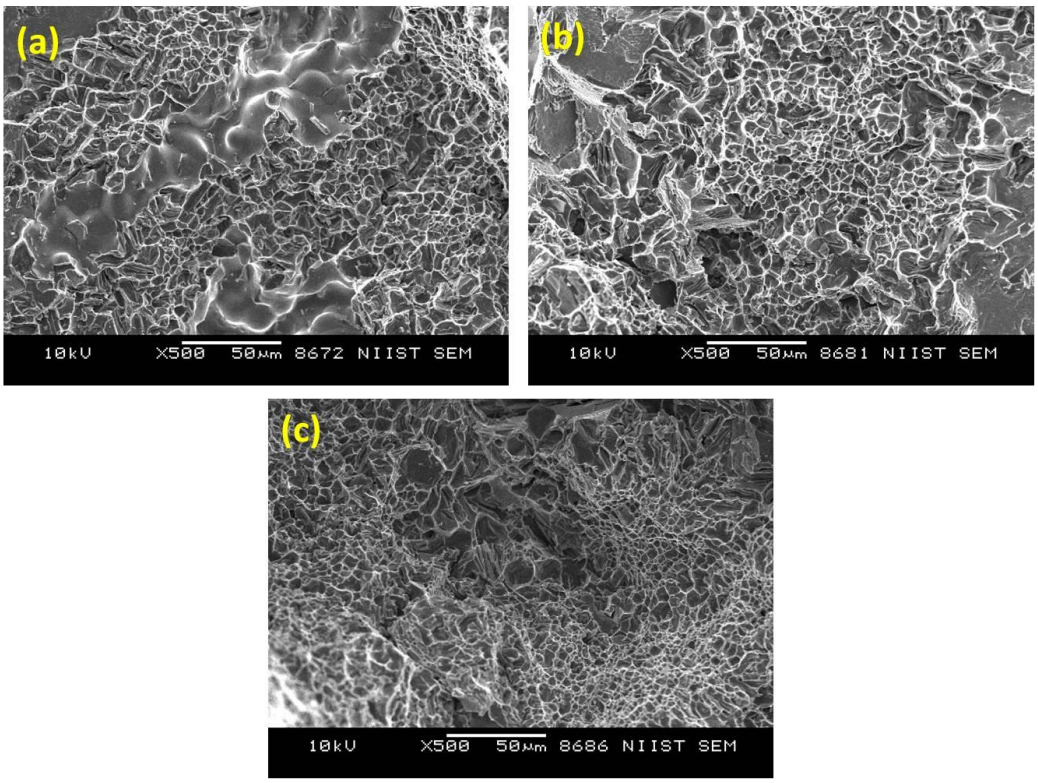

Figure 5.34 SEM analysis of fracture surface of A390-1.5 wt. % Mg (a) outer specimen (b) middle specimen and (c) inner specimen

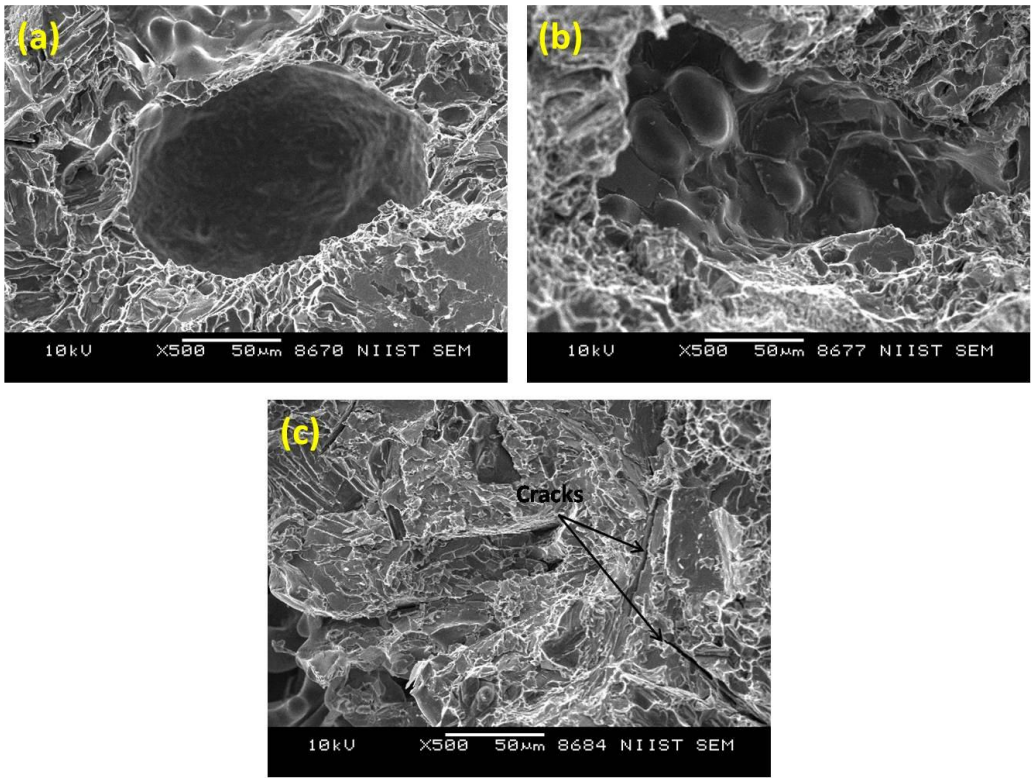

Figure 5.35 SEM analysis of fracture surface of A390-0.03 wt. % Sr (a) outer specimen (b) middle specimen and (c) inner specimen

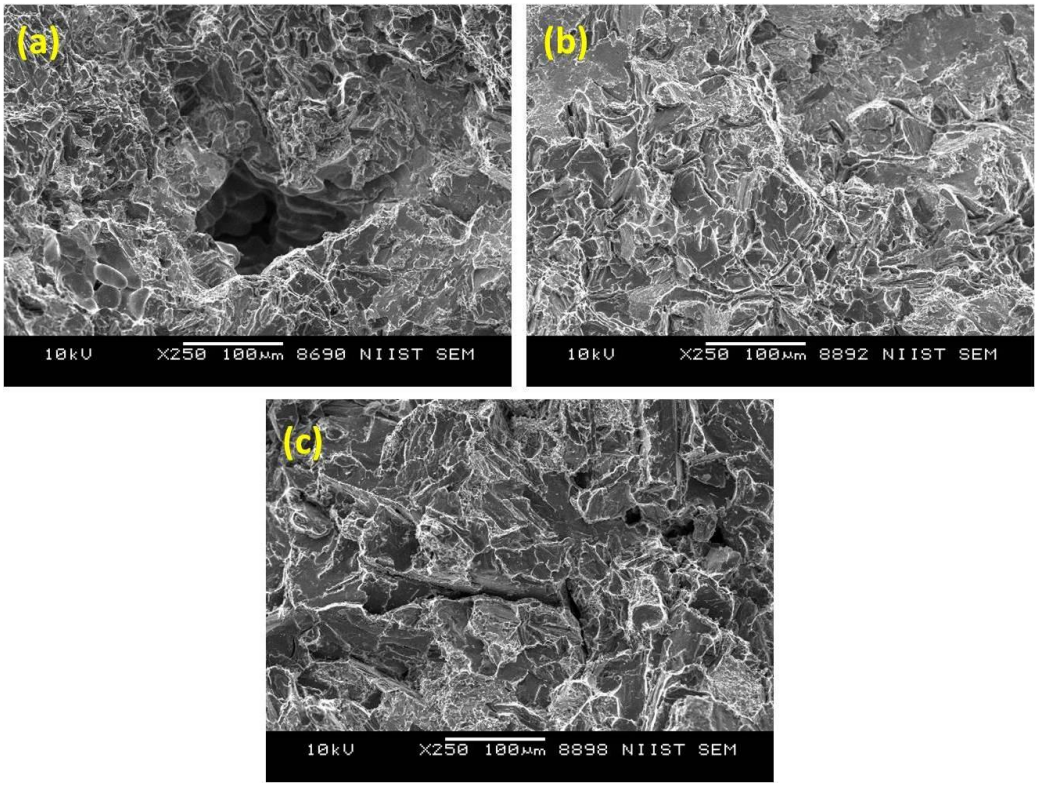

Figure 5.36 SEM analysis of fracture surface of A390-0.03 wt. % Zr (a) outer specimen (b) middle specimen and (c) inner specimen

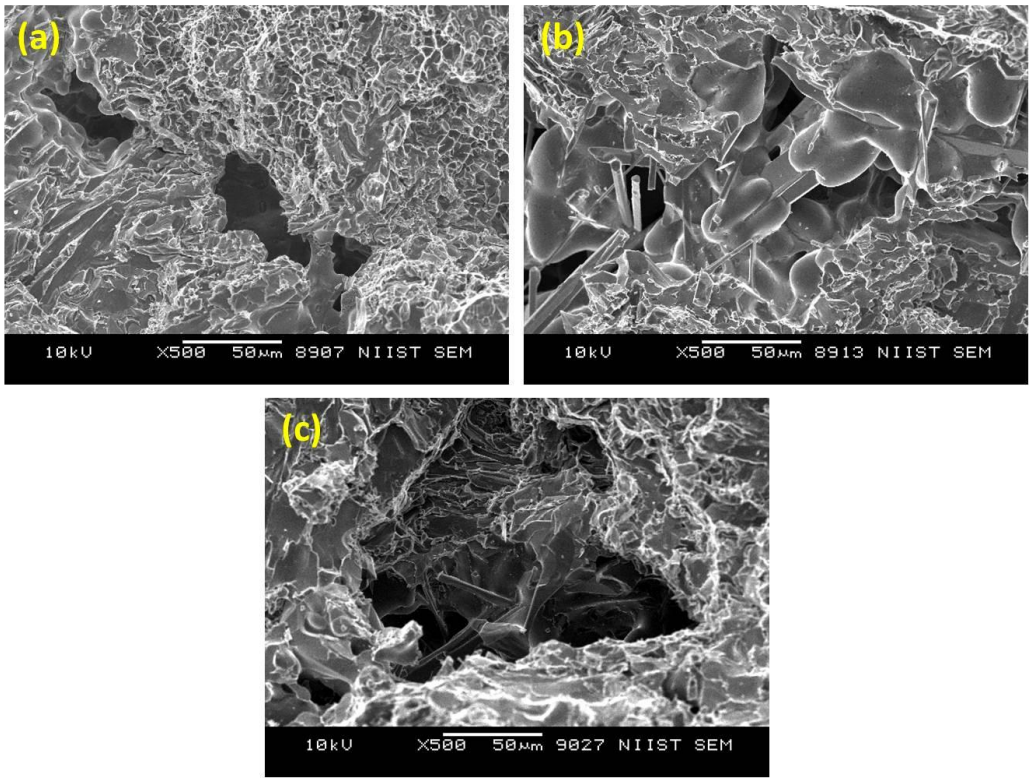

Figure 5.37 SEM analysis of fracture surface of A390-1.5 wt. % Mg-0.03 wt. % Sr (a) outer specimen (b) middle specimen and (c) inner specimen

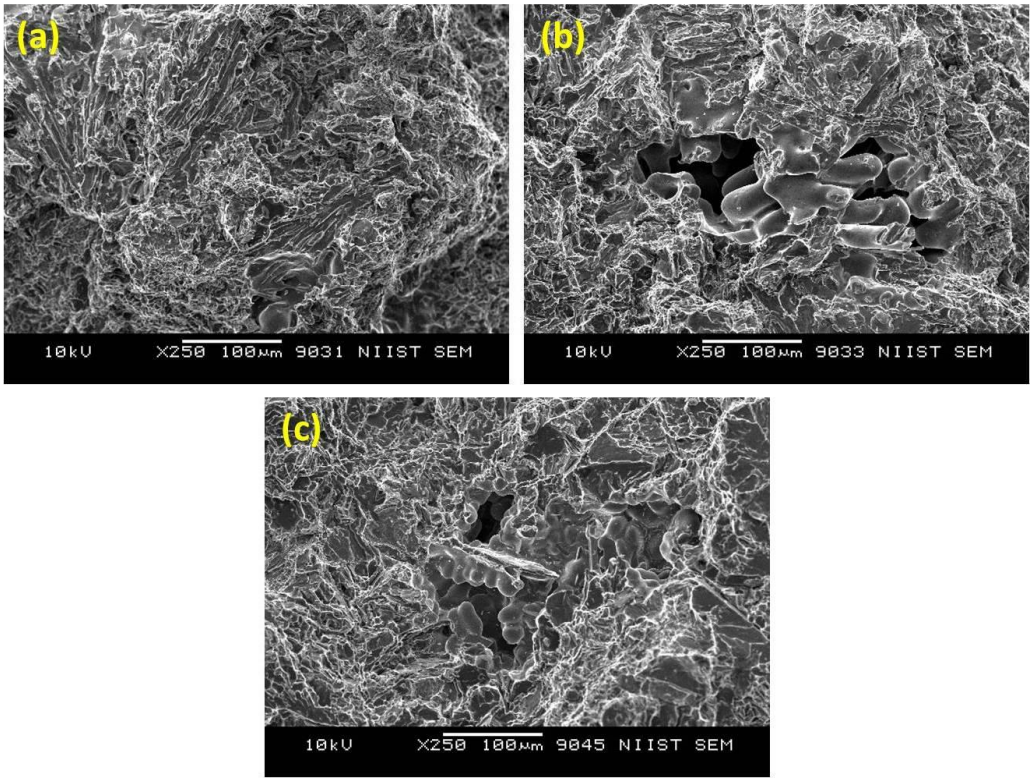

Figure 5.38 SEM analysis of fracture surface of A390-1.5 wt. % Mg-0.03 wt. % Zr (a) outer specimen (b) middle specimen and (c) inner specimen

Figure 5.39 is the bar chart showing the compressive strengths of A390-1.5 wt. % Mg, A390-0.03 wt. % Sr, A390-0.03 wt. % Zr, A390-1.5 wt. % Mg-0.03Sr and A390-1.5 wt. % Mg-0.03 wt. % Zr at outer, middle and inner regions. The outer, middle and inner regions of A390-1.5 wt. % Mg provides compressive strengths of 540, 578 and 590 MPa respectively. The inner region gives higher compression strength than the outer and the middle regions due to the presence of primary silicon at this region that gives brittleness to the component at the inner region. A390-0.03 wt. % Sr centrifugal cast alloy system gives 585, 598 and 592 MPa at the outer, middle and inner regions, respectively. The 0.03 wt. % added Zr alloy system provides a compressive strength of 551, 576 and 553 MPa. Also the combined addition of Mg-Sr and Mg-Zr in the A390 aluminium alloy cast disc gives the compressive strength values as 583, 612 and 522 MPa for Mg-Sr system and 470, 537, 570 MPa for Mg-Zr systems at the three regions.

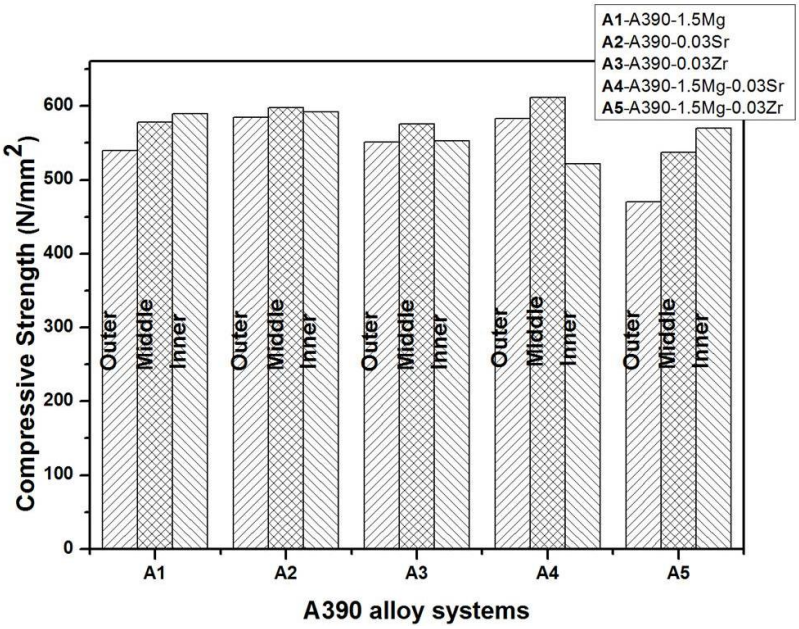

Figure 5.39 Compression strengths of Mg, Sr, Zr, combined addition of Mg-Sr and Mg-Zr in A390 aluminium alloy

5.5.6 Wear studies

The wear rate of centrifugal cast disc of A390-1.5 wt. % Mg, A390-0.03 wt. % Sr, A390-0.03 wt. % Zr, A390-1.5 wt. % Mg-0.03 wt. % Sr and A390-1.5 wt. % Mg-0.03 wt. % Zr are represented in the Figure 5.40a-e. The wear rate values are calculated by taking the difference in the weight of the wear specimens before and after the test and the rate of wear is represented in mm^3/Nm by considering the volume of the

wear. Figure 5.40a illustrates the wear rate values of outer, middle and inner specimens of A390-1.5 wt. % Mg. The graph reveals that at lower loads the wear specimens shows nearly same magnitude of wear rate for the specimens from the three regions. The wear rate of the middle region shows a minimum wear rate of 3.08787 x 10^{-5} mm^3/Nm at 19.62 N and shows a maximum wear rate value of 53.26578 x 10^{-5} mm^3/Nm at 78.48 N, among the other specimens at lower and higher loads. The outer and inner specimens of the Mg added A390 alloy system shows almost close values at all the loads. This is because the outer and inner region specimens acquired a fine structured aluminum phases at outer region and primary silicon rich phases at the inner region which gives a higher hardness values than the middle region as represented in the hardness graph in Figure 5.27. The specimens from the middle regions are with coarser phases of aluminium and this region has the lowest hardness among the other two regions which shows a higher wear rate as compared with the outer and inner specimens.

Figure 5.40b indicates the wear rate values of Sr added A390 centrifugal cast aluminium alloy system. In this, the outer region shows the minimum wear rate, the middle region shows the maximum wear rate and the inner region specimens shows an intermediate wear rate values at all the loads. The outer region specimen shows a minimum wear rate of 1.05909 x 10^{-5} mm^3/Nm at 19.62 N and a maximum wear rate of 6.30157 x 10^{-5} mm^3/Nm at 78.48 N. The specimens of middle regions give a minimum wear rate at a load of 39.24 N of 12.83064 x 10^{-5} mm^3/Nm and maximum of 18.74757 x 10^{-5} mm^3/Nm at 78.48 N. The outer specimens underwent minimum wear rate than the inner regions that contains primary silicon particles. This is because, the outer specimens have very fine grain size of aluminium than the inner where, porosities at micron levels are observed in microstrcture and the hardness is also lower as observed in hardness profile of Sr added system.

The wear rate of A390-0.03 wt. % Zr is presented in the Figure 5.40c. The graph reveals that the specimens of the outer regions show higher wear rate at almost all the loads and minimum wear rate for the specimens of the inner region due to the presence of primary silicon particles at this region. The maximum wear rate of the inner specimen is 12.20462 x 10^{-5} mm^3/Nm, while that of the outer specimen is 62.43324 x 10^{-5} mm^3/Nm at 78.48 N. The wear rates of combined addition of best combinations of Mg and Sr in A390 aluminium alloy is depicted in the Figure 5.40d. The combined addition of 1.5 wt. % Mg and 0.03 wt. % Sr

provides least wear rate for the specimens of the middle region where the silicon and the magnesium reacts and form Mg_2Si and is visible in the microstructures gives strength and hardness in this region. The outer specimen shows the maximum wear rate at the lower and higher load, i.e., 13.02678 x 10^{-5} mm^3/Nm and 63.61356 x 10^{-5} mm^3/Nm, respectively. The specimens of the inner region show a minimum of 9.82779 x 10^{-5} mm^3/Nm and a maximum of 44.26988 x 10^{-5} mm^3/Nm wear rate at 19.62 N and 78.48 N, respectively. The A390-1.5 wt. % Mg-0.03 wt. % Zr system in Figure 5.40e indicates a maximum wear for the middle specimens at all the loads. The outer and inner specimens shows almost close values of wear rate at 19.62, 39.24 and 58.86 N loads, but at 78.48 N load the inner specimen underwent a higher wear rate than the outer specimen at the same load due to the reduced hardness values obtained at the inner region in Figure 5.31 for the combined addition of the Mg and Zr in A390 aluminium alloy. The outer specimen of A390-0.03 wt. % Sr shows the maximum wear resistance among the other alloy systems and regions. The wear resistance of the outer specimen shows a reduced wear rate even at the higher loads, due to the finer grain size of alpha aluminium and short needle shaped eutectic silicon attained during solidification process. In general, as the load increases the wear rate also increases. At lower loads of 19.62 N and 39.24 N the A390-0.03wt. % Sr middle region specimens show maximum wear rate and at higher loads, the A390-1.5Mg-0.03Sr inner region specimens show the maximum wear rate.

5.5.7 Worn surface and wear debris analysis

SEM and EDAX analysis carried out on the worn surfaces and worn debris at the outer, middle and inner specimens of the A390-1.5 wt. % Mg, A390-0.03 wt. % Sr, A390-0.03 wt. % Zr, A390-1.5 wt. % Mg-0.03 wt. % Sr and A390-1.5 wt. % Mg-0.03 wt. % Zr at 39.24 and 78.48 N loads are depicted in Figure 5.41-5.50. The worn surface of all the samples ensures a typical sliding wear characteristic. The analyses show a distinct pattern of grooves over the surfaces of the samples that are mostly running parallel to one another. Fine and deep scratches are observed on the surface analyses at lower and higher loads. The fine grooves are because of the lower pressure exerted to the pin surface due to the loading during the experiment. The deeper grooves are due to the penetration of high intensity asperities from the counter surface to the surface of the pin and may also due to the rubbing of the surfaces of the detached particles between the surfaces. In the Figure 5.41-5.50, a and b represents the outer region, c and d represents the middle region and the Figure e and f represents the inner region as well as the Figures a, c and e represents the analyses at 39.24 N and b, d and f at 78.48 N loads. The SEM analysis of the worn surfaces of A390-1.5 wt. % Mg is provided in the Figure 5.41 and the corresponding wear debris obtained are shown in Figure 5.42.

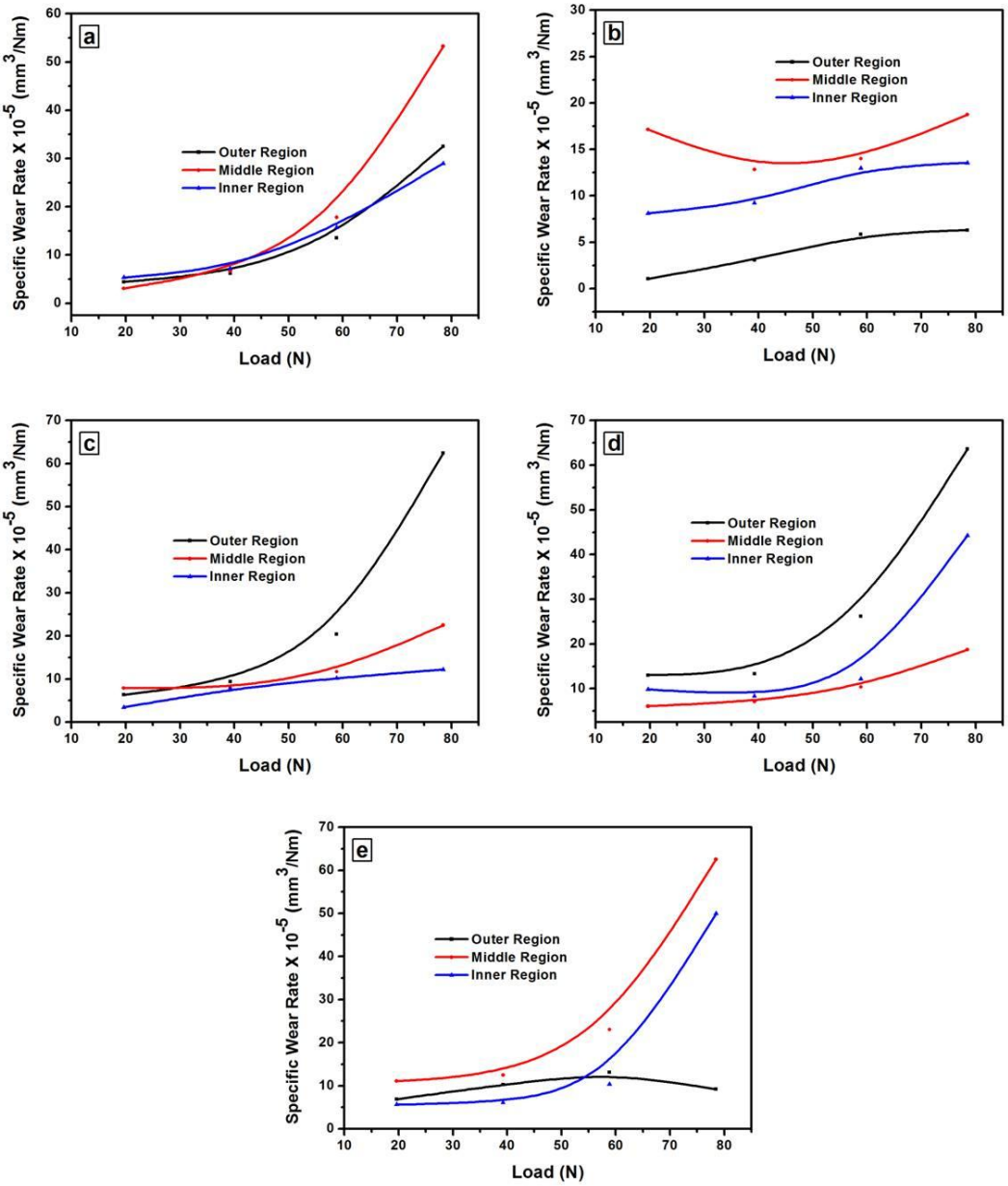

Figure 5.40 Wear rate values of (a) A390-1.5 wt. % Mg, (b) A390-0.03 wt. % Sr, (c) A390-0.03 wt. % Zr, (d) A390-1.5 wt. % Mg-0.03 wt. % Sr and (e) A390-1.5 wt. % Mg-0.03 wt. % Zr centrifugal cast disc

Figure 5.41a-f shows the worn surface analyses of outer, middle and inner wear specimens of A390-1.5 wt. % Mg at a load of 39.24 and 78.48 N. The SEM analyses at the lower load of 39.24 N at outer, middle and inner region shows very fine scars of wear. The outer and inner specimen at this load shows finer scars of wear than the middle region due to the hardness at this region. The hardness at the outer region is acquired during the solidification process where very fine grains of α-

aluminium and short eutectic silicon phases. The higher hardness at the inner region is due to the accumulation of low density primary silicon at the inner region due to the rotation of the mould during the casting process. However, in the middle pin at lower load reveals the presence of oxide layers which helps the surface of the material in further severe wearing. The SEM analyses at a higher load of 78.48 N shows plastically deformed delaminated and sheared surfaces in all the micrographs. But in the inner specimen that underwent wear at 78.48 N loads the surface is not much damaged such as delamination and shear, it only shows the initiation of the

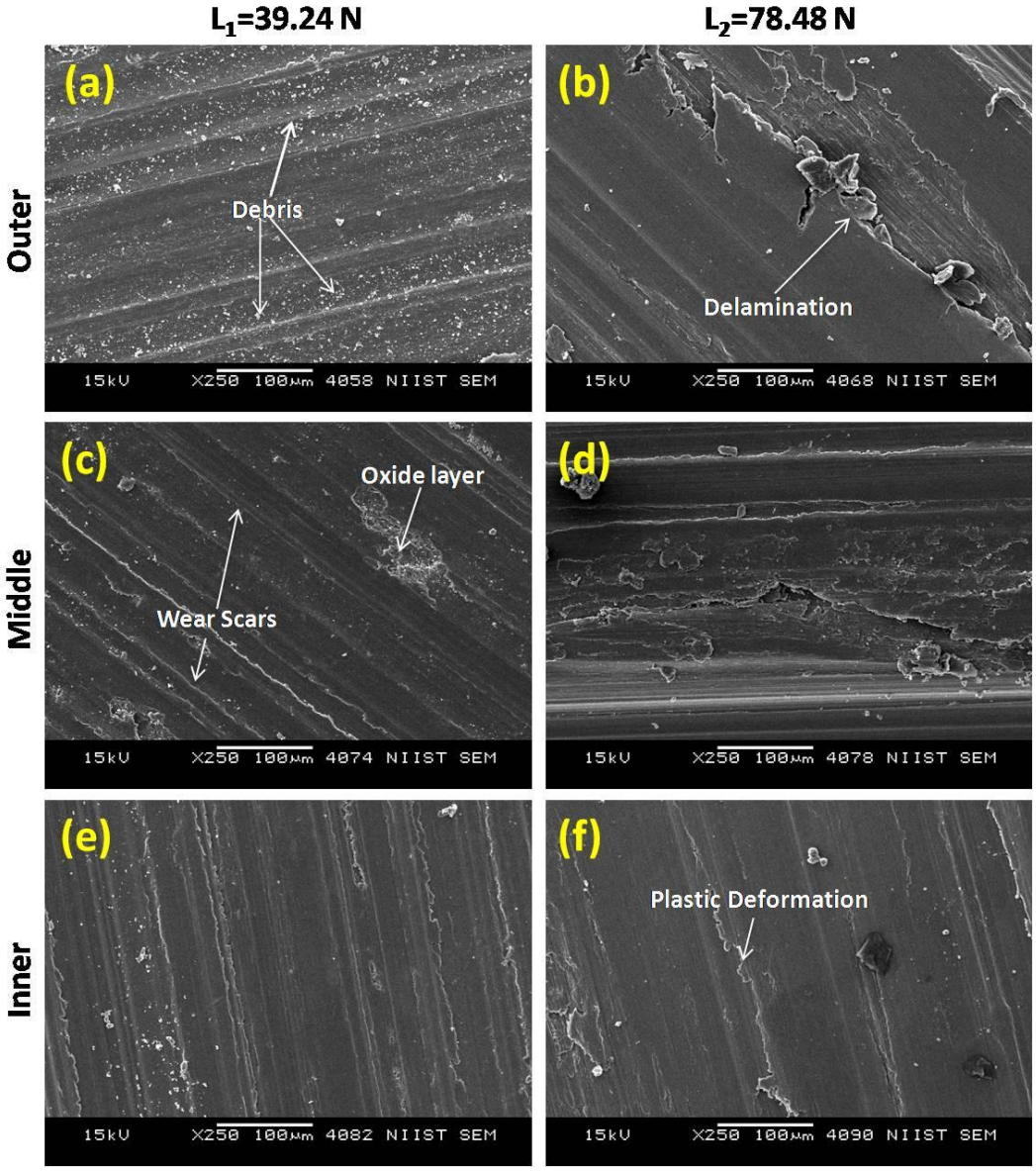

Figure 5.41 SEM micrographs of the worn surface of A390-1.5 wt. % Mg (a, b) at outer, (c, d) at middle and (e, f) at inner region specimen (L_1 at 39.24 N and L_2 at 78.48 N)

plastic deformation. The resistance to severe wear is due to the presence of primary silicon phases at the inner regions which provides better hardness and wear resistance properties. Figure 5.42 shows the wear debris analysis of outer, middle and inner pin specimens of A390-1.5 wt. % Mg at 39.24 and 78.48 N loads. At the lower load of 39.24 N, the outer and middle pin specimens show a thin sheet-like structured derbies whereas the inner specimens show more of a small crystal shaped debris due to the brittleness achieved by the presence of primary silicon. The wear debris analyses at 78.48 N shows a fine equiaxed grains at outer specimens due to the hardness obtained through the grain size of aluminum at this region whereas the debris from the middle region gives more coarser pieces due to the ductile nature of the material. Obviously, the presence of primary silicon phases provided brittle nature at the inner region shows very small debris.

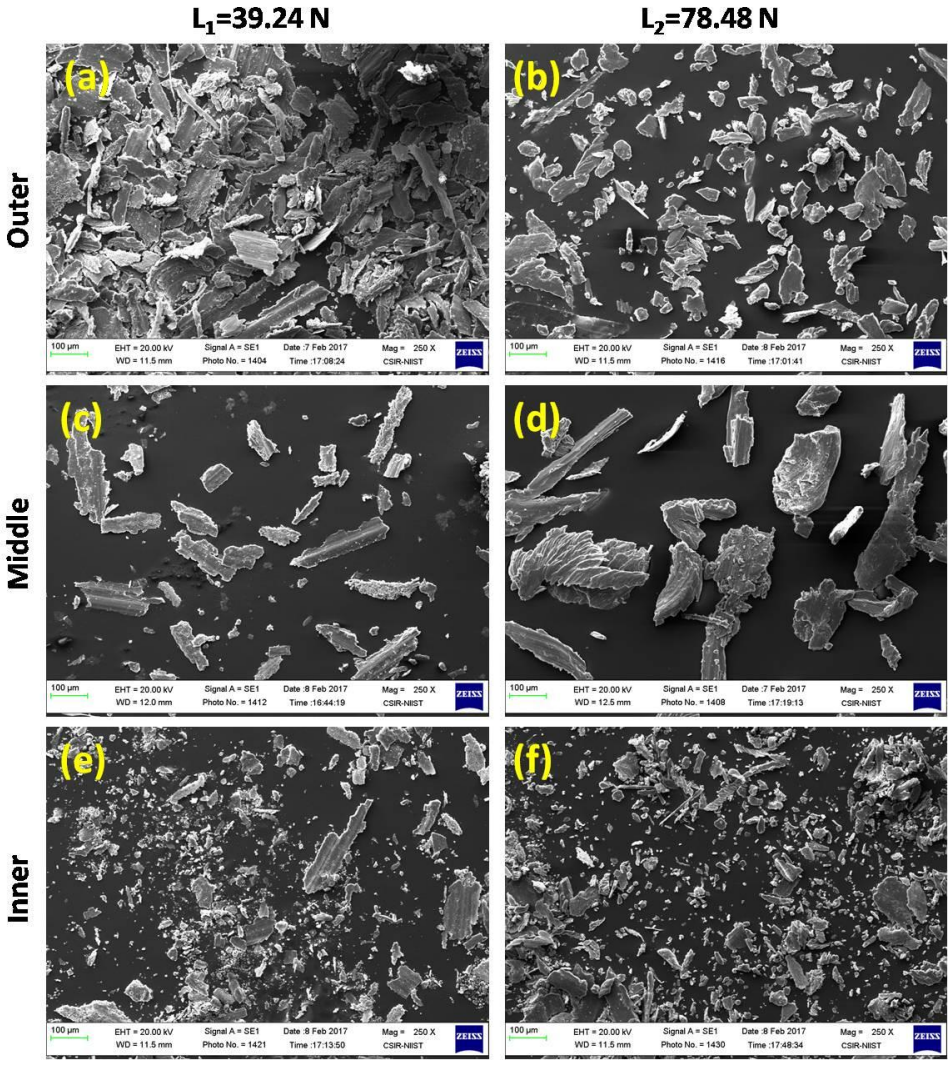

Figure 5.42 SEM images of wear debris of A390-1.5 wt. % Mg (a, b) at outer, (c, d) at middle and (e, f) at inner region specimen (L_1 at 39.24 N and L_2 at 78.48 N)

Figure 5.43 shows the worn surface analysis of Sr added A390 outer, middle and inner pin specimens and the corresponding wear debris analyses is provided in the Figure 5.44a-f. At lower load the wear scars are seen fine and running parallel to each other. The middle region shows slightly wider wear grooves than the outer region. The specimen of the outer region shows a wider wear grooves and at this

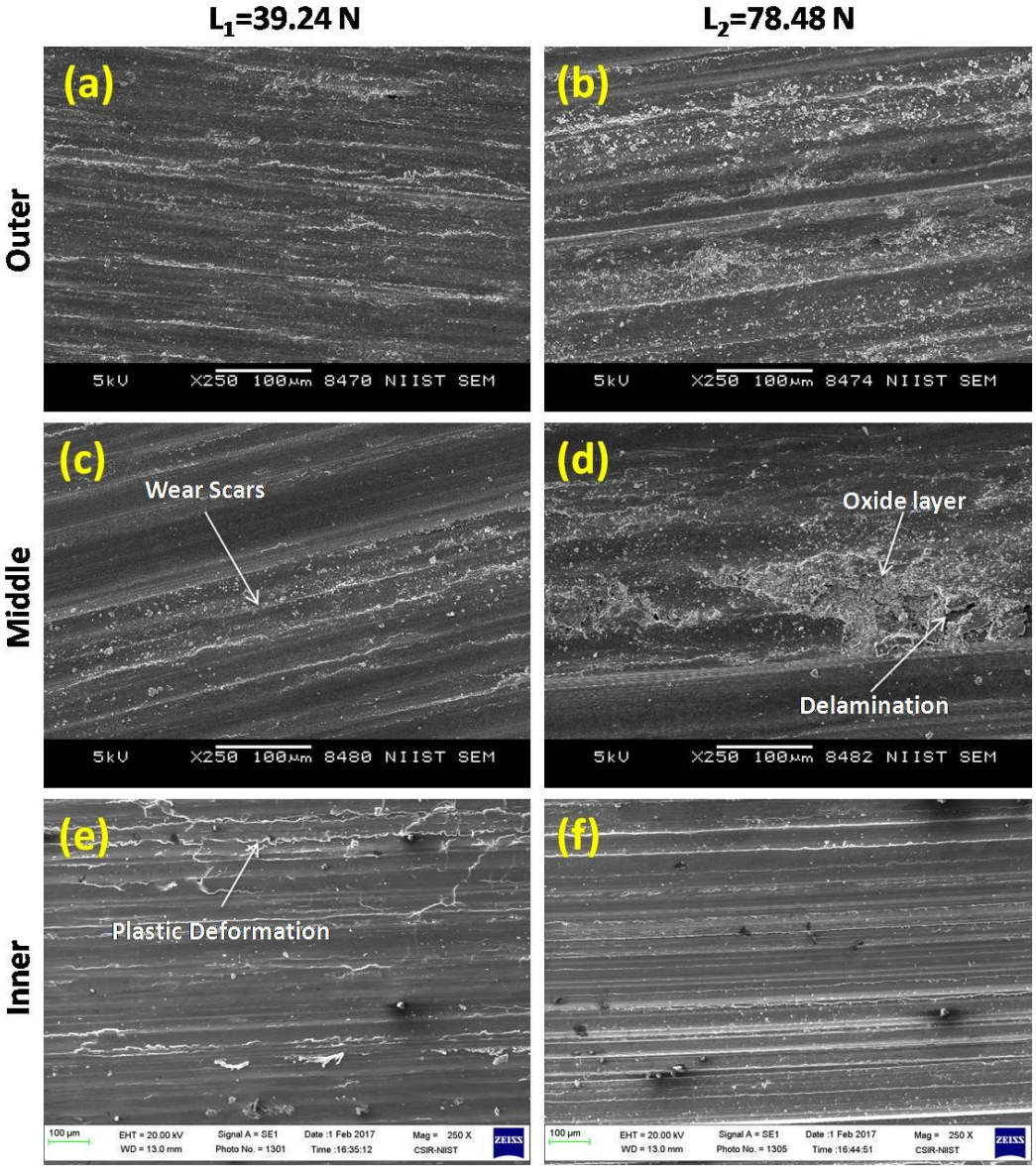

Figure 5.43 SEM micrographs of the worn surface of A390-0.03 wt. % Sr (a, b) at outer, (c, d) at middle and (e, f) at inner region specimen (L_1 at 39.24 N and L_2 at 78.48 N)

region it is seen the starting of the oxidative wear mechanism. The middle specimen at the higher load clearly shows the layer of oxidation formed. But the inner pin specimens of A390-0.03 wt. % Sr shows a partially deformed worn surface at the lower and the higher loads. This may be due to the presence of porosities that found

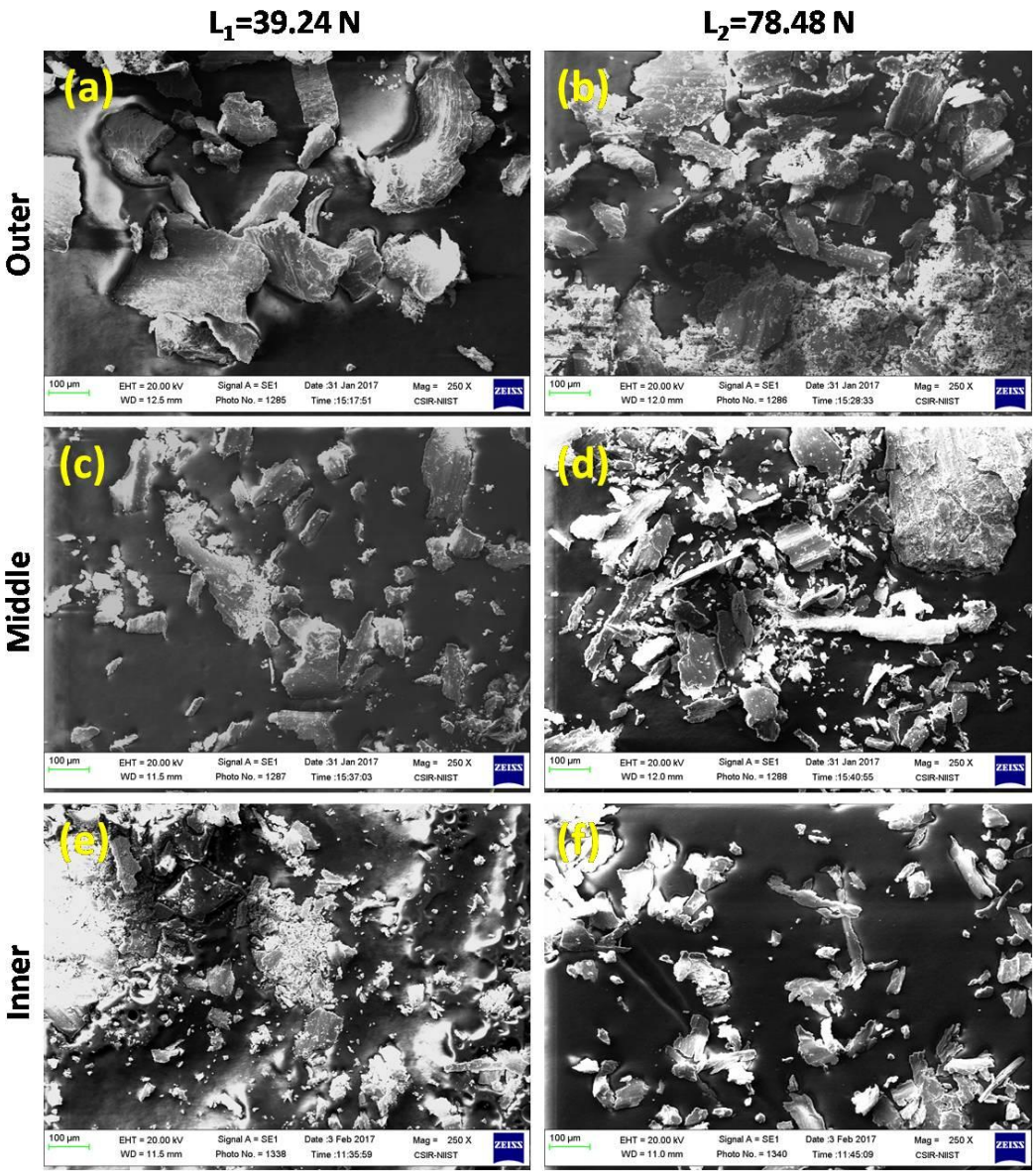

Figure 5.44 SEM images of wear debris of A390-0.03 wt. % Sr (a, b) at outer, (c, d) at middle and (e, f) at inner region specimen (L_1 at 39.24 N and L_2 at 78.48 N)

in the microstructures at this region in the microstructural analysis. The porosities present in the material gives rise to excessive wear and plastic deformation due to the jerking of the samples during the rubbing of the specimen and the counter surface on the uneven surfaces. The inner specimens of A390-0.03Sr at all loads shows only a medium wear rate than when compared with the outer region even the hard cuboids of primary silicon accumulated at this region is evident from the Figure 5.40b. The wear debris analysis in the Figure 5.44a for outer specimen at 39.24 N load shows small plate-like structures while at the higher load of 78.48 N load shows large sheet-like structures that squeezed out from the hard surfaces of the specimen and the

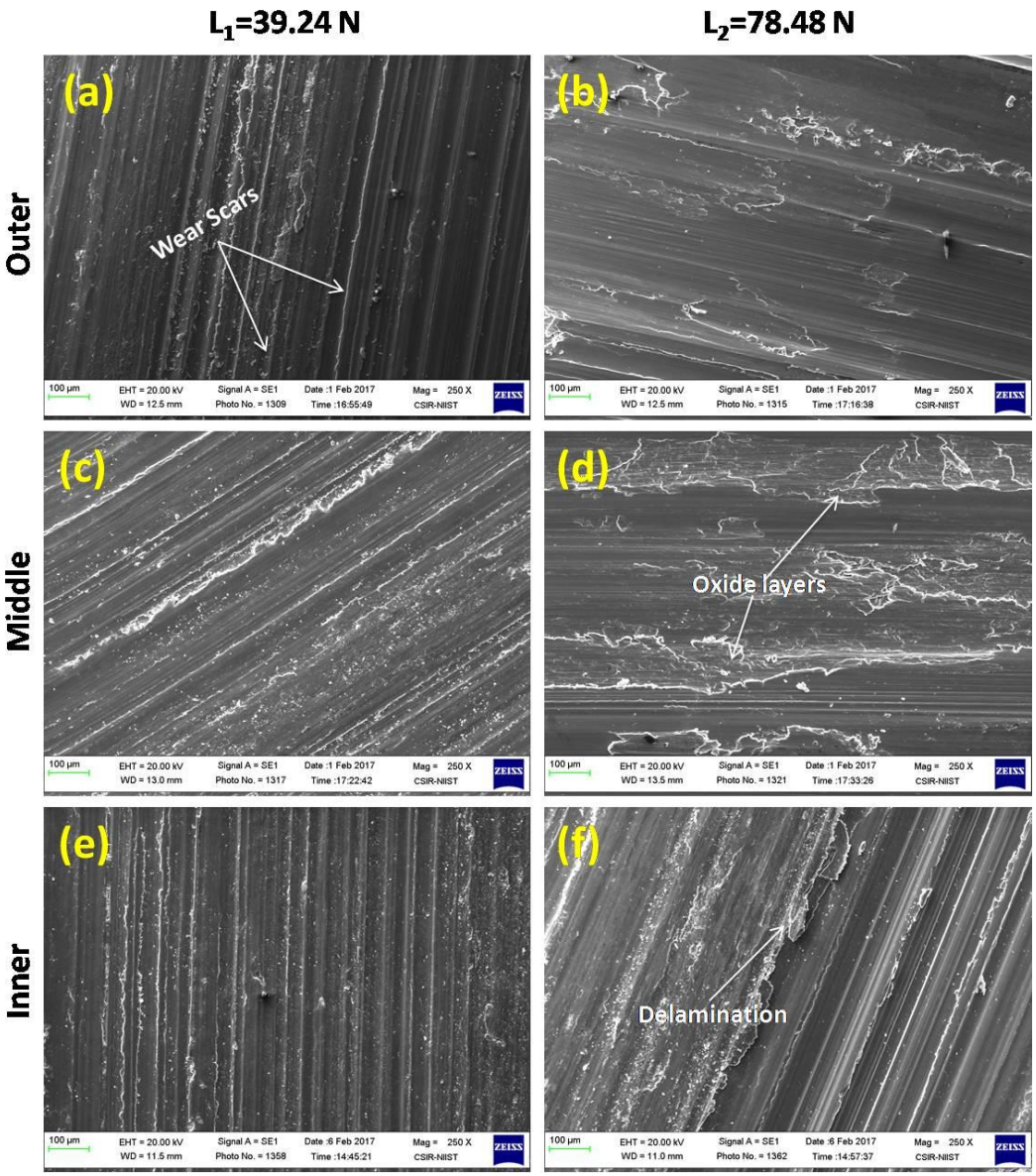

Figure 5.45 SEM micrographs of the worn surface of A390-0.03 wt. % Zr (a, b) at outer, (c, d) at middle and (e, f) at inner region specimen (L_1 at 39.24 N and L_2 at 78.48 N)

counter surface. The middle specimen is plastically deformed and hot extruded due to the heat developed in the system during the process of continuous running of the specimen and due to the coarser grain size. The inner specimens of A390-0.03 wt. % Sr exhibits very fine debris since the region is enriched with the brittle primary silicon at 39.24 and 78.48 N loads. Figure 5.45 and 5.46 corresponds to the worn surface analysis and the wear debris of A390-0.03 wt. % Zr FGM alloy system. At the lower load of 39.24 N the specimens show fine wear scars at the outer and inner

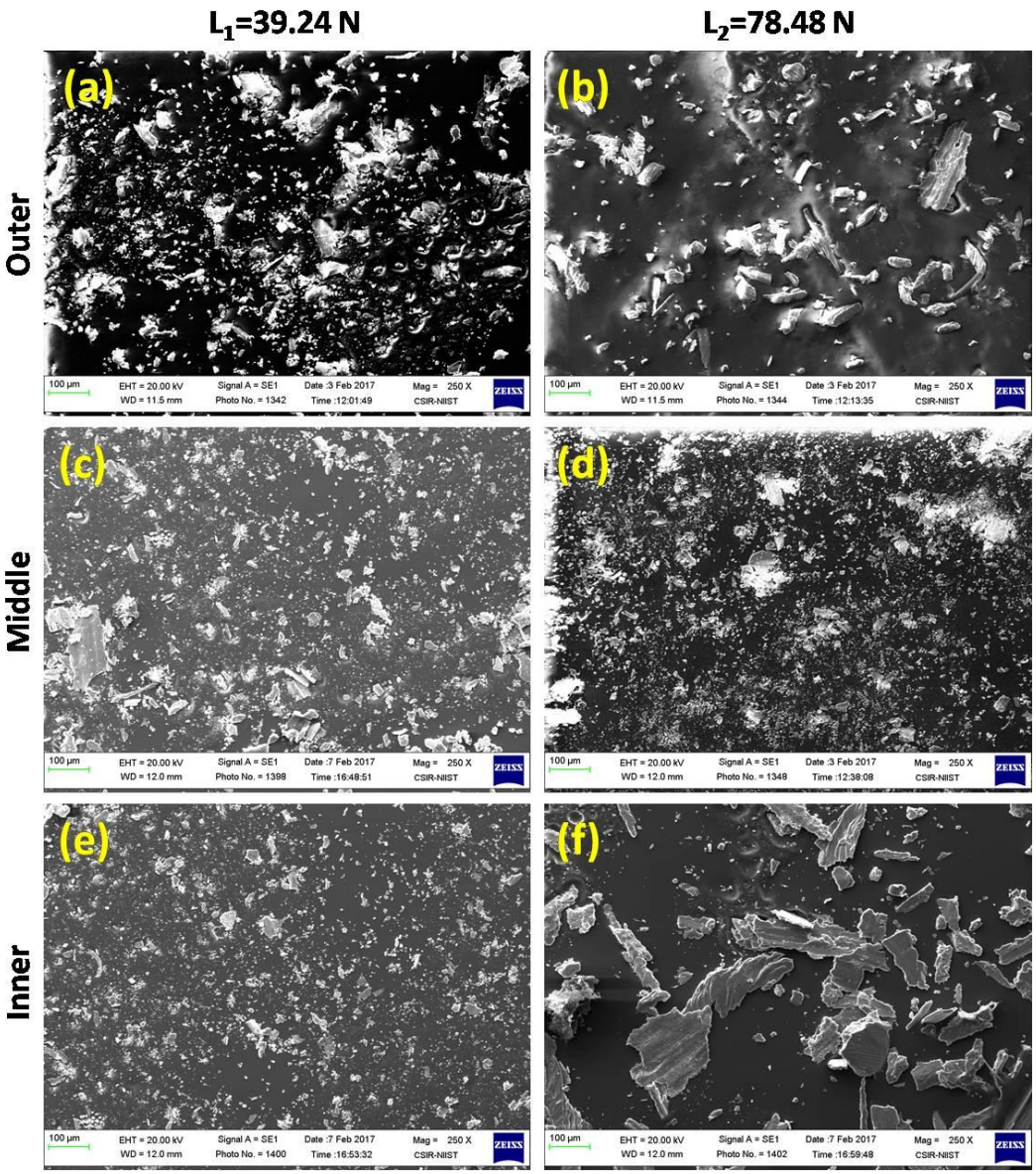

Figure 5.46 SEM images of wear debris of A390-0.03 wt. % Zr (a, b) at outer, (c, d) at middle and (e, f) at inner region specimen (L_1 at 39.24 N and L_2 at 78.48 N)

specimens due to the fine grain size and the presence of primary silicon particles respectively at the regions. The middle specimen at the higher load is completely damaged due to the coarser grain size at the region obtained. But at the higher load of 78.48 N also the surface is plastically deformed even at the presence of primary silicon particle. This is due to the low hardness values achieved at the inner region in the A390-0.03 wt. % Zr alloy system in Figure 5.29. The result of the worn surface analysis and the hardness values reflects in the wear debris analysis. The debris from the inner region shows large plate-like structures due to the less hardness at this region.

Figure 5.47 and 5.48 represents the worn surface analyses and the wear debris analyses of A390-1.5 wt. % Mg-0.03 wt. % Sr FGM alloy system respectively. At lower loads, the wear specimens of all the regions are seen as fine and the grooves are clearly visible due to the low pressure acting normally to the pin specimen. The outer specimen at 78.48 N load plastically deformed and delamination occurs due to the excessive pressure and the region contains mostly of soft aluminium phases. The middle specimen at lower loads shows fine grooves and the fine detached particles from the specimen surface during the sliding process. But the middle specimen at a higher load of 78.48 N is a cleaned surface without the detached particles on the surface because of the excessive pressure acting on the pin specimen. The wear debris analyses of A390-1.5 wt. % Mg-0.03 wt. % Sr at all the regions shows a similar type of wear debris formation as in the previous cases. Apart from the previous conditions of the inner specimens the wear debris shows a sheet-like structure at the lower and the higher loads because of the presence of Sr in the A390 aluminium alloy that contains microporosities as mentioned in the microstructural analyses section of A390-1.5 wt. % Mg-0.03 wt. % Sr aluminium alloy system.

The Figure 5.49 and 5.50 represents the worn surface analysis and wear debris analysis of A390-1.5 wt. % Mg-0.03 wt. % Zr FGM system. The worn surface analysis at the inner region shows a plane area that is washed out during the wearing process due to the less hardness obtained at the inner region in the combined addition of Mg and Zr in A390 alloy. The wear debris analysis shows large flakes at the middle region and finer particles of aluminium at outer region. The debris analysis at the inner region shows long plates of aluminium due to the lesser hardness value.

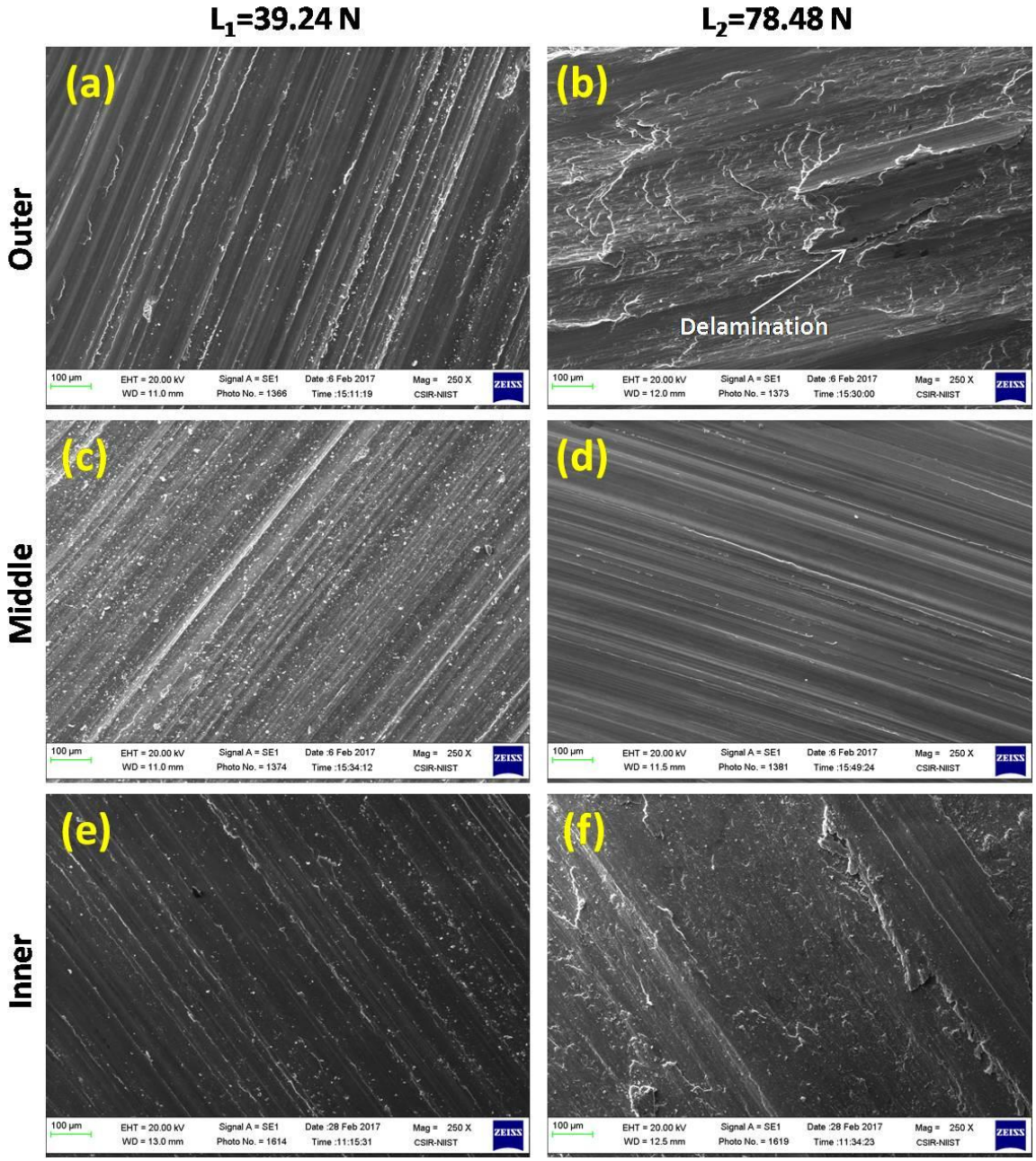

Figure 5.47 SEM micrographs of the worn surface of A390-1.5 wt. % Mg-0.03 wt. % Sr (a, b) at outer, (c, d) at middle and (e, f) at inner region specimen (L_1 at 39.24 N and L_2 at 78.48 N)

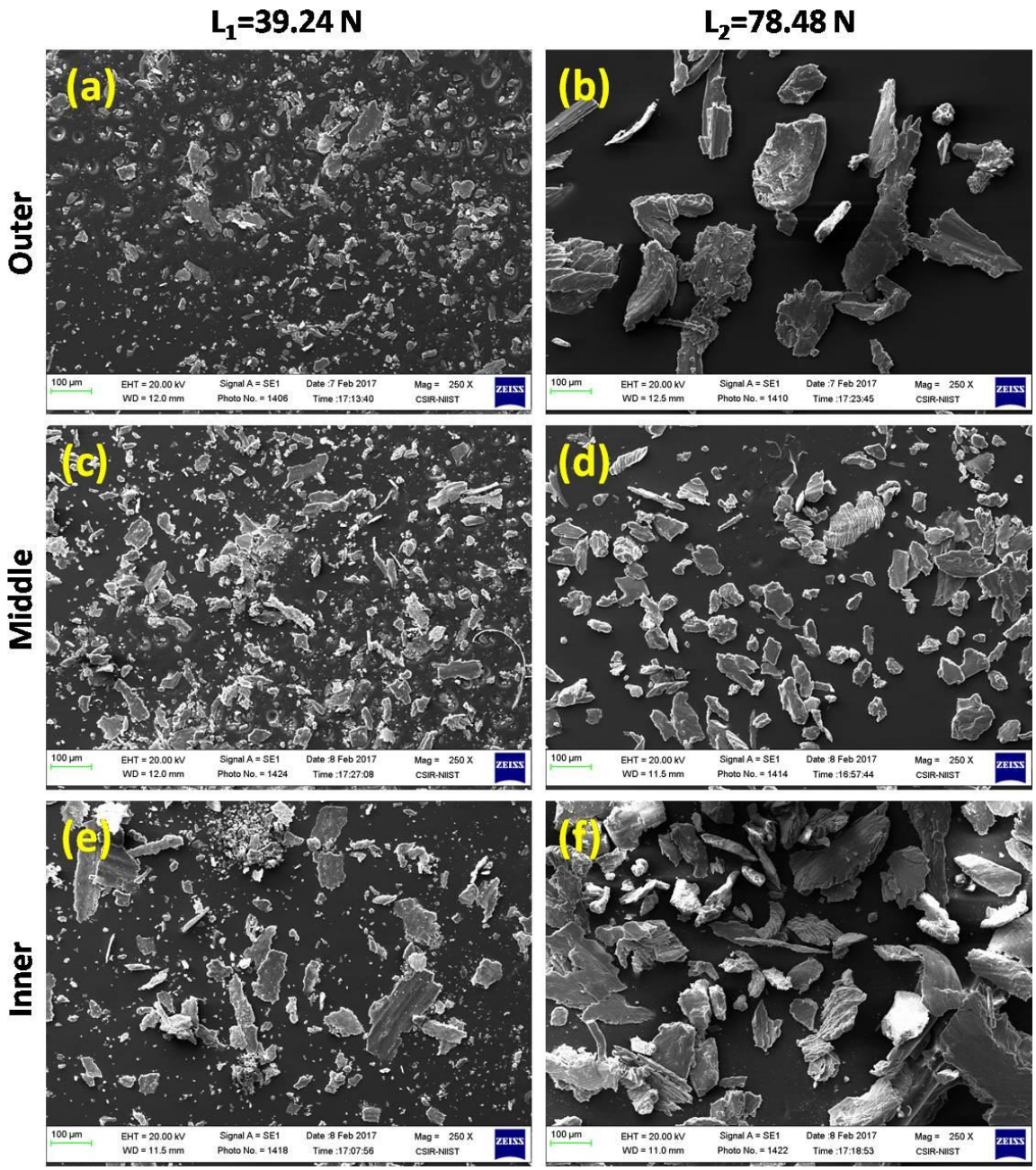

Figure 5.48 SEM images of wear debris of A390-1.5 wt. % Mg-0.03 wt. % Sr (a, b) at outer, (c, d) at middle and (e, f) at inner region specimen (L_1 at 39.24 N and L_2 at 78.48 N)

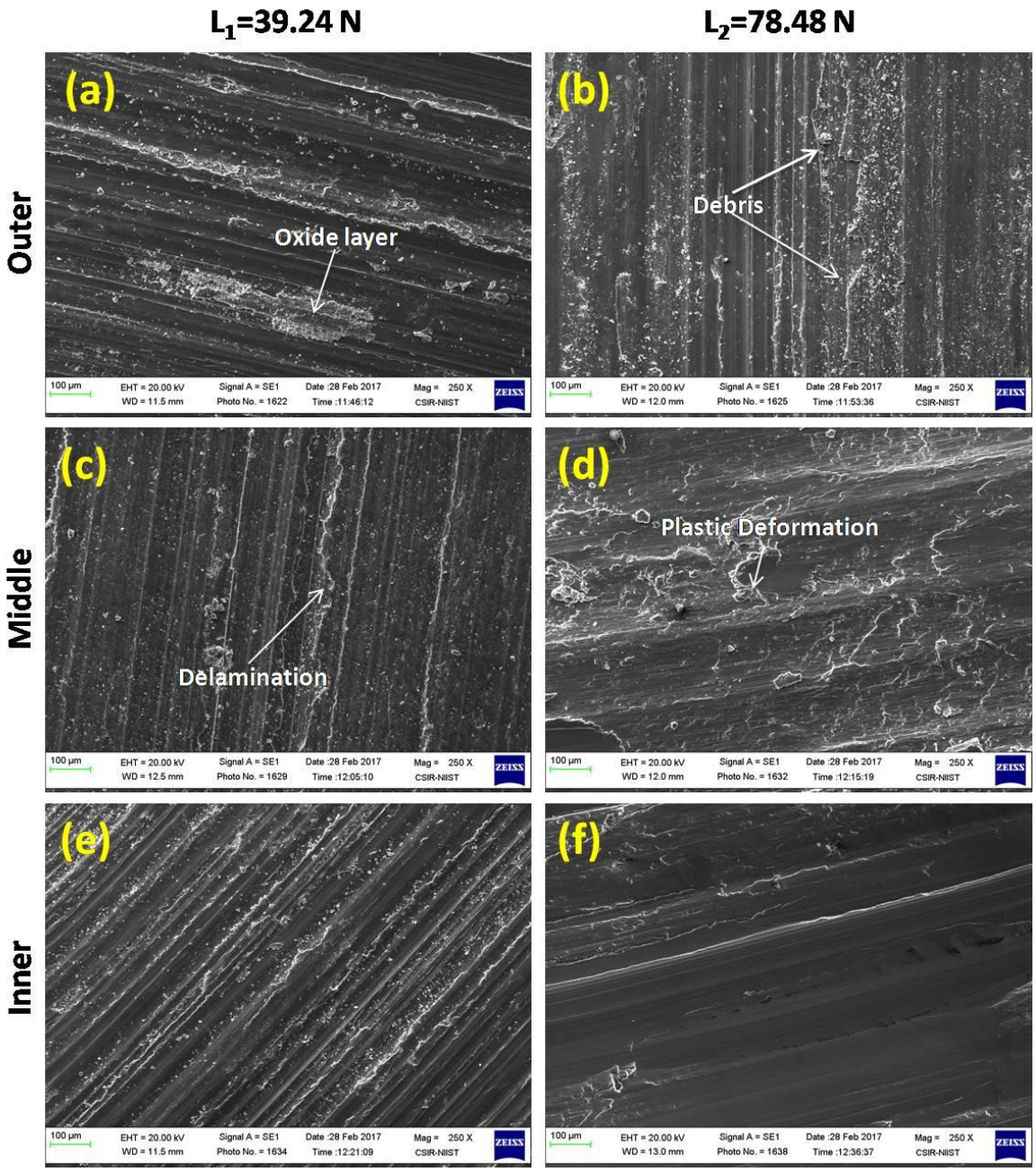

Figure 5.49 SEM micrographs of the worn surface of A390-1.5 wt. % Mg-0.03 wt. % Zr (a, b) at outer, (c, d) at middle and (e, f) at inner region specimen (L_1 at 39.24 N and L_2 at 78.48 N)

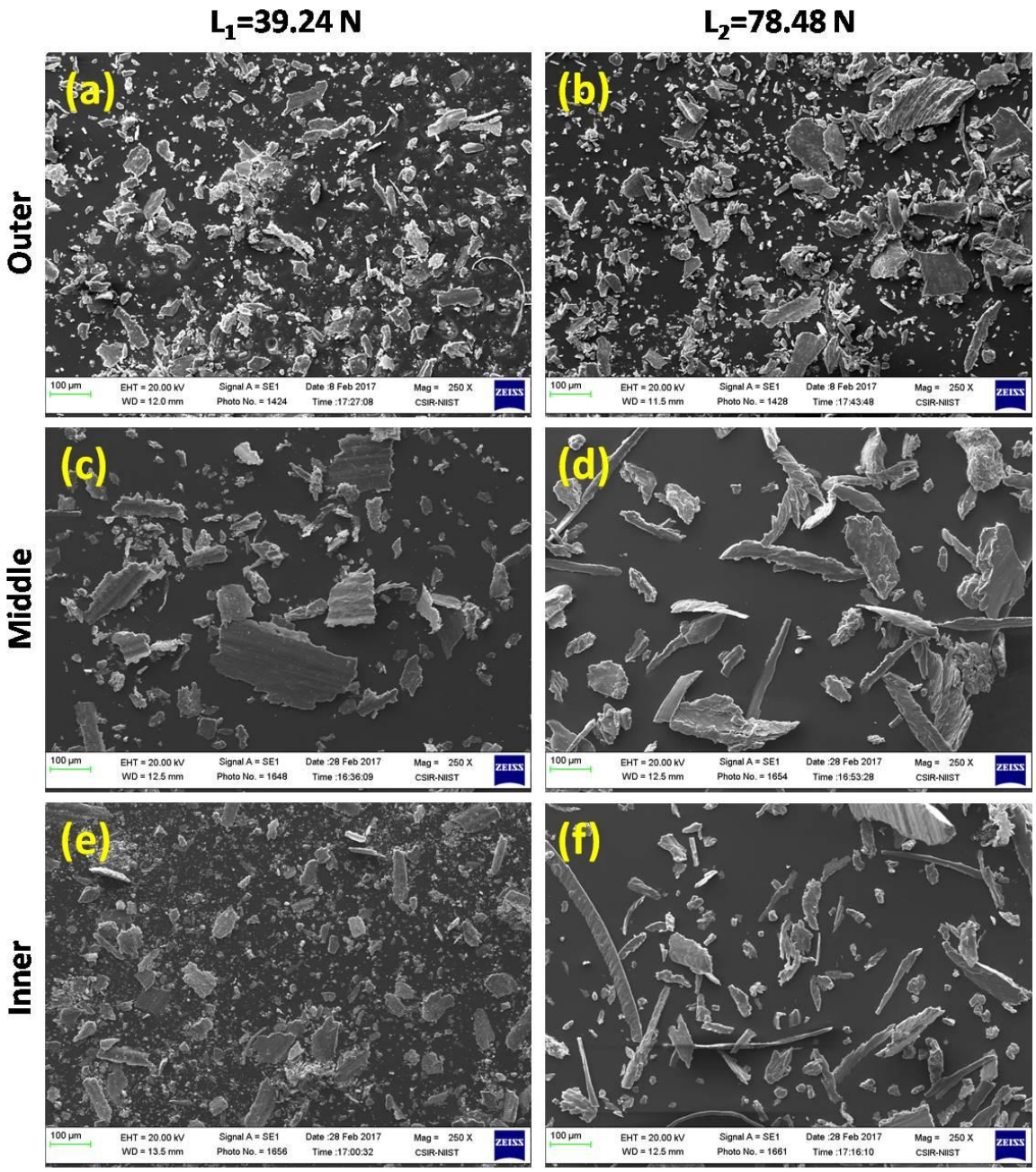

Figure 5.50 SEM images of wear debris of A390-1.5 wt. % Mg-0.03 wt. % Sr (a, b) at outer, (c, d) at middle and (e, f) at inner region specimen (L_1 at 39.24 N and L_2 at 78.48 N)

The EDAX analyses at the worn surfaces of the pin specimens from different regions are shown in Figure 5.51. The EDAX analyses are carried out at the outer specimen of Mg and Sr added A390 aluminium alloy at 78.48 N load, the middle specimens of Mg added A390 at 39.24 N and Sr added A390 alloy at 78.48 N and the inner specimens of Mg and Sr added A390 system at 78.48 N and 39.24 N, respectively. The surface of the worn out pin was covered with a thin layer of a white

compound or white layers called oxide layers. The EDAX analyses at all the conditions exhibit strong oxygen peaks corresponding to the formation of aluminium oxide. This is a clear evidence for the oxidative wear phenomenon at the surfaces. The oxidative wear phenomenon is taking place due to the frictional heating occurring during the sliding mechanism of wear. The formation of such type of oxide layers protect the surface of the specimen from further wearing of the specimen. The further running of the specimen over the counter surface pushes the layers of oxides into the grooves of the specimens and its acts as a protective agent at the grooves. This helps the specimens from the excessive wear of the material. The oxide layers are always associated with the grooves on the surface is clearly evident from the SEM surface analysis of the worn surfaces.

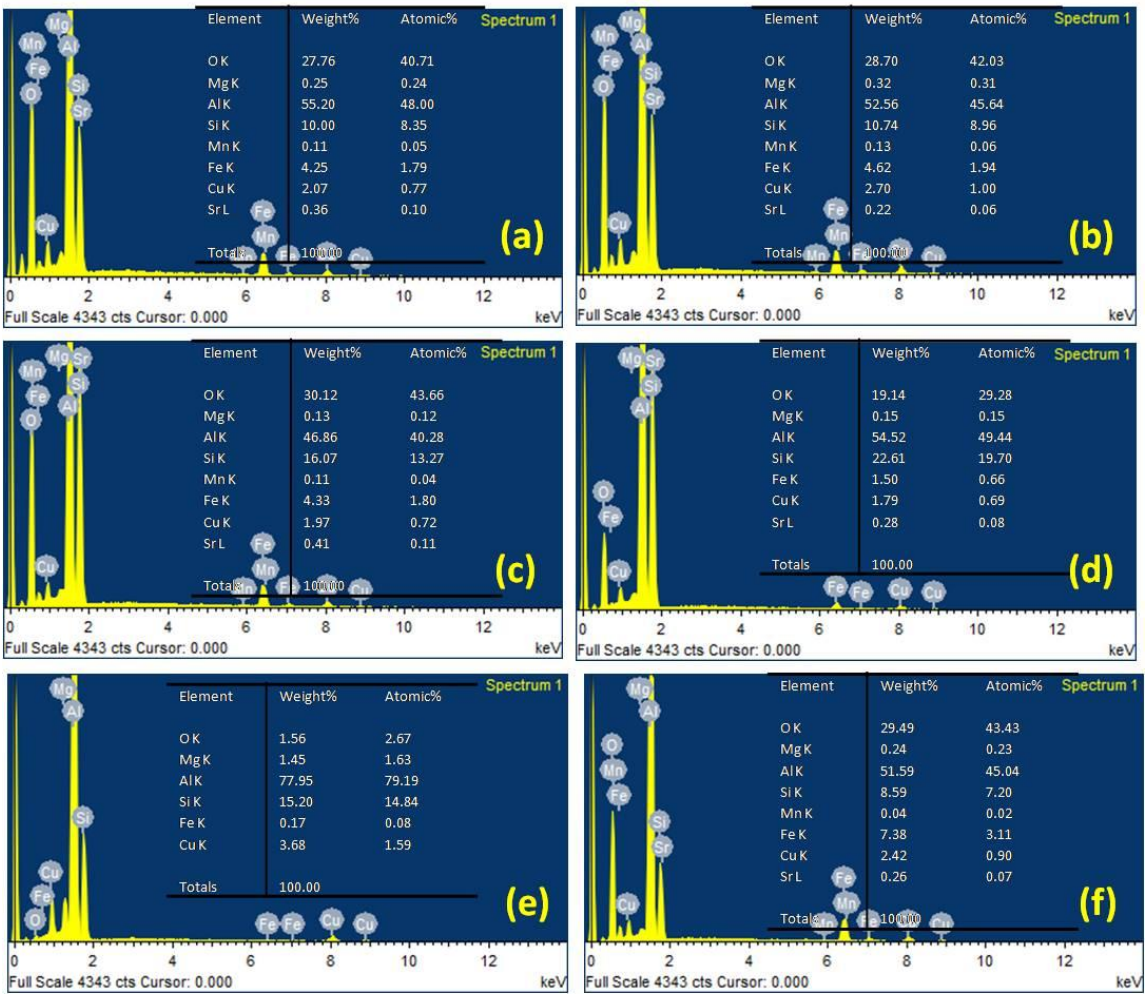

Figure 5.51 EDAX analysis of worn surfaces of (a) outer specimen of A390-1.5 wt. % Mg at 39.24 N, (b) inner specimen of A390-1.5 wt. % Mg at 78.48 N, (c) middle specimen of A390-0.03 wt. % Sr at 78.48 N, (d) inner specimen of A390-0.03 wt. % Sr at 39.24 N, (e) outer specimen of A390-1.5 wt. % Mg-0.03 wt. % Sr at 78.48 N and (f) middle specimen of A390-1.5 wt. % Mg-0.03 wt. % Sr at 39.24 N

5.5.8 Conclusions

- Functionally graded aluminium A390 alloy systems with varying percentages of Mg, Sr and Zr are successfully fabricated using the cylindrical mould for cylinder liner applications and the best conditions are successfully processed and characterized in the centrifugal disc mould.
- The microstructural observations of the gravity cast pure A390 aluminium alloy and the modifiers added A390 aluminium alloy shows a homogeneous distribution of α-aluminium, eutectic silicon, primary silicon and Mg_2Si phases in the cast components.
- The gravity cast samples of A390-0.01 wt. % Sr alloy system indicated 152.5 BHN as maximum hardness due to the modification of silicon phases in comparison to A390 alloy which showed a hardness of 134 BHN.
- Among varying content of Mg, Sr and Zr added in centrifugally cast cylinders, maximum hardness were observed in A390-1.5 wt. % Mg and A390-0.03 wt. % Sr/Zr in respective systems.
- The combined addition of 1.5 wt. % Mg and 0.03 wt. % Sr in A390 hypereutectic aluminium alloy shows the maximum hardness of 158 BHN at the inner periphery of the disc casting. The individual addition of Zr and combined addition of Mg and Zr tend to decrease the hardness towards the inner periphery even in the presence of primary silicon particles due to segregation of dense Al-Zr phases to outer periphery.
- The maximum tensile strength of 295 MPa is obtained at the outer periphery and 264 MPa is obtained at the inner specimen of the A390-0.03 wt. % Zr centrifugal cast disc.
- Generally, a higher wear resistance is obtained at the inner periphery of the cast discs. However, the transition region specimens show better wear resistances than the inner regions because of the micro porosities present in the inner most periphery of the A390-1.5 wt. % Mg-0.03 wt. % Sr aluminium alloy system.
- The middle regions of all the alloy systems show an adhesive and oxidative type of wear due to the coarse grain size of the aluminium attained at this middle region. The inner periphery shows an abrasive type of wear mechanism due to the presence of hard brittle primary silicon segregated at the inner periphery of the centrifugal cast discs.

CHAPTER 6

Functionally Graded A2219 Al Composite Turbine Exit Vane Guide

6.1 Abstract

Enhanced tribological and location-specific properties achieved in functionally graded metallic composites make them potential materials for futuristic engineering components. The present investigation aims on the processing of functionally graded A2219 aluminium matrix composites reinforced with SiC particles (SiC_p) of 14 and 23 μm average particle size (APS) by centrifugal casting techniques for the application of turbine exit vane guide. The sizes of the primary aluminium phases are finer towards the outer periphery due to the higher solidification rate attained during the centrifugal casting technique. Functionally graded Al–SiC_p composite turbine exit vane guide produced by centrifugal casting show higher concentration of SiC_p towards outer periphery, followed by a gradient transition region and the particle depleted zone towards the inner periphery. Particle agglomerates formed due to partially wetted particles associated with voids and gas porosities segregate towards the inner periphery. The higher concentration of reinforcement particles near the outer periphery in FGM enhances the hardness and wear resistance. Centrifugal cast alloys at the outer region also show an enhanced wear resistance than the inner region specimens due to the fine grains of primary aluminium phases. The pin-on-disc wear tests show the abrasive, adhesive and oxidative type of wear mechanisms in the Al-SiC FGM.

6.2 Introduction

Functionally graded metal matrix composites (FGMMCs) are relatively new advanced class of inhomogeneous engineering materials which contains ceramic reinforcement particles, where the elemental composition and the volume fraction of the reinforcement particles varies continuously thereby bearing a non-uniform microstructure in a specific direction leading to the variation in the functional performance of the component within a part (Vieira et al., 2009 and Akhil et al., 2016). The concepts of functionally graded materials (FGMs) are rampant in the

environment such as in human teeth and bones, bark of wood, etc. Japan proposed the concept of making FGMs in 1980s. Since the developments of the FGMs are still in the early stages of evolution, hence there exist an immense scope for the fabrication and development of the FGMs suitable for various specific engineering applications for thermal protection systems in automotive, aerospace, defence sectors and so on. The FGMs are advised for the strategic sectors because of their high thermal properties such as high-temperature resistance at the surface of the component, increased toughness of fracture and increased bonding between the ceramic reinforcement particles and the alloy matrix (Rajan et al., 2008). Most of the FGM studies are multiphase composite materials where the volume fraction of reinforcement particles or phases varies continuously from one location to the other within a component or structure leading to the formation of controlled non-uniform microstructure with continuous change in properties. Processing of FGM and their engineering components with gradient properties are very much exigent and has a lot of technological relevance. Out of various processing methods for FGM such as chemical vapour deposition, physical vapour deposition, sol–gel technique, plasma spraying, molten metal infiltration, self-propagating, centrifugal casting, diffusion bonding laser cladding and controlled mould filling, etc. centrifugal casting is the simplest and cost-effective technique for producing large-size engineering components.

Centrifugal casting or rotocasting is a pressure casting technique which is used to produce functionally graded metal matrix composites by the aid of centrifugal force applied to the pool of molten metal for the high quality of the results attainable, particularly for precise control of their metallurgy and microstructure at specific locations of the cast component by rotating the casting mould. Both horizontal and vertical centrifugal casting methods are used for making FGM. In vertical centrifugal casting method, a centrifugal force applied to a homogeneous semi-liquid composite, (containing ceramics or intermetallic compound particles) drives the formation of the desired gradient, resulting in composition gradient that is produced by the difference in density between the molten metal and the particles under the same centrifugal force in a vertical axis. Mechanical properties of FGM fabricated by this method have been investigated using relatively large samples (Rodrıguez-Castro et al., 2002a;

Rodrıguez-Castro et al., 2002b; Watanabe et al., 2000 and Velhinho et al., 2003). Velhinho et al. produced functionally graded SiC_p reinforced aluminium–matrix composites by centrifugal casting and observed that SiC_p is partially clustered with some pores due to imperfect wetting of ceramic particles by the molten aluminium alloy (Velhinho et al., 2003). Hence, proper wetting between the particles and the matrix is necessary to reduce particle clustering. A gradient in the microstructure and the hardness of the centrifugally cast Al alloy is also observed due to the differences in the solidification rates. Sharper gradients in the distribution of the reinforcing particles are obtained in the higher centrifugal speeds and a smoother in the lower speeds (Vieira et al., 2009).

Most of the tribological studies were carried out using pin-on-disc (rotating) wear tester and ball-on- ring tribometer (Corrochano et al., 2011; Yang, 2003; Herbert et al., 2008; Wilson et al., 1997; Shivamurthy et al., 2011; Perez-Bustamante et al., 2012; Cree et al., 2011 and Edalati et al., 2014). The concept of FGM can be effectively used in automobile components such as engine blocks, cylinder liners, piston rings, strategic sectors, etc. in which these parts are subjected to wear by direct contact of the materials or by indirect means. The wear performance of aluminium alloys and metal matrix composites/FGM not only depends on the service conditions (load, sliding distance, sliding speed, counter surface temperature and roughness of the surface) but also depends upon various material- related mechanical properties (hardness, ductility and toughness) and microstructure (Clarke et al., 1979 and Chandrasekharaiah et al., 2009). In aluminium based alloys and composites, the dominant wear mechanisms found are two-body abrasive wear, adhesive wear, oxidative wear and delamination.

The objective of the present investigation is to process functionally graded A2219 aluminium alloy reinforced with 15 wt. % SiC particle (SiC_p) of 14 and 23 μm average particle size (APS) using liquid metal stir casting and centrifugal casting techniques for turbine exit vane guide application and evaluation of microstructure, mechanical properties, pin-on-disc wear characteristics. A2219 aluminium alloys are used as it finds potential applications in diverse fields such as in automotive parts; aircraft fittings and control parts; water-cooled cylinder blocks due to the excellent

castability and good weldability, pressure tightness and excellent resistance to corrosion.

6.3 Experimental Methods

The standard elemental composition and the properties of the A2219 aluminium alloy is depicted in Table 6.1a and 1b, respectively. Green SiC particles of 14 μm and 23 μm average particles sizes (APS) and a density of 3.2 g/cm^3 are used as the reinforcements for the processing of metal matrix composites/FGMs by adding

Table 6.1a Standard elemental compositions of A2219 aluminium alloy (wt. %)

Alloy	Al	Cu	Fe	Mg	Mn	Si	Ti	V	Zn	Zr
A2219	91.5-93.5	5.8-6.8	Max. 0.3	0.02-0.65	0.2-0.4	Max.0.2	0.02-0.1	0.05-0.15	Max. 0.1	0.1-.25

Table 6.1b Standard properties of A2219 aluminium alloy

Properties	A2219
Density	2.84 g/cm^3
Liquidus Temperature	643 ^{o}C
Solidus Temperature	543 ^{o}C
Co-efficient of thermal Expansion	24.1 μm/m-^{o}C at 20-300 ^{o}C
Thermal Conductivity	121 W/m-K at 25 ^{o}C
Solutionizing Temperature	535 ^{o}C
Aging Temperature	190 ^{o}C for 18 hr
Hardness	130 BHN
UTS	476 MPa
% Elongation	10
Modulus of Elasticity	73.1 GPa
Fatigue Strength	103 MPa
Shear Strength	280 MPa

15 wt. % into the A2219 aluminium alloy matrix. The SiC particles of 14 μm and 23 μm APS reinforced composites are primarily processed in a 15 kg capacity clay graphite crucible. Magnesium was added at 1 wt. % to the A2219 molten melt to improve the wettability of the matrix alloy with the SiC reinforcement particles. The SiC particles are preheated at 600 °C and are introduced to the A2219 molten aluminium at 740 °C at a controlled feed rate. The reinforcement particles were added to the vortex of the molten metal, to ensure the proper mixing of the SiC particles, achieved with the help of a specially designed mechanical impeller rotated at 250 to 300 rpm with the help of an electric motor. Degassing of the melt was carried out at 740 °C by passing N_2 gas to the composite slurry through sulphuric acid to remove the hydrogen entrapment. Before pouring the composite melt into the permanent gravity mould, the centrifugal disc mould of 240 mm outer diameter and 30 mm thickness and the centrifugal turbine molud, the melt was superheated above the liquidus temperature. The melt was poured into the gravity as well as the centrifugal mould at 760 °C. For centrifugal casting the disc mould was rotated at 1300 rpm and the centrifugal turbine mould was rotated at 750 rpm. The as-cast samples were subjected to T6 heat treatment condition. The base alloy samples were solution heat treated at 535 °C for 1 h and the composite samples were heat treated at 515 °C for 1 h. And the alloy and the composite samples were aged at 190 °C for 18 h.

Microstructural evaluations of the alloys and composite as-cast samples were carried out using a Leica – DMRX optical microscope by using standard metallographic procedures. The as cast samples of alloys and composites were etched using Keller's reagent to reveal the phases present in the cast component. The hardness tests of the as-cast and the heat treated samples were evaluated using a TINUS OLSEN hardness tester using a 2.5 mm steel ball indenter with an applied load of 62.5 kg for a dwell time of 20 s to study the effect of heat treated samples over the as cast samples and the calculated values were in Brinell Hardness Number (BHN). An average of 5 values is reported though out the work. In centrifugal cast FGM samples of alloy and composites, the values were taken from outer periphery to the inner periphery of the castings. The thermal characteristics of the cast components of the alloys and composite FGMs are carried out using a HITACHI STA7300 thermal

analyser. In FGM components, the differential thermal analysis (DTA) samples are taken from outer, middle, transition and from the inner regions of the casting since the compositional changes at different regions affect the thermal properties of the cast components at different locations. The DTA studies were executed upto a temperature of 800 °C beyond the alloy processing temperature and the melting point of the alloy at a standard heating rate of 10 °C/min. X-ray diffraction (XRD) analysis of the A2219 cast alloy and composite FGM was done with the XRD-PAN analytical machine. The tensile samples were machined confirming to the ASTM B557M Standard and tested using the E-8 standard performed at 1 mm/min in a KIC-2-1000-C 100 kN capacity universal testing machine. The wear tests of the alloy and the FGM composite specimens were conducted on a Ducom wear and friction monitor – 20LE pin-on-disc wear testing machine which can measure the tribological properties. A stationary pin holder of 6 mm internal diameter holds the wear specimen of 6 mm diameter and 30 mm length against hardened high-carbon En 31 alloy steel having a diameter of 165 mm and hardness of 63 HRC. The 6 mm cross sections of the cylindrical specimens were firmly contacted with the En 31 counter body steel with the aid of special pulley arrangement and dead weights that can bear a maximum load of 20 kg. The wear tests were finished at a constant sliding distance of 1800 m and a constant velocity of 1 m/s. The surface morphologies of the worn out wear specimens and the wear debris analysis were carried out using the JEOL JSM-5600LV and Carl Zeiss EVO-18 scanning electron microscope (SEM) and using energy dispersive spectroscopy (EDAX).

6.4 Results and Discussion

6.4.1 Characteristics of gravity cast materials

6.4.1.1 Microstructural observations

Figure 6.1 shows the typical variation in the optical microstructures of gravity cast A2219 base alloy, A2219-15 wt. % SiC composite of 14 μm APS and A2219-15 wt. % SiC composite of 23 μm APS. In Figure 6.1a the presence of pure aluminium phase and undissolved secondary phases are visible while in 1b and 1c, apart from the presence of α-aluminium phase and the un-dissolved secondary phases it also indicated the presence of SiC particles of 14 and 23 μm respectively. Almost uniform sized columnar Al dendrites are observed throughout the microstructure of the base

A2219 alloy. By the addition of SiC particles in the matrix alloy, the size of the primary aluminium phases are reduced and is evident from the Figure 6.1b and c. The size of the primary aluminium phases are much less in the case of 14 µm size SiC particles. Particle agglomerates are found in the composite system added with 23 µm size SiC particles. Nevertheless, the metal matrix composite systems with 14 and 23 µm SiC particles shows an even distribution of particles throughout the microstructure.

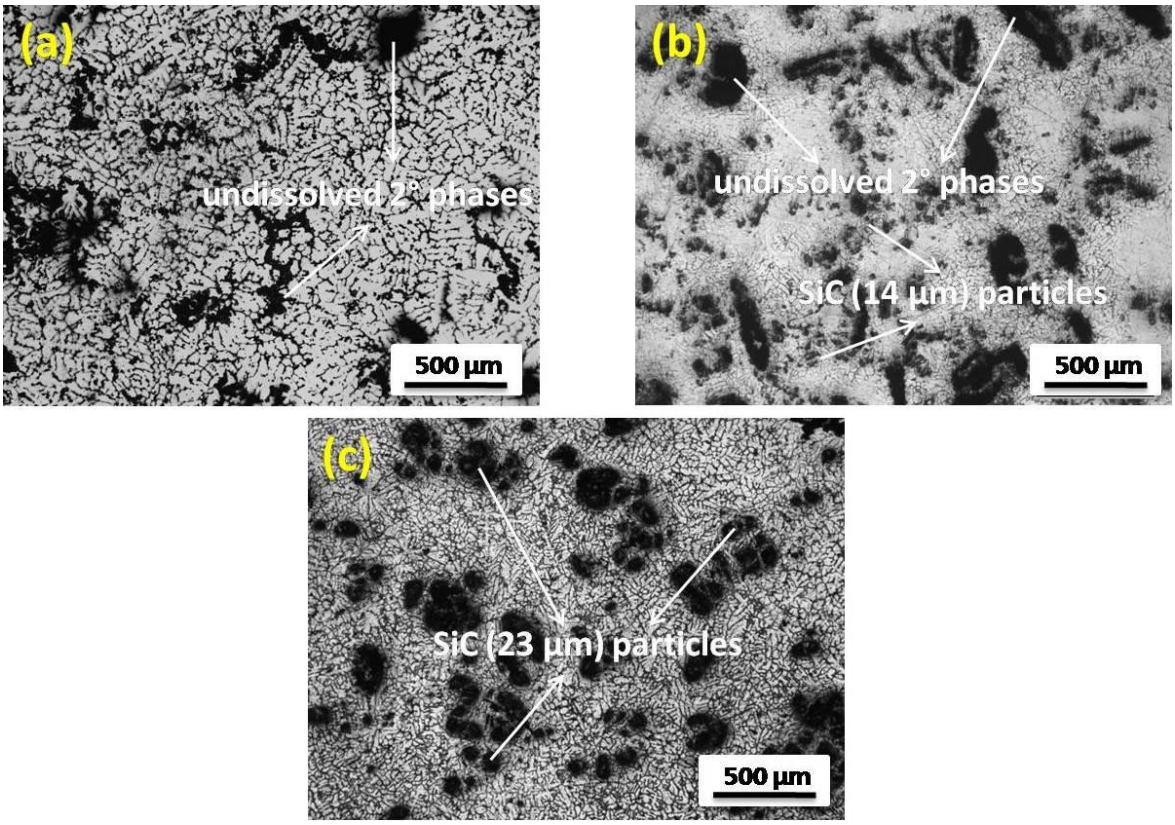

Figure 6.1 Optical microstructures of gravity cast (a) A2219 alloy, (b) A2219-15 wt. % SiC (14 µm) composite and (c) A2219-15 wt. % SiC (23 µm) composite

6.4.1.2 Hardness

Table 6.2 presents the hardness values of gravity cast A2219 base alloy, A2219-15 wt. % SiC with 14 µm APS and A2219-15 wt. % SiC with 23 µm APS. The base A2219 alloy gives a hardness of 76 BHN in the as-cast condition and 110 BHN in the heat treated condition. The composites A2219-15 wt. % SiC with 14 µm and 23 µm gives a hardness value of 96 and 109.5 BHN, respectively in the as-cast condition whereas the MMCs shows almost same hardness of 133 and 133.5 BHN, respectively in the heat treated conditions. This is due to the smaller grain size of the

primary aluminium phases achieved due to hindrance in the growth of alpha aluminium phases leading to higher hardness of the component by the addition of 14 μm SiC particles in the A2219-SiC of 14 μm composite system. The 23 μm APS SiC added composite system also shows the similar hardness may be due to the higher size of the SiC particle in the 2219 aluminium matrix alloy (Akhil et al., 2016).

Table 6.2 Hardness of A2219 alloy and composite systems (BHN)

Alloy System	As cast	Heat treated
A2219 base alloy	76	110
A2219-15%SiC (14μm)	96	133
A2219-15%SiC (23μm)	109.5	133.5

6.4.2 Characteristics of centrifugal cast FGM disc

6.4.2.1 Microstructural observations

Figure 6.2 shows the optical micrographs of functionally graded A2219 base alloy formed by centrifugal casting in disc mould. The microstructures as shown are from the outer periphery of the disc casting to the inner periphery of the disc. The outer periphery of the cast A2219 shows very fine grain structures of primary aluminium phases and some undissolved secondary phases observed as dark phases in Figure 6.2a. As the microstructures proceed to the inner regions of the castings, it reveals that the primary aluminium phases become coarser and coarser are evident from the Figure 6.2a-d. The difference in the grain size from the outer region of the casting to the inner region is due to the difference in the solidification rate experienced from the outer to the inner periphery during the casting process due to the centrifugal action. Due to the centrifugal action, the mould experiences different G factor at different locations. The outer region grains are almost circular or nearly circular shaped grains while the inner grains of the aluminium phases are almost similar shaped equally spaced dendritic structures.

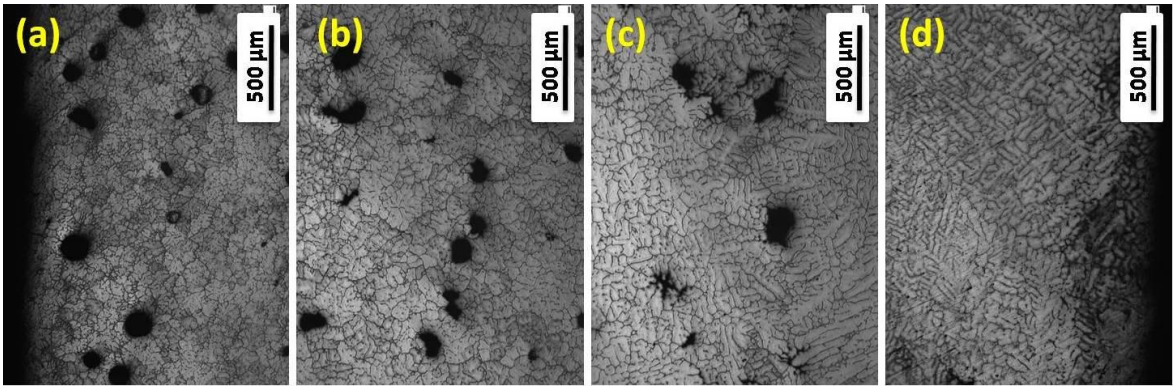

Figure 6.2 Optical microstructures of functionally graded centrifugal cast A2219 base alloy disc at (a) 0.5 mm, (b) 20 mm, (c) 50 mm and (d) 85 mm from the outer to the inner periphery

Figure 6.3 and 6.4 shows the optical microstructures of A2219-15 wt. % SiC with 14 and 23 µm functionally graded ex-situ composites produced by vertical centrifugal casting, respectively. The micro structures are taken at 0.5 mm, 20 mm, 60 mm and 80 mm from the outer diameter to the inner periphery of the 14 µm and 23 µm added MMCs. The outer periphery at 20 mm of the castings shows higher concentration of SiC particle reinforcement than the subsequent regions towards the inner side and the particle depleted zone at the inner most regions due to the propagation of high density of 3.2 g/cm^3 SiC particles to the outer periphery of the castings by the action of centrifugal force during centrifugal casting that will emphatically clout the mechanical properties such as hardness, toughness and high wear resistance where the inner region of the cast disc is mainly constituted with the A2219 aluminium alloy matrix of 2.67 g/cm^3 density. The outer region close to the centrifugal disc mould at 0.5 mm in the microstructures shows very less particles concentration in comparison with the adjoining region between 10 and 20 mm, due to the formation of the chill zone because of the high temperature (350 °C) in the preheated mould. The region after the chill zone towards the inner side is enriched with higher concentration of SiC particle, because of the movement of the high density SiC reinforcement particle from the inner region of the molten melt to the outer diameter of the castings, where the solidification of the molten metal taking place slowly as compared with the chill zone. The gradation of particles is observed at 10 to 40 mm from the outer periphery between the particle rich region and the particle depleted region. The inner peripheries of the castings are enriched with coarse grains of primary aluminium as visible in the case of centrifugal cast A2219

base alloy. The innermost regions close to the internal diameter of the castings exhibits the presence of few porosities due to the accumulation of the gas bubbles, low density slag inclusions, agglomerations and due to the less centrifugal gravitational G factor near the axis of rotation, that provides lesser rate of solidification at the inner region of the cast component. The grain sizes of the FGMMCs with 14 μm size SiC particles are finer than that of the 23 μm size added FGMMCs. This is due to the finer size of the reinforcement particles and also due to the large number of particles of 14 μm compared with the 23 μm particles since the small sized particles increase the surface area and the area of contact with that of the matrix alloy which will act as new centers of nucleation.

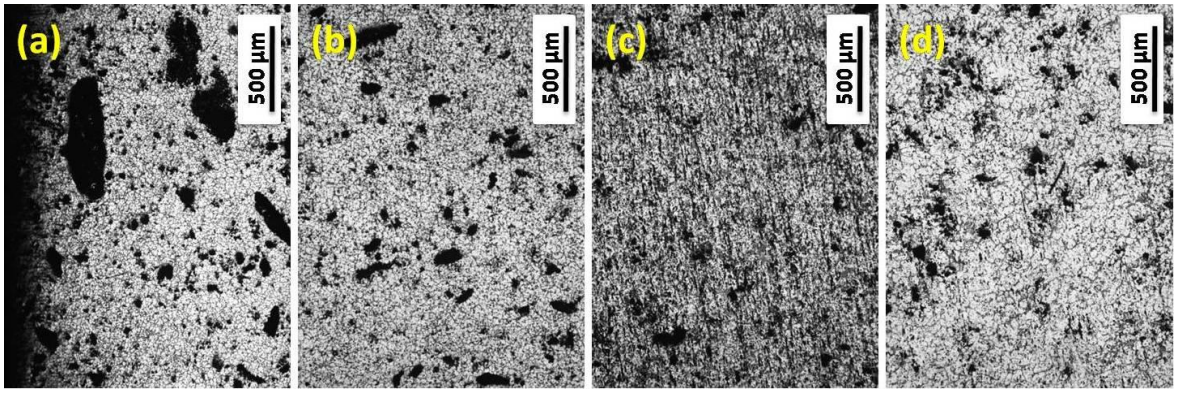

Figure 6.3 Optical microstructures of functionally graded centrifugal cast A2219-15%SiC (14 μm) disc at (a) 0.5 mm, (b) 20 mm, (c) 60 mm and (d) 80 mm from the outer to the inner periphery

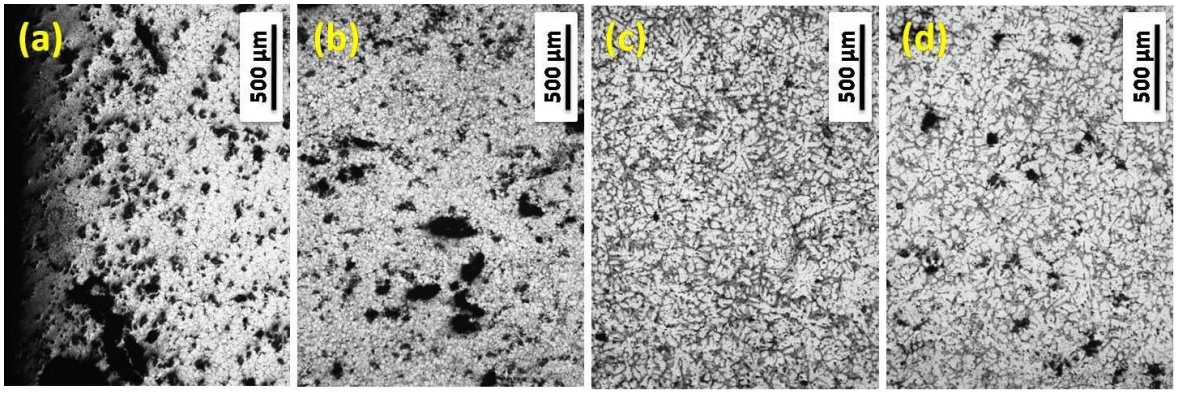

Figure 6.4 Optical microstructures of functionally graded centrifugal cast A2219-15%SiC (23 μm) disc at (a) 0.5 mm, (b) 20 mm, (c) 60 mm and (d) 80 mm from the outer to the inner periphery

6.4.2.2 Hardness

Figure 6.5 illustrates the hardness profiles of centrifugal cast functionally graded A2219 base alloy, A2219-15 wt. % SiC (14 μm) composite and A2219-15 wt. % SiC (23 μm) composite. The heat treated samples always showed an enhanced hardness values than the as-cast samples at every location. Figure 6.5a shows the hardness profile of functionally graded A2219 base alloy which shows a gradual increase in the hardness from the inner periphery towards the outer periphery of the castings. It gives a maximum hardness of 122 BHN at 40 mm from the outer periphery and 95 BHN at the inner most regions at 85 mm from the outer surface. This increase in the hardness values towards the outer periphery is because of the smaller grain size achieved at the outer periphery due to the faster solidification rate at the outer regions than the inner regions by the centrifugal casting process. The

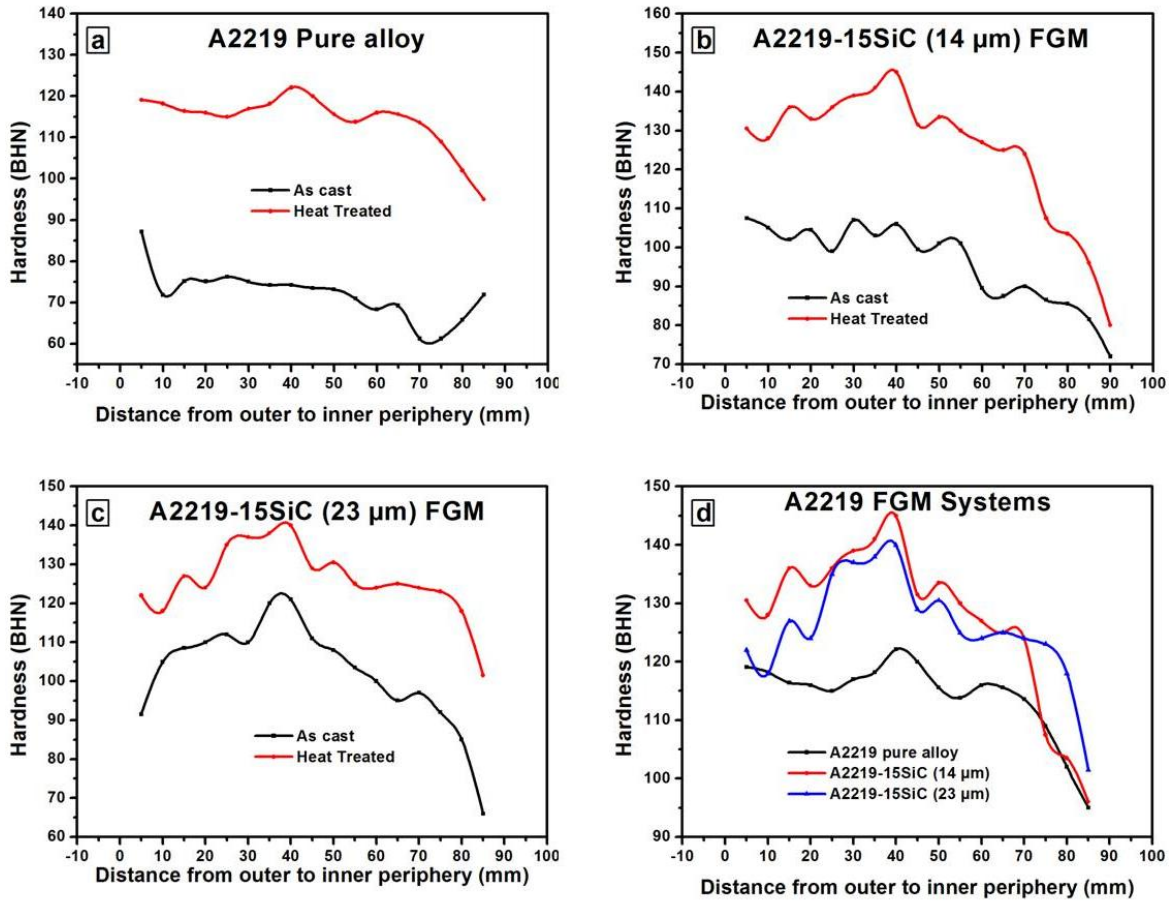

Figure 6.5 Hardness profile of the as-cast and precipitated-treated centrifugal cast FGM discs of (a) A2219 base alloy, (b) A2219–15 wt. % SiC (14 μm), (c) A2219–15 wt.% SiC (23 μm) and (d) combined A2219-FGM heat treated systems

inner periphery shows the lowest hardness values due to the coarser grain size of primary aluminum phases. An increase in the hardness values of as-cast at the inner most region is also attributed to the evenly distributed undissolved secondary phases at this region.

The as-cast and precipitation-treated samples of A2219-SiC FGM composites with 14 μm and 23 μm sizes also show an increase in the hardness values towards the outer periphery of the castings. This increase in the hardness values towards the outer periphery is due to the combined effect of the finer grains at the outermost regions and due to the segregation of the high density SiC reinforcement particles towards the outer regions of the castings by the centrifugal action. The FGM A2219-15 wt. % SiC of 14 μm and A2219-15 wt. % SiC of 23 μm shows a maximum hardness of 145 BHN and 140 BHN at 40 mm from the outer periphery of the cast disc, respectively that reveals the maximum segregation of the SiC particles at this region [Figure 6.5b and c]. And a minimum hardness of 80 BHN at 90 mm and 101 BHN at 85 mm from the outer diameter of the castings are observed in the 14 μm and 23 μm APS added composite systems, respectively. The inner periphery of the 14 μm added system shows a lesser hardness value than the 23 μm added system is due to the agglomeration took place due to improper wetting of SiC particles at the inner periphery of the casting. The outer periphery of the casting shows only a lower hardness than the hardness at 40 mm because of the segregated SiC particles are maximum at this region and chill zone formation towards the outer edge leading to lower particle concentration. And beyond 40 mm from the outer periphery it shows only lesser hardness than the preceding regions due to the decrease in the SiC particles and gradation towards the inner region. Figure 6.5d represents the hardness profiles of the functionally graded alloys and composites at the heat treated conditions together. The hardness curves clearly reveal that the composite system with 14 μm SiC gives the maximum values than the functionally graded alloy and the composite with the 23 μm SiC since when the particle sizes are finer the grain sizes are also finer which will increase the hardness values positively. The hardness values of the alloy and composites system shows initially an increase in the hardness upto 40 mm and then decreases. The centrifugal cast A2219 alloy also shows maximum hardness at 40 mm due to the segregation of the undissolved secondary phases

present in A2219 alloy. Similarly, the hardness for the corresponding FGM composite systems shows the maximum values at 40 mm itself due the segregation of the SiC reinforcement particles at this region. And the difference in the maximum values of the alloy system and in the FGM composite system is because of the presence of SiC particles present in the FGM composite systems.

6.4.3 Characteristics of functionally graded turbine exit vane guide

Figure 6.6 and 6.7 displays solid model and photograph of the centrifugal mould of the turbine exit vane guide respectively for the production of functionally graded composites by centrifugal casting technique. The model of the lower half of the centrifugal turbine exit vane guide is provided in the Figure 6.6a while the full assembly of the turbine exit vane guide is provided in the Figure 6.6b. The designed mould using the SOLIDWORKS is fabricated using oil hardening non-shrinking (OHNS) steel. Computer numerical control (CNC) milling process is used for the fabrication of the turbine exit vane guide. The photograph of the fabricated centrifugal mould for the turbine exit vane guide is as shown in Figure 6.7. The photograph of the centrifugal cast functionally graded turbine exit vane guide is

provided in Figure 6.8. Figure 6.9 shows the first angle projection of the turbine exit vane guide that clearly indicates the important terminologies of the exit vane guide. The plan of the projection clearly shows two types of edges in the vane guide, one is the leading edge and the other is the trailing edge.

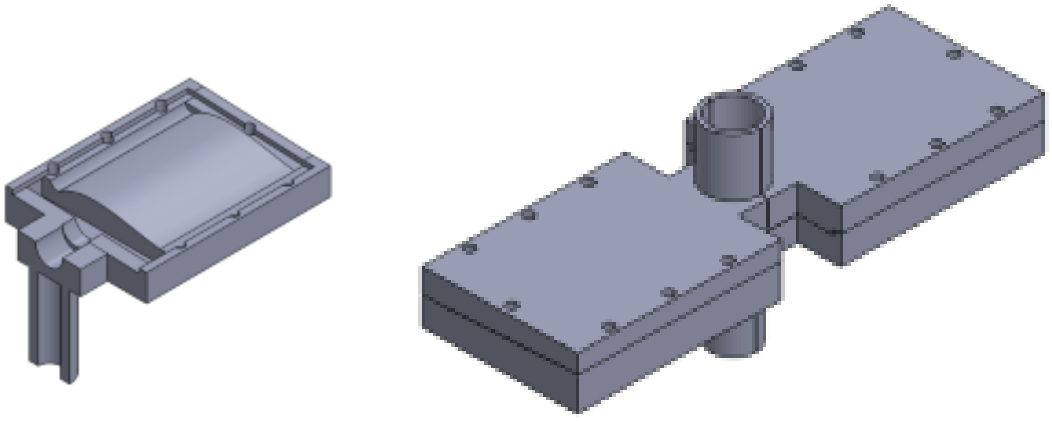

(a) **(b)**

Figure 6.6 Solid works model of the centrifugal cast mould for turbine exit vane guide (a) lower half of the mould and (b) whole assembly of the lower and upper half of the centrifugal mould

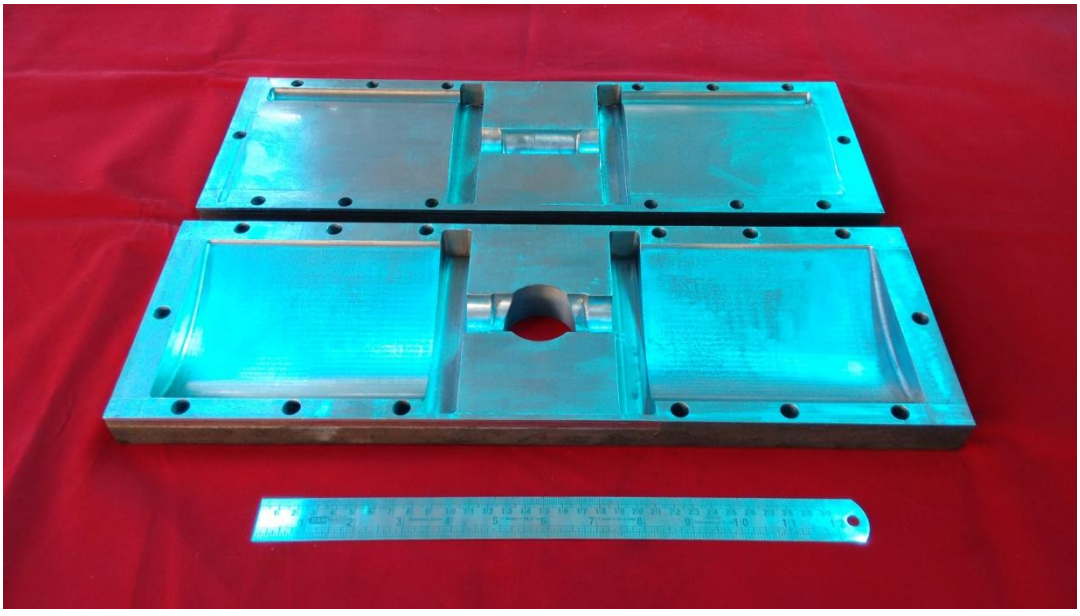

Figure 6.7 Fabricated mould for the centrifugal casting of the turbine exit vane guide

Figure 6.8 Photograph of the centrifugal cast functionally graded turbine exit vane guide

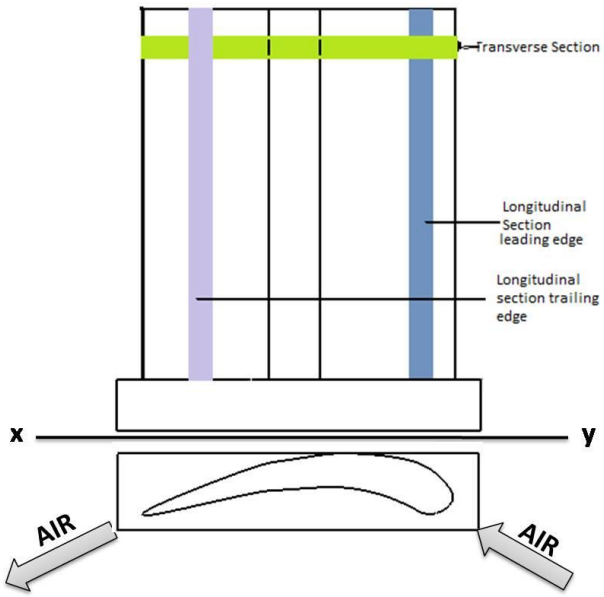

Figure 6.9 First angle projection of the turbine exit vane guide

6.4.3.1 Microstructural observations

The optical microstructures of the functionally graded turbine exit vane guide are considered along the transverse as well as in the longitudinal direction. Figure 6.10 shows the optical microstructures of the centrifugal cast turbine exit vane guide using A2219 base alloy along the transverse direction from the trailing edge to the leading edge. Figure 6.10a shows the tip of the tailing edge showing the fine grain sized primary aluminium phases which are achieved due to the lower thickness of the mould at the trailing edge where the solidification took place faster than the other regions. The smaller grain size at the trailing edge improves the mechanical properties of the turbine vane guide at this region. As the microstructures proceed towards the leading edge of the functionally graded turbine exit vane guide, the size of the primary aluminium phases become larger and larger. The larger size of the

grains is due to the increase in the rate of solidification. The leading edge has the coarser size primary aluminium phases in the FGM turbine exit vane guide. The undissolved secondary phases in the A2219 aluminium alloy is seen as round towards the outer periphery of the casting and towards the trailing edge is due to the centrifugal action and the thickness of the mould cavity, respectively.

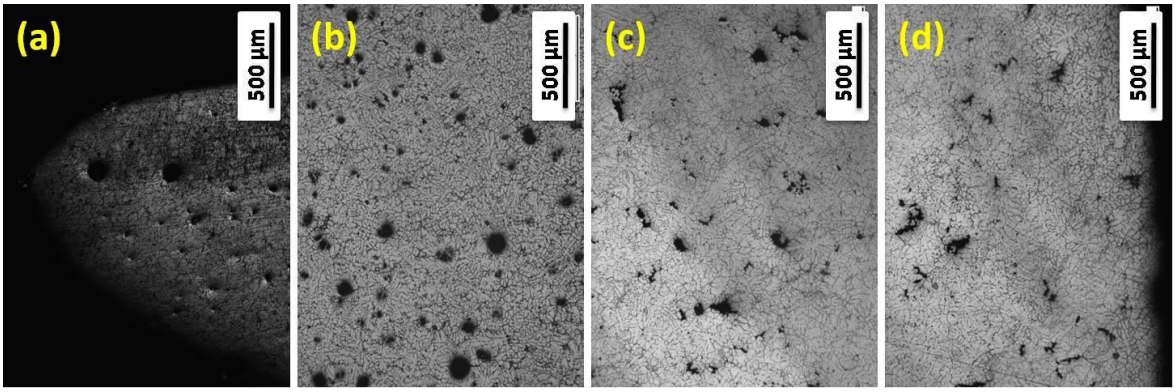

Figure 6.10 Optical microstructures of functionally graded centrifugal cast A2219 base alloy exit vane guide along the transverse direction from the trailing edge to the leading edge at (a) 0.5 mm, (b) 20 mm, (c) 60 mm and (d) 125 mm

Figure 6.11 shows the optical micrographs of the A2219-15 wt. % SiC of 14 µm APS functionally graded centrifugal cast turbine exit vane guide from the trailing edge to the leading edge at 0.5 mm, 20 mm, 60 mm and 120 mm. The trailing edge at 0.5 mm shows only a less SiC particle concentration than the subsequent region at 10 and 20 mm. The less particle concentration at the trailing edge is because of the chill zone formation due to the preheat temperature in the mould. The maximum concentrations of the SiC particles are observed in between 10 mm and 25 mm from the trailing edge. The leading edge is showing only a lesser particle concentration. The trailing edge shows a higher percentage of particle concentration than the leading edge because of the propagation of the high density reinforcement particles towards the trailing edge since the leading edge possesses as the rotational front of the mould. So the reinforcement particles are forced to segregate towards the trailing edge of the exit vane guide. Also, the size of the primary aluminium phases is finer towards the trailing edge due to the reduced thickness of the mould cavity towards the trailing edge. And it is also noticed that the grain size of the FGM composite with 14 µm size SiC is finer than the centrifugal cast A2219 base alloy. This is due to the hindrance to the growth of primary aluminum phases in the matrix due to the presence of smaller size (14 µm) reinforcement particles.

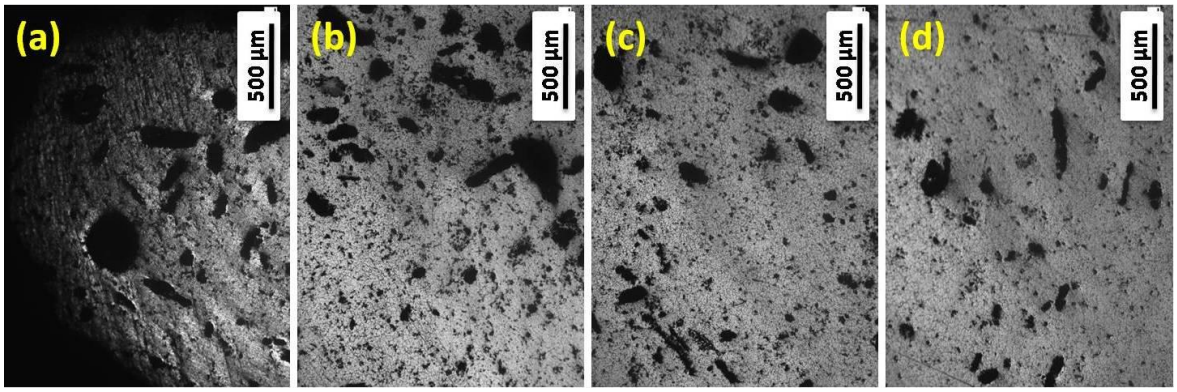

Figure 6.11 Optical microstructures of functionally graded centrifugal cast A2219-15 wt. % SiC (14 µm) exit vane guide along the transverse direction from the trailing edge to the leading edge at (a) 0.5 mm, (b) 20 mm, (c) 60 mm and (d) 120 mm

Figure 6.12 represents the microstructures of A2219-15 wt. % SiC of 23 µm APS functionally graded centrifugal cast turbine exit vane guide. The microstructures are taken from the trailing edge to the leading edge at 0.5 mm, 20 mm, 60 mm and 120 mm. The 23 µm size SiC reinforcement particles are seen as almost evenly distributed in the matrix. Nevertheless, a gradual increase in the gradation can be observed up to 60 mm and some particle agglomerates are observed in the Figure 6.12d at 120 mm from the trailing edge. The particle agglomeration seen at the leading edges may be due to the restriction of the movement of the high density SiC particles through the matrix from the rotation front of the mould. But, the microstructures of the 23 µm size SiC added 2219 functionally graded composite system clearly reveals that the sizes of the primary aluminium phases are coarser than that of the 14 µm size added 2219 functionally graded composite system.

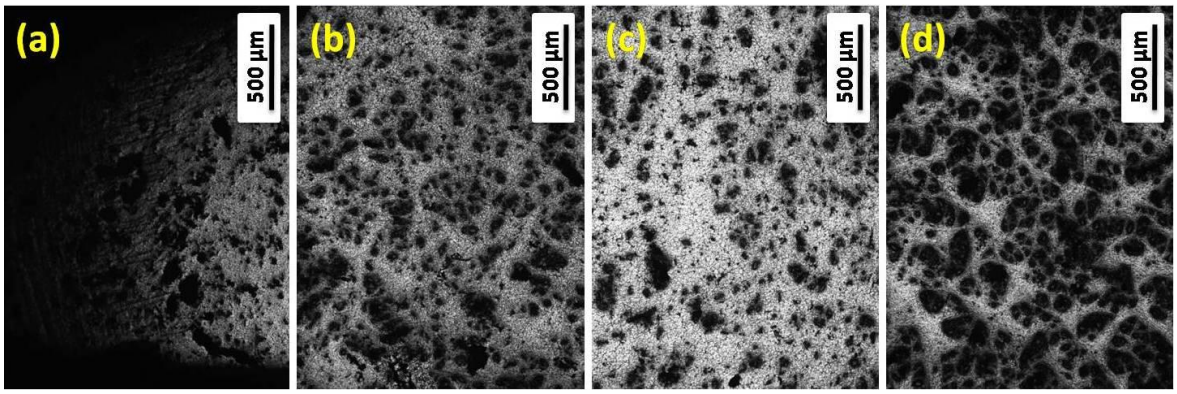

Figure 6.12 Optical microstructures of functionally graded centrifugal cast A2219-15 wt. % SiC (23 µm) exit vane guide along the transverse direction from the trailing edge to the leading edge at (a) 0.5 mm, (b) 20 mm, (c) 60 mm and (d) 120 mm

Figure 6.13 and 6.14 displays the optical micrographs of the A2219 FGM composite systems with 14 and 23 μm APS along the longitudinal direction at 35 mm, 70 mm, 105 mm and 140 mm from the outer to the inner periphery of the castings. In A2219-15 wt. % SiC composite with 14 μm APS in Figure 6.13 shows finer grains of primary aluminium phases towards the outer region of the casting due to the forced solidification of the molten melt during the centrifugal casting. And the distribution of the SiC reinforcement particles is found homogeneously up to 80 mm from the outer periphery and there is a slight increase in the concentration of the 14 μm SiC added FGMMC towards the inner periphery of the casting. The slight increase in the concentration of the SiC particle of 14 μm size towards the inner periphery of the castings as visible in the Figure 6.13c and d may due to the faster solidification of the molten metal from the outer most region and may also due to the relative density of the fine SiC particle of 14 μm with the aluminium matrix. Figure 6.14 shows the optical micrographs of the functionally graded A2219-15 wt. % SiC of 23 μm APS. The micrographs of the longitudinal section from the outer to the inner periphery of the casting show an almost homogeneous distribution of the SiC particles throughout in the Figure 6.14a-d. But the primary aluminium phases show finer grain size towards the outer periphery of the casting due to the forced solidification of the melts during the centrifugal casting process. As the microstructures proceed to the inner periphery of the castings in Figure 6.14b and c, it is clear that the grain size of the primary aluminium phases become coarser and coarser, since the inner regions of the castings were experienced with only low centrifugal gravitational effect due to the rotation of the mould.

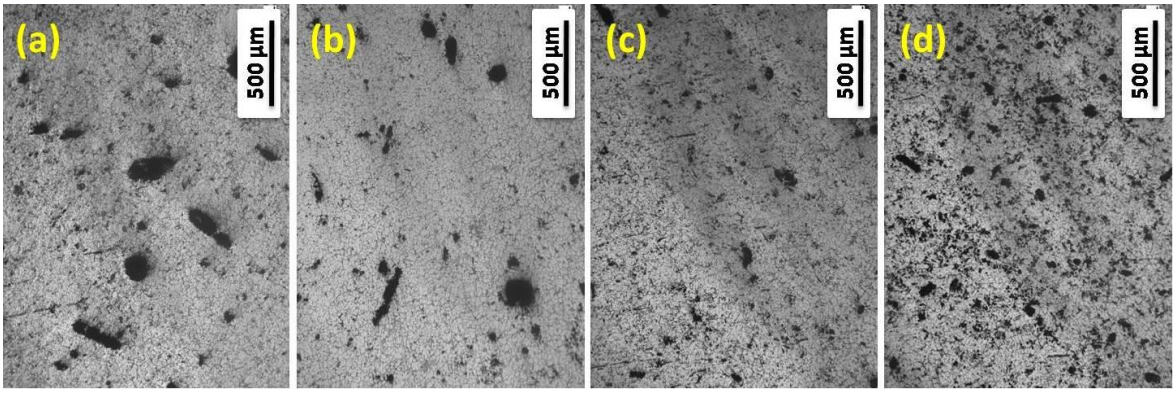

Figure 6.13 Optical microstructures of functionally graded centrifugal cast A2219-15 wt. % SiC (14 μm) exit vane guide along the longitudinal direction at (a) 35 mm, (b) 70 mm, (c) 105 mm and (d) 140 mm from the outer to the inner periphery of the casting

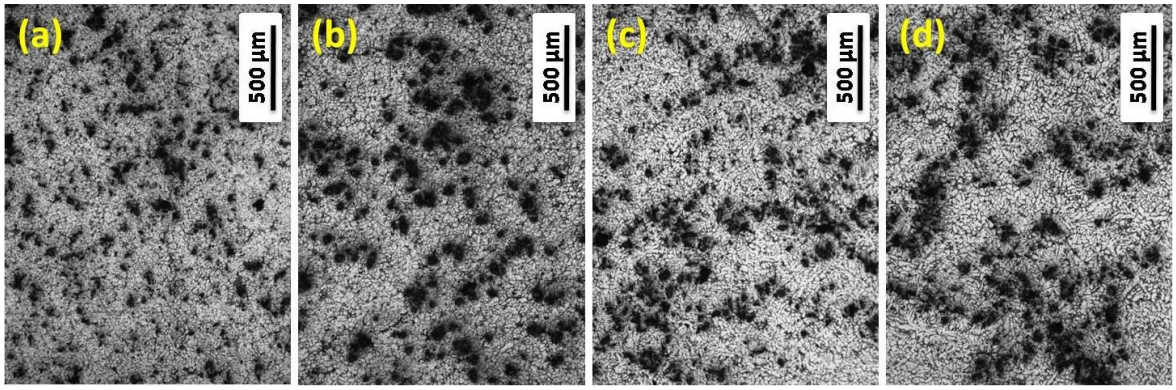

Figure 6.14 Optical microstructures of functionally graded centrifugal cast A2219-15 wt. % SiC (23 µm) exit vane guide along the longitudinal direction at (a) 35 mm, (b) 70 mm, (c) 105 mm and (d) 140 mm from the outer to the inner periphery of the casting

6.4.3.2 Hardness

Figure 6.15 and 6.16 indicates the hardness profiles of the functionally graded centrifugal cast A2219 base alloy and the A2219- SiC systems in the as-cast and the heat treated conditions. The hardness values are taken along the transverse and longitudinal direction of the functionally graded centrifugal cast turbine exit vane guide. The heat treated values show an enhanced hardness than the as-cast values of hardness at every location. Figure 6.15a shows the hardness profile of functionally graded centrifugal cast A2219 base alloy turbine exit vane guide along the transverse direction (aerofoil profile). It can be seen that there is an increase in the hardness values towards the leading edge of the turbine exit vane guide from the trailing edge in the heat treated condition. But the as-cast hardness values show a decreased value towards the leading edge. A maximum hardness of 128 BHN was obtained at the leading edge and a minimum hardness of 118 BHN is obtained at 75 mm from the leading edge in the heat treated condition. The increase in the values of the heat treated conditions towards the leading edge from the trailing edge is due to a large amount of secondary phases precipitated out during the solution heat treatment process, since the vane guide cross section is bigger at the leading edge than the trailing edge.

A2219-15 wt. % SiC of 14 µm size centrifugal cast FGM also shows an increase in the hardness values towards the leading edge from the trailing edge, due to the large number of precipitation phases and the presence of the SiC particles. The FGM composite A2219-15 wt. % SiC (14 µm) system gives a maximum hardness of 162

BHN at the leading edge and a minimum hardness of 141 BHN at 110 mm from the leading edge. But in the 23 μm size SiC particle added A2219 composite FGM system in Figure 6.15c shows a higher hardness towards the trailing edge than the leading edge. This is because of the presence of high density SiC particles of 23 μm at the trailing edge and also due to the refined fine grain structure of the primary aluminium phases at this region acquired due to the faster solidification of the melt in the trailing edge than the leading edge. The agglomeration of the SiC particles at the leading edges reduces the hardness of the vane guide at this region than the trailing edge, which is evident from the microstructure [Figure 6.12d]. The hardness profiles of all the FGM systems shows an increased hardness at the two ends i.e., at the leading edge and the trailing edge because of the finer grain size due to chill zone formation during the process of centrifugal casting. The middle region of the transverse direction is showing the lower hardness values than the trailing and leading edges since this being the last solidified region. The combined hardness profiles of heat treated samples of centrifugal cast functionally graded A2219 base alloy and the A2219 composites are provided in the Figure 6.15d. The combined profile of hardness in the Figure 6.15d reveals that the maximum hardness is obtained at the leading edge of the functionally graded A2219-SiC composite with 14 μm APS SiC. And the profile of the hardness also shows the large increase in the values of the hardness in the A2219-SiC composite of 14 μm APS in comparison with the centrifugal cast A2219 base alloy FGM and the A2219-SiC composite of 23 μm APS. The increased hardness values at the leading edges in the centrifugal cast A2219 base alloy and the A2219-SiC composite of 14 μm APS gives more strength and wear resistance at this region where the air enters to the exit vane guide in the aero turbine engines.

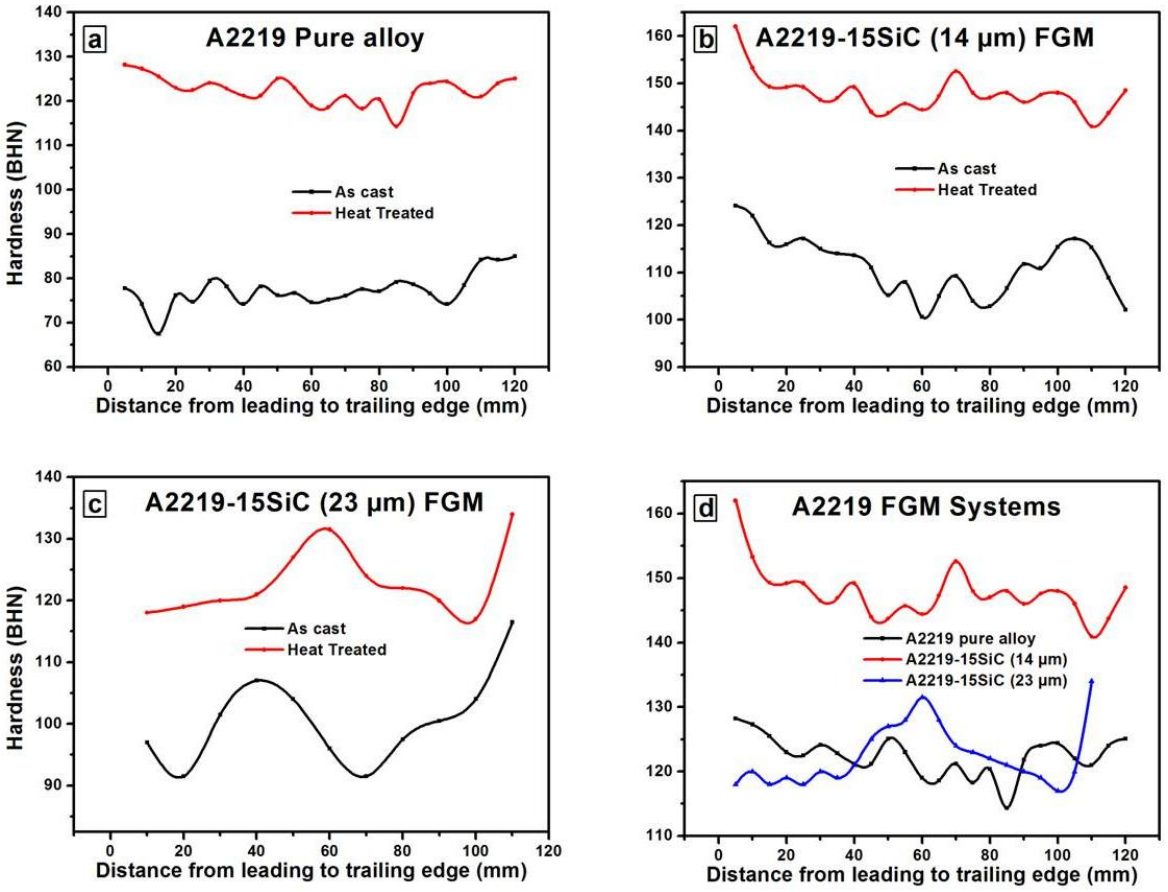

Figure 6.15 Hardness profile of the as-cast and precipitated-treated centrifugal cast turbine exit vane guide FGM of (a) A2219 base alloy, (b) A2219–15 wt. % SiC (14 μm) (c) A2219–15 wt. % SiC (23 μm) along the transverse section (aerofoil cross-section) and (d) combined A2219-FGM heat treated systems

Figure 6.16 indicates the hardness values of the functionally graded centrifugal cast A2219 base alloy and composite systems reinforced with SiC particles of 14 and 23 μm APS in the longitudinal direction from outer to the inner periphery of the castings. As in the previous cases, the heat treated samples shows enhanced hardness values than the as-cast samples. Figure 6.16a shows the hardness profiles of centrifugal cast A2219 base alloy turbine exit vane guide from the outer to the inner periphery in the longitudinal direction. There is an increase in the hardness observed from the inner periphery to the outer periphery, achieved due to the forced solidification of the molten melt during centrifugal rotation of the mould. Due to the forced solidification of the melt, the outer region of the cast component contains fine grains of the primary aluminium phases which are evident from the

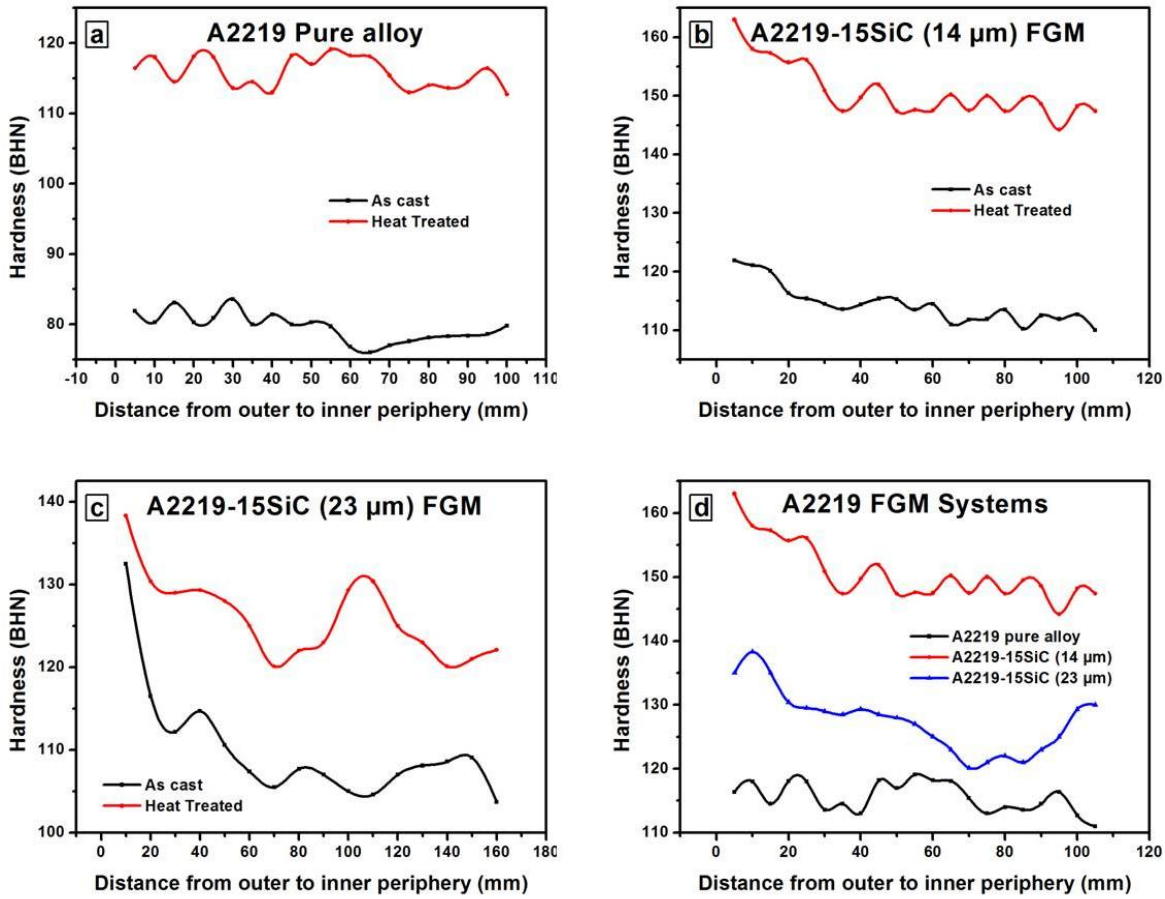

Figure 6.16 Hardness profile of the as-cast and precipitated-treated centrifugal cast turbine exit vane guide FGM of (a) A2219 base alloy, (b) A2219–15 wt. % SiC (14 µm) (c) A2219–15 wt. % SiC (23 µm) along the longitudinal direction from the outer to the inner periphery of the castings and (d) combined A2219-FGM heat treated systems

microstructure evaluation [Figure 6.12 and 6.13]. The heat treated samples in the outer region at 5 mm shows a maximum hardness of 128 BHN and a minimum hardness of 114 BHN at 85 mm from the outer periphery. The hardness profiles in Figure 6.16b and c of FGM composite systems of A2219 with 14 and 23 µm APS shows an increased hardness towards the outer region because of the segregation of the higher concentration of the high density SiC particles towards the outer most regions of the casting and also due to the fine grain size of the primary aluminium phases due to the forced solidification by the centrifugal casting process. The FGM with 14 µm size SiC particle added A2219 aluminium composite system shows a maximum hardness of 163 BHN at 5 mm from the outer region and 147 BHN at 105 mm from the outer region, whereas the 23 µm added composite shows 138 BHN

at 10 mm and 120 BHN at 140 mm from the outer region of the castings as the maximum and the minimum values of hardness, respectively [Figure 6.16b and c]. Also, the FGM with 23 μm shows and increase in the hardness after 100 m from the outer periphery due to the agglomeration of the SiC particles at this region. The value of the hardness is then decreased to a value that is less than that of the outer most region due to the segregation of low density particles towards the axis of rotation during the centrifugal casting process. Figure 6.16d represents the combined hardness profile of the FGM alloy and composite systems which shows an increase in the hardness towards the outer periphery of the castings than the inner periphery and also the hardness profiles clearly reveals that the 14 μm size SiC particle added A2219 aluminium composite system provides the maximum hardness values at every location among the other systems.

6.4.3.3 Tensile Properties

The tensile properties of centrifugal cast functionally graded A2219-15 wt.% SiC of 14 μm APS composites were evaluated with ASTM E8M standard using flat tensile specimens of dimensions 60 mm length, 12 mm width and 4 mm thickness with a gauge length of 20 mm. For the tensile test of the centrifugal cast functionally graded SiC composite, the turbine exit vane guide is divided into 6 equal sections from the outer to the inner portion of the casting as shown in Figure 6.17.

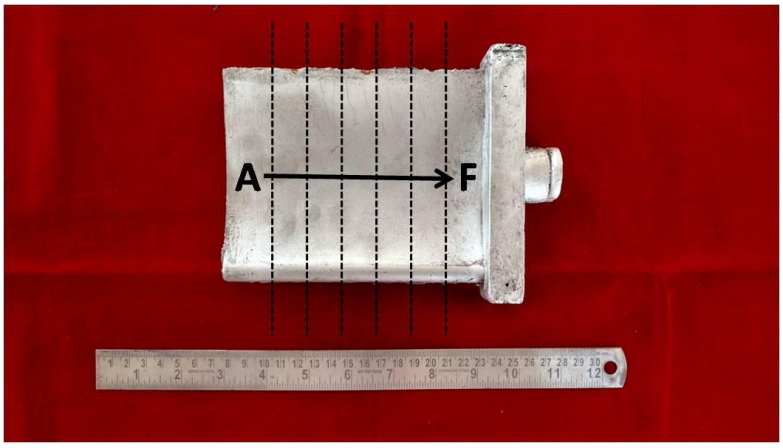

Figure 6.17 Section considered from the outer to the inner periphery of the cast turbine exit vane guide

Figure 6.18 shows the tensile strengths of gravity cast and centrifugal cast functionally graded A2219 base alloy and A2219-SiC (14 μm) composite. The gravity cast A2219 base alloy shows the higher tensile strength of 316 N/mm^2 and the

A2219-SiC composite shows 150 N/mm^2. The lesser value in the tensile strength in the composite system is due to the incorporation of the SiC particles causing increased of porosity and agglomeration of particles. The centrifugal cast functionally graded A2219 base alloy and A2219-SiC composite from the outer to the inner portion of the cast turbine exit vane guide displays an increase in the tensile strengths towards the inner portion of the castings due to the ductile nature of the coarse grains of the aluminium alloys towards the inner region of the castings achieved during the centrifugal casting process. The alloy FGM from the section A to F shows a tensile strength of 156, 233, 234, 266, 270 and 322 N/mm^2. The functionally graded composite A2219-15 wt. % SiC (14 μm) FGM gives 121, 133, 137, 140, 158 and 272 N/mm^2 from the Section A to F towards the inner portion of the casting. The inner section F shows a large increase in the tensile value due to the lower concentration of reinforcement particles towards the inner region.

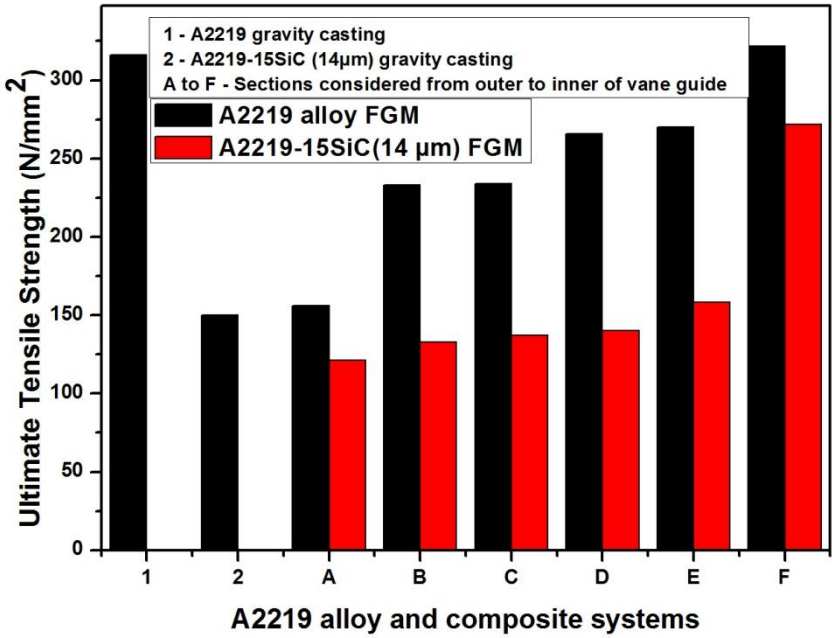

Figure 6.18 Tensile strengths of gravity and centrifugal cast functionally graded A2219 alloy and A2219-SiC (14 μm) composite turbine exit vane guide

6.4.3.4 Wear properties

The pin-on-disc wear analysis of the gravity cast A2219 base alloy and the A2219-15 wt. % SiC of 14 μm APS is provided in the Figure 6.19a. The wear tests were conducted using heat treated samples at 19.62, 39.24, 58.86 and 78.48 N loads and the specific wear rates are reported in mm^3/Nm. A2219-SiC composite samples show better wear resistance than the gravity cast 2219 Al alloy samples at all the loads. The gravity cast A2219 alloy specimens shows a minimum wear rate of 6.01647 x 10^{-5} mm^3/Nm at a load of 19.62 N and a maximum of 9.16301 x 10^{-5} mm^3/Nm at 58.86 N. But in the composite specimens with 15 wt. % SiC of

14 μm APS gives only a maximum wear rate of 7.09617 x 10^{-5} mm^3/Nm at 58.86 N load which is almost close value of wear rate with the minimum value for alloy specimen at lower load and the composite system which gives a minimum wear rate of 3.30695 x 10^{-5} mm^3/Nm at a load of 19.62 N. At a load of 78.48 N both the alloy and SiC composite FGM system of A2219 aluminium matrix shows slightly lesser wear rate of 8.97283 x 10^{-5} mm^3/Nm and 6.8981 x 10^{-5} mm^3/Nm than the 58.86 N load. This decrease in the wear rate at a maximum load of 78.48 N is due to the formation of mechanically mixed layers (MMLs) on the rubbing surface between the pin and the counter surface. The formation of the MML protects the specimen surface from further wearing of the specimen, which results in the lower value of the wear rate at the maximum load.

Figure 6.19b indicates the wear rate of the functionally graded centrifugal cast A2219-15 wt. % SiC of 14 μm APS turbine exit vane guide from the outer to the inner periphery of the castings. For the wear test of the composite FGM turbine exit vane guide, six sections (A to F) were considered from the outer to the inner periphery of the castings as considered for the tensile tests for the turbine exit vane guide in the Figure 6.17. The outer specimens at section A shows a maximum wear resistance at all loads of 19.62, 39.24, 58.86 and 78.48 N than the inner sections from sections B to F. The functionally graded composite turbine exit vane guide at Section A shows a minimum wear rate of 0.85103 x 10^{-5} mm^3/Nm at 19.62 N load and a maximum wear rate of 3.88281 x 10^{-5} mm^3/Nm at 78.48 N. The specific wear rate from the Section A to F from the outer to the inner periphery of the turbine exit vane guide casting at all the loads shows an increase in the wear rate. The maximum wear rate occurred at all the loads can be observed in the innermost regions of Section F. The minimum rate of wear at a lower load of 19.62 N is 4.47375 x 10^{-5} mm^3/Nm and the maximum rate of wear is 8.81193 x 10^{-5} mm^3/Nm at a load of 58.86 N. The wear rate at the higher load of 78.48 N shows a lower wear rate than at the 58.86 N because of the formation of the mechanically mixed layer during the continuous run of the wear specimen over the counter surface. The outer region (Section A) of the Al FGM turbine exit vane guide shows enhanced wear resistance due to the presence of higher concentration of SiC particles as well as the undissolved secondary phases in the matrix as evident from the microstructures. The sections A, B and C shows very low wear rate due to particle enriched zone compared to sections D, E and F. Also, it can be observed that there is a difference in the closest values of wear rates of the curves between Section C and Section D because, upto Section C the concentration of the SiC particles are more than Section D due to the forced segregation of the SiC particles towards the outer region (Sections A, B and C) during the centrifugal force involved in the casting process.

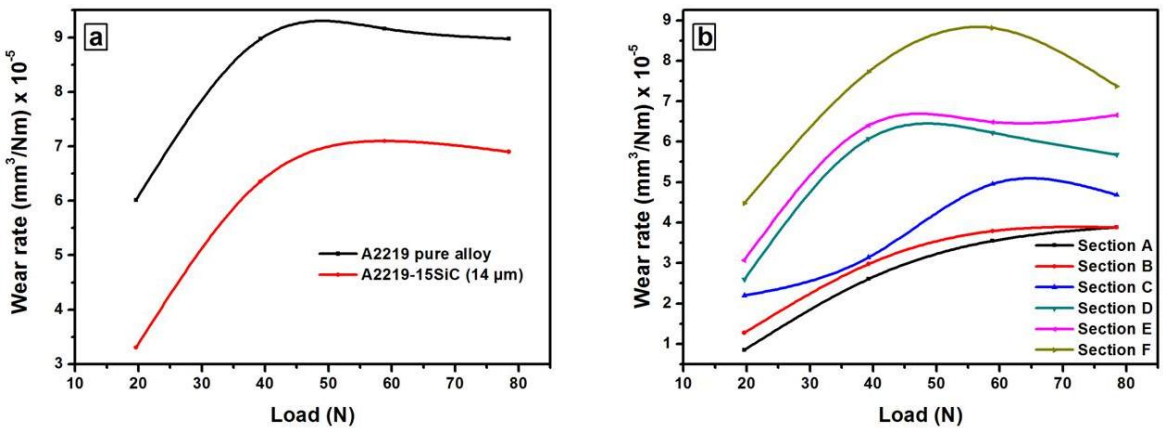

Figure 6.19 Wear rate values of (a) gravity cast A2219 base alloy and A2219-SiC (14 µm) and (b) functionally graded centrifugal cast and A2219-15 wt.% SiC (14µm) turbine exit vane guide from the outer to the inner periphery of the castings

6.4.3.5 Worn surface analysis

Worn surface SEM analyses of the wear specimens from the outer to the inner periphery of the functionally graded A2219-15 wt. % SiC (14 µm) composite turbine exit vane guide produced by centrifugal castings are shown in Figure 6.20. The worn surface SEM analyses were conducted at the specimens from the sections A to F, one at a lower load of 39.24 N and another at a higher load of 78.48 N. Figure 6.20a shows the SEM images of the worn surface of wear pin specimen from the outermost periphery of the castings at a lower load of 39.24 N. It shows a very fine wear scars which are running parallel to each other. The wear debris formed due to the continuous run of the wear specimen is visible in the SEM analysis which is a clear evidence of abrasive type of wear mechanism that took place due to the fine grain size of the primary aluminum phases and also due to the presence of higher concentration of 14 µm APS SiC reinforcements at the outer periphery of the

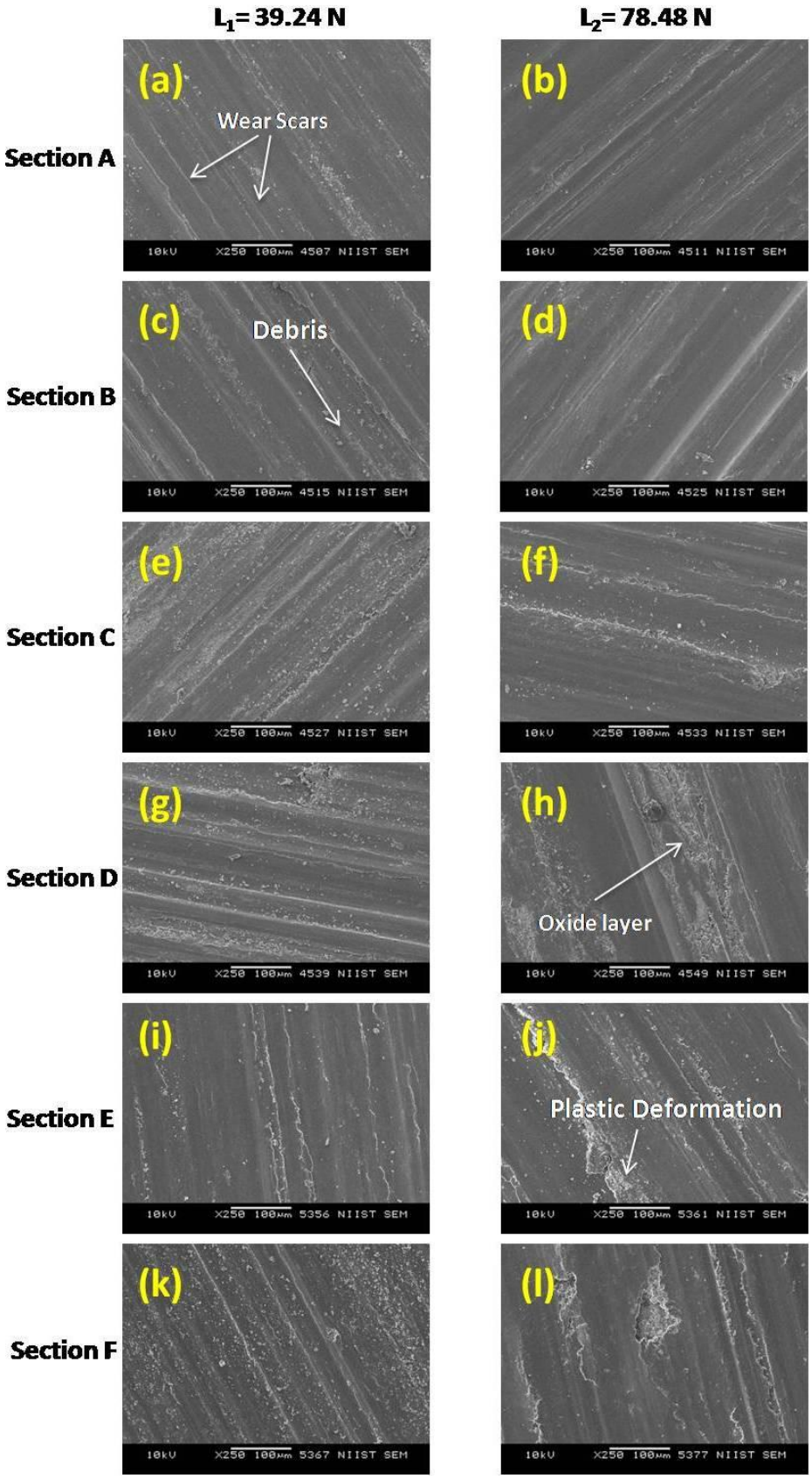

Figure 6.20 Worn surface analysis of centrifugal cast functionally graded A2219-15 wt. % SiC (14 μm) composite turbine exit vane guide from outer to inner periphery of the casting

centrifugal cast turbine exit vane guide achieved due to the centrifugal force involved in the casting process. Figure 6.20b shows the SEM image of the worn surface of the wear specimen at section A at a load of 78.48 N. At the higher load also it can be visible that the surface is not damaged much when compared with the worn surface at the lower load. This resistance to the surface of the wear specimen was offered by the higher concentration of the fine SiC particles and the fine grain size at the outer regions of the centrifugal cast samples. In the SEM analysis, at the higher load the wear scars are slightly wider than that at the lower load in Figure 6.20a. The worn surface analysis of Section B specimens at the lower load shows almost similar type of surface as observed in the case of Section A. But the specimen of Section B at a load of 78.48 N shows slight delaminated worn surface than the higher load at the Section A. This is due to the higher concentration of SiC particles, the undissolved secondary phases as well as coarser gain size of the primary aluminium phases in the matrix of section A in comparison with Section B gained through the centrifugal casting process. The analysis also indicates the presence of the initiation of the oxide layers at this location under the higher load.

Section C shows almost similar types of wear phenomenon at the lower and the higher load without much surface damage than from the Section B. At the higher load of 78.48 N at the Section D, the SEM analysis shows that the surface is enriched with more layers of oxide layers which helped the material from further wearing and severe surface damage to the material surface which can be seen in the wear rate graph in Figure 6.19b, where at the higher load the graphs falls to a lesser value than from the previous value of were rate. As the worn surface analysis proceeds to the inner region of the cast turbine exit vane guide the width of the wear scars increases at the lower load of 39.24 N and at the higher load of 78.48 N. The oxide layers came into existence which spreads through a large area on the surface of the wear specimen, especially at the inner Section of D, E and F that protects the surface from severe adhesive wear of the material which reflects in the wear rate graphs of sections D, E and F at the loads of 58.86 and 78.48 N. The specimens from the inner periphery of the casting underwent delamination on the surface layers at Section E and the surface was severely plastically deformed at the Section F. The worn out surface of the wear pin specimens always show a specific pattern of wear scars,

grooves and projections on the surface of the specimen that gives a clear picture of the peculiarity of the wear mechanisms at various loads and running conditions. The penetration that seen on the surface of the worn specimens in depth may be due to the existence of the asperity peaks in high altitudes present on the counter surface and/or due to the presence of the hard ceramic reinforcement particles got detached from the surfaces and trapped during the wear test in between the mating surfaces. Generally, the surface of the pin specimens underwent an abrasive type of wear mechanism due to the presence of fine SiC particles, especially at the outer regions. Nevertheless, the specimens at the inner specimen had undergone with the adhesive type of wear due to the coarser grain size of the primary aluminium phases towards the inner periphery of the castings. In the functionally graded composites, at certain loads, the formation of the oxide layers and MMLs cannot be completely neglected. Aluminium oxide, iron and iron oxide, intermetallic compounds of Al-Fe and Al-Fe-O formed during the continuous sliding operation during the pin-on-disc wear test plays a vital role in the development of the MMLs between the pin surface and counter body during the rubbing of the both together at the test duration. The formation of oxides and MMLs on the rubbing surfaces usually protects the surface of the material under sliding from severe wear and catastrophic failure due to the repeated rotation of the counter body through the same path which develops the heat of the counter body. But MMLs cannot perform as a barrier to protect the wear surface from every service condition like higher loads and lower sliding speed as well as lower loads and higher sliding velocity for a prolonged period. Even though the oxides and MMLs protect the wear surface, the wearing of the MML layers and the formation of oxide layers are a continuous process which finally results in a swift decrease and increase in the wear magnitude when the material is mating at higher loads with high pressure at the pin specimen. The oxide layers and the MML formations in the specimen surfaces are approximately very much good agreement with the worn surface analysis, microstructures and the hardness properties of the corresponding material systems were reported in the previous studies (Rajaram et al., 2010; Young et al., 2000; Ghazali et al., 2007 and Rosenberger et al., 2005). Also, Rajaram et. al., observed and reported that the debris of oxides are deposited in the wear grooves and restricts further wear of the material by forming wear resistant layers (Rajaram et al., 2010). John et al. had given a detailed report on the formation

and destruction of the MMLs during the sliding contact during the wear test (Young et al., 2000). Depending upon the elemental composition, its properties and the service conditions, the morphology and the thickness of the MMLs vary by providing different types of strengthening behavior to the material under wearing (Ghazali et al., 2007). Rosenberger et al. also reported that the MMLs are always formed from the matrix alloy, reinforcing phases and the reinforcement particles removed from the surface of the specimen during wear reported and 20 % of Fe worn from the counter surface removed due to the hard reinforcing particles present on the specimen surface (Rosenberger et al., 2005). The observations of MML formation in Al alloy and MMC reported in the above mentioned literature are in good agreement with the present observations in Al FGMs.

6.5 Conclusions

Exit vane guide for turbine was successfully designed and A2219 based SiC reinforced functionally graded metal matrix composites are successfully fabricated especially at the thinner sections of the guides by centrifugal casting without any axial symmetry which is normally difficult to process through gravity casting process. The SiC particles are mostly segregated gradually towards the outer periphery of the casting due to the high centrifugal force factor owing to the rotation of the mould during casting. The hardness results show an increase in the hardness magnitudes towards the outer periphery of the castings due to the segregation of the SiC particles and also due to the finer grain sizes of primary aluminium phases because of the higher solidification rate achieved at the outer region of the castings. The hardness values are increasing towards the leading edge from the trailing edge. The increase in the hardness values at the leading edge will help the edge to protect the region from high erosive wear since the air enters to the vane guide for the exhaust through the leading edge. The hardness values are in very good agreement with the microstructures of the cast turbine exit vane guide. The tensile strength increases from the outer periphery towards the inner periphery of the cast turbine exit vane guide. The pin-on-disc wear tests show mostly an abrasive and oxidative type of wear mechanisms and higher resistance to wear were observed towards the outer periphery of the cast component due to the presence of high density SiC particles and the fine grain size of the primary aluminium phases.

CHAPTER 7

Functionally Graded SCF Reinforced Epoxy Composites

7.1 Abstract

Epoxy resins are extensively used in aerospace and cryogenic engineering applications. Functionally graded epoxy polymers can be advantageously used for tribological applications to attain better properties than the homogeneous polymers/ composites. The wear properties can be improved by incorporating fibers/particles in the epoxy matrix. The present investigation aims at the processing and the characterization of functionally graded short carbon fiber (SCF) reinforced epoxy matrix composites by centrifugal casting technique using various volume percentages (0, 1, 2 and 3 vol. %) of short carbon fibers. As the volume percentage of the short carbon fibers increases in the epoxy matrix, the viscosity also increases. A maximum hardness is obtained at the outer periphery of 1 volume percentage short carbon fiber reinforced functionally graded material (FGM). The fiber rich region exhibits excellent tribological properties at the outer region of the fabricated item of polymer composite system.

7.2 Introduction

Functionally graded materials (FGMs) are the most advanced class of inhomogeneous composite materials, where the volume fractions of reinforcement particles/fibers are altered locally to achieve specific properties at specific locations within a component (Vieira et al., 2009; Duquea et al., 2005 and Akhil et al., 2016). The developments of FGMs are in the immature stage only so, there exists various scopes in the production and development of the FGM for heat exchangers, turbine blades, flywheels, thermal protection systems for aerospace applications, nuclear fuel pellets, frame components for space shuttles, thermo electric generators, sports goods, automotive industry, defence sector etc. due to their high thermal properties, fracture toughness and interfacial bonding between the matrix and the reinforcement. However epoxy resins have poor crack resistance at room temperature, it has been widely used in cryogenic engineering sectors since it is brittle and posses good cryogenic mechanical properties at cryogenic temperatures

(Chen et al., 2009). Modification versatility to improve the properties by incorporating aromatic and aliphatic monomers and good chemical resistance makes epoxy resins attractive for the researchers (McGrath et al., 2008). Compared to homogeneous materials FGM shows enhanced functional properties since the materials are engineered with different gradients of constituent elements. FGMs are the most advanced materials in the composite family that is used for strategic engineering applications where the operating conditions are severe. Since the FGM possess continuous gradient structure, it can avoid sudden failures or changes in properties during operation. Nowadays FGM finds its potential applications in various sectors even in medicinal fields such as in optical fibers, lenses, artificial skins, teeth, and bone transplantation (Akhil et al., 2016 and Tarlochan et al., 2012).

Centrifugal casting technique seems to be one of the most cost effective and efficient processes to produce FGM among the various other processes such as controlled mould filling, molten metal infiltration, sol-gel technique, self propagating, diffusion bonding laser cladding plasma spraying, chemical and physical vapour deposition, etc. Rotocasting or centrifugal casting is a pressure casting process to produce FGM where the matrix liquid or composite mixture is poured into a rotating mould till the matrix solidifies under centrifugal force, acting continuously towards the mould wall (Akhil et al., 2016). Fukui et al. carried out a ring crushing test of plaster model composite produced by centrifugal casting and showed that as the gradient of the composition increases in a component the maximum strain and load increases at this point and leads to breakage (Fukui et al., 1992 and Lee et al., 1997).

Thermosetting epoxy resins are normally used polymer matrix for the high temperature applications below 160 °C since it can accommodate higher temperatures than other polymers, good rheological behaviour during processing, low cost, low shrinkage, easiness in the processing, alterable structure, environmental resistance, better adhesion properties, improved mechanical properties especially for strategic sectors and recyclability (Chatterjee et al., 2010; Zhou et al., 2008; Green et al., 2009; Xu et al., 2008; Zhao et al., 2012 and El-Sayed et al., 1995). Due to the polymerisation reaction, flow condition and increase in temperature during the processing the viscosity of the epoxy matrix changes. Even though the polymers have been used in various sectors in engineering including

aerospace industry, it has only short running life when exposed to high temperature and tribological applications. So it is very essential to enhance the tribological properties including higher hardness and wear resistance for the outstanding performance of the polymers by improving the mechanical properties. To attain the enhanced tribological properties, a small amount of fillers are added to the polymer matrix, especially glass and carbon fibers. An improved wear resistance can also be accrued by introducing some solid or liquid lubricants (Thostenson et al., 2001; Friedrich et al., 2005; Khun et al., 2014; Ajayan et al., 2000 and Khun et al., 2013). The remarkable properties of three-dimensional composites such as fracture toughness, resistance to impact loading and delamination tolerances differentiate the material from unidirectional fiber composites (Bonfield et al., 1976). Liquid paraffin is the commonly used liquid lubricant in polymers. The usages of liquid lubricants like paraffin in the polymer matrix upgrade the wear resistance between the rubbing surfaces during the operation. The accommodation of solid and liquid lubricants in the polymer matrix depends on the types of application. Because of the difficulty in the proper dispersion of solid lubricants in the polymer matrix liquid lubricants are also used (Khun et al., 2013 and Wan et al., 2005). Carbon fibers are the reinforcements that are widely used in epoxy matrix composites such as in carbon fiber reinforced materials like plastics, carbon-carbon composites, cement reinforced with carbon fibers due to their high specific strength and modulus (Donnet et al., 1990; Tiwari et al., 2014 and Smith et al., 1987). Pitch and PAN-based carbon fibers are broadly used in polymer composites as reinforcements due to its resistance to corrosive environment, good electrical and thermal conductivity, outstanding mechanical properties, etc. The interfacial adhesion between fiber and matrix, the volume fraction of fiber in the polymer, the application of load in the composite material with respect to fiber direction, etc. affects the overall mechanical property of the composite (Li et al., 2015). Carbon fiber reinforcements added into the epoxy matrix act as a solid lubricant during the sliding wear condition. Even though the curing process for epoxy takes enormous time, carbon fiber-epoxy composites got mass attention from researchers' side due to its light weight and simple processing techniques. Various engineering industries developed curing agents for the faster curing of epoxy matrix, to reduce the time in the processing of the composites and to save the energy (Shimamoto et al., 2014). Polymer matrix has no interface reaction

and bonding with carbon fibers since the fiber surface maintains inert atmosphere (Tiwari et al., 2014). However, the adhesion between the matrix and the fiber plays the dominant role in improving the mechanical properties of the polymer composites. The load applied to the composites is transferred and redistributed equally to the entire material through the matrix fiber interfaces. Better the bonding between the matrix and the reinforcement, better will be the strength of the composites (Zhang et al., 2004). Since carbon fibers possess weak bonding between the epoxy matrix due to the inert and smooth surface, Park and Kim reported that the oxidative and non-oxidative treatment approaches for carbon fibers helps to improve the bonding properties of the matrix and the fibers (Park et al., 2000). Hui Zhang found that the cryogenic and oxidative treatments significantly improves the surface roughness of the carbon fibers and thereby confirms the mechanical interlocking of the carbon fibers and the matrix by better adhesion (Zhang et al., 2004). Cryogenic treatment is an eco-friendly treatment that improves the strength and modulus than other treatments. Carbon fibers have been used in nuclear, aerospace industries and other engineering components such as polymer cams and gears, exhaust fan blades, etc. since the fiber composites have a low linear coefficient of thermal expansion, good thermal and electrical conductivity, high damping capacity and no corrosion to the chemical environment (Tiwari et al., 2014). Khun et al. reported that the fabrication and tribological properties of epoxy composites reinforced with varying percentages of short carbon fibers (SCFs) (Khun et al., 2013). The wear and friction coefficient comparably decreased with increase in the short carbon fiber reinforcement content due to the combined effect of the fiber and matrix in the composite and also due to the solid lubricating effect of the carbon fiber present in the composite (Khun et al., 2014). Recent studies in epoxy-carbon fiber composites improve the life time, composite performance and durability by giving thermoplastic sizing treatments in carbon fiber (Broyles et al., 1998). Studies on functionally graded carbon fiber reinforced polymer matrix are limited.

In the present work, the fabrication of epoxy-carbon fiber composite reinforced with varying percentages (0, 1, 2 and 3 vol. %) of carbon fiber by centrifugal casting and their characterization. The microstructure, mechanical properties and pin-on-disc wear test results are discussed.

7.3 Experimental Methods

7.3.1 Materials

The commercially available low temperature curing epoxy resin XY-100 of density 1.2 g/cm^3 and hardener HY 951 IN supplied by Huntsman were used. Polyacrylonitrile (PAN) based short carbon fibers of density 1.74 g/cm^3 supplied by Courtaulds of 3 mm length and 7 μm diameter were used as the reinforcements for the manufacturing of the epoxy-SCF composite by centrifugal casting.

7.3.2 Composite preparation

The composites were processed in a 600 ml capacity plastic beaker. A quantity of 340 ml of epoxy resin was taken for all the experiments. The as-received short carbon fibers were cleaned using distilled water in an ultrasonicator for 30 minutes. The epoxy resin was continuously stirred with the help of a mechanical impeller fitted to a low torque AC motor to ensure the proper mixing and wetting of the reinforcement. Carbon fibers of varying percentages (0, 1, 2 and 3 vol. %) were

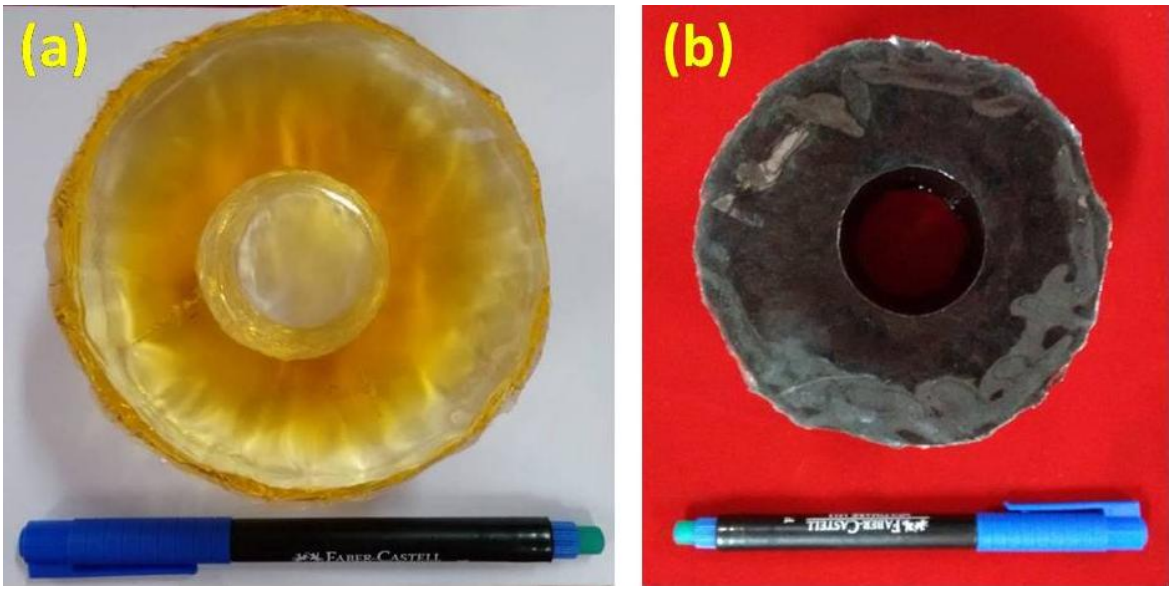

Figure 7.1 Photograph of epoxy and epoxy-SCF reinforced composite cylinder produced by centrifugal casting technique. (a) Pure epoxy and (b) epoxy- 3 vol. % SCF

manually introduced into the epoxy resin at a controlled feed rate. The epoxy resin was kept in a water bath during the addition of reinforcement while stirring, to avoid the generation of heat due to exothermic reaction in the composite slurry. After the addition of carbon fibers, 34 ml of curing agent (epoxy to hardner ratio is 10:1) was added to the composite liquid and allowed it to stir for 5 more minutes. Then, the

composite liquid was poured into a rotating cylindrical mould of diameter 100 mm and height 50 mm rotating at 1300 rpm till the composite slurry get cured. The centrifugal force at 1300 rpm is around 220 times more than that of earth's gravitational force. The photographs of the fabricated polymer cylinders and cut sections of the cylinder using epoxy and epoxy-SCF FGM composites are depicted in Figure 7.1 and 7.2 respectively.

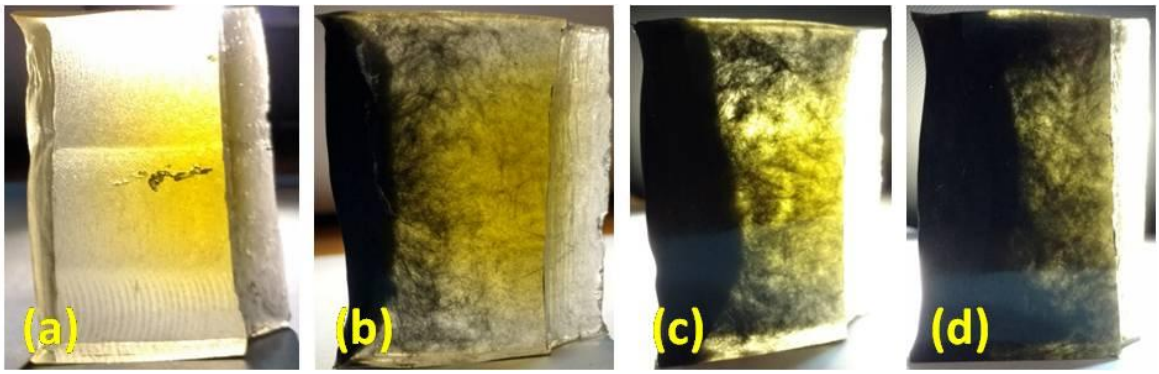

Figure 7.2. Photograph of cut section of epoxy and epoxy-SCF composite cylinder produced by centrifugal casting technique. (a) Pure epoxy (EPC0), (b) epoxy- 1 vol. % SCF (EPC1), (c) epoxy-2 vol. % SCF (EPC2) and (d) epoxy-3 vol. % SCF (EPC3)

7.3 Results and Discussion

7.3.1 Rheology

The variation of complex viscosity with time in the curing of epoxy-hardener and epoxy-hardener composite blend systems under an isothermal condition in the presence of a catalyst is shown in Figure 7.3. From the graph, it is revealed that the complex viscosity in case of blended systems is progressively increasing with time and exhibits a sudden increase in viscosity after gelation. As the percentage of the short carbon fiber reinforcements increases in the epoxy matrix, the viscosity also increases. Epoxy-hardener blend without reinforcement has the minimum value of viscosity and the maximum is obtained for the blend with 3 vol. % short carbon fiber reinforcement.

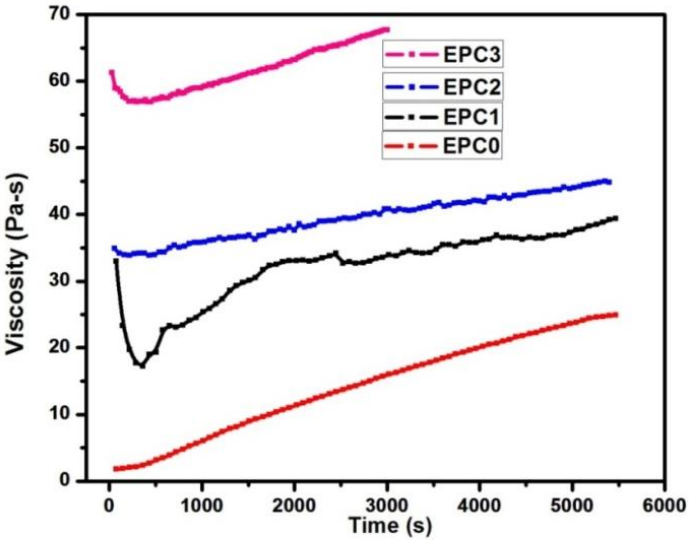

Figure 7.3 Viscosity variation in the epoxy-hardener and epoxy-hardener-SCF composite systems with time

7.3.2 Microstructural observations

The optical microstructures of the centrifugally cast functionally graded epoxy without reinforcement and epoxy-SCF composites are shown in Figure 7.4. The optical images are taken from the outer periphery to the inner periphery of the cast polymer mainly in three different regions, i.e., at the reinforcement rich region, transition region and the reinforcement depleted region. Figure 7.4a shows the optical images of centrifugal cast epoxy polymer (EPC0) cured with the hardener without any reinforcements. In this, the microstructural features are seen similar from the outer to the inner periphery in the three regions since it contains only the epoxy resin matrix which is transparent. The epoxy is more densely packed to the outer periphery due to the effect of centrifugal force and the outer region is less transparent in comparison to the inner region as shown in the photograph in Figure 7.2a. Figures 7.4b-d represents the optical micrographs of epoxy-SCF composites. The cut cross sections of the carbon fibers are clearly visible [Figure 7.2b] in the carbon fiber rich region and transition region of the epoxy-1 vol. % SCF (EPC1) reinforced functionally graded composite. The carbon fibers are accumulated towards the outer periphery of the polymer casting due to its comparatively higher density than the resin and the effect of centrifugal force. Moreover, the inner region indicates the reinforcement depleted region which contains only the epoxy resin due to the difference in the density. Due to the higher volume percentages of carbon fibers in the epoxy matrix of epoxy-2 (EPC2) and 3 vol. % SCF (EPC3) reinforced composite

[Figure 7.2c and d], the density of the carbon fibers at the reinforcement rich region is very high in the functionally graded epoxy matrix composites that when compared with epoxy-1 vol. % SCF reinforced composite. Also, a clear transition and SCF depleted regions are not completely transparent in the epoxy composites with 2 and 3 volume percentages. However, in both 2 and 3 vol. % SCF reinforced composites a transition region is observed from the optical micrographs. As the volume fraction of the SCF increases in the FGM composites, the effective fiber rich region thickness increases towards the outer periphery [Figure 7.2]. The average width of the SCF rich outer region is 6 mm, 8.5 mm and 8.75 mm for 1, 2, and 3 vol. % SCF reinforced FGM composites respectively. Figure 7.5 represents the calculated volume percentages by Archimedes principle, at the fiber rich outer regions are 58 vol. %, 63 vol. % and 69 vol. % respectively for 1, 2, and 3 vol. % SCF reinforced epoxy FGM composites.

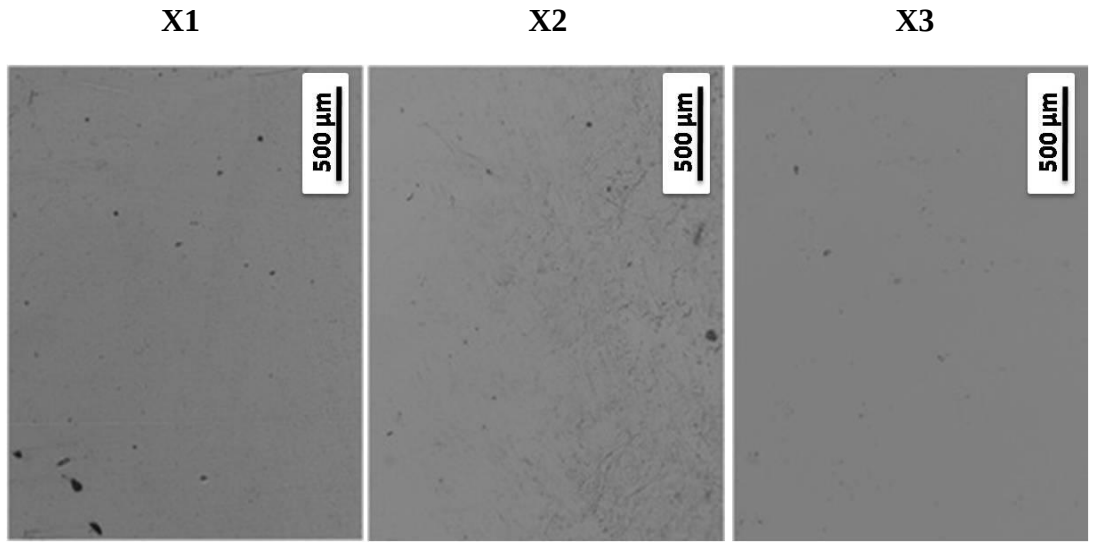

(a)

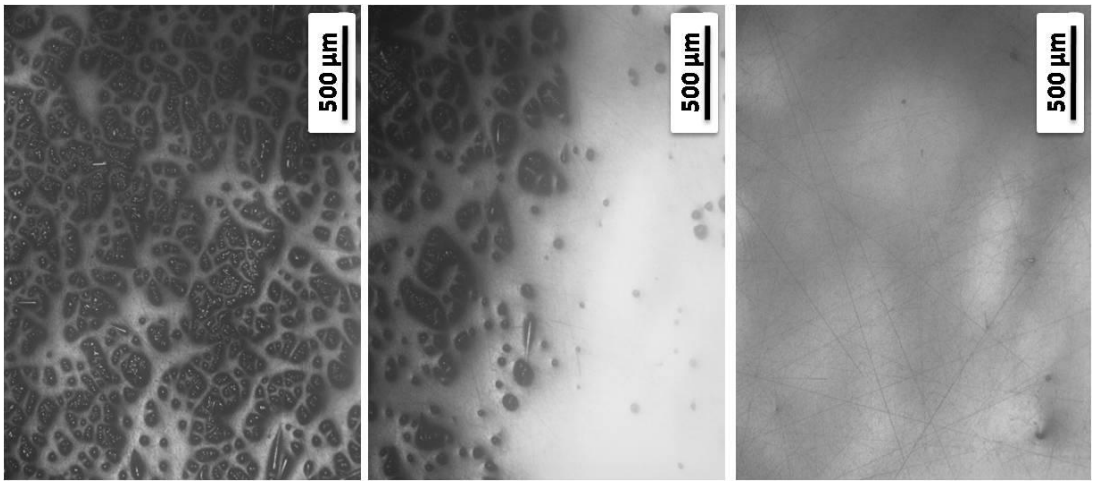

(b)

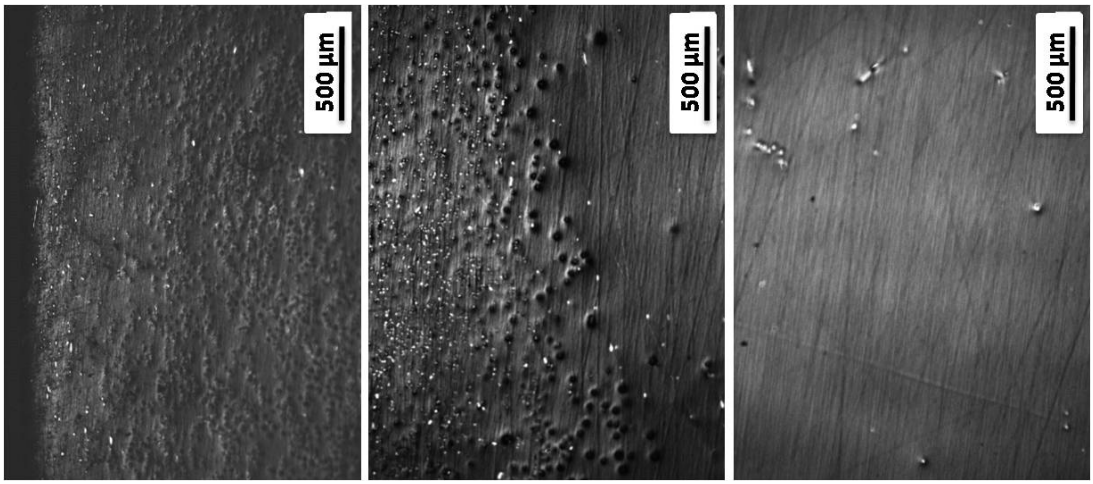

(c)

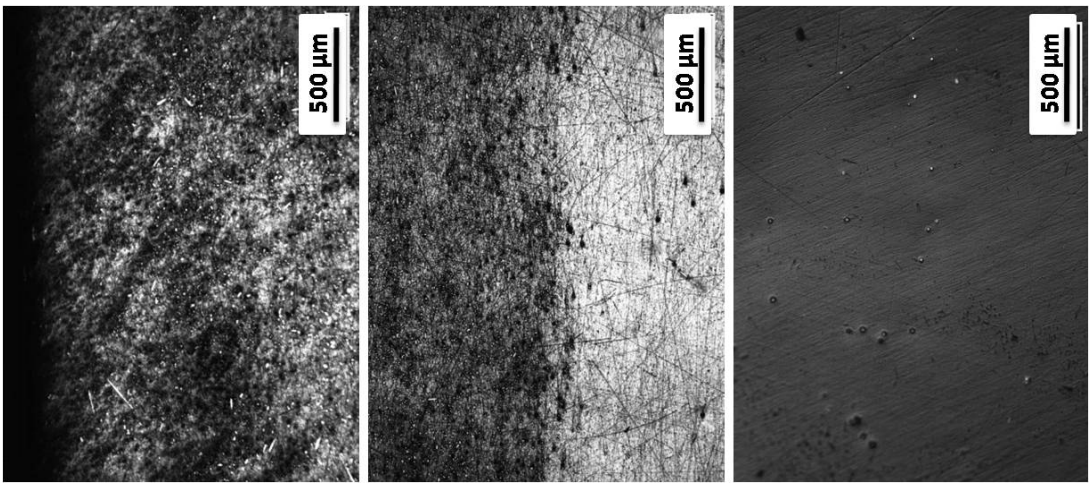

(d)

Figure 7.4 Optical micrographs of functionally graded epoxy and epoxy-FGM systems (X1 at 0.5 mm in SCF rich region, X2 at transition region and X3 at SCF depleted region from outer periphery of the centrifugal castings). (a) Epoxy base polymer, (b) epoxy-1, (c) epoxy-2 and (d) epoxy-3 vol. % SCF reinforced composites

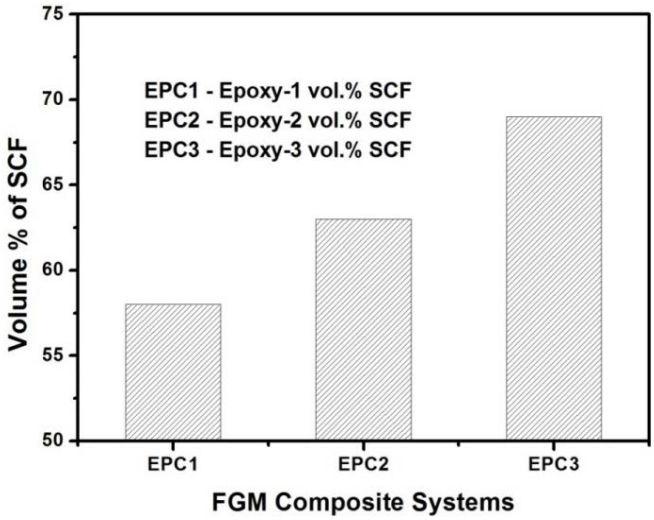

Figure 7.5 Volume percentage of SCF at outer regions of centrifugal cast FGM composites

7.3.3 Hardness

Figure 7.6 illustrates the variation in the Shore D hardness values from outer to the inner periphery of the polymer and polymer composite castings by the centrifugal casting method at 3 mm apart. Composites at outer periphery have higher hardness when compared with the subsequent regions in the pure polymer and polymer composite castings. Epoxy blended with 1 vol. % of SCF composite shows higher hardness than the other composite systems. It gives a maximum hardness of 80 Shore D at the outermost region (3 mm apart from the outer periphery) and a minimum value of Shore D 73.5 is obtained in the innermost regions. A maximum Shore D hardness value of 78.5 at 3 mm and a minimum value of 67 at 21 mm are obtained for the epoxy-composite system reinforced with 2 vol. % SCF. The epoxy-composite system reinforced with a higher volume percentage of SCF (3 vol. %) gives a hardness value of 78 and 74 at 3 mm and 6 mm respectively. However, it shows lesser values than the other systems beyond 6 mm. The cast epoxy system without SCF reinforcement gives better hardness values than the epoxy-composite system (3 vol. % SCF) after 6 mm.

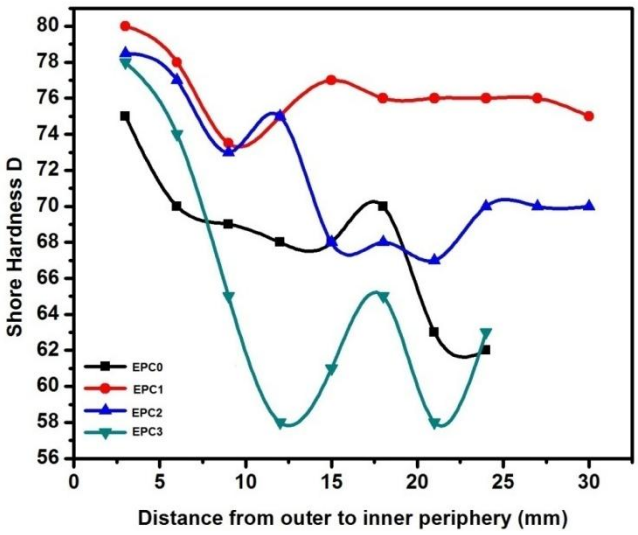

Figure 7.6 Shore D hardness values of centrifugally cast epoxy resin and epoxy composite systems from outer to inner periphery of the fabricated systems

7.3.4 Wear properties

Figures 7.7a-c represents the specific wear rate values of outer and inner specimens of the cast epoxy, epoxy-2 vol. % SCF and epoxy-3 vol. % SCF systems. The wear specimens are taken from the outer carbon fiber enriched zone and the inner fiber depleted zone. The outer pin of the epoxy cast without reinforcement [Figure 7.7a] shows similar wear resistance compared to the inner pin at the lower loads of 9.81 N and 19.62 N. But at higher loads, the wear resistance is more for inner pins. This resistance is due to the resin and the hardener distribution during the centrifugal casting of the component. Figure 7.7b is the specific wear rate curves of outer and inner specimens of epoxy-2 vol. % SCF reinforced composite. The outer pin shows better wear resistance than the inner pin since the outer pin specimen is enriched with reinforced short carbon fibers. The outer pin gives a minimum specific wear rate value of 2.7155 X 10^{-5} mm^3/Nm at 39.24 N compared to 231.1528 X 10^{-5} mm^3/Nm for the pin in the inner region. Figure 7.7c indicates the specific wear rate of outer and inner pin material reinforced with the higher volume percentage (epoxy-3 vol. % SCF). The outer pin specimen has the higher wear resistance than the inner pin specimen in all the loads which gives lower wear value at 7.93 X 10^{-5} mm^3/Nm at higher load of 39.24 N. The outer pin specimens always gives better wear resistance than the inner pin specimens in functionally graded composites due to the solid lubricating effect of carbon fibers during dry sliding.

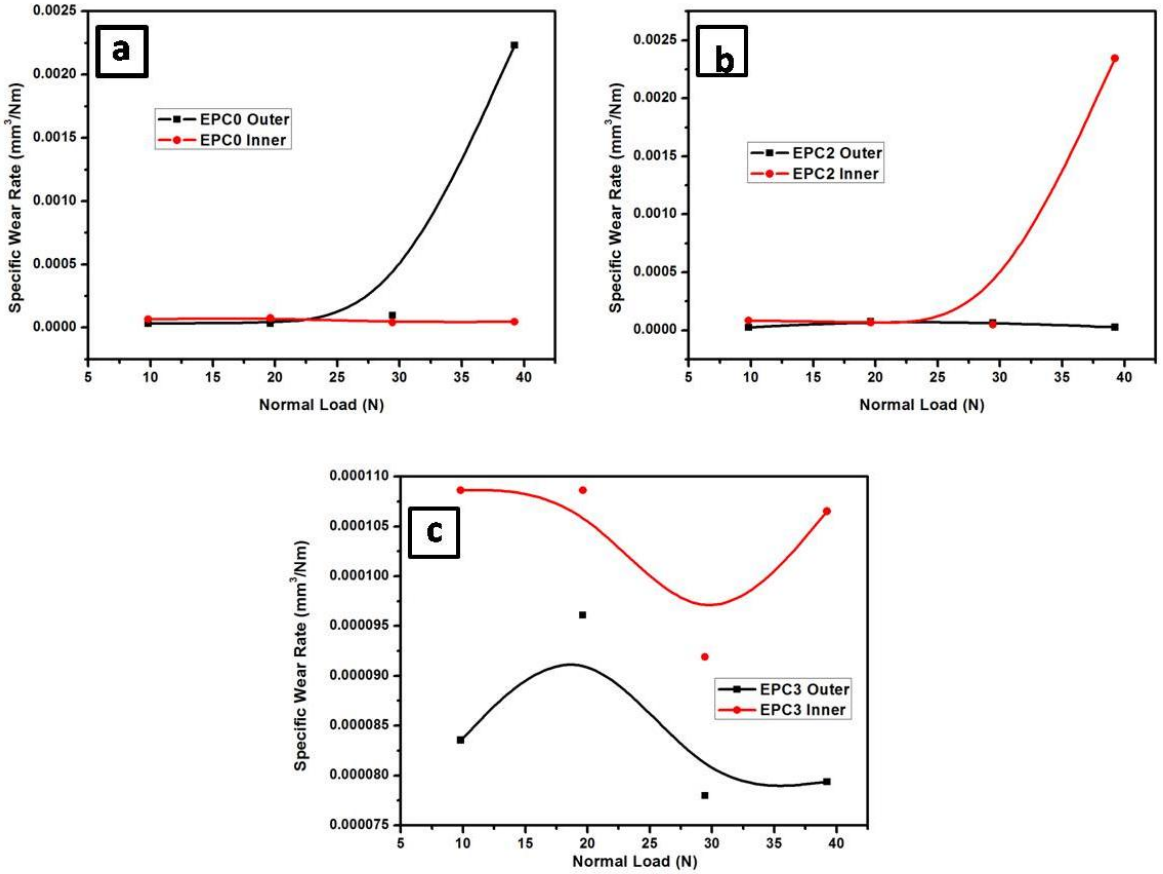

Figure 7.7 Wear rate values of outer and inner pins of epoxy systems with and without SCF reinforcement (a) epoxy-0 vol. % SCF, (b)epoxy-2 vol. % SCF and (c) epoxy-3 vol. % SCF

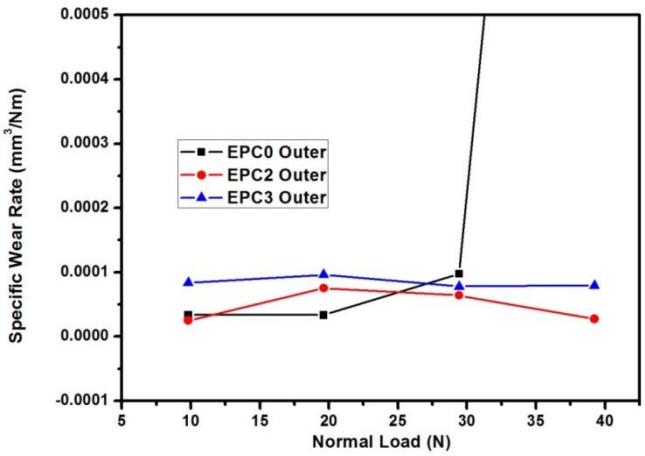

Figure 7.8 Wear rate values of outer pins of centrifugally cast epoxy, epoxy-2 vol. % SCF and epoxy-3 vol. % SCF

Figure 7.8 shows the specific wear rate of outer pins of epoxy, epoxy-2 vol. % SCF and epoxy-3 vol. % SCF functionally graded composites. The graph reveals that the epoxy specimens without reinforcements have good wear resistance than the

composite reinforced with short carbon fibers at lower loads but, at higher loads, the specimens undergoes severe wear and leads to breakage. The epoxy-2 vol. % SCF shows better wear resistance than the composite reinforced with 3 vol. % at all the loads, which also reflects in lower hardness for 3 vol. % SCF FGM.

7.3.5 Worn surface analysis

Figure 7.9 shows the stereo macro photographs of outer and inner wear pin specimens of the cast polymer systems at a load of 19.62 N and 39.24 N. Tribological phenomenon involves the interaction between the specimen to be tested and the counter surface. Figure 7.9a exhibits the stereo macrographs of worn surface of centrifugally cast epoxy without reinforcement. From the figure, it is clearly seen the wear scars at 19.62 N and 39.24 N in the inner region. At the load of 19.62 N the pin surface shows fine wear scars, but at a maximum load of 39.24 N, wide and deep wear scars are visible because the material is fully thrown out and undergoes excessive wear at this load. It is observed that for the outer pin, at a load of 39.24 N much higher wear takes place in comparison to that of 19.62 N. At 39.24 N the removal of material is more and the pin specimen undergoes bending and a part of the pin gets sheared off and cause excessive wear due to the absence of reinforcements. But at lower loads, the outer pins shows better wear resistance than the inner pins as indicated in the specific wear rate graph. In the case of epoxy-2 vol. % SCF composite specimens [Figure 7.9b] the surface of the outer pin is not much affected by a lower load of 19.62 N because the wear scars are fine when compared with a load of 39.24 N. And at the higher load the inner specimen get fractured and ultimately breaks. Stereo micrographs of worn surfaces of epoxy-3 vol. % SCF composites reveal that the outer specimens have only a smooth surface at lower and higher loads. The wear scars are not clearly visible in this case. However, for the inner specimens wear scars are clearly seen as in the previous cases. From the stereo micrographs, the epoxy-SCF system with 2 vol. % SCF exhibits good wear resistance than the other functionally graded composite and the polymer system. The lubrication effect of the incorporated carbon fibers in the epoxy matrix is clearly evident from the stereo micrograph of the composite reinforced with 2 vol. % SCF.

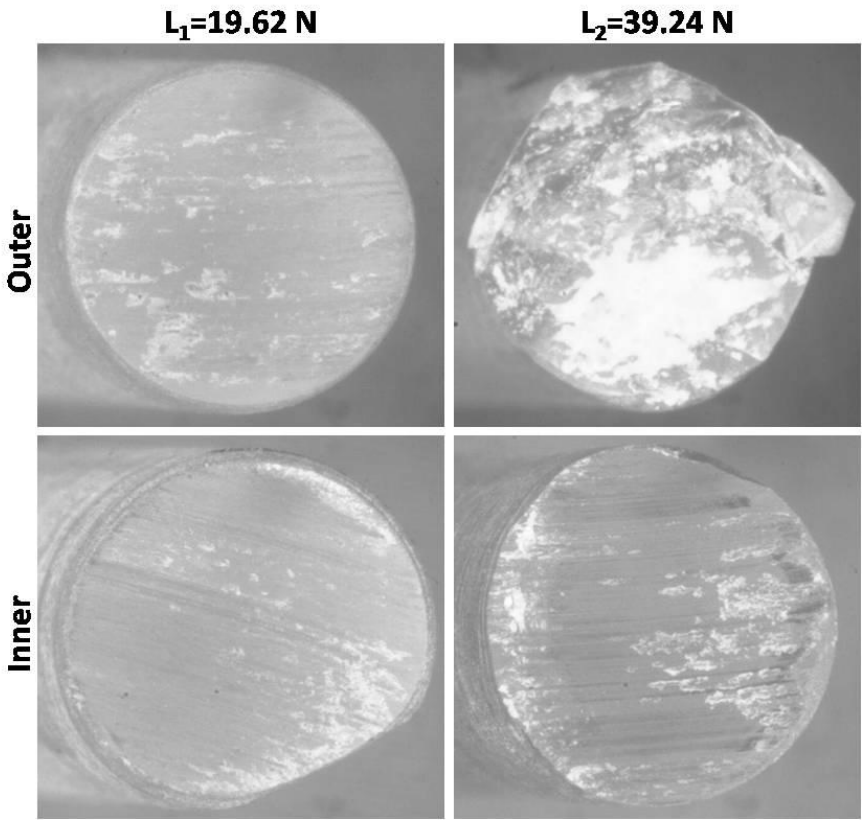

(a)

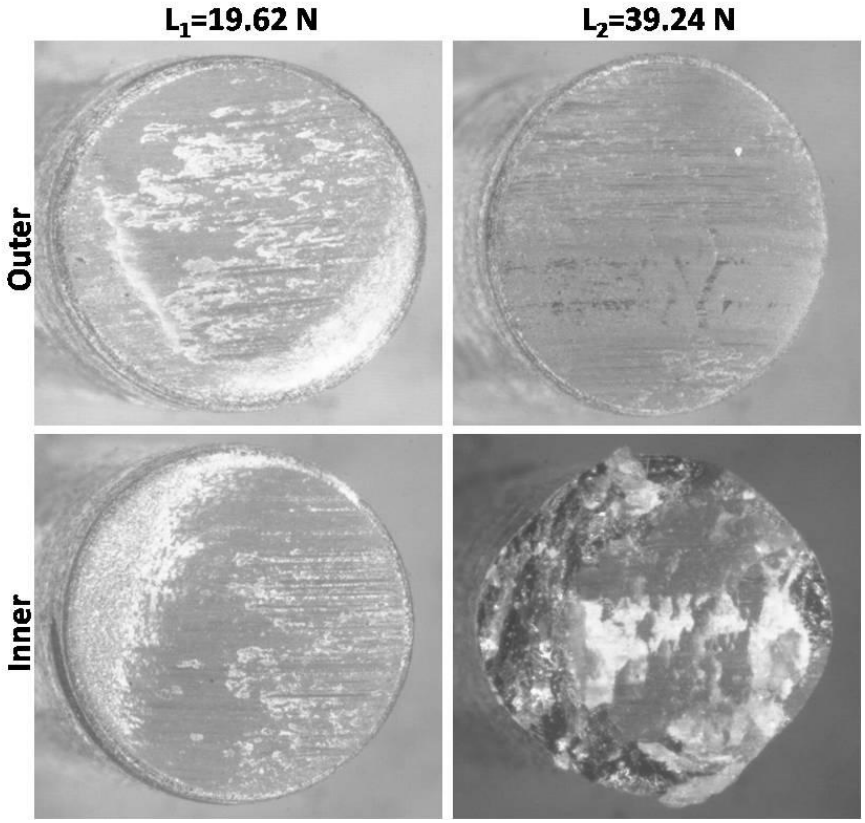

(b)

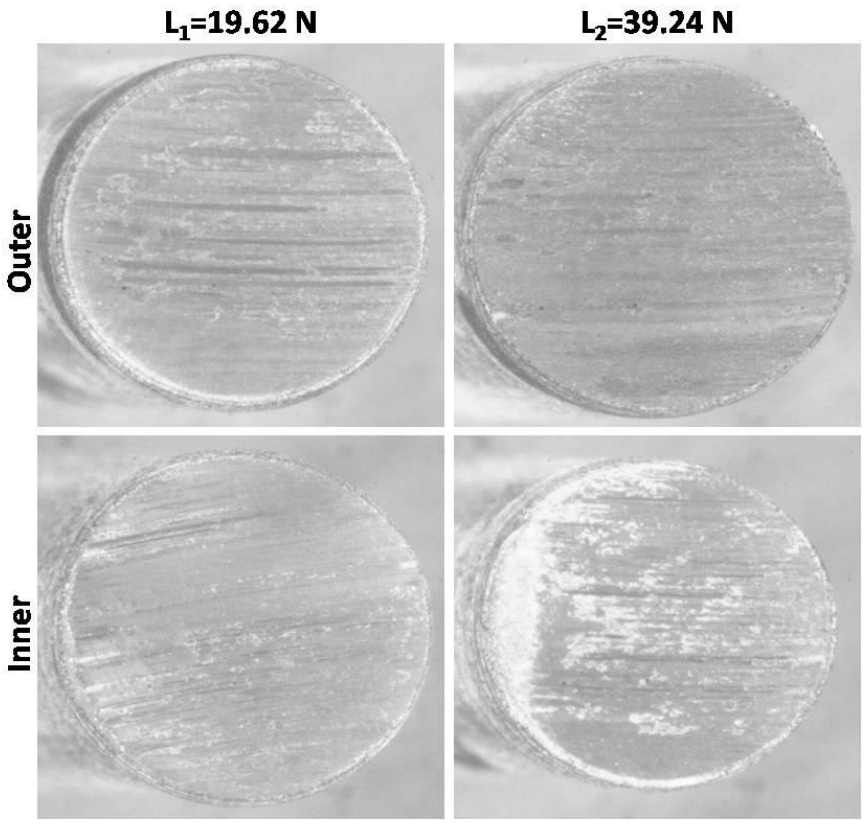

(c)

Figure 7.9 Stereo micrographs of worn surface of outer and inner pins - centrifugal cast (a) pure epoxy, (b) epoxy-2 vol. % SCF and (c) epoxy-3 vol. % SCF (L_1 at 19.62 N and L_2 at 39.24 N)

SEM analysis carried out on the worn surfaces of the pure epoxy, epoxy-2 vol. % SCF and epoxy-3 vol. % SCF composites at 19.62 N and 39.24 N are depicted in Figure 7.10 and 7.11 respectively. Adhesion, abrasion and fatigue were the dominant mechanisms found in the polymer materials. The frictional coefficient is understood by the type of the wear mechanism involved during sliding. In this pin-on-disc wear testing process, adhesive type of wear mechanism is revealed from the SEM images by which the mechanism involves the creation of adhesive bonds, their growth and breaking of the created bonds when the material transfer is taking place between the rubbing surfaces. In polymer composites, no material transfer takes place between the mating surfaces since the lubricating effect of the carbon fibers incorporated in the epoxy that act as a solid lubricant during the rubbing. For pure polymers or fiber depleted region, abrasive wear is particularly interesting. Abrasive wear occurs due to the cutting and ploughing of the surface by harder particles or asperities present on the counter surface. The wear scars in the epoxy sample are small when compared

with the scars on 3vol. % reinforced SCF for the outer specimens because of the agglomeration of SCF in the polymer composite since it acts as a solid lubricant. For the same sample, higher magnification clearly explains the surface corrugations. The outer surface of the epoxy sample is much better and smoother than the surface of the composite with 3 vol. % SCF reinforcement. However, the wear scar of 2 vol. % SCF reinforced composite is finer than the other two systems because the reinforcement is within the particular limit in the epoxy matrix that is already reported by the earlier researchers in terms of hardness (Khun et al., 2014). The higher magnification of the inner sample shows some corrugations over the surface with negligible surface irregularity. The surfaces of the samples with reinforcement exhibit a large number of laminar planes detached from the sample surface due to the poor wear resistance since the concentration of the carbon fiber at the inner region is negligible when compared to the outer region of the centrifugal cast samples. Even though the percentage of the reinforcement increases from 0 to 3 vol. % SCF, the same laminar planes were observed in the case of inner samples because the inner region of all the samples with various volume percentages, only having nearly 0 vol. % SCF in this region. The outer pin SEM images of worn surfaces of epoxy without reinforcement is smoother when compared with 3 vol. % SCF reinforcement, but the wear is more in without reinforcement since it does not have any reinforcement and lubricating effect. The FGM system with 3 vol. % SCF exhibits a higher surface irregularity when compared with 2 vol. % SCF and without reinforcement. However, we can see that the surface of FGM system with 2 vol. % SCF is only having less surface irregularity when compared with other surfaces of the FGM systems. And it is also important to note that wear is usually not the result of a single mechanism but a combination of different mechanisms.

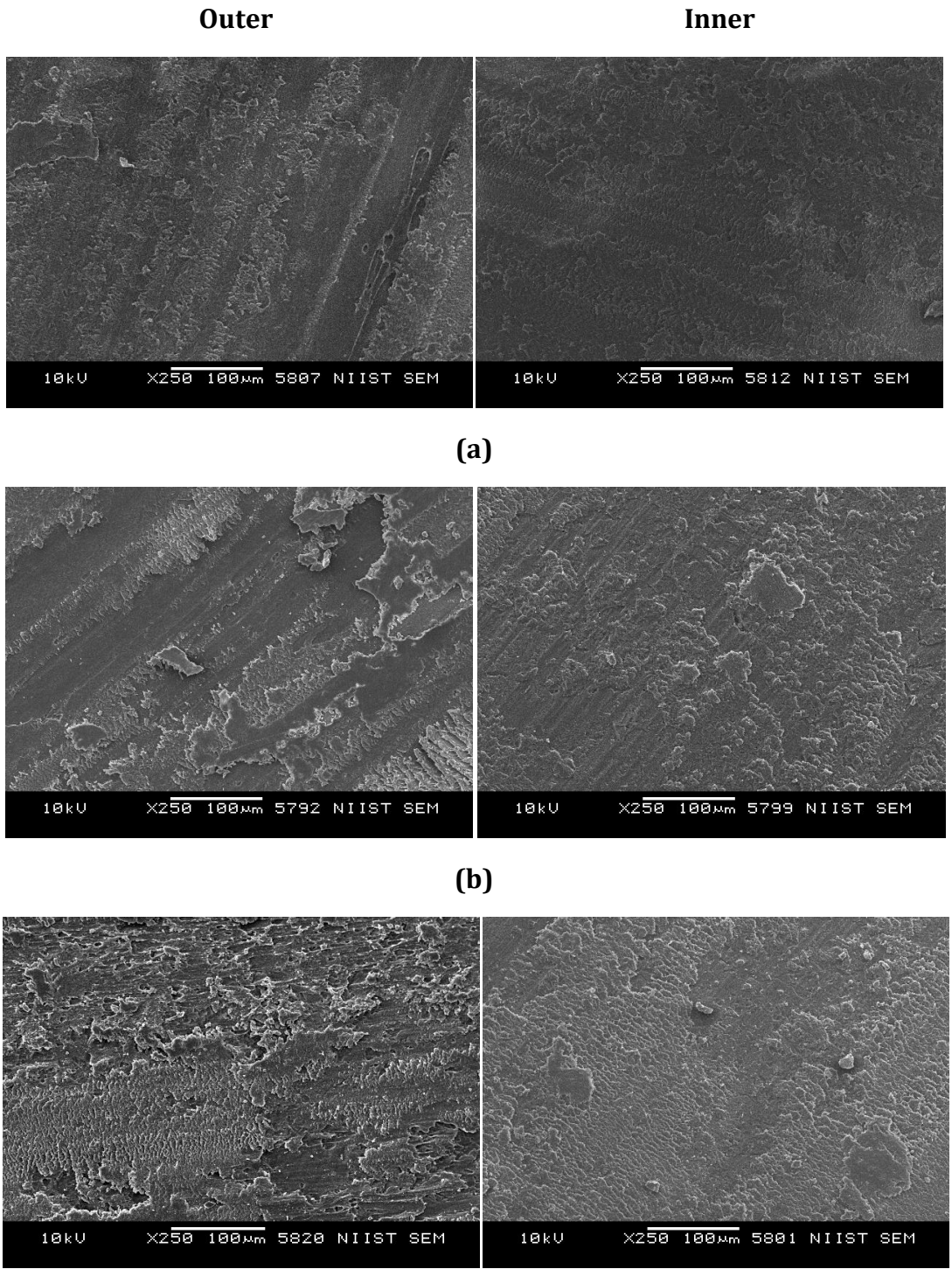

Figure 7.10 SEM images of worn surfaces of outer and inner pins at a normal load of 19.62N (a) pure epoxy, (b) epoxy-2 vol. % SCF and (c) epoxy-3 vol. % SCF reinforced composites

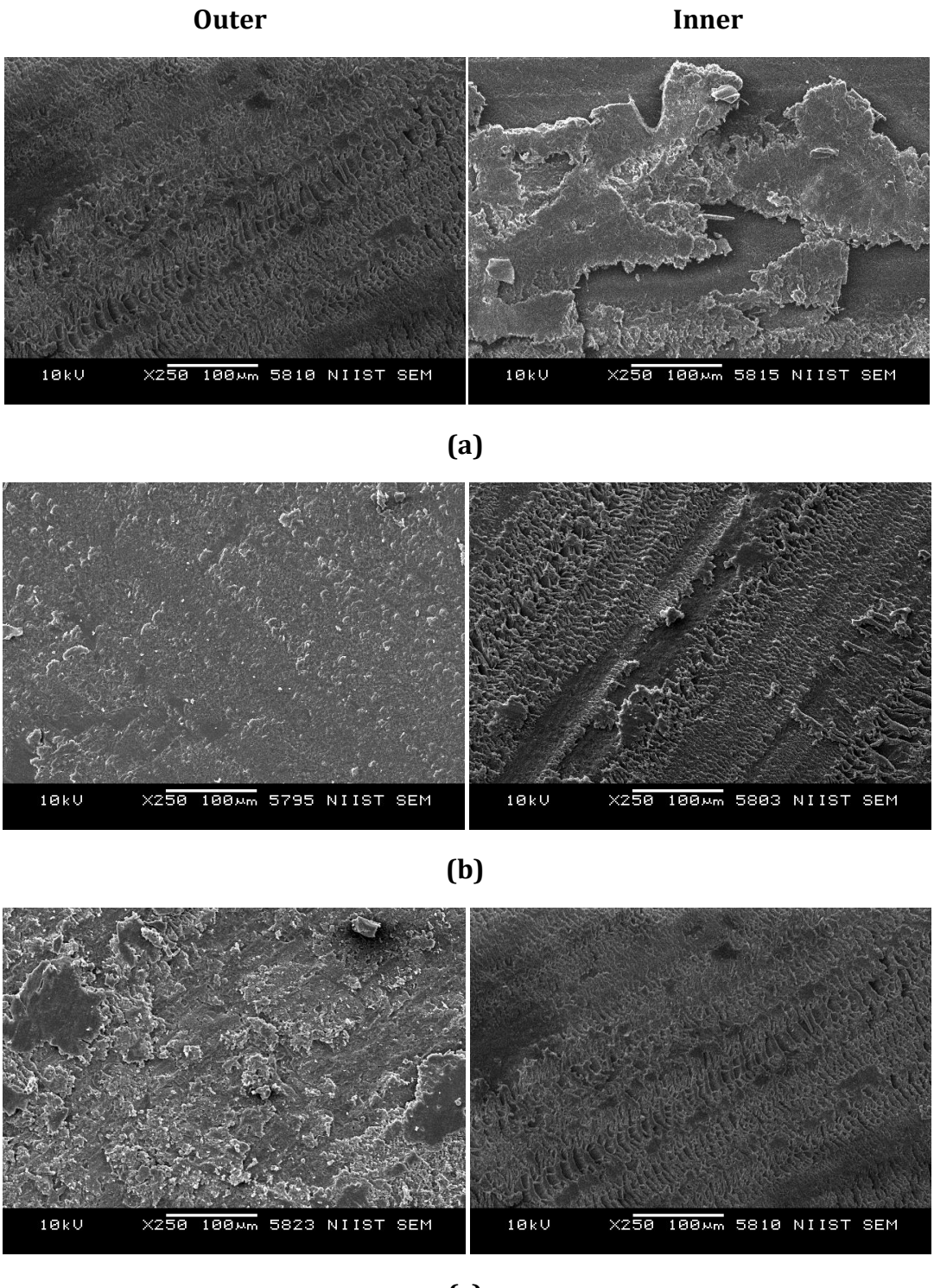

Figure 7.11 SEM images of worn surfaces of outer and inner pins at a normal load of 39.24N (a) pure epoxy, (b) epoxy-2 vol. % SCF and (c) epoxy-3 vol. % SCF reinforced composite

7.4 Conclusions

Centrifugal casting has been successfully used to fabricate short carbon fiber reinforced epoxy functionally graded composites. FGM formed by centrifugal casting shows an apparent variation in concentration of short carbon fibers due to centrifugal force, from the inner to the outer periphery of the casting.

- Rheological studies show that the viscosity increases as the volume percentage of SCF increases. The maximum viscosity is found for epoxy with 3 vol. % and the minimum is for pure polymer.
- Microstructural features of the FGM notably exhibit a clear variation of three regions namely matrix rich region, fiber rich region and transition region.
- The hardness of centrifugal cast pure epoxy is comparatively lower than that of the epoxy centrifugal cast with 1 vol. % SCF reinforcement. Hardness value is maximum for the outer periphery of epoxy polymer cast with 1 vol. % SCF reinforcement. As the volume percentage of SCF increases the value of hardness found to be decreased in the outer region of the centrifugal cast product.
- The addition of short carbon fibers to the epoxy matrix under the action of centrifugal force result in the creation of FGM with excellent wear resistant properties to the outer periphery due to self lubricating behaviour up to a particular volume percentage of SCF. Wear resistance is maximum in case of the specimen taken from the outer periphery of the epoxy-2 vol. % SCF composite system at a maximum load of 39.24 N. Wear resistance increases as the volume percentage of SCF increase up to a particular limit of reinforcement.
- Surface morphology analysis of worn out samples was also done and the major wear mechanism is abrasive type in pure epoxy and adhesive in polymer composites.

CHAPTER 8

Summary and Scope of Future Investigation

8.1 Summary

The present investigation on fabrication and characterization of functionally graded metal and polymer composites has accomplished the application by sequential and centrifugal casting techniques, by tailoring the location specific material properties using aluminium as the metal and the epoxy as the polymer matrix for the production of functionally graded materials and components. A new method of casting technique called 'sequential casting' was introduced for the production of bimetallic aluminium alloys. The fabrication of the composites with aluminium alloy was achieved by both in-situ and ex-situ particle methods. The in-situ functionally graded composites for automotive cylinder liner applications are fabricated by the centrifugal casting technique using hypereutectic aluminium alloy by generating primary silicon particles segregated to the inner most region of the cast cylinder. A precursor of functionally graded turbine exit vane guide was fabricated successfully by ex-situ centrifugal casting without any axial symmetry in the mould and component using SiC particles as the reinforcements in aluminium alloy, shows enhanced properties especially at the thinner sections which are difficult to process through other casting techniques. Also, functionally graded epoxy composites were fabricated by dispersing the short carbon fibers (SCFs) as reinforcement, gives an enhanced hardness and wear properties towards the outer diameter of the cast cylinder.

The major conclusions drawn from the present investigation are summarised as follows:

Sequential cast bimetallic Al FGMs

- A390-A319 and A390-A6061 functionally graded bimetallic aluminium alloys were successfully fabricated by sequential gravity casting technique.

- Two entirely different types of properties were attained in a single cast component with enhanced interfacial bonding between the alloys.

- A maximum hardness of 160 BHN is obtained at the A390 region in both sequential gravity cast alloy systems (A390–A319 and A390–A6061), and a minimum hardness of 105 BHN and 91 BHN are also obtained at the A319 and A6061 alloy regions in the respective systems at the heat-treated samples.

- The sequential cast materials provide improved tensile and compressive strength compared to parent materials. The A390–A319 sequential cast system has a tensile strength of 337 MPa and a compressive strength of 490 MPa, whereas A390–A6061 sequential cast system shows 364 MPa and 401 MPa, respectively. The tensile strengths of bimetallic alloys are higher than the standard values of the individual base alloys in the respective systems.

- The wear study performed at the two different regions of the both sequential cast system shows a gradient performance within the same sequential cast bimetallic component.

Centrifugally cast Mg, Sr and Zr added in-situ A390 Al FGMs

- The segregation of in-situ generated low density primary Si phases towards the inner periphery of cast cylinder and disc by centrifugal casting technique are observed in A390 alloy systems with Mg, Sr and Zr modifiers.

- The individual addition of varying percentages of Mg, Sr and Zr in centrifugal cast A390 alloy cylinders shows maximum hardness in A390-1.5 wt. % Mg and A390-0.03 wt. % Sr/Zr.

- The combined addition of 1.5 wt. % Mg and 0.03 wt. % Sr in A390 hypereutectic aluminium alloy provides a maximum hardness of 158 BHN at the inner periphery of the cast disc. The individual addition of Zr and combined addition of Mg and Zr shows a decrease in the hardness values even in the presence of primary silicon particles towards the inner periphery due to segregation of dense Al-Zr phases to the outer periphery.

- The maximum tensile strength of 295 N/mm^2 is obtained at the outer periphery and 264 N/mm^2 is obtained at the inner specimen of the A390-0.03 wt. % Zr centrifugal cast disc.

- In general, a higher wear resistance is obtained at the inner periphery of the cast discs. Nevertheless, the transition region specimens also shows enhanced wear resistance than the inner regions of the A390-1.5 wt. % Mg-0.03 wt. % Sr aluminium alloy system because of the micro porosities present in the inner most periphery. The middle region specimens of all the alloys systems show an adhesive and oxidative type of wear due to the coarse grain size of the aluminium phases attained at this middle region, while the inner periphery shows an abrasive type wear due to the presence of hard, brittle primary silicon phases.

Centrifugal cast turbine exit vane guide using SiC reinforced A2219 Al FGMs

- Turbine exit vane guide was successfully designed and fabricated using A2219 based SiC of 14 and 23 μm average particle size (APS) reinforced functionally graded metal matrix composites (FGMMCs), especially with thinner trailing edge sections by centrifugal casting without any axial symmetry which is normally difficult to process through gravity casting method.

- The leading edges of exit vane guide provide higher hardness and wear resistance due to increased graded particle concentration. The increase in the hardness magnitude at the leading edge will help the edge to protect the region from high erosive wear.

- The tensile strength of the A2219-SiC FGM is higher towards the interior region of the turbine exit vane guide. The exit vane guide with fine SiC reinforcement particle of 14 μm provides an enhanced hardness and thereby improves the wear resistance.

SCF reinforced epoxy composite FGMs

- Short carbon fiber (SCF) dispersed epoxy functionally graded composites has been successfully developed by centrifugal casting technique.

- Rheological studies on the composite slurry with varying volume percentage of SCF show that the viscosity increases as the volume percentage of SCF increases. The maximum viscosity is obtained for epoxy with 3 vol. % and the minimum is for the pure polymer.

- The hardness values are higher for the epoxy polymer centrifugal cast FGM with 1 vol. % SCF reinforcement. Further, increase in the volume percentage of SCF in epoxy reduced the hardness. An enhanced wear resistance at the fibre rich region is achieved due to the self lubricating behaviour of the SCFs. The wear resistance is maximum for the specimen from the outer periphery of the epoxy-2 vol. % SCF composite system.

8.2 Scope of Future Investigation

The sequential casting is comparatively a new method of casting for the production of functionally graded components. Since the casting process involves only simple technique and the non requirement of any special equipment are the main advantages of the sequential casting process. The centrifugal castings also have many advantages such as good quality castings can be produced in terms of surface finish with close dimensional accuracy, tolerances and reduced gas porosities.

The present investigation can be further extended to,

- Sequential gravity casting of alloy and composite combination with graded properties. Sequential centrifugal and squeeze casting of FGMs using alloys and composites can also be explored.

- Modification of hypereutectic aluminium alloys using phosphorous master alloys for the modification of primary silicon phases for centrifugal cast cylinder liner applications.

- Change in the design aspects of the exit vane guide with complicated profiles.

- Effect of different fibre lengths of SCF on dispersion, distribution and orientation in metal and polymer matrix by centrifugal casting technique.

References

Abramov, V. O., Abramov, O. V., Straumal, B. B., & Gust, W. (1997). Hypereutectic Al-Si based alloys with a thixotropic microstructure produced by ultrasonic treatment. *Materials & Design*, *18*(4), 323-326.

Adachi, M. (1984). Modification of Hypereutectic Al--Si System Casting Alloys. *J. Jpn. Inst. Light Met.*, *34*(7), 430-436.

Ajayan, P. M., Schadler, L. S., Giannaris, C., & Rubio, A. (2000). Single-walled carbon nanotube–polymer composites: strength and weakness. *Advanced materials*, *12*(10), 750-753.

Akbari-Mousavi, S. A. A., Barrett, L. M., & Al-Hassani, S. T. S. (2008). Explosive welding of metal plates. *Journal of materials processing technology*, *202*(1), 224-239.

Akhil S. Karun, Rajan, T. P. D., Pillai, U. T. S., Pai, B. C., Rajeev, V. R., & Farook, A. (2016). Enhancement in tribological behaviour of functionally graded SiC reinforced aluminium composites by centrifugal casting. *Journal of Composite Materials*, *50*(16), 2255-2269.

Alshmri, F., Atkinson, H. V., Hainsworth, S. V., Haidon, C., & Lawes, S. D. A. (2014). Dry sliding wear of aluminium-high silicon hypereutectic alloys. *Wear*, *313*(1), 106-116.

Apelian, D., Shivkumar, S., & Sigworth, G. A. F. S. (1989). Fundamental aspects of heat treatment of cast Al-Si-Mg alloys. *AFS transactions*, *97*, 727-742.

Asensio-Lozano, J., & Suarez-Peña, B. (2006). Effect of the addition of refiners and/or modifiers on the microstructure of die cast Al–12Si alloys. *Scripta materialia*, *54*(5), 943-947.

B.A. Srinivasan. (2006) Dissertation, CSIR-National Institute for Interdisciplinary Science and Technology, Trivandrum, India.

Babu, P. E., Rajan, T. P. D., Savithri, S., Pillai, U. T. S., & Pai, B. C. (2004). Theoretical Analysis and Computer Simulation of the Particle Gradient Distribution in a Centrifugally Cast Functionally Gradient Material. *parameters*, *4*, 6.

Banerjee, D., Lao, J. Y., Wang, D. Z., Huang, J. Y., Ren, Z. F., Steeves, D., Kimball, B. & Sennett, M. (2003). Large-quantity free-standing ZnO nanowires. *Applied Physics Letters*, *83*(10), 2061-2063.

Banerji, A., Rohatgi, P. K., & Reif, W. (1984). Role of wettability in the preparation of metal-matrix composites(a review). *Metall*, *38*(7), 656-661.

Bates, A. P. (1960). Hypereutectic Aluminum-Silicon Alloys: A Review of Published Information. *Metallurgia*, *61*(364), 70-79.

Benedyk, J. C. (2006). Novelis Fusion™ Process: Breakthrough in the Simultaneous DC Casting of Multiple Al Alloy Layers for Rolling Ingot. *Light Metal Age-Chicago-*, *64*(4), 48.

Bever, M. B., & Duwez, P. E. (1972). Gradients in composite materials. *Materials Science and Engineering*, *10*, 1-8.

Boileau, J. M., & Allison, J. E. (2003). The effect of solidification time and heat treatment on the fatigue properties of a cast 319 aluminum alloy. *Metallurgical and materials transactions A*, *34*(9), 1807-1820.

Bonfield, W. B. C. A. J. J. R., Edwards, B. C., Markham, A. J., & White, J. R. (1976). Wear transfer films formed by carbon fibre reinforced epoxy resin sliding on stainless steel. *Wear*, *37*(1), 113-121.

Brook, R. J. (1996). Materials Science and Technology, Volume 17B, Processing of Ceramics Part II. *Masters Thesis*, *17*, 379.

Broyles, N. S., Verghese, K. N. E., Davis, S. V., Li, H., Davis, R. M., Lesko, J. J., & Riffle, J. S. (1998). Fatigue performance of carbon fibre/vinyl ester composites: the effect of two dissimilar polymeric sizing agents. *Polymer*, *39*(15), 3417-3424.

Caceres, C. H., Svensson, I. L., & Taylor, J. A. (2003). Strength-ductility behaviour of Al-Si-Cu-Mg casting alloys in T6 temper. *International Journal of Cast Metals Research*, *15*(5), 531-543.

Chandrashekharaiah, T. M., & Kori, S. A. (2009). Effect of grain refinement and modification on the dry sliding wear behaviour of eutectic Al–Si alloys. *Tribology international*, *42*(1), 59-65.

Chang, J. (2001). Crystal morphology of eutectic Si in rare earth modified Al-7wt% Si alloy. *Journal of materials science letters*, *20*(14), 1305-1307.

Chang, J., Moon, I., & Choi, C. (1998). Refinement of cast microstructure of hypereutectic Al-Si alloys through the addition of rare earth metals. *Journal of materials science*, *33*(20), 5015-5023.

Chatterjee, A., & Gillespie, J. W. (2010). Room temperature-curable VARTM epoxy resins: Promising alternative to vinyl ester resins. *Journal of applied polymer science*, *115*(2), 665-673.

Chen, C. M., Yang, C. C., & Chao, C. G. (2005). A novel method for net-shape forming of hypereutectic Al–Si alloys by thixocasting with powder preforms. *Journal of Materials Processing Technology*, *167*(1), 103-109.

Chen, Z. K., Yang, J. P., Ni, Q. Q., Fu, S. Y., & Huang, Y. G. (2009). Reinforcement of epoxy resins with multi-walled carbon nanotubes for enhancing cryogenic mechanical properties. *Polymer*, *50*(19), 4753-4759.

Cheng, G. S., Zhang, L. D., Chen, S. H., Li, Y., Li, L., Zhu, X. G., ... & Mao, Y. Q. (2000). Ordered nanostructure of single-crystalline GaN nanowires in a honeycomb structure of anodic alumina. *Journal of Materials Research*, *15*(02), 347-350.

Chirita, G., Soares, D., & Silva, F. S. (2008). Advantages of the centrifugal casting technique for the production of structural components with Al–Si alloys. *Materials & Design*, *29*(1), 20-27.

Chirita, G., Stefanescu, I., Barbosa, J., Puga, H., Soares, D., & Silva, F. S. (2009). On assessment of processing variables in vertical centrifugal casting technique. *International Journal of Cast Metals Research*, *22*(5), 382-389.

Choi, H., Konishi, H., & Li, X. (2012). Al_2O_3 nanoparticles induced simultaneous refinement and modification of primary and eutectic Si particles in hypereutectic Al–20Si alloy. *Materials Science and Engineering: A*, *541*, 159-165.

Clarke, J., & Sarkar, A. D. (1979). Wear characteristics of as-cast binary aluminium-silicon alloys. *Wear*, *54*(1), 7-16.

Clyne, T. W. (2001). Metal matrix composites: matrices and processing. *Encyclopaedia of Materials: Science and Technology*, 1.

Corrochano, J., Walker, J. C., Lieblich, M., Ibáñez, J., & Rainforth, W. M. (2011). Dry sliding wear behaviour of powder metallurgy Al–Mg–Si alloy-$MoSi_2$ composites and the relationship with the microstructure. *Wear*, *270*(9), 658-665.

Cree, D., & Pugh, M. (2011). Dry wear and friction properties of an A356/SiC foam interpenetrating phase composite. *Wear*, *272*(1), 88-96.

Crosley, Phillip Bernard, and L. F. Mondolfo. *Modification of aluminum-silicon-alloys*. Diss. Illinois Institute of Technology, 1966.

Cruz, K. S., Meza, E. S., Fernandes, F. A., Quaresma, J. M., Casteletti, L. C., & Garcia, A. (2010). Dendritic arm spacing affecting mechanical properties and wear behavior of Al-Sn and Al-Si alloys directionally solidified under unsteady-state conditions. *Metallurgical and Materials Transactions A*, *41*(4), 972-984.

Cui, C., Schulz, A., Schimanski, K., & Zoch, H. W. (2009). Spray forming of hypereutectic Al–Si alloys. *Journal of Materials Processing Technology*, *209*(11), 5220-5228.

Das, S. K. (1994). Al-rich intermetallics in aluminum alloys. *Intermetallic compounds*, *2*, 175-198.

Dezellus, O., Milani, L., Bosselet, F., Sacerdote-Peronnet, M., Rouby, D., & Viala, J. C. (2008). Mechanical testing of titanium/aluminium–silicon interfaces by push-out. *Journal of Materials Science*, *43*(6), 1749-1756.

Diouf, P., & Jones, A. (2010). Investigation of bond strength in centrifugal lining of babbitt on cast iron. *Metallurgical and Materials Transactions A*, *41*(3), 603-609.

Divandari, M., & Golpayegani, A. V. (2009). Study of Al/Cu rich phases formed in A356 alloy by inserting Cu wire in pattern in LFC process. *Materials & Design*, *30*(8), 3279-3285.

Donnet, J. B., Bansal, R. C., & Wang, M. J. (1990). CFs.

Duque, N. B., Melgarejo, Z. H., & Suárez, O. M. (2005). Functionally graded aluminum matrix composites produced by centrifugal casting. *Materials Characterization*, *55*(2), 167-171.

Edalati, K., Ashida, M., Horita, Z., Matsui, T., & Kato, H. (2014). Wear resistance and tribological features of pure aluminum and Al–Al_2O_3 composites consolidated by high-pressure torsion. *Wear*, *310*(1), 83-89.

Eizadjou, M., Manesh, H. D., & Janghorban, K. (2008). Investigation of roll bonding between aluminum alloy strips. *Materials & Design*, *29*(4), 909-913.

El-Hadad, S., Sato, H., Miura-Fujiwara, E., & Watanabe, Y. (2010). Fabrication of Al-Al_3Ti/Ti_3Al functionally graded materials under a centrifugal force. *Materials*, *3*(9), 4639-4656.

El-Sayed, A. A., El-Sherbiny, M. G., Abo-El-Ezz, A. S., & Aggag, G. A. (1995). Friction and wear properties of polymeric composite materials for bearing applications. *Wear*, *184*(1), 45-53.

Enjyo, T., Ikeuchi, K., Kanai, M., & Maruyama, T. (1977). Diffusion welding of aluminum to titanium. *Transactions of JWRI*, *6*(1), 123-130.

Feller, J. F., Linossier, I., & Grohens, Y. (2002). Conductive polymer composites: comparative study of poly (ester)-short carbon fibres and poly (epoxy)-short carbon fibres mechanical and electrical properties. *Materials Letters*, *57*(1), 64-71.

Friedrich, K., Zhang, Z., & Schlarb, A. K. (2005). Effects of various fillers on the sliding wear of polymer composites. *Composites Science and Technology*, *65*(15), 2329-2343.

Fukui, Y., & Watanabe, Y. (1996). Analysis of thermal residual stress in a thick-walled ring of duralcan-base Al-SiC functionally graded material. *Metallurgical and Materials Transactions A*, *27*(12), 4145-4151.

Fukui, Y., Kinoshita, H., & Nakanishi, K. (1992). A Simulative Experiment for Characterizing the Strength of Functionally Gradient Material: The Analysis for the Case of Radial Crushing Test. *JSME international journal. Ser. 1, Solid mechanics, strength of materials*, *35*(1), 95-101.

Fukui, Y., Takashima, K., & Ponton, C. B. (1994). Measurement of Young's modulus and internal friction of an in situ Al-Al_3Ni functionally gradient material. *Journal of materials science*, *29*(9), 2281-2288.

Fuxiao, Y., Jianzhong, C., Ranganathan, S., & Dwarakadasa, E. S. (2001). Fundamental differences between spray forming and other semisolid processes. *Materials Science and Engineering: A*, *304*, 621-626.

G. Sigworth, S. Shivkumar and D. Apelian. (1989) ibid. 97 81L.

Gao, J. W., & Wang, C. Y. (2000). Modeling the solidification of functionally graded materials by centrifugal casting. *Materials Science and Engineering: A*, *292*(2), 207-215.

Gao, J. W., & Wang, C. Y. (2001). Transport phenomena during solidification processing of functionally graded composites by sedimentation. *Transactions-American Society of Mechanical Engineers Journal of Heat Transfer*, *123*(2), 368-375.

García-García, G., Espinoza-Cuadra, J., & Mancha-Molinar, H. (2007). Copper content and cooling rate effects over second phase particles behavior in industrial aluminum–silicon alloy 319. *Materials & design*, *28*(2), 428-433.

Gautam, G., Ghose, A. K., & Chakrabarty, I. (2015). Tensile and Dry Sliding Wear Behavior of In-Situ Al_3Zr+Al_2O_3-Reinforced Aluminum Metal Matrix Composites. *Metallurgical and Materials Transactions A*, *46*(12), 5952-5961.

Ge, L. L., Liu, R. P., Li, G., Ma, M. Z., & Wang, W. K. (2004). Solidification of Al–50at.% Si alloy in a drop tube. *Materials Science and Engineering: A*, *385*(1), 128-132.

Ghazali, M. J., Rainforth, W. M., & Jones, H. (2007). The wear of wrought aluminium alloys under dry sliding conditions. *Tribology International*, *40*(2), 160-169.

Gomes, J. R., Miranda, A. S., & Soares, D. (2000). Tribological Characterization of Al-Si/SiC_p Composites: MCs vs FGMs.

Green, K. J., Dean, D. R., Vaidya, U. K., & Nyairo, E. (2009). Multiscale fiber reinforced composites based on a carbon nanofiber/epoxy nanophased polymer matrix: synthesis, mechanical, and thermomechanical behavior. *Composites Part A: applied science and manufacturing*, *40*(9), 1470-1475.

Gui, M., & Kang, S. B. (2001). Dry sliding wear behavior of plasma-sprayed aluminum hybrid composite coatings. *Metallurgical and Materials Transactions A*, *32*(9), 2383-2392.

Guzowski, M. M., Sigworth, G. K., & Sentner, D. A. (1987). The role of boron in the grain. *Metallurgical and Materials Transactions A*, *18*(5), 603-619.

Hajjari, E., Divandari, M., Razavi, S. H., Emami, S. M., Homma, T., & Kamado, S. (2011). Dissimilar joining of Al/Mg light metals by compound casting process. *Journal of materials science*, *46*(20), 6491-6499.

Hajjari, E., Divandari, M., Razavi, S. H., Homma, T., & Kamado, S. (2012). Intermetallic compounds and antiphase domains in Al/Mg compound casting. *Intermetallics*, *23*, 182-186.

Halvaee, A., & Talebi, A. (2001). Effect of process variables on microstructure and segregation in centrifugal casting of C92200 alloy. *Journal of Materials Processing Technology*, *118*(1), 122-126.

Henning, W., Melzer, C., & Mielke, S. (1992). Keramische Gradientenwerkstoffe für Komponenten in Verbrennungsmotoren. *Metall*, *46*(5), 436-439.

Herbert, M. A., Maiti, R., Mitra, R., & Chakraborty, M. (2008). Wear behaviour of cast and mushy state rolled Al–4.5 Cu alloy and in-situ Al_4-5Cu–5TiB_2 composite. *Wear*, *265*(11), 1606-1618.

Heremans, J., Thrush, C. M., Lin, Y. M., Cronin, S., Zhang, Z., Dresselhaus, M. S., & Mansfield, J. F. (2000). Bismuth nanowire arrays: Synthesis and galvanomagnetic properties. *Physical Review B*, *61*(4), 2921-2930.

Herling, D. R., & Hunt, W. (2004). *Low cost cast aluminum metal matrix composites have arrived* (No. PNNL-SA-39566). Pacific Northwest National Laboratory (PNNL), Richland, WA (US).

Hernandez, F. R., & Sokolowski, J. H. (2006). Comparison among chemical and electromagnetic stirring and vibration melt treatments for Al–Si hypereutectic alloys. *Journal of alloys and compounds*, *426*(1), 205-212.

Hirai T. (1996). Processing of Ceramics; Weinheim: New York, NY, USA, 17B 293.

Hogg, S. C., & Atkinson, H. V. (2005). Inhibited coarsening of a spray-formed and extruded hypereutectic aluminum-silicon alloy in the semisolid state. *Metallurgical and Materials Transactions A*, *36*(1), 149-159.

Ji, C., & Searson, P. C. (2002). Fabrication of nanoporous gold nanowires. *Applied physics letters*, *81*(23), 4437-4439.

Jiangwei, R., Yajiang, L., & Tao, F. (2002). Microstructure characteristics in the interface zone of Ti/Al diffusion bonding. *Materials Letters*, *56*(5), 647-652.

Jinlong, W. Z. M. X. Z., & Zhiying, O. (2005). Modification of Al-Si Hypereutectic Alloys by Sr-PM [J]. *Special Casting & Nonferrous Alloys*, *4*, 021.

Jorstad, J. L. (1971). The hypereutectic aluminum-silicon alloy used to cast the Vega engine block. *Modern Casting*, *60*(4), 59-64.

Jorstad, J., & Apelian, D. (2004). Hypereutectic Al-Si Alloys: Practical Processing Techniques. *Die Casting Engineer*, *48*(3), 50-58.

K. Durai Babu. (2005). Dissertation, CSIR-National Institute for Interdisciplinary Science and Technology, Trivandrum, India.

Kang, C. G., & Rohatgi, P. K. (1996). Transient thermal analysis of solidification in a centrifugal casting for composite materials containing particle segregation. *Metallurgical and Materials Transactions B*, *27*(2), 277-285.

Karaköse, E., & Keskin, M. (2012). Microstructure properties and microhardness of rapidly solidified $Al_{64}Cu_{20}Fe_{12}Si_4$ quasicrystal alloy. *Metals and Materials International*, *18*(2), 257-263.

Kawasaki, A., & Watanabe, R. (1997). Concept and P/M fabrication of functionally gradient materials. *Ceramics international*, *23*(1), 73-83.

Kennedy, A. R. (2002). The microstructure and mechanical properties of Al-Si-B_4C metal matrix composites. *Journal of materials science*, *37*(2), 317-323.

Kennedy, A. R., & Brampton, B. (2001). The reactive wetting and incorporation of B_4C particles into molten aluminium. *Scripta Materialia*, *44*(7), 1077-1082.

Kevorkijan, V. (2003). Functionally graded aluminum-matrix composites. *American Ceramic Society Bulletin*, *82*(2), 60-64.

Khun, N. W., & Liu, E. (2013). Thermal, mechanical and tribological properties of polycarbonate/acrylonitrile-butadiene-styrene blends. *Journal of Polymer Engineering*, *33*(6), 535-543.

Khun, N. W., Zhang, H., Lim, L. H., Yue, C. Y., Hu, X., & Yang, J. (2014). Tribological properties of short carbon fibers reinforced epoxy composites. *Friction*, *2*(3), 226-239.

Khun, N. W., Zhang, H., Tang, X. Z., Yue, C. Y., & Yang, J. (2014). Short Carbon Fiber-Reinforced Epoxy Tribomaterials Self-Lubricated by Wax Containing Microcapsules. *Journal of Applied Mechanics*, *81*(12), 121004.

Khun, N. W., Zhang, H., Yang, J., & Liu, E. (2013). Mechanical and tribological properties of epoxy matrix composites modified with microencapsulated mixture of wax lubricant and multi-walled carbon nanotubes. *Friction*, *1*(4), 341-349.

Kieback, B., Neubrand, A., & Riedel, H. (2003). Processing techniques for functionally graded materials. *Materials Science and Engineering: A*, *362*(1), 81-106.

Kim, J. K., & Yu, T. X. (1997). Forming and failure behaviour of coated, laminated and sandwiched sheet metals: a review. *Journal of Materials Processing Technology*, *63*(1-3), 33-42.

Knuutinen, A., Nogita, K., McDonald, S. D., & Dahle, A. K. (2001). Porosity formation in aluminium alloy A356 modified with Ba, Ca, Y and Yb. *Journal of Light Metals*, *1*(4), 241-249.

Kori, S. A., Murty, B. S., & Chakraborty, M. (2000). Development of an efficient grain refiner for Al–7Si alloy and its modification with strontium. *Materials Science and Engineering: A*, *283*(1), 94-104.

Korkut, M. H. (2004). Effect of particulate reinforcement on wear behaviour of aluminium matrix composites. *Materials Science and Technology*, *20*(1), 73-81.

Krishnan, B. P., & Rohatgi, P. K. (1984). Modification of Al–Si alloy melts containing graphite particle dispersions. *Metals Technology*, *11*(1), 41-44.

Kumar, S., Panwar, R. S., & Pandey, O. P. (2013). Wear behavior at high temperature of dual-particle size zircon-sand-reinforced aluminum alloy composite. *Metallurgical and Materials Transactions A*, *44*(3), 1548-1565.

Kumar, S., Sarma, V. S., & Murty, B. S. (2010). Functionally graded Al alloy matrix in-situ composites. *Metallurgical and Materials Transactions A*, *41*(1), 242-254.

Kuo, C. G., & Chao, C. G. (2007). A novel method of centrifugal processing for the synthesis of lead–bismuth eutectic alloy nanospheres and nanowires. *The International Journal of Advanced Manufacturing Technology*, *32*(5), 468-472.

Kyffin, W. J., Rainforth, W. M., & Jones, H. (2001). Effect of treatment variables on size refinement by phosphide inoculants of primary silicon in hypereutectic Al–Si alloys. *Materials science and technology*, *17*(8), 901-905.

Lajoye, L., & Suery, M. (1987). Solidification Processing Reprints of 3'rd International Conference. *Sheffield, Sept*, *473*.

Lajoye, L., & Suery, M. (1988). Modelling of particle segregation during centrifugal casting of Al-matrix composites. *Cast reinforced metal composites*, 15.

Lao, J. Y., Wen, J. G., & Ren, Z. F. (2002). Hierarchical ZnO nanostructures. *Nano Letters*, *2*(11), 1287-1291.

Lavernia, E. J., & Grant, N. J. (1987). Aluminium-lithium alloys. *Journal of Materials Science*, *22*(5), 1521-1529.

Lee, J. S., Son, H. T., Oh, I. H., Kang, C. S., Yun, C. H., Lim, S. C., & Kwon, H. C. (2007). Fabrication and characterization of Ti–Cu clad materials by indirect extrusion. *Journal of Materials Processing Technology*, *187*, 653-656.

Lee, N. J., Jang, J., Park, M., & Choe, C. R. (1997). Characterization of functionally gradient epoxy/carbon fibre composite prepared under centrifugal force. *Journal of Materials Science*, *32*(8), 2013-2020.

Lee, T. H., Lee, Y. J., Park, K. T., Nersisyan, H. H., Jeong, H. G., & Lee, J. H. (2013). Controlling Al/Cu composite diffusion layer during hydrostatic extrusion by using colloidal Ag. *Journal of Materials Processing Technology*, *213*(3), 487-494.

Li, F., Liu, Y., Qu, C. B., Xiao, H. M., Hua, Y., Sui, G. X., & Fu, S. Y. (2015). Enhanced mechanical properties of short carbon fiber reinforced polyethersulfone composites by graphene oxide coating. *Polymer*, *59*, 155-165.

Li, H. P., & Sekhar, J. A. (1993). Rapid solidification by unstable combustion synthesis. *Journal of materials research*, *8*(10), 2515-2523.

Li, X., Liang, W., Zhao, X., Zhang, Y., Fu, X., & Liu, F. (2009). Bonding of Mg and Al with Mg–Al eutectic alloy and its application in aluminum coating on magnesium. *Journal of Alloys and Compounds*, *471*(1), 408-411.

Liao, H., Sun, Y., & Sun, G. (2002). Correlation between mechanical properties and amount of dendritic α-Al phase in as-cast near-eutectic Al–11.6% Si alloys modified with strontium. *Materials Science and Engineering: A*, *335*(1), 62-66.

Liu, C. Y., Wang, Q., Jia, Y. Z., Jing, R., Zhang, B., Ma, M. Z., & Liu, R. P. (2012). Microstructures and mechanical properties of Mg/Mg and Mg/Al/Mg laminated composites prepared via warm roll bonding. *Materials Science and Engineering: A*, *556*, 1-8.

Liu, J. C., Hu, J., Nie, X. Y., Li, H. X., Du, Q., Zhang, J. S., & Zhuang, L. Z. (2015). The interface bonding mechanism and related mechanical properties of Mg/Al compound materials fabricated by insert molding. *Materials Science and Engineering: A*, *635*, 70-76.

Liu, K., Ma, Y. C., Gao, M., Rao, G. B., Li, Y. Y., Wei, K., Wu, X. & Loretto, M. H. (2005). Single step centrifugal casting TiAl automotive valves. *Intermetallics*, *13*(9), 925-928.

Liu, T., Wang, Q., Sui, Y., Wang, Q., & Ding, W. (2015). An investigation into aluminum–aluminum bimetal fabrication by squeeze casting. *Materials & Design*, *68*, 8-17.

Liu, T., Wang, Q., Sui, Y., Wang, Q., & Ding, W. (2016). An investigation into interface formation and mechanical properties of aluminum–copper bimetal by squeeze casting. *Materials & Design*, *89*, 1137-1146.

Liu, Z. Q., Pan, Z. W., Sun, L. F., Tang, D. S., Zhou, W. Y., Wang, G., Qian, L. X., & Xie, S. S. (2000). Synthesis of silicon nanowires using AuPd nanoparticles catalyst on silicon substrate. *Journal of physics and chemistry of solids*, *61*(7), 1171-1174.

Lu, D., Jiang, Y., Guan, G., Zhou, R., Li, Z., & Zhou, R. (2007). Refinement of primary Si in hypereutectic Al–Si alloy by electromagnetic stirring. *Journal of Materials Processing Technology*, *189*(1), 13-18.

Lu, S. Z., & Hellawell, A. (1987). The mechanism of silicon modification in aluminum-silicon alloys: impurity induced twinning. *Metallurgical Transactions A*, *18*(10), 1721-1733.

Mandal, A., & Makhlouf, M. M. (2007). *Improving Aluminum Casting Alloy and Process Competitiveness* (pp. 07-02). ACRC Report.

Martın-González, M. S., Prieto, A. L., Gronsky, R., Sands, T., & Stacy, A. M. (2002). Insights into the electrodeposition of Bi_2Te_3. *Journal of the Electrochemical Society*, *149*(11), C546-C554.

Marukovich, E. I., Anisovich, A. G., Dozmarov, V. V., & Muchin, Y. V. (1999). Structure of contact layer of the bimetals obtained by connection of components in liquid state. *Foundry*, *9*, 12-5.

Marukovich, E. I., Branovitsky, A. M., Na, Y. S., Lee, J. H., & Choi, K. Y. (2006). Study on the possibility of continuous-casting of bimetallic components in condition of direct connection of metals in a liquid state. *Materials & design*, *27*(10), 1016-1026.

Marukovich, E. I., Dozmarov, V. V., & Voytenko, I. G. (1998). Research of zone of contact of bimetals by a method of high-frequency hypersonic sondage. *Foundry Prod Metall*, *1*, 24-6.

Matsuda, K., Watanabe, Y., & Fukui, Y. (2000). Particle Size Distributions in in situ Al-Al~ 3Ni FGMs Fabricated by Centrifugal in situ Method. *CERAMIC TRANSACTIONS*, *114*, 491-500.

McGrath, L. M., Parnas, R. S., King, S. H., Schroeder, J. L., Fischer, D. A., & Lenhart, J. L. (2008). Investigation of the thermal, mechanical, and fracture properties of alumina–epoxy composites. *Polymer*, *49*(4), 999-1014.

Melgarejo, Z. H., Suárez, O. M., & Sridharan, K. (2006). Wear resistance of a functionally-graded aluminum matrix composite. *Scripta Materialia*, *55*(1), 95-98.

Melgarejo, Z. H., Suárez, O. M., & Sridharan, K. (2008). Microstructure and properties of functionally graded Al–Mg–B composites fabricated by centrifugal casting. *Composites Part A: Applied Science and Manufacturing*, *39*(7), 1150-1158.

Miao, Z., Xu, D., Ouyang, J., Guo, G., Zhao, X., & Tang, Y. (2002). Electrochemically induced sol– gel preparation of single-crystalline TiO_2 nanowires. *Nano Letters*, *2*(7), 717-720.

Miller, W. S., Zhuang, L., Bottema, J., Wittebrood, A., De Smet, P., Haszler, A., & Vieregge, A. (2000). Recent development in aluminium alloys for the automotive industry. *Materials Science and Engineering: A*, *280*(1), 37-49.

Miriyev, A., Levy, A., Kalabukhov, S., & Frage, N. (2016). Interface evolution and shear strength of Al/Ti bi-metals processed by a spark plasma sintering (SPS) apparatus. *Journal of Alloys and Compounds*, *678*, 329-336.

Miyamoto, Y., Kaysser, W. A., Rabin, B. H., Kawasaki, A., & Ford, R. G. (Eds.). (2013). *Functionally graded materials: design, processing and applications* (Vol. 5). Springer Science & Business Media.

Mordike, B. L., & Ebert, T. (2001). Magnesium: Properties—applications—potential. *Materials Science and Engineering: A*, *302*(1), 37-45.

Moroz, A. (1999). Three-dimensional complete photonic-band-gap structures in the visible. *Physical Review Letters*, *83*(25), 5274-5277.

Mortensen, A., & Suresh, S. (1995). Functionally graded metals and metal-ceramic composites: Part 1 Processing. *International Materials Reviews*, *40*(6), 239-265.

Moses, J. J., Dinaharan, I., & Sekhar, S. J. (2016). Prediction of influence of process parameters on tensile strength of AA6061/TiC aluminum matrix composites produced using stir casting. *Transactions of Nonferrous Metals Society of China*, *26*(6), 1498-1511.

Nai, S. M. L., Gupta, M., & Lim, C. Y. H. (2004). Synthesis and wear of Al based, free standing functionally gradient materials: effects of different reinforcements. *Materials science and technology*, *20*(1), 57-67.

Neubrand, A., & Rödel, J. (1997). Gradient materials: an overview of a novel concept. *Zeitschrift für Metallkunde*, *88*(5), 358-371.

Nie, X. Y., Liu, J. C., Li, H. X., Du, Q., Zhang, J. S., & Zhuang, L. Z. (2014). An investigation on bonding mechanism and mechanical properties of Al/Ti compound materials prepared by insert moulding. *Materials & Design*, *63*, 142-150.

Nie, X. Y., Zhao, K. N., Li, H. X., Du, Q., Zhang, J. S., & Zhuang, L. Z. (2015). Comparisons of interface microstructure and mechanical behavior between Ti/Al and Ti-6Al-4V/Al bimetallic composites. *China Foundry*, *12*(1).

Ning H.L., Wang Y.P., Huang F.X., Ma J.S., Geng Z.T. & Chen Z.H., (2002). J Funct Mater, 2166–2168.

Nogita, K., Drennan, J., & Dahle, A. K. (2003). Evaluation of silicon twinning in hypo-eutectic Al-Si alloys. *Materials transactions*, *44*(4), 625-628.

Pacz, A. (1921). United States Patent 358555, 0–7

Papis, K. J. M., Hallstedt, B., Löffler, J. F., & Uggowitzer, P. J. (2008). Interface formation in aluminium–aluminium compound casting. *Acta Materialia*, *56*(13), 3036-3043.

Papis, K. J. M., Löffler, J. F., & Uggowitzer, P. J. (2010). Interface formation between liquid and solid Mg alloys—An approach to continuously metallurgic joining of magnesium parts. *Materials Science and Engineering: A*, *527*(9), 2274-2279.

Papis, K. J., Loeffler, J. F., & Uggowitzer, P. J. (2009). Light metal compound casting. *Science in China Series E: Technological Sciences*, *52*(1), 46-51.

Park, S. J., & Kim, M. H. (2000). Effect of acidic anode treatment on carbon fibers for increasing fiber-matrix adhesion and its relationship to interlaminar shear strength of composites. *Journal of materials science*, *35*(8), 1901-1905.

Perez-Bustamante, R., Bueno-Escobedo, J. L., Jimenez-Lobato, J., Estrada-Guel, I., Miki-Yoshida, M., Licea-Jimenez, L., & Martínez-Sánchez, R. (2012). Wear behavior in Al 2024–CNTs composites synthesized by mechanical alloying. *Wear*, *292*, 169-175.

Polmear, I. J. (1994). Magnesium alloys and applications. *Materials science and technology*, *10*(1), 1-16.

Ragab, K. A., Samuel, A. M., Al-Ahmari, A. M. A., Samuel, F. H., & Doty, H. W. (2013). Influence of Fluidized Bed Quenching on the Mechanical Properties and

Quality Index of T6 Tempered B319. 2-Type Aluminum Alloys. *Journal of materials engineering and performance*, *22*(11), 3476-3489.

Rajan T. P. D, R.M. Pillai & B.C. Pai, (2004). Proceedings of 3rd International Conference on Materials Processing for Properties and Performance, Singapore, 24–26 November 2004, ed. by K.A. Khor (Institute of Materials (East Asia), Singapore, 33.

Rajan T. P. D, R.M. Pillai & B.C. Pai. (2008) Proceedings of 68th World Foundry Congress., 63–68.

Rajan, T. P. D, & Pai, B. C. (2009). Formation of solidification microstructures in centrifugal cast functionally graded aluminium composites. *Transactions of the Indian Institute of Metals*, *62*(4), 383-389.

Rajan, T. P. D., & Pai, B. C. (2014). Developments in processing of functionally gradient metals and metal–ceramic composites: a review. *Acta Metallurgica Sinica (English Letters)*, *27*(5), 825-838.

Rajan, T. P. D., Pillai, R. M., & Pai, B. C. (2003). Solidification Processing of Functionally Gradient Metals and Metal-Ceramic Composites. *Indian Foundry Journal*, *49*(9), 19-30.

Rajan, T. P. D., Pillai, R. M., & Pai, B. C. (2008). Functionally graded Al–Al_3Ni in situ intermetallic composites: fabrication and microstructural characterization. *Journal of Alloys and Compounds*, *453*(1), L4-L7.

Rajaram, G., Kumaran, S., & Rao, T. S. (2010). High temperature tensile and wear behaviour of aluminum silicon alloy. *Materials Science and Engineering: A*, *528*(1), 247-253.

Rao, A. G., Mohape, M., Katkar, V. A., Gowtam, D. S., Deshmukh, V. P., & Shah, A. K. (2010). Fabrication and characterization of aluminum (6061)-boron-carbide functionally gradient material. *Materials and Manufacturing Processes*, *25*(7), 572-576.

Rodriguez-Castro, R., & Kelestemur, M. H. (2002a). Processing and microstructural characterization of functionally gradient Al A359/SiC_p composite. *Journal of materials science*, *37*(9), 1813-1821.

Rodrıguez-Castro, R., Wetherhold, R. C., & Kelestemur, M. H. (2002b). Microstructure and mechanical behavior of functionally graded Al A359/SiC_p composite. *Materials Science and Engineering: A*, *323*(1), 445-456.

Rosenberger, M. R., Schvezov, C. E., & Forlerer, E. (2005). Wear of different aluminum matrix composites under conditions that generate a mechanically mixed layer. *Wear*, *259*(1), 590-601.

Rosenhain W. & Grogan G.D. and Schofield T.H. (1930).

Rübner, M., Günzl, M., Körner, C., & Singer, R. F. (2011). Aluminium–aluminium compound fabrication by high pressure die casting. *Materials Science and Engineering: A*, *528*(22), 7024-7029.

S. T. Chiu: Z. Metallkde. (1966). 57, 396–401.

Samuel, F. H., Samuel, A. M., Ouellet, P., & Doty, H. W. (1998). Effect of Mg and Sr additions on the formation of intermetallics in Al-6 wt pct Si-3.5 wt pct Cu-(0.45) to (0.8) wt pct Fe 319-type alloys. *Metallurgical and Materials Transactions A*, *29*(12), 2871-2884.

Schatt, W. (1992). *Sintervorgänge: Grundlagen*. VDI-Verlag.

Sequeira, P. D., Watanabe, Y., & Rocha, L. A. (2005). Aluminum matrix texture and particle characterization in Al-Al_3Ti FGMs produced by a centrifugal solid-particle method. In *Solid State Phenomena* (Vol. 105, pp. 415-420). Trans Tech Publications.

Sequeira, P. D., Watanabe, Y., & Rocha, L. A. (2005). Particle distribution and orientation in Al-Al_3Zr and Al-Al_3Ti FGMs produced by the centrifugal method. In *Materials Science Forum* (Vol. 492, pp. 609-614). Trans Tech Publications.

Shabestari, S. G., & Moemeni, H. (2004). Effect of copper and solidification conditions on the microstructure and mechanical properties of Al–Si–Mg alloys. *Journal of Materials Processing Technology*, *153*, 193-198.

Shen, M., & Bever, M. B. (1972). Gradients in polymeric materials. *Journal of Materials science*, *7*(7), 741-746.

Shen, S., Cai, S., Xu, G., Li, Y., Zhang, T., & Zhang, M. (2015). Bond strength and corrosion resistance of bioglass coated magnesium alloy fabricated by uniaxial pressing and microwave hybrid heating. *Materials & Design*, *86*, 610-615.

Shimamoto, D., & Yusuke Imai, Y. H. (2014). Kinetic study of resin-curing on carbon fiber/epoxy resin composites by microwave irradiation. *Open Journal of Composite Materials*, *2014*.

Shivamurthy, R. C., & Surappa, M. K. (2011). Tribological characteristics of A356 Al alloy–SiC_p composite discs. *Wear*, *271*(9), 1946-1950.

Shivkumar, S., Ricci Jr, S., Steenhoff, B., Apelian, D., & Sigworth, G. (1989). An experimental study to optimize the heat treatment of A356 alloy. *AFS Transactions*, *97*, 791-810.

Show, B. K., Mondal, D. K., & Maity, J. (2014). Wear behavior of a novel aluminum-based hybrid composite. *Metallurgical and Materials Transactions A*, *45*(2), 1027-1040.

Sigworth, G. K. (1983). Theoretical and practical aspects of the modification of Al-Si alloys. *AFS Trans*, *66*, 7-16.

Sigworth, G. K., Shivkumar, S., & Apelian, D. AFS Transactions, 97 (1989). *Google Scholar*, 811-824.

Smith, W. S. (1987). Engineered materials handbook. *ASM International, Ohio*, *1*.

Song, X. Y., Sun, J. B., Zhong, D. S., Yu, Y. S., Wang, T. M., Cao, Z. Q., & Li, T. J. (2012). Study on Al/Mg compound materials by solid–liquid bonding method. *Materials Research Innovations*, *16*(1), 51-55.

Stefanescu, D. M., Davis, J. R., & Destefani, J. D. (1988). Metals Handbook, Vol. 15--Casting. *ASM International, 1988,*, 937.

Strzelecka, M., Iwaszko, J., Malik, M., & Tomczyński, S. (2015). Surface modification of the AZ91 magnesium alloy. *Archives of Civil and Mechanical Engineering*, *15*(4), 854-861.

Sun, J., Song, X., Wang, T., Yu, Y., Sun, M., Cao, Z., & Li, T. (2012). The microstructure and property of Al–Si alloy and Al–Mn alloy bimetal prepared by continuous casting. *Materials Letters*, *67*(1), 21-23.

Tarlochan, F. (2012). Functionally Graded Material: A New Breed of Engineered Material. *Journal of Applied Mechanical Engineering, November*.

Tavitas-Medrano, F. J., Gruzleski, J. E., Samuel, F. H., Valtierra, S., & Doty, H. W. (2008). Effect of Mg and Sr-modification on the mechanical properties of 319-type aluminum cast alloys subjected to artificial aging. *Materials Science and Engineering: A*, *480*(1), 356-364.

Telang, Y. P. (1963). Process variables in Al-21Si alloys refinement. *AFS Transactions*, *71*, 232-240.

The Aluminum Automotive Manual: Design-Design with Aluminum, European Aluminum Association. (2011).

Thostenson, E. T., Ren, Z., & Chou, T. W. (2001). Advances in the science and technology of carbon nanotubes and their composites: a review. *Composites science and technology*, *61*(13), 1899-1912.

Tiwari, S., & Bijwe, J. (2014). Surface treatment of carbon fibers-a review. *Procedia Technology*, *14*, 505-512.

Velhinho, A., Sequeira, P. D., Martins, R., Vignoles, G., Fernandes, F. B., Botas, J. D., & Rocha, L. A. (2003). X-ray tomographic imaging of Al/SiC_p functionally graded composites fabricated by centrifugal casting. *Nuclear Instruments and Methods in Physics Research Section B: Beam Interactions with Materials and Atoms*, *200*, 295-302.

Vencl, A., Bobic, I., Arostegui, S., Bobic, B., Marinković, A., & Babić, M. (2010). Structural, mechanical and tribological properties of A356 aluminium alloy reinforced with Al_2O_3, SiC and SiC+ graphite particles. *Journal of Alloys and Compounds*, *506*(2), 631-639.

Viala, J. C., Peronnet, M., Barbeau, F., Bosselet, F., & Bouix, J. (2002). Interface chemistry in aluminium alloy castings reinforced with iron base inserts. *Composites Part A: Applied Science and Manufacturing*, *33*(10), 1417-1420.

Vieira, A. C., Sequeira, P. D., Gomes, J. R., & Rocha, L. A. (2009). Dry sliding wear of Al alloy/SiC_p functionally graded composites: Influence of processing conditions. *Wear*, *267*(1), 585-592.

Volder, J. P. (1993). An overview of a number of casting processes. *Aluminium*, *4*, 11-16.

W. Sufei & L. Steve. (2008). "ASM Handbook: Centrifugal Casting," ASM International, 15, 667-673.

Wagner, R. S. (1960). On the growth of germanium dendrites. *Acta metallurgica*, *8*(1), 57-60.

Wagstaff, R. B., & Bischoff, T. F. (2011). *U.S. Patent No. 7,882,887*. Washington, DC: U.S. Patent and Trademark Office.

Wagstaff, R. B., Lloyd, D. J., & Bischoff, T. F. (2006). Direct chill casting of CLAD ingot. In *Materials Science Forum* (Vol. 519, pp. 1809-1814). Trans Tech Publications.

Wan, Y. Z., Luo, H. L., Wang, Y. L., Huang, Y., Li, Q. Y., Zhou, F. G., & Chen, G. C. (2005). Friction and wear behavior of three-dimensional braided carbon fiber/epoxy composites under lubricated sliding conditions. *Journal of materials science*, *40*(17), 4475-4481.

Wang D.Q., Shi Z.Y & Qi R.B. (2007). Scripta Mater 56, 369–372.

Wang, K., Sun, W., Li, B., Xue, H., & Liu, C. (2011). Microstructures in centrifugal casting of SiC_p/AlSi9Mg composites with different mould rotation speeds. *Journal of Wuhan University of Technology-Mater. Sci. Ed.*, *26*(3), 504-509.

Wang, L., & Shivkumar, S. (1995). Strontium modification of aluminium alloy castings in the expendable pattern casting process. *Journal of materials Science*, *30*(6), 1584-1594.

Wang, Q. D., & Jin, J. Z. (1997). In situ gradient double-layer composites of Al-Fe alloy by centrifugal casting. *Transactions of Nonferrous Metals Society 0f China*, *7*(1), 125-130.

Wang, Q. G. (2003). Microstructural effects on the tensile and fracture behavior of aluminum casting alloys A356/357. *Metallurgical and materials Transactions A*, *34*(12), 2887-2899.

Wang, Q. G. (2004). Plastic deformation behavior of aluminum casting alloys A356/357. *Metallurgical and Materials Transactions A*, *35*(9), 2707-2718.

Wasilewski, P. (1993). Siluminy-modyfikacja i jej wpływ na strukturę i właściwości. PAN Krzepnięcie metali i stopów, Zeszyt 21. *Monografia, Katowice*.

Watanabe, Y., & Fukui, Y. (2000). Fabrication of functionally-graded aluminum materials by the centrifugal method. *Aluminum Transactions*, *2*(2), 195-208.

Watanabe, Y., & Fukui, Y. (2000). Microstructures and mechanical properties of functionally graded material fabricated by centrifugal casting method.

Watanabe, Y., & Nakamura, T. (2001). Microstructures and wear resistances of hybrid Al–(Al_3Ti+ Al_3Ni) FGMs fabricated by a centrifugal method. *Intermetallics*, *9*(1), 33-43.

Watanabe, Y., & Oike, S. (2005). Formation mechanism of graded composition in Al–Al_2Cu functionally graded materials fabricated by a centrifugal in situ method. *Acta materialia*, *53*(6), 1631-1641.

Watanabe, Y., Eryu, H., & Matsuura, K. (2001). Evaluation of three-dimensional orientation of Al_3Ti platelet in Al-based functionally graded materials fabricated by a centrifugal casting technique. *Acta Materialia*, *49*(5), 775-783.

Watanabe, Y., Inaguma, Y., Sato, H., & Miura-Fujiwara, E. (2009). A novel fabrication method for functionally graded materials under centrifugal force: the centrifugal mixed-powder method. *Materials*, *2*(4), 2510-2525.

Watanabe, Y., Kurahashi, M., Kim, I. S., Miyazaki, S., Kumai, S., Sato, A., & Tanaka, S. I. (2006). Fabrication of fiber-reinforced functionally graded materials by a centrifugal in situ method from Al–Cu–Fe ternary alloy. *Composites Part A: Applied Science and Manufacturing*, *37*(12), 2186-2193.

Watanabe, Y., Yamanaka, N., & Fukui, Y. (1997). Orientation of Al_3Ti platelets in Al-Al3Ti functionally graded material manufactured by centrifugal method. *Zeitschrift für Metallkunde*, *88*(9), 717-721.

Watanabe, Y., Yamanaka, N., & Fukui, Y. (1999). Wear behavior of Al-Al_3Ti composite manufactured by a centrifugal method. *Metallurgical and Materials Transactions A*, *30*(12), 3253-3261.

Williams S. Ebhota, Akhil S. Karun, & Inambao, F. L. (2016). Principles and Baseline Knowledge of Functionally Graded Aluminium Matrix Materials (FGAMMs): Fabrication Techniques and Applications. In *International Journal of Engineering Research in Africa* (Vol. 26, pp. 47-67). Trans Tech Publications.

Wilson, S., & Alpas, A. T. (1997). Wear mechanism maps for metal matrix composites. *Wear*, *212*(1), 41-49.

Wu, Y., & Yang, P. (2000). Germanium nanowire growth via simple vapor transport. *Chemistry of Materials*, *12*(3), 605-607.

Xiangfa, L., Jinguo, Q., Yuxian, L., Shitong, L. I., & Xiufang, B. I. A. N. (2004). Modification performance of the Al-P master alloy for eutectic and hypereutectic Al-Si alloys. *Acta Metall Sin*, *40*(5), 471-476.

Xu, Y., & Van Hoa, S. (2008). Mechanical properties of carbon fiber reinforced epoxy/clay nanocomposites. *Composites Science and Technology*, *68*(3), 854-861.

Yang, L. J. (2003). The effect of casting temperature on the properties of squeeze cast aluminium and zinc alloys. *Journal of Materials Processing Technology*, *140*(1), 391-396.

Yang, L. J. (2003). Wear coefficient equation for aluminium-based matrix composites against steel disc. *Wear*, *255*(1), 579-592.

Yilmaz, F., Atasoy, O. A., & Elliott, R. (1992). Growth structures in aluminium-silicon alloys II. The influence of strontium. *Journal of crystal growth*, *118*(3-4), 377-384.

Yoshida, F., & Hino, R. (1997). Forming limit of stainless steel-clad aluminium sheets under plane stress condition. *Journal of materials processing technology*, *63*(1-3), 66-71.

Young, J. L., Kuhlmann-Wilsdorf, D., & Hull, R. (2000). The generation of mechanically mixed layers (MMLs) during sliding contact and the effects of lubricant thereon. *Wear*, *246*(1), 74-90.

Yu, H., Tieu, A. K., Lu, C., & Godbole, A. (2014). An investigation of interface bonding of bimetallic foils by combined accumulative roll bonding and asymmetric rolling techniques. *Metallurgical and Materials Transactions A*, *45*(9), 4038-4045.

Yu, L., Liu, X., Ding, H., & Bian, X. (2007). A new nucleation mechanism of primary Si by peritectic-like coupling of AlP and TiB_2 in near eutectic Al–Si alloy. *Journal of alloys and compounds*, *432*(1), 156-162.

Zhang, B., & Gasik, M. M. (2002). Stress evolution in graded materials during densification by sintering processes. *Computational materials science*, *25*(1), 264-271.

Zhang, G., Karger-Kocsis, J., & Zou, J. (2010). Synergetic effect of carbon nanofibers and short carbon fibers on the mechanical and fracture properties of epoxy resin. *Carbon*, *48*(15), 4289-4300.

Zhang, H., Chen, Y., & Luo, A. A. (2014). A novel aluminum surface treatment for improved bonding in magnesium/aluminum bimetallic castings. *Scripta Materialia*, *86*, 52-55.

Zhang, H., Zhang, Z., & Breidt, C. (2004). Comparison of short carbon fibre surface treatments on epoxy composites: I. Enhancement of the mechanical properties. *Composites science and technology*, *64*(13), 2021-2029.

Zhang, J. C., Ding, D. Y., Zhang, W. L., Kang, S. H., Xu, X. L., Gao, Y. J., Chen, G.Z., Chen, W.G. & You, X. H. (2014). Effect of Zr addition on microstructure and properties of Al–Mn–Si–Zn-based alloy. *Transactions of Nonferrous Metals Society of China*, *24*(12), 3872-3878.

Zhang, J., Chen, H., Yu, H., & Jin, Y. (2015). Study on dual modification of Al-17% Si alloys by structural heredity. *Metals*, *5*(2), 1112-1126.

Zhang, J., Fan, Z., Wang, Y., & Zhou, B. (2000). Hypereutectic aluminium alloy tubes with graded distribution of Mg_2Si particles prepared by centrifugal casting. *Materials & Design*, *21*(3), 149-153.

Zhang, K., Shen, W. P., & Ge, C. C. (2007). Properties of W/Cu FGMs containing 1% TiC or 1% La_2O_3 prepared using GSUHP. *Acta Metallurgica Sinica (English Letters)*, *20*(1), 59-64.

Zhao, C., Zhang, G., & Zhao, L. (2012). Effect of curing agent and temperature on the rheological behavior of epoxy resin systems. *Molecules*, *17*(7), 8587-8594.

Zhao, J. L., Jie, J. C., Fei, C. H. E. N., Hang, C. H. E. N., Li, T. J., & Cao, Z. Q. (2014). Effect of immersion Ni plating on interface microstructure and mechanical properties of Al/Cu bimetal. *Transactions of nonferrous metals society of China*, *24*(6), 1659-1665.

Zhao, K. N., Liu, J. C., Nie, X. Y., Li, Y., Li, H. X., Du, Q., ... & Zhang, J. S. (2016). Interface formation in magnesium–magnesium bimetal composites fabricated by insert molding method. *Materials & Design*, *91*, 122-131.

Zhao, P., Guo, S., Liu, G., Chen, Y., & Li, J. (2014). Fabrication of W–Cu functionally graded material with improved mechanical strength. *Journal of Alloys and Compounds*, *601*, 289-292.

Zhou, B. L. (1998). Functionally graded Al/Mg_2Si in-situ composites, prepared by centrifugal casting. *Journal of materials science letters*, *17*(19), 1677-1679.

Zhou, G., Movva, S., & Lee, L. J. (2008). Nanoclay and long-fiber-reinforced composites based on epoxy and phenolic resins. *Journal of applied polymer science*, *108*(6), 3720-3726.

Zuo, M., Liu, X., Dai, H., & Liu, X. (2009). Al-Si-P master alloy and its modification and refinement performance on Al-Si alloys. *Rare metals*, *28*(4), 412-417.